Evaluation and Remediation of Low Permeability and Dual Porosity Environments

Martin N. Sara and
Lorne G. Everett

EDITORS

STP 1415

ASTM
INTERNATIONAL
Standards Worldwide

STP 1415

Evaluation and Remediation of Low Permeability and Dual Porosity Environments

Martin N. Sara and Lorne G. Everett, editors

ASTM Stock Number: STP 1415

ASTM
100 Barr Harbor Drive
PO Box C700
West Conshohocken, PA 19428-2959

Printed in the U.S.A.

Library of Congress Cataloging-in-Publication Data
Evaluation and remediation of low permeability and dual porosity environments / Martin N. Sara and Lorne G. Everett, editors.
p. cm.
"ASTM stock number: STP 1415."
Includes bibliographical references and index.
ISBN 0-8031-3452-5
1. Soil remediation--Congresses. 2. Soil permeability--Congresses. I. Sara, Martin N., 1946- II. Everett, Lorne G. III. Symposium on Evaluation and Remediation of Low Permeability and Dual Porosity Environments (2001 : Reno, Nev.)

TD878 .E923 2002
628.5'5--dc21

2002034262

Photocopy Rights

Peer Review Policy

Each paper published in this volume was evaluated by two peer reviewers and at least one editor. The authors addressed all of the reviewers' comments to the satisfaction of both the technical editor(s) and the ASTM Committee on Publications.

To make technical information available as quickly as possible, the peer-reviewed papers in this publication were prepared "camera-ready" as submitted by the authors.

The quality of the papers in this publication reflects not only the obvious efforts of the authors and the technical editor(s), but also the work of the peer reviewers. In keeping with long-standing publication practices, ASTM maintains the anonymity of the peer reviewers. The ASTM Committee on Publications acknowledges with appreciation their dedication and contribution of time and effort on behalf of ASTM.

Printed in Saline, MI
2002

Foreword

The Symposium on Evaluation and Remediation of Low Permeability and Dual Porosity Environments was held in Reno, Nevada on 25 Jan. 2001. The Symposium was sponsored by ASTM Committee D18 on Soil and Rock. The co-chairmen were Martin N. Sara, Environmental Resource Management, Inc. and Lorne G. Everett, Chancellor, Lakehead University; Chief Scientist, Stone & Webster Consultants. They both served as editors for this publication.

Contents

SESSION I: TEST PROCEDURES

SESSION II: LABORATORY TO FIELD EVALUATIONS

SESSION III: LOW PERMEABILITY ENVIRONMENTS AND REMEDIATION ISSUES

TEST PROCEDURES

David Cazaux[1] and Gérard Didier[2]

Comparison between various Field and Laboratory Measurements of the Hydraulic Conductivity of three Clay Liners

Reference: Cazaux, D and Didier, G., "**Comparison between various Field and Laboratory Measurements of the Hydraulic Conductivity of three Clay liners**", *Evaluation and Remediation of Low Permeability and Dual Porosity Environments, ASTM STP 1415,* M.N. Sara and L.G. Everett, Eds., ASTM International, West Conshohocken, PA, 2002.

Abstract: For waste facilities, field assessment of the hydraulic conductivity of fine-grained soils has been a real challenge for the past decades that has led to several types of test methods. Although standards (ASTM, NF, etc.) have been adopted in many countries, any test method needs careful application for constructing quality-control programs. The type of apparatus, its geometry, and even specimen preparation may be major sources of discrepancy. We compared hydraulic-conductivity values obtained from various field-testing methods (open, sealed, single and double infiltrometers, and borehole methods), and laboratory-testing methods such as oedometer cells or rigid and flexible-wall permeameters. Three materials were tested in this study: a compacted sand-bentonite mixture, compacted clayey silt, and natural sandy clay. The field tests were run on soil-test pads whose characteristics were defined beforehand in the laboratory and the field. Comparison of the results shows a large range of hydraulic-conductivity values for a single soil sample. Such variability can commonly be explained by a scale effect, as demonstrated by the use of various types of diameter or geometry for the field or laboratory tests. Soil behavior (swelling or shrinkage) and test-analysis methods (saturated or unsaturated-flow analysis) are other important parameters. In conclusion, we identified the main problems affecting tests with infiltrometers and permeameters, and how they can be reduced or avoided by the improvement of current techniques.

Keywords: infiltration, hydraulic conductivity, clay liner, ring, infiltrometer, borehole, scale effect

---

[1] Research Engineer, BRGM, Industrial Environment and Processes Division, BP6009, 45060 Orléans, France, d.cazaux@brgm.fr.

[2] Lecturer, URGC Géotechnique, INSA Lyon, BAT JCA Coulomb, 34, Avenue des Arts, 69621 Villeurbanne, France, geot@insa-lyon.fr

Introduction

On of the most important geotechnical parameters for clay liners used in waste facilities is hydraulic conductivity. Regulatory agencies increasingly require field tests as well as laboratory tests. In the early 1990s, a Standards for Waste Facilities Committee was set up in France, in order to establish standards for hydraulic-conductivity testing. Eight standards concern ring-infiltrometer field methods (two standards published in 1999), field borehole methods (three standards), and laboratory methods (three standards). The French Environmental Agency (ADEME) further co-financed two research programs that compared methods used in France for determining hydraulic conductivity in the field (surface and borehole techniques) and in the laboratory.

The success of a hydraulic conductivity field test is a major issue. Failures are as much due to errors of procedure as to the type of tested soil, and affect borehole and surface methods. Such failures have led to increased vigilance during installation of the devices, to the application of lower hydraulic heads in sealed infiltrometers, and to a greater awareness of any abnormalities of the test zones that would help in understanding some of the failures. In addition, several other parameters can affect a test result, such as borehole installation (Chapuis and Sabourin, 1989), or the testing method hypothesis (Neuzil, 1982). Many papers have been written on this topic (Day and Daniel, 1985; Herzog and Morse, 1990; Sai and Anderson, 1991; Elrick and Reynolds, 1992; Picornell and Guerra, 1992; Dunn and Palmer, 1994; Trautwein and Boutwell, 1994; Purdy and Ramey, 1995; Benson *et al.*, 1997). Daniel (1994) and Benson *et al.* (1994) compared the available methods for recommending a representative specimen size that will reproduce field-test conditions in the laboratory. Benson *et al.* (1994) suggested that field-scale hydraulic conductivity can be measured on specimens with a diameter of at least 300 mm.

It is assumed that a logical alternative to field-testing is to conduct hydraulic-conductivity tests in the laboratory on specimens large enough to simulate field conditions. The objective of our research was to determine the influence of specimen size through surface and borehole tests in the field and the laboratory. The comparisons took place on three sites, during September 1994 (sites A and B) and 1995 (site C). Sites A and B are both test pads; the first with compacted clayey silt and the second with a compacted sand-bentonite mixture. Site C is a natural kaolinitic-clay deposit. After presenting the results obtained with the various testing methods used in this program, we compare them with results of additional laboratory tests on samples taken from the three sites. We try to explain any discrepancy by correlating the obtained results with the soil characteristics and geometry of the tested specimen.

Many different field tests have been proposed in this research. They are discussed with reference to their suitability for clay-barrier evaluation. Reasons for the preference of a particular test over other methods are also discussed.

Infiltrometer field-test methods

Summary

The infiltrometer-ring method consists in determining the infiltration rate under one or more hydraulic heads. With double-ring infiltrometers, the outer ring allows maintaining a vertical flow through the soil under the inner ring where the infiltration rate is measured. This is particularly useful for highly permeable material, when the wetting front can reach the base of both rings. The following nomenclature is generally found in ASTM references: *ODRI* for Open Double Ring Infiltrometer, *SSRI* for Sealed Single Ring Infiltrometer, and *SDRI* for Sealed Double Ring Infiltrometer. The field techniques and apparatus that were used in the programs are summarized in Table 1, which also gives the ring geometry (the first number is the inner ring diameter, the second is that of the outer ring).

Table 1 - *Apparatus and test methods used in the programs.*

ODRI 1 ∅100/300 mm	*SDRI 3 ∅800/1200 mm*
ODRI 2 ∅ 76/300 mm	*SSRI 1 ∅200 mm*
SDRI 1 ∅500/800 mm	*SSRI 1a ∅500 mm*
SDRI 1a ∅200/500 mm	*SSRI 2 ∅100 mm*
SDRI 2 ∅100/300 mm	

Open-Ring Infiltrometers – Open-ring infiltrometers are commonly used for soil/sewage applications. They are very easily applied simple devices, but they are limited to a middle-range hydraulic conductivity of 1×10^{-5} to 1×10^{-8} m/s. Several standards are available: ASTM D3385, AFNOR X30-418, DIN 19682, OENORM L1066, NVN 5790. The *ODRI* device consists of two concentric rings that are driven into the soil, filled with the same level of water. Water levels within both rings can be measured. The hydraulic head is maintained below the ring top, which is the main difference with sealed infiltrometers (Figure 1). Water-level fall is monitored in the inner ring with a specific instrument: if it remains low compared to the water height in the rings, it is assumed that infiltration into the soil proceeds under a constant hydraulic head. Water levels can be checked with various devices, such as a float, level transducer, graduated stick, or Mariotte bottle. Two *ODRI* were used in this research (Table 1).

Sealed-ring infiltrometers - Sealed-ring infiltrometers are driven into the soil and filled with water through a pressure-volume controller (*PVC*). The *PVC* is used for supplying water and recording the infiltration in one or both rings that are sealed with caps maintaining a constant hydraulic head. The hydraulic head is commonly higher than the level of the top of rings caps; which is the main difference from open-ring infiltrometers. Many types of *PVC* are available: Mariotte bottle, pressurized tank or tubes, piston volumeter, horizontal capillary, or bags. The infiltration rate is controlled by measuring water levels in different *PVC*, or by weighing bags at successive times. In some cases, the application of a confining load may be needed to avoid rising of the infiltrometer, particularly when a high hydraulic head is applied in the rings. During tests, a dial gauge can be used for checking a possible rise of the ring cap under the hydraulic head. Seven types of sealed infiltrometers, three single and four double, were used in this study; three are described on Figure 2 and Figure 3. Two standards are available: ASTM D5093 and AFNOR X30-420.

Tension infiltrometer - Tension infiltrometers, also known as disk infiltrometers, are used to determine the hydraulic characteristics of nearly saturated soils. The infiltrometer consists of a disk with a nylon mesh. Volumes are recorded with a system of Mariotte tubes (Figure 3b). The analysis is done under unsaturated conditions (White and Sully, 1992).

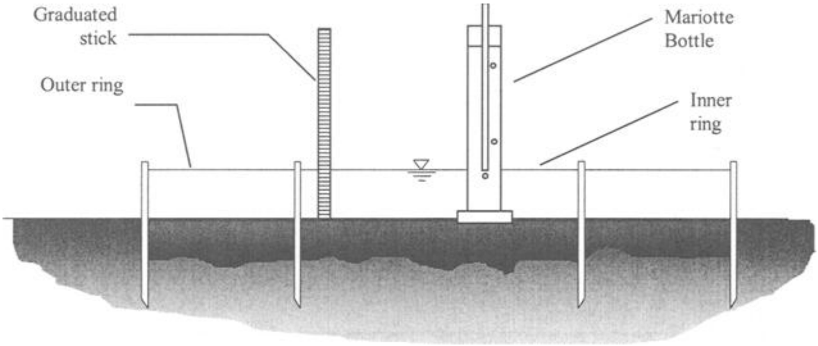

Figure 1 - *Schematic layout of an Open Double Ring Infiltrometer (ODRI)*

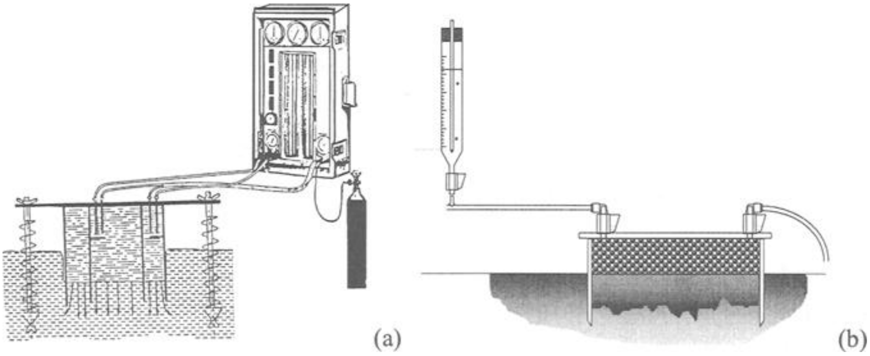

Figure 2 - *Schematic layouts of SDRI 2 with pressurized burettes and of SSRI 1 with Mariotte bottle and confined soil surface*

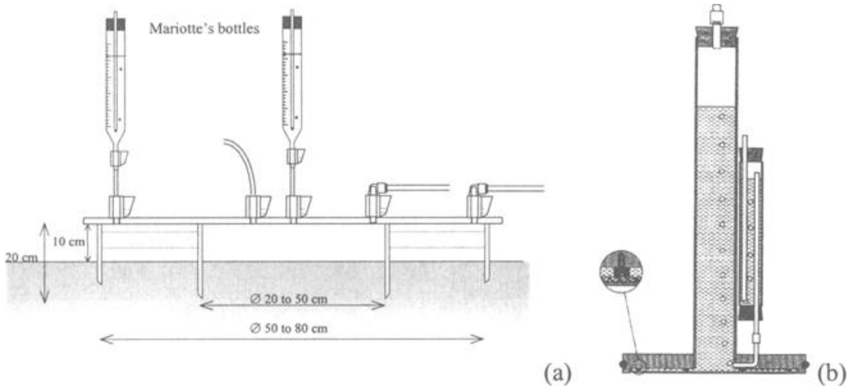

Figure 3 - *Schematic layouts of SDRI 1 with Mariotte bottle and an unconfined soil surface, and of a Mariotte-tube-based Tension infiltrometer (right)*

Test-failure criteria

Surface field-tests are subject to various problems that can be due to soil conditions or to the testing device. Table 2 and Figure 4 summarize the main problems that can be encountered during tests with ring infiltrometers (Cazaux, 1998).

Table 2 - *Main sources of uncertainty associated with open and sealed ring infiltrometers (after Cazaux, 1998)*

<table>
<tr><th>Open-Ring Infiltrometer</th><th>Sealed-Ring Infiltrometer</th></tr>
<tr><td colspan="2">▪ Side-wall leakage
▪ Temperature effects on fluid and devices
▪ Divergent flow under the ring due to too high permeability or excessive infiltration time compared to device capacity
▪ Swelling and alteration of soil surface
▪ Glazing of infiltration surface
▪ Diffusion process of non-aqueous liquid
▪ Fingering of flow</td></tr>
<tr><td>▪ Evaporation can exceed infiltration rate
▪ Infiltration rate too low for volume controller capacity</td><td>▪ Hydraulic head too high, led to ring rising
▪ Hydraulic fracturing due to excessive hydraulic head</td></tr>
</table>

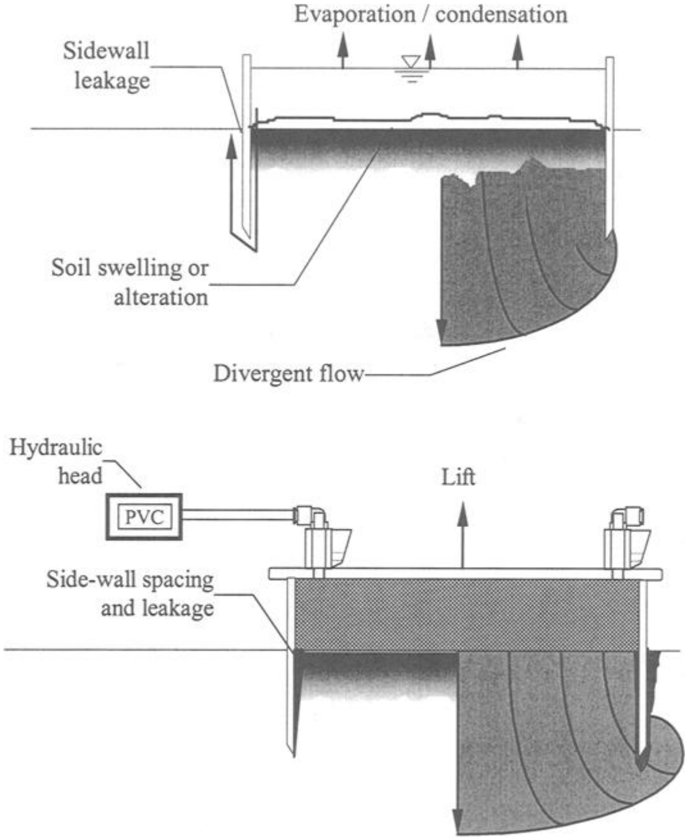

Figure 4 - *Schematic layout of problems associated with ring-infiltrometer methods (after Cazaux, 1998)*

Borehole field-test methods

The three main types of borehole techniques for measuring hydraulic conductivity correspond to three different hydraulic situations: constant head, variable or falling head, and pressure pulse. Hydraulic conductivity tests are done in deep boreholes for characterizing natural geological subgrades, or in shallow (<1 m) wells for checking thin and compacted soil layers. For deep and shallow tests, the following nomenclature and standards were used: *CHBT*, for Constant Hydraulic-head Borehole Technique (ASTM D4630-96, AFNOR X30-424); *VHBT*, for Variable Hydraulic-head Borehole Technique (ASTM D5912, AFNOR X30-423); and *PPBT*, for Pressure hydraulic-Pulse Borehole Technique (ASTM D4631, AFNOR X30-425). The three techniques were compared in this research. All the holes were core-drilled with water and then dry-reamed to a larger diameter (1 cm larger) to remove altered and moistened material around the borehole wall. This test procedure allowed preserving soil integrity before testing. In a last stage the testing cavities were scarified with a cylindrical steel brush to re-open soil porosity partially closed by coring process. In this condition, the saturation of the soil around cavity wall was not modified.

Laboratory test methods

Three types of laboratory-hydraulic conductivity testing are commonly used for assessing hydraulic conductivity of a clay soil. The following nomenclature is taken from (mainly North American) scientific references: *FWP*, for flexible-wall permeameters; *RWP*, for rigid-wall permeameters; and *ODP*, for oedopermeameters or consolidation cells. Schematic diagrams of the testing methods are given in Figure 5. Table 3 summarizes the three types of laboratory test, used in our research with various types of specimen geometry.

The flexible-wall permeameter (FWP) confines the specimen to be tested with porous disks and end caps on top and bottom, and with a latex membrane on the sides (DIN 18130, BS 1377, ASTM 5084, prISO 17313, CSN 72-1020, etc.).

The rigid-wall permeameter (RWP) consists of a rigid, generally cylindrical, metal or PVC tube containing the test specimen. Various types of RWP include compaction-mold permeameters and sampling-tube permeameters (DIN 18130-1).

An oedo-permeameter (ODP) is a consolidation cell with a loading cap that consists of a rigid tube containing the specimen to be tested. It is useful only for fine-grained soils that contain no gravel or coarse sand (Daniel, 1994, DIN 18130).

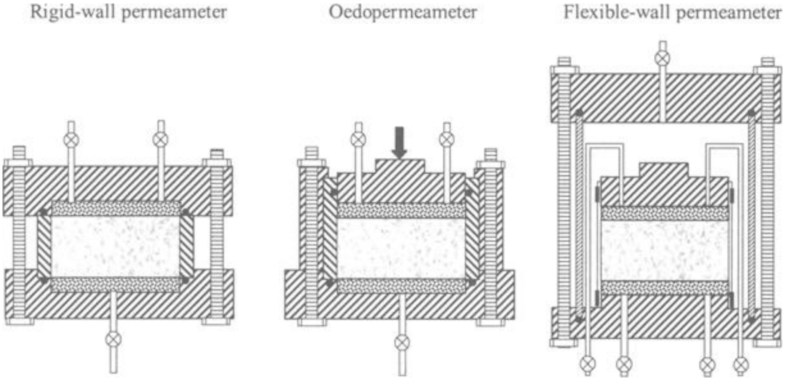

Figure 5 - *Schematic diagrams of rigid wall permeameter, oedo-permeameter, and flexible-wall permeameter*

Table 3 - *Dimensions of the different permeameters (FWP, ODP, and RWP).*

Sites A and B		
Apparatus	Diameter (mm)	Height (mm)
FWP 1	70	70
FWP 2	35	40
FWP 3	50	100
FWP 4	100	100
FWP 5	38	38
FWP 6	50	80
ODP 1	70	25
ODP 2	65	25
ODP 3	70	25
ODP 4	100	40
ODP 5	50	25
RWP 1	100	40
RWP 2	100	100

Site C		
Apparatus	Diameter (mm)	Height (mm)
FWP 1	35	40
FWP 2	38	40
FWP 3	70	70
ODP 1	50	25
ODP 2	50	20
RWP 1	100	40

Soil characteristics

Site A

This test pad was created of a sand-bentonite mixture (fine factory-treated sand with 5% of Na-activated bentonite) as two 50-cm layers, compacted with a vibrating roller. Characteristics of the clean sand are summarized in Table 4. About 30 samples were taken with thin-wall tubes (150-mm diameter) near the hydraulic conductivity-test sites, in order to determine the average values of the weight moisture content w, the initial dry weight γ_d, and the bentonite content $B_{\%}$ (in percentage of dry soil weight). The following average values were determined:

$$w = 12.3\% \qquad \gamma_d = 17.3\ \text{kN/m}^3 \qquad B_{\%} = 4.5$$

Site B

The test pad was built up of clayey silt in three layers of 30 cm each, compacted with a sheep-foot roller. The main characteristics of the silt are summarized in Table 4. Samples were taken with thin-wall tubes (150-mm diameter) near the test sites in order to determine the average values of the moisture content w and the initial dry weight γ_d:

$$w = 19.5\ \% \qquad \gamma_d = 16.9\ \text{kN/m}^3$$

Table 4 - *Soil characteristics on site A and B*

	Site A (less bentonite)	Site B
Average methylene blue value (g/100g)	1.7	2.6
Optimum moisture content, w_{OPT} (%)	11.0	15.0
Optimum dry density, $\gamma_{d\,OPN}$ (kN/m^3)	18.2	17.5
Maximum grain size (mm)	2	0.2
Grain size fraction < 80 μm (% of weight)	35	91
Grain size fraction < 2 μm (% of weight)	<1	10

Site C

Site C is a natural kaolinite-clay deposit. The tests were done on the current quarry floor. Spatial variations in the sand content are marked by color contrasts from white to purple brown, easily seen in the quarry. Considering this heterogeneity, it was impossible to select a relatively homogeneous area for setting up all the devices, and the tests were done on a varying lithology that made it difficult to compare the devices. At the end, the site was mostly used for comparing borehole methods. A 2-m-thick purple level that was tested is located between 1.5 and 3.5 m depth. All the holes were core-drilled with water, and the samples were then sent to various laboratories. These laboratory samples were then immediately cut to a smaller diameter to remove about 1 to 2 cm of altered and moistened material due to core-drilling process. This test procedure allowed preserving field soil saturation before testing. Before testing, the laboratories identified the physical sample characteristics, such as natural moisture content w_n, volumetric dry weight γ_d, degree of saturation S, Methylene blue value VB, and Atterberg plasticity index IP. The results are summarized in Table 5 and show that the material was not initially saturated.

Table 5 - *Soil characteristics of clay-quarry samples at various depths.*

Depth (m)	w_n (%)	γ_d (kN/m^3)	S (%)	VB (g/100g)	IP
2.10	12.0-14.6	17.9-18.8	74.0 -77.0	2.5	53
2.40	10.9-17.1	18.1-18.9	67.0 - 94.0	3.1	56
2.60	10.2-12.1	19.2	67.3	2.1	44
2.75	12.1	19.2	63.0	-	-

Field Testing

Site A

The results obtained on the sand-bentonite pad (Site A) show two groups that correspond to the two equipment types: open-ring infiltrometers (ODRI 1, 2) with a hydraulic conductivity close to 1×10^{-9} m/s and sealed infiltrometers (SSRI 1, 1a, SDRI 1, 2, 3) with a hydraulic conductivity around $3\text{-}4\times10^{-11}$ m/s (Table 6). Dispersion of the results is of the order of 1 or 2 degrees of magnitude, with the exception of the tension (disc) infiltrometer that gave a much higher hydraulic conductivity than the other devices. These differences between open and sealed rings confirm the hypotheses on the application domains of open-type infiltrometers. Figure 6 shows the relationship between hydraulic-conductivity results and bentonite content, i.e. the bentonite content only slightly influences hydraulic conductivity. The minimum bentonite content was initially chosen to avoid discrepancy between results allowing to compare testing devices.

Table 6 - *Field hydraulic conductivity on the Site A test pad (logarithmic scale).*

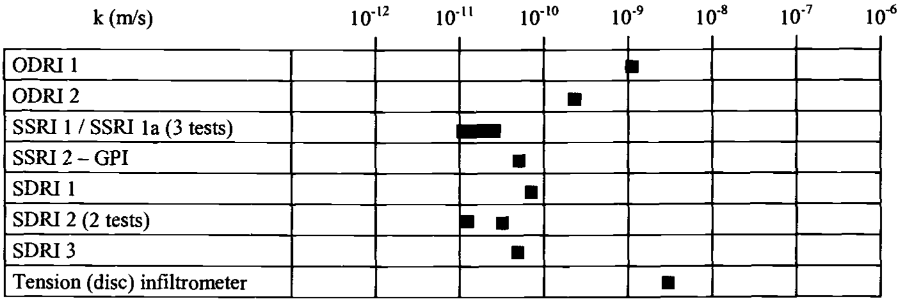

Site B

On the compacted silt pad of Site B, the data dispersion is lower than on Site A, except for the tension infiltrometer (Table 7). The difference between open and closed rings was partially confirmed, with the exception of ODRI 2 that gave a hydraulic conductivity value close to the average one obtained with the other devices.

In addition, we determined the moisture-content profile at the end of a test and for each ring, in order to verify whether confining the wet surface of a potentially swelling material influences the flow pattern. The profiles show that, in the case of the sand-bentonite of Site A, most of the tests led to a much higher final moisture content than the saturated moisture content (Figure 7). The tests done with open rings (ODRI 1 and 2) have almost identical final profiles, but much higher maximum moisture contents, than closed rings except for SDRI 1.

Table 7 - *Field hydraulic conductivity on the Site B test pad (logarithmic scale)*

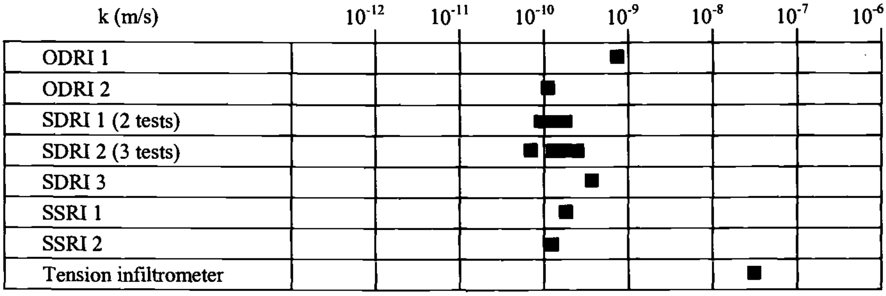

Both tests done with SSRI 1 show maximum moisture contents close to the theoretical saturation value. These results are confirmed by the same analyses made on silt (Figure 8). As a consequence, confinement of the soil surface (as for SSRI 1), even without additional loading, helps in maintaining the integrity of the soil during infiltration. This is of value with sand-bentonite, as the confinement of the wetting surface avoid over-saturation due to swelling of the bentonite. For silt, confinement of the surface in certain cases allowed to avoid the unsticking of the lamination produced under compaction. This phenomenon is particularly valid for Site B where soil was compacted to 3 to 4% over the optimum moisture value.

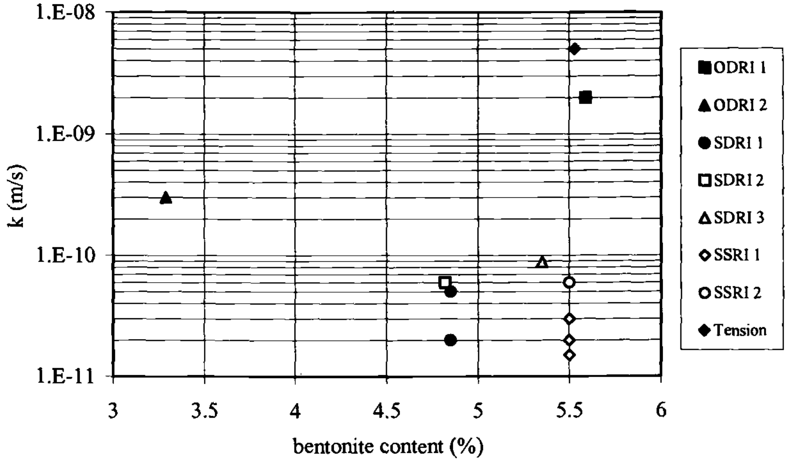

Figure 6 - *Field hydraulic conductivity vs. bentonite content on the Site A test pad.*

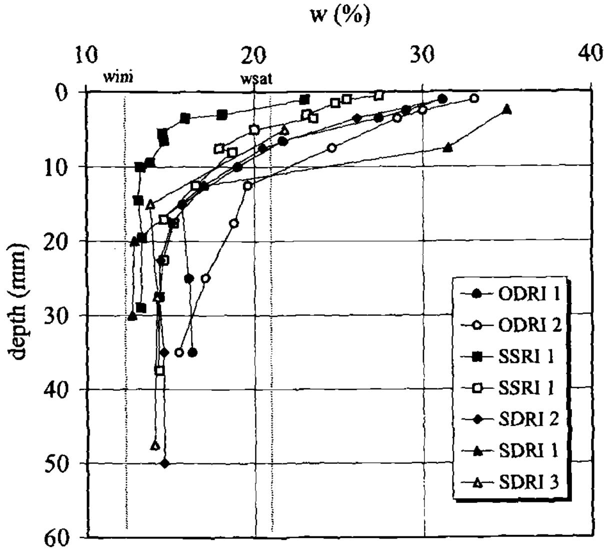

Figure 7 - *Soil-moisture profiles at the end of the infiltrometer test on Site A.*

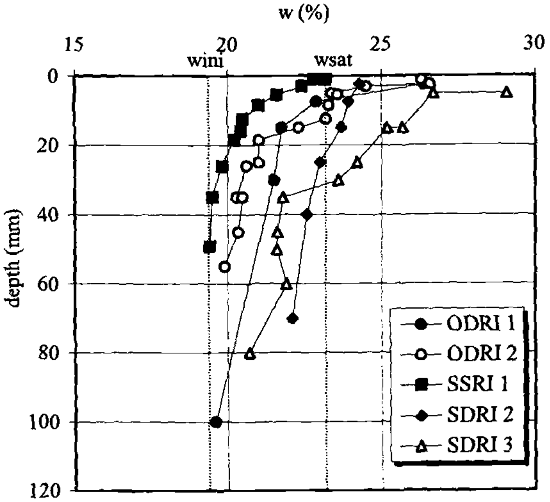

Figure 8 - *Soil-moisture profiles at the end of the infiltrometer test on Site B.*

Site C

Surface testing - Because of the local conditions, only five surface devices were used on the site. Most of the results fall between 2.10^{-10} and 1.10^{-9} m/s; the tested material and its spatial heterogeneity cause part of this dispersal. The exception is ODRI 1, where the used technique explains the difference, as it cannot measure this order of hydraulic conductivity. One test with SSRI 1 was done in a zone containing coarser sand, which gave a hydraulic conductivity of about 1.10^{-8} m/s; the increase in hydraulic head at the end of the test led to the hydraulic fracturing of this sand.

Table 8 - *Surface field hydraulic conductivity on the Site C test pad (logarithmic scale).*

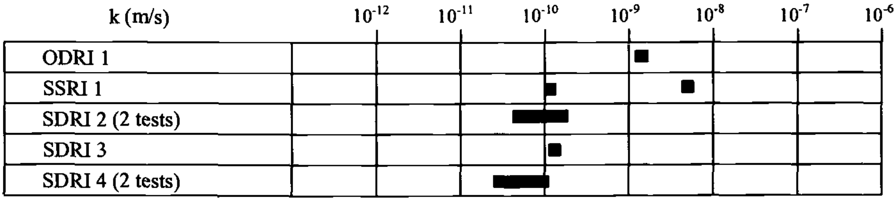

Borehole testing- Nine methods were tested in the program. Borehole diameters are identical but testing cavity height and test procedures vary depending of the operators. Table 9 summarizes the results. They show good homogeneity and the average value is around 2.10^{-10} to 1.10^{-9} m/s. The relative dispersion of results probably is more related to soil heterogeneities than to the testing methods. Even for testing zones located in the same level, visual observation showed a well-marked spatial heterogeneity. However, two techniques gave results more than one order of magnitude outside the average: pressure-pulse test PPBM 1 made in the same borehole as the constant-head test CHMB 2, probably caused by a wrong estimation of the compressibility of the system. The second erroneous result comes from the CHBM 3 permeameter that overestimated the hydraulic conductivity (3 tests made). As for tension infiltrometer for surface testing, interpretation of the test results assumed unsaturated conditions (Elrick and Reynolds, 1994). All other techniques gave comparable results.

Table 9 - *Hydraulic conductivity values in boreholes on Site C (logarithmic scale).*

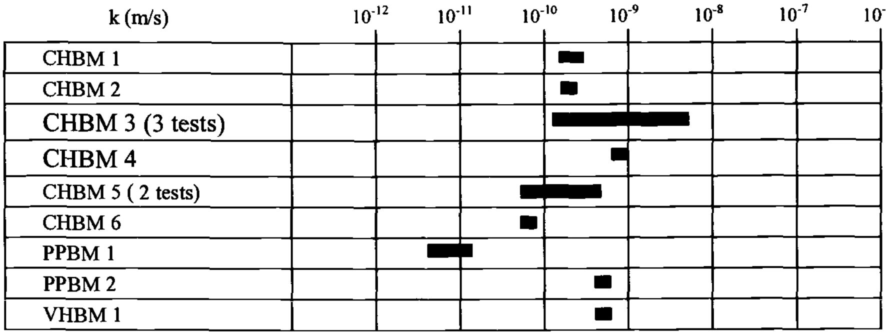

Laboratory tests

Site A

Results obtained on the sand-bentonite mixture are relatively homogeneous with an average k_L (laboratory) value of 3.10^{-11} m/s. There is no notable variation of the values according to the type of equipment used (Figure 9). Despite the high swelling potential of this material due to its bentonite content, the *ODP* gave hydraulic conductivity values only very slightly above than those obtained with other techniques. This surprisingly small difference may be due to the relatively high bentonite content.

Figure 10 shows the hydraulic conductivity versus sample geometry in terms of their diameter and height. The hydraulic conductivity is clearly influenced by sample geometry, confirming the observations and modeling by Benson *et al.* (1994). The scale effect is small and the threshold minimum specimen diameter and height are about 50 mm. Below this value, the hydraulic conductivity much more varies. Benson (1994) had noticed limit diameters of the order of 300 mm in certain materials. Our results must be related to the nature of the sand itself, which has a uniform and fine grain-size distribution. Furthermore, any joints caused by compaction remained localized to the liner lifts and no interfaces due to clod flattening were seen.

Figure 11 shows the relationship between hydraulic conductivity and bentonite content: the influence of bentonite is clearer than for field tests. This can be explained by a scale effect since the larger the (field) sample area, the more homogeneous will be the average bentonite content. The much smaller laboratory samples may include quite variable bentonite volumes that will affect the hydraulic conductivity.

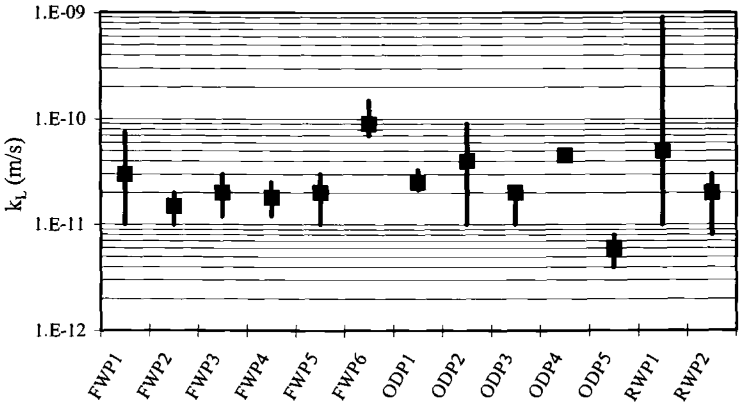

Figure 9 - *Laboratory hydraulic conductivity of the sand-bentonite mixture (black squares indicate the average k_L value).*

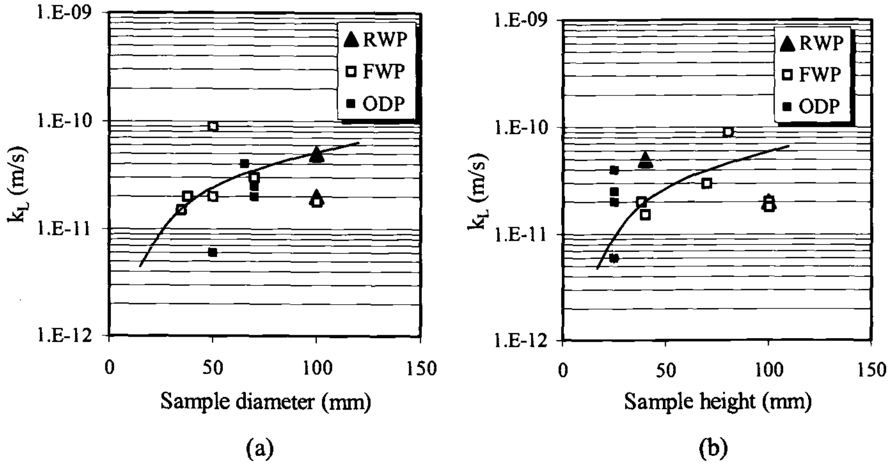

Figure 10 - *Laboratory hydraulic conductivity vs. (a) sample diameter and (b) height for the sand-bentonite mixture.*

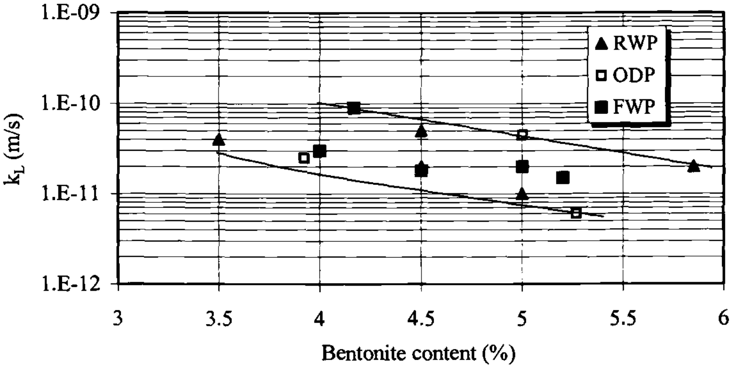

Figure 11 - *Laboratory hydraulic conductivity against bentonite content*

Site B

The results obtained on silt are scattered over two orders of magnitude (Figure 12), but without a visible variation due to the type of device. This dispersion is not explained by the tested sample geometry (Figure 13), but may be due to the sample sizes that are too small in terms of the discontinuities included in the material. This can be explained by sampling that did not protect the initial sample geometry (compression in the sampling tube for example). Compaction discontinuities are very common and large (decimeters).

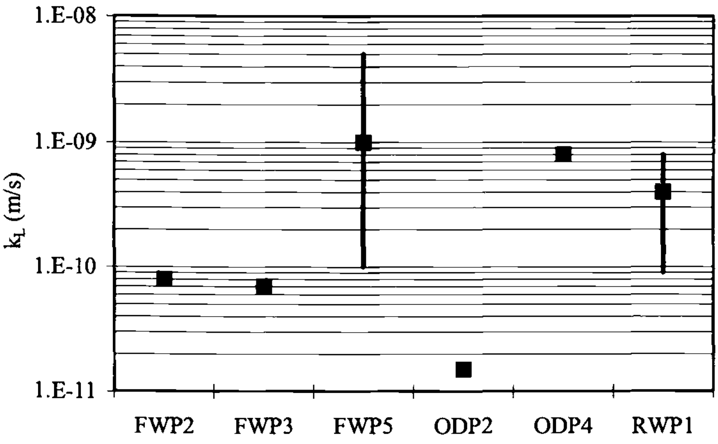

Figure 12 - *Laboratory hydraulic conductivity on Site B silt (black squares indicate the average k_L value)*

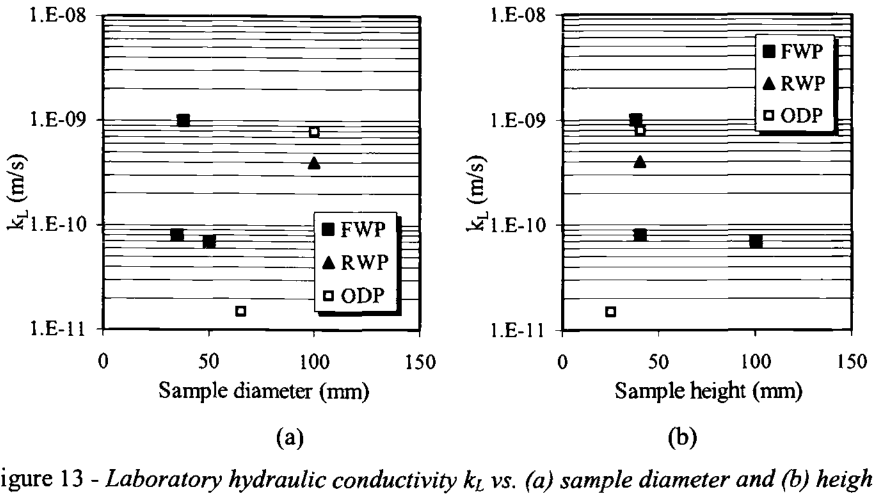

(a) (b)

Figure 13 - *Laboratory hydraulic conductivity k_L vs. (a) sample diameter and (b) height on Site B silt*

Site C

The results, obtained on borehole-core samples, show a mostly homogeneous hydraulic conductivity with an average value close to 2×10^{-11}/s (Figure 14). The exception are the RWP 1 values (2 tests), but this divergence from the average may be explained by the larger diameter of these samples (100 mm against 35-70 mm for the other samples). Figure 15 shows the hydraulic conductivity against infiltration-surface area (a) and height/diameter ratio (b). The scale effect is clear for the infiltration-surface area but the relationship does not show any discontinuity. In the graph of k_L versus height/diameter ratio (Figure 15b), a discontinuity can be observed around 0.5.

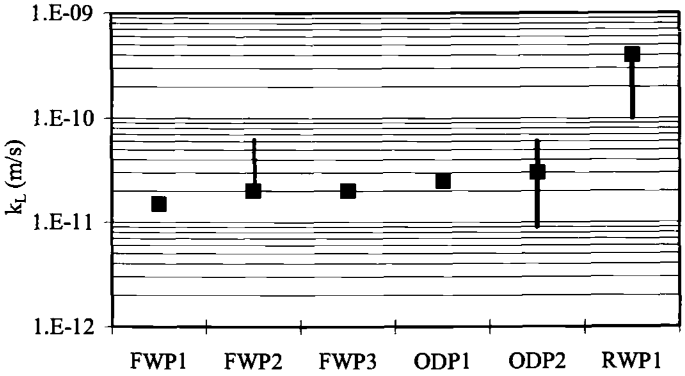

Figure 14 - *Laboratory hydraulic conductivity on Site C clay (black squares indicate the average k_L value)*

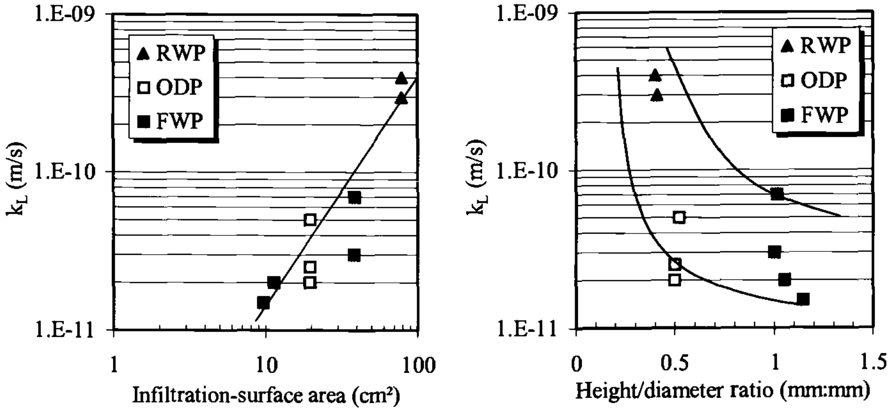

(a) (b)

Figure 15 - *Laboratory hydraulic conductivity against (a) sample surface-area and (b) height/diameter ratio on Site C clay.*

Discussion

Plotting the tests results from test pads A and B against to the sample diameter, we notice that the scale-effect is obvious for both soils (Figure 16). This last point confirms that the specimens tested in the laboratory, even if they gave coherent results, were not representative of the test pads as they were too small. The critical diameter is situated near 100 mm. Comparison of laboratory and field tests on boreholes is more difficult; an additional problem is that hydraulic conductivity is not measured in the same direction: one-dimensional vertical flow in the lab and radial horizontal flow in the borehole. To assess the scale effect, it is best to compare hydraulic-conductivity values with the infiltration surface area; comparison with diameter is not significant of flow geometry for radial flow. Figure 17 shows a good relationship between k and surface area.

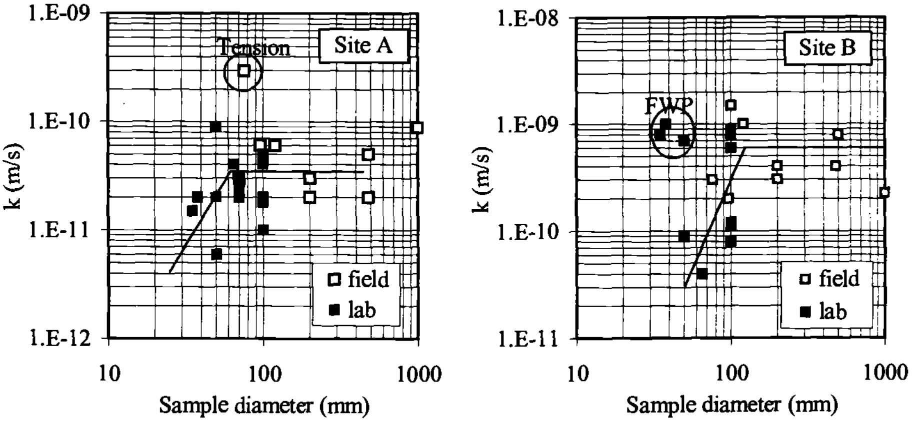

(a) (b)

Figure 16 - *Field and laboratory hydraulic conductivity against sample diameter for (a) sand-bentonite mixture (Site A) and (b) silt (site B).*

Conclusions and recommendations

Field measurements of hydraulic conductivity with a ring infiltrometer are influenced by the surface condition of the tested soil (glazing), the surface area of infiltration (minimum diameter), and the used technique. When carrying out such hydraulic-conductivity tests, the sample scale of the *in situ* tested soil will influence the representativeness of a test for a given soil. Though there is no set rule for the optimum diameter of an infiltrometer in soil testing, our experiments established that rings should have a diameter of at least 200 mm. It seems that this minimum size helps in accounting for most of the macropores in a natural soil or a compacted fine soil. In addition, we observed that the confining of a field-tested surface, even through simple contact, helps in preventing most swelling and over-saturation.

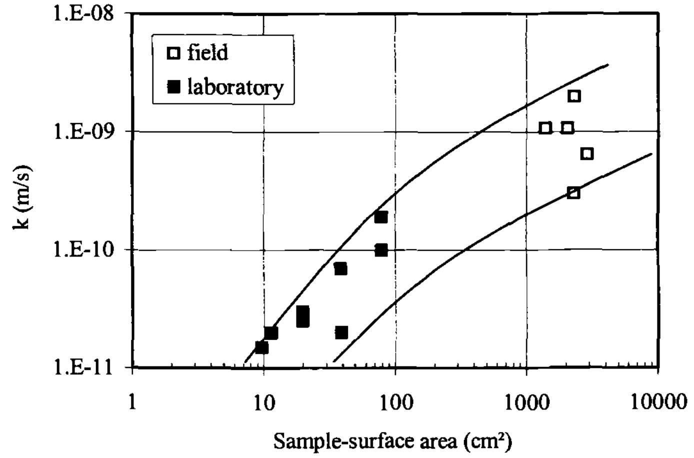

Figure 17 - *Field and laboratory hydraulic conductivity against sample surface area on Site C clay.*

Table 10 summarizes the advantages and disadvantages of the devices used in this research; for each, we mention the measured hydraulic conductivity range, the installation conditions (from difficult – to very easy ++), the analysis method, the scale, the need for confining or not of the infiltration surface, the sensitivity of the device to temperature, and the sensitivity to evaporation or dilatation.

Among borehole techniques, the constant-head injection method appears to be the simplest to interpret when hydraulic conductivity is low. A sufficiently long injection time (several hours generally) provides good estimates of the hydraulic conductivity. Variable head tests, though relatively reliable, for a hydraulic conductivity below 1.10^{-9} m/s require very long test times to obtain a significant level fall. Replacing the pipe by a smaller-diameter tube could be a satisfactory alternative for accelerating the fall of the water. Pressure-pulse tests tend to underestimate the value of the hydraulic conductivity.

The three types of test (surface field, borehole field and laboratory) and their interpretation methods were developed to answer the specific problems of water flow in fine-grained soil. Such devices are subject to different procedures that render the comparison of results difficult. Certain observations were nevertheless possible from a careful comparison of the results obtained on field-test pads. The borehole tests, the laboratory tests and the surface tests, with some exceptions, produced comparable results. The comparison between the three testing types is more risky, and observed differences in hydraulic conductivity reach several orders of magnitude. In conclusion, it seems necessary that all these techniques be developed with a unique procedure, which only standardization can provide.

Table 10 - *Summary table of surface field-testing methods (in italics, technique not tested in this research program).*

Device	*k range (m/s)*	*Ease of installation (– difficult to ++ very easy*	*Analysis*	*Scale*	*Confining*	*Testing time*	*Cost*	*Sensitivity*
OSRI	$\geq 1.10^{-7}$	*++*	*Darcy's Law*	*–*	*No*	*+*	*++*	*– (Evaporation)*
ODRI 1	$\geq 1.10^{-8}$	++	Darcy's Law	–	No	+	++	– (Evaporation)
ODRI 2	$\geq 1.10^{-8}$	++	Darcy's Law	–	No	+	++	– (Evaporation)
SDRI 2	$1.10^{-11} \leq \leq 1.10^{-8}$	–	Darcy's Law	–	No	+	+	+ (Dilatation)
SSRI 1	$1.10^{-11} \leq \leq 1.10^{-8}$	+	Darcy's Law	+	Porous disc	+	+	+ (Dilatation)
SSRI 2	$1.10^{-11} \leq \leq 1.10^{-8}$	+	Fallow et al. (1994)	–	No	++	+	– (Plexiglass)
Tension	$1.10^{-11} \leq \leq 1.10^{-8}$	+	White et al. (1992)	+	Nylon disc	++	+	– (Plexiglass)
SDRI 1	$1.10^{-10} \leq \leq 1.10^{-8}$	0	Darcy's Law	+	No	+	+	+
SDRI 3	$1.10^{-10} \leq \leq 1.10^{-8}$	--	Darcy's Law	++	No	+	--	+

References

Benson, C.H., Hardianto, F.S. and Motan, E.S., 1994, Representative specimen size for hydraulic conductivity assessment of compacted soil liners, *in* Hydraulic Conductivity and Waste Contaminant Transport in soil, D.E. Daniel and S.J. Trautwein, Eds., American Society for Testing and Materials, ASTM STP 1142, pp 3-29.

Benson, C.H., Gunter, J.A., Boutwell, G.P., Trautwein, S.J. and Berzanskis, P.H., 1997, Comparison of four methods to assess hydraulic conductivity, *Journal of Geotechnical and Geoenvironmental Engineering,* Vol. 123, pp. 929-937.

Bredehoeft J.D., and Papadopulos, S.S., 1980, A method for determining the hydraulic properties of tight formations, *Water Resources Research*, Vol. 16, pp. 233-238.

Cazaux, D., 1998, Mesure et contrôle in situ de la perméabilité des matériaux utilisés dans les dispositifs d'étanchéité pour la protection de l'environnement, Etat de l'art et Développements, *Doctoral thesis, Institut National des Sciences Appliquées de Lyon,* 335 p.

Chapuis, R.P, and Sabourin, L., 1989, Effects of installation of piezometers and wells on groundwater characteristics and measurements, *Canadian Geotechnical Journal*, Vol. 26, pp. 604-613.

Daniel D.E., 1994, State of the art: laboratory hydraulic conductivity tests for saturated soils, *in* Hydraulic Conductivity and Waste Contaminant Transport in soil, D.E. Daniel and S.J. Trautwein, Eds., American Society for Testing and Materials, ASTM STP 1142, pp 30-78.

Day, S.R. and Daniel, D.E., 1985, Field permeability test for clay liners, *in* Hydraulic barriers in soil and rock, A.I. Johnson, R.K. Frobel, N.J. Cavalli, and C.B. Petterson, Eds., American Society for Testing and Materials, ASTM STP 874, pp. 276-288.

Dunn, R.J. and Palmer, B.S., 1994, lessons learned from the application of standard test methods for field and laboratory hydraulic conductivity measurement, *in* Hydraulic Conductivity and Waste Contaminant Transport in soil, D.E. Daniel and S.J. Trautwein, Eds., American Society for Testing and Materials, ASTM STP 1142, pp. 335-352.

Elrick, D.E. and Reynolds, W.D., 1992, Infiltration from constant-head well permeameters and infiltrometers, *in* Advances in Measurement of Soil Physical Properties: Bringing theory into practice, *Soil Science Society of America Journal*, Special Publication No. 30, pp. 1-24

Fallow, D.J., Elrick, D.E., Reynolds, W.D., Baumgartner, N. and Parkin, G.W., 1994, Field measurement of hydraulic conductivity in slowly permeable materials using early-time infiltration measurements in unsaturated media, *in* Hydraulic Conductivity and Waste Contaminant Transport in soil, D.E. Daniel and S.J. Trautwein, Eds., *American Society for Testing and Materials*, ASTM STP 1142, pp. 375-389.

Herzog, B.L. and Morse, W.J, 1990, Comparison of slug test methodologies for determining hydraulic conductivity in fine grained sediments, *in* Ground Water and Vadose Zone Monitoring, D.M. Nielsen and A.I. Johnson Eds., American Society for Testing and Materials, ASTM STP 1053, pp. 152-164.

Johnson, G.W., Crumley, W.S. and Boutwell, G.P., 1994, Field verification of clay liner hydraulic conductivity, *in* Hydraulic Conductivity and Waste Contaminant Transport in soil, D.E. Daniel and S.J. Trautwein, Eds., American Society for Testing and Materials, ASTM STP 1142, pp. 226-245.

Neuzil, C.E., 1982, On conducting the modified slug test in tight formations, *Water Resources Research*, Vol. 18, pp. 439-441.

Picornell, M. and Guerra, A., 1992, A comparison of field and laboratory measurements of hydraulic measurements of hydraulic conductivity, *in* Current Practices in Ground Water and Vadose Zone Investigations, D.M. Nielsen and M.N. Sara Editors, American Society for Testing and Materials, Philadelphia, ASTM STP 1118, pp. 346-361.

Purdy, S.D. and Ramey, T.V., 1995, "Comparison of Hydraulic Conductivity test methods", *5th International Landfill Symposium, Sardinia 95,* Cagliari, Italy, Proceedings, pp 321-329.

Sai, J.O. and Anderson, D.C., 1991, State-of-the-art field hydraulic conductivity testing of compacted soils, *Cincinnati: EPA*, Report No EPA/600/2-91/022, 85 p.

Trautwein, S.J. and Boutwell, G.P., 1994, In situ hydraulic conductivity tests for compacted liners and caps, *in* Hydraulic Conductivity and Waste Contaminant Transport in soil, D.E. Daniel and S.J. Trautwein, Eds., American Society for Testing and Materials, ASTM STP 1142, pp 184-223.

White, I., Sully, M.J. and Perroux, K.M., 1992, Measurement of Surface-soil hydraulic properties: disk permeameters, tension infiltrometers, and other techniques, *Advances in Measurement of Soil Physical Properties: Bringing theory into practice*, Soil Science Society of America, Special Publication No. 30, pp. 69-103.

Tarek Abichou[1], Craig H. Benson[2], Michael Friend[3], and Xiaodong Wang[2]

Hydraulic Conductivity of a Fractured Aquitard

Reference: Abichou, T., Benson, C., Friend, M., and Wang, X., **"Hydraulic Conductivity of a Fractured Aquitard,"** *Evaluation and Remediation of Low Permeability and Dual Porosity Environments, ASTM STP 1415,* M. N. Sara and L. G. Everett, Eds., ASTM International, West Conshohocken, PA, 2002.

Abstract: An investigation was conducted to characterize the hydraulic conductivity of a shallow clay till aquitard over which a municipal solid waste landfill was being sited. Hydraulic conductivity tests were conducted in the laboratory on specimens removed from the till in thin-wall sampling tubes (71 mm diameter) and as large hand-carved blocks (460 mm diameter). Field hydraulic conductivity was measured using a slug test. Tests on specimens from the sampling tubes indicated that the hydraulic conductivity of the till was very low (10^{-9} to 10^{-8} cm/s). The slug test and tests on large blocks containing fractures yielded much higher hydraulic conductivities, on the order of 10^{-6} cm/s. This difference in hydraulic conductivities is attributed to fractures, which were evident in the block specimens. Testing of the block specimens at higher overburden stresses showed that the hydraulic conductivity decreased by one order of magnitude as the overburden stress increased from 35 kPa to 175 kPa, apparently due to closure of the fractures.

Key Words: aquitard, field hydraulic conductivity, scale effects, fractures, fractured till, glacial till, block sample, sampling tube, slug test, fractured till

Introduction

Field-testing is often recommended to determine the in situ hydraulic conductivity of glacial tills, especially those containing fractures (Hendry 1982, D'Astous et al. 1989, Bradbury and Muldoon 1990, Bruner and Lutenegger 1994). This recommendation is made because a sufficiently large volume of undisturbed soil needs to be tested to ensure that it contains a representative distribution of macroscopic features (fractures, seams, fissures, slickensides, etc.) that can control the hydraulic conductivity. However, field tests can be misleading if disturbance occurs or a smear zone develops when the testing equipment is installed (D'Astous et al. 1989). Field tests also do not address how hydraulic conductivity can be affected by an increase in overburden stress. The

---

[1] Assistant Professor, Dept. of Civil and Environ. Engr., Florida State University – Florida A&M University, 2525 Pottsdamer street, Tallahassee, FL 32310, abichou@eng.fsu.edu;
[2] Professor, GeoEngineering Lab. Manager, Dept. of Civil and Environ. Engr., University of Wisconsin-Madison, 1415 Engineering Drive, Madison, WI, 53706, benson@engr.wisc.edu, wang1@cae.wisc.edu;
[3] Senior Project Engineer, Andrews Environmental Engineering, 215 West Washington St., Pontiac, IL 61674.

significance of stress is important for landfill applications, since filling of a landfill can result in a substantial increase in the effective stress in the underlying soils. An alternative approach is to conduct laboratory tests on large undisturbed specimens of till obtained from test pits over a range of potential stresses. If the specimens are large enough, they can contain a representative network of macroscopic features and have hydraulic conductivity representative of the field condition.

This paper describes an investigation that was conducted to characterize the hydraulic conductivity of a glacial clay till aquitard above which a landfill was being sited. Field and laboratory measurements of hydraulic conductivity were performed. The laboratory measurements were conducted on small specimens obtained with thin-walled sampling tubes and on large specimens collected by hand-carving large blocks of undisturbed till. The laboratory tests on the large specimens were conducted over the range of effective stresses expected as the landfill was filled.

Background

Clayey till is common in the upper midwestern United States and Canada, and frequently it is fractured or contains other macroscopic features (Herzog and Morse 1984, Keller et al. 1986, Bosscher and Connell 1988, Sims et al. 1996). These features can control the field hydraulic conductivity of clay tills because they act as preferential flow paths (Hendry 1982, Bosscher et al. 1988, D'Astous et al. 1989). Natural mechanisms that cause fractures include vertical stress release due to overburden reduction during thinning of the glacial ice sheet, horizontal tensile stresses resulting from isostatic crustal rebound, freeze-thaw cycling, and desiccation (Boulton 1976, Hendry 1982, Bosscher and Connell 1988, Kirkaldie and Talbot 1992, Albrecht and Benson 2001).

The presence of fractures and other macroscopic features generally results in hydraulic conductivity that is scale dependent. That is, the hydraulic conductivity generally increases as the volume of soil that is tested increases since a greater number of preferential flow paths become engaged in flow (Bradbury and Muldoon 1990, Benson et al. 1994). For fractured tills, hydraulic conductivities operative at field scale tend to be on the order of 10^{-7} to 10^{-4} cm/s, whereas the hydraulic conductivity at the scale of the clay matrix tends to be in the range of 10^{-9} to 10^{-8} cm/s. Examples of scale dependence throughout the midwest are illustrated in case histories described by Keller et al. (1986), Bradbury and Muldoon (1990), McKay et al. (1993), and Bruner and Lutenegger (1994).

Keller et al. (1986) compared field and laboratory measurements of the hydraulic conductivity of a fractured clay till. Oedometer tests conducted in the laboratory on specimens 64 mm in diameter yielded an average hydraulic conductivity of 3.5×10^{-9} cm/s. None of the oedometer specimens contained fractures. In situ hydraulic conductivities measured using slug tests were 5×10^{-7} cm/s, on average. Keller et al. attributed the difference in hydraulic conductivities to the lack of a representative distribution of fractures in the small oedometer specimens.

Bradbury and Muldoon (1990) conducted hydraulic conductivity tests on specimens of tills obtained using thin-walled sampling tubes and compared these hydraulic conductivities to those obtained from slug tests on tills from eastern and central Wisconsin. The laboratory tests were conducted using rigid-wall and flexible-wall permeameters. Bradbury and Muldoon report that the small laboratory specimens from the tills in eastern Wisconsin had hydraulic conductivities near 10^{-8} cm/s. For the tills in central Wisconsin, the hydraulic conductivity of the small laboratory specimens ranged from 10^{-8} to 10^{-7} cm/s. The field hydraulic conductivities were typically 10^{-6} cm/s for the tills from eastern Wisconsin and ranged from 6×10^{-6} to 2×10^{-4} cm/s for the tills from central Wisconsin. Thus, for both tills, hydraulic conductivities of the small laboratory specimens were two or more orders of magnitude lower than the hydraulic conductivities measured in the field using slug tests.

McKay et al. (1993) measured the field hydraulic conductivity of a glacial clay till by measuring the rate of infiltration into large trenches. The field hydraulic conductivities ranged from 1×10^{-5} to 3×10^{-5} cm/s. Undisturbed specimens tested in the laboratory using oedometers had an average hydraulic conductivity of 2×10^{-8} cm/s. McKay et al. report that the field hydraulic conductivity was much higher than that obtained from the laboratory oedometer tests because the small laboratory specimens did not contain fractures.

Bruner and Lutenegger (1994) compared hydraulic conductivities measured in the field and laboratory on a glacial clay till in Iowa. Bailer tests and pumping tests were used for the field measurements. Laboratory tests were conducted in flexible-wall permeameters on specimens having a diameter of 70 mm and a height of 50 mm. Specimens used for the laboratory tests were collected in thin-wall sampling tubes. The geometric mean hydraulic conductivity of the laboratory specimens was 1×10^{-8} cm/s, whereas the field hydraulic conductivity ranged between 3×10^{-6} cm/s and 2×10^{-5} cm/s.

Stress is also an important issue affecting the hydraulic conductivity of fractured clay tills. Sims et al. (1996) conducted laboratory hydraulic conductivity tests at different effective stresses on fractured specimens of till collected near Sarnia, Ontario. Sims et al. found that the hydraulic conductivity of some specimens decreased more than two orders of magnitude as the effective stress was increased from 10 to 320 kPa.

Site Characteristics

The geology of the site consists of unconsolidated Pleistocene deposits of glacial origin overlaying Pennsylvanian bedrock. The Pleistocene deposits consist of a 0.6-m-thick layer of Richland loess above a layer of Yorkville till 4-m thick, on average. Beneath the Yorkville till is a lacustrine deposit formed by an ancient lake. Yorkville till is a clayey gray till that includes small dolomite pebbles. Hairline fractures, root holes, gypsum crystals, and silt and sand lenses also exist in the till. The liquid limit of the till varies between 25 and 52 (39 on average) and the plasticity index varies from 11 to 27 (20 on average). Yorkville till is described as a silty clay with low to moderate plasticity, is assigned a designation of CL in the Unified Soil Classification System.

Methods

Thin-Wall Sampling Tubes

Forty-one samples were collected from the aquitard in thin-wall sampling tubes (71 mm diameter). The samples were extruded in the laboratory using a hydraulic ram and then trimmed into specimens having an aspect ratio of 1. Twenty-four specimens were permeated in the vertical direction. Seventeen specimens were trimmed for hydraulic conductivity testing in the horizontal direction. All of the laboratory tests were conducted using flexible-wall permeameters in accordance with ASTM Standard Test Methods for Measurement of Hydraulic Conductivity of Saturated Porous Materials Using a Flexible Wall Permeameter (D 5084). The effective stress during these tests ranged from 27 to 45 kPa.

Block Samples

Large undisturbed block samples were removed from the base of an excavation in the aquitard using a procedure described in Othman et al. (1994). The samples were trimmed into polyvinyl chloride (PVC) trimming rings having a beveled cutting shoe at the base. A synopsis of the sampling procedure is as follows. A trimming ring with a diameter of 610 mm was placed on the surface of the soil in the base of the excavation. A trench was then excavated around the area of the ring using a shovel. This resulted in a cylindrical block of soil with a diameter approximately 200 mm larger than that of the trimming ring (Figure 1). The soil remaining around the ring was then trimmed away using hand tools until the ring could be slid downward over the soil being sampled with modest effort. When the ring was filled with soil, the sample was separated from the underlying soil using a shovel. Excess soil was then trimmed away from the upper and lower surfaces and plastic sheeting was affixed to prevent the sample from desiccating. The sample was shipped to the laboratory on a reinforced pallet. Three samples were removed from the aquitard using this technique.

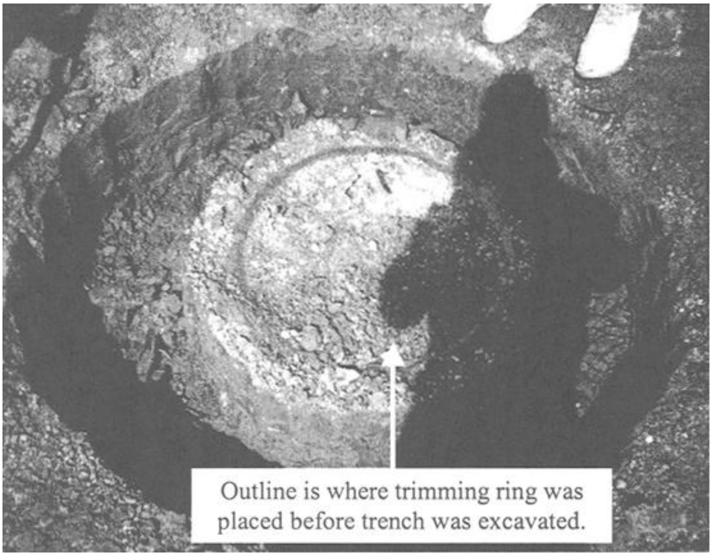
Outline is where trimming ring was placed before trench was excavated.

Figure 1 -- *Trench excavated around block of soil.*

In the laboratory, the samples were removed from their rings and trimmed into specimens having a diameter of 460 mm and height of 300 mm. The specimens were placed in a large-scale flexible-wall permeameter and tested using procedures described in ASTM D 5084. The specimens were initially consolidated to an average effective stress of 27 kPa under a backpressure of 275 kPa and then permeated under a hydraulic gradient of 14. This gradient was selected as a compromise between two competing objectives: simulating field conditions and reasonable testing time; however, the gradient that was used is consistent with the guidelines in ASTM D 5084.

After the termination criteria in D 5084 were met, two of the specimens were tested again at higher effective stresses. The hydraulic gradient was removed and the cell pressure was increased to induce consolidation. The inflow and outflow burettes were monitored to determine when consolidation was complete. These specimens were then permeated again at the higher effective stress until the termination criteria were satisfied. Hydraulic conductivity tests were conducted on these specimens at effective stresses of 27, 96, and 172 kPa.

Slug Test

Only one slug test was conducted because only one of the piezometers previously installed in the till contained water when the testing program was conducted. The slug test was performed in accordance with procedures described in ASTM Standard Test Method for Field Procedure for Instantaneous Change in Head (Slug) Tests for Determining Hydraulic Properties of Aquifiers (D 4044). A slug of water 1-m long was manually removed from the well. The rate at which the water level returned to equilibrium was measured using a pressure transducer and a datalogger.

The Bouwer and Rice method (Bouwer and Rice 1976, Bouwer 1989) was used to calculate the hydraulic conductivity of the till from the water level data, i.e.

$$K = \frac{r_c^2 \ln\left(\frac{R_e}{r_w}\right)}{2L} \frac{1}{t} \ln\left(\frac{H_o}{H_t}\right) \qquad (1)$$

where r_c is the radius of the casing (25 mm), r_w is the radius of the hole or filter pack (45 mm), R_e is the effective radius (400 mm) that was empirically estimated using the well geometry in accordance with Bower and Rice (1976), L is the length of the filter pack (2.1 m), H_0 is initial head, and H_t is the head at time t. Herzog (1994) shows that the Bouwer and Rice method yields hydraulic conductivities similar to those computed with other common methods when applied to data from less conductive units, such as unfractured and fractured tills. The hydraulic conductivity computed from the slug test was 1.5×10^{-6} cm/s.

Results and Discussion

Summary of Hydraulic Conductivities

A summary of the hydraulic conductivities measured during the study is in Table 1. Horizontal (K_h) and vertical hydraulic (K_v) conductivities are reported for the specimens collected in sampling tubes since tests were conducted on these specimens in both directions. Only vertical hydraulic conductivities were measured on the block specimens.

Table 1 -- *Summary of hydraulic conductivities.*

Type of Sample or Test	K_v (cm/s)	Effective Stress (kPa)	K_h (cm/s)	Effective Stress (kPa)
Thin-Wall Tube	$6.4\text{x}10^{-8}$	27	$1.5\text{x}10^{-9}$	38
	$1.0\text{x}10^{-8}$	27	$2.0\text{x}10^{-8}$	40
	$3.6\text{x}10^{-9}$	27	$2.6\text{x}10^{-9}$	38
	$3.9\text{x}10^{-9}$	45	$3.7\text{x}10^{-9}$	45
	$1.5\text{x}10^{-8}$	38	$1.2\text{x}10^{-8}$	38
	$9.1\text{x}10^{-9}$	52	$1.2\text{x}10^{-9}$	52
	$2.4\text{x}10^{-9}$	38	$3.3\text{x}10^{-9}$	38
	$7.8\text{x}10^{-9}$	45	$3.5\text{x}10^{-8}$	45
	$1.6\text{x}10^{-8}$	38	$4.2\text{x}10^{-9}$	38
	$8.2\text{x}10^{-9}$	41	$4.6\text{x}10^{-9}$	41
	$7.7\text{x}10^{-9}$	38	$3.8\text{x}10^{-9}$	38
	$2.6\text{x}10^{-8}$	41	$1.5\text{x}10^{-9}$	41
	$6.4\text{x}10^{-8}$	52	$2.0\text{x}10^{-8}$	52
	$1.0\text{x}10^{-8}$	41	$2.6\text{x}10^{-9}$	41
	$3.9\text{x}10^{-8}$	41	$4.5\text{x}10^{-6}$	41
	$1.5\text{x}10^{-8}$	48	$4.6\text{x}10^{-9}$	48
	$3.7\text{x}10^{-9}$	41	$3.8\text{x}10^{-9}$	41
	$1.2\text{x}10^{-8}$	41	--	--
	$1.2\text{x}10^{-9}$	41	--	--
	$3.3\text{x}10^{-9}$	48	--	--
	$3.5\text{x}10^{-8}$	48	--	--
	$4.2\text{x}10^{-9}$	43	--	--
	$3.6\text{x}10^{-9}$	41	--	--
	$9.1\text{x}10^{-9}$	45	--	--
Block (B1)	$6.2\text{x}10^{-9}$	27	--	--
Block (B2)	$9.5\text{x}10^{-7}$	27	--	--
Block (B3)	$8.3\text{x}10^{-7}$	27	--	--
Block (B1)	$5.5\text{x}10^{-9}$	96	--	--
Block (B3)	$2.0\text{x}10^{-7}$	96	--	--
Block (B1)	$4.8\text{x}10^{-9}$	172	--	--
Block (B3)	$5.4\text{x}10^{-8}$	172	--	--
Slug	--	--	$1.5\text{x}10^{-6*}$	36

*This hydraulic conductivity is representative of an overall hydraulic conductivity since flow to the screen is three-dimensional

The hydraulic conductivity measured using the slug test is listed in the column for horizontal hydraulic conductivities, although this hydraulic conductivity is more representative of an overall hydraulic conductivity since flow induced by the slug test is three dimensional.

Hydraulic conductivities of the small specimens from sampling tubes ranged from 1.2 x 10^{-9} to 6.4 x 10^{-8} cm/s, regardless of orientation, with the exception of one "outlier" (K_h=4.5x10^{-6} cm/s). The geometric mean vertical and horizontal hydraulic conductivities of the small specimens were 8.5x10^{-9} cm/s and 6.9x10^{-9} cm/s, respectively. When tested at an effective stress (27 kPa) comparable to the in situ stress (≈35 kPa at depth of the slug test), hydraulic conductivity of the block specimens varied from 6.2 x 10^{-9} to 9.5 x 10^{-7} cm/s. Blocks B2 and B3 had similar hydraulic conductivities (9.5 x 10^{-7} cm/s and 8.3 x 10^{-7} cm/s). Block B1 (K_v=6.2x10^{-9} cm/s) was approximately two orders of magnitude less permeable than Blocks B2 and B3.

Influence of Scale

The influence of scale is depicted in Figure 2, which shows hydraulic conductivity vs. volume of soil that was permeated. Volume associated with the slug test was assumed to equal the volume of the slug divided by the porosity, which was assumed to equal 0.3. The other volumes were computed from the geometry of the test specimens.

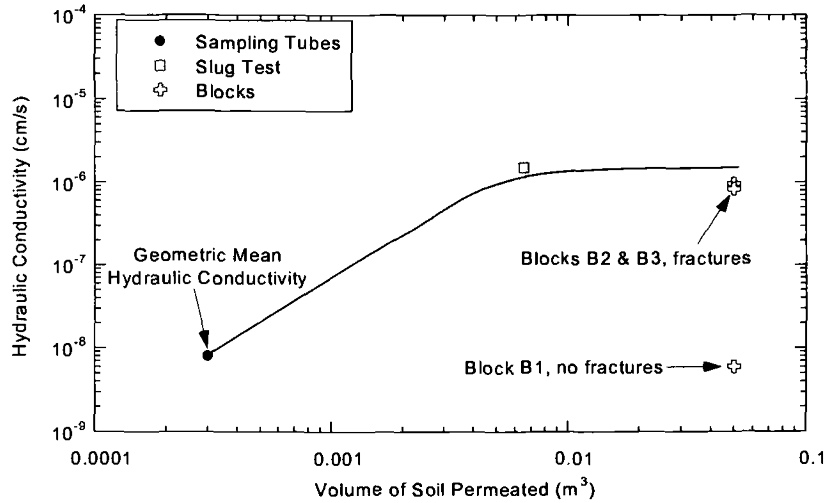

Figure 2 -- *Hydraulic conductivity as a function of volume of soil tested.*

The trend in Figure 2 indicates that testing methods that permeate a larger volume of soil tend to yield hydraulic conductivities representative of the fracture network operative in the field. Hydraulic conductivities of the small specimens from sampling tubes are 200 times lower, on average, than the in situ hydraulic conductivity measured using the slug test. The only small specimen with hydraulic conductivity comparable to that obtained from the slug test is the specimen considered to be an 'outlier'. The hydraulic conductivities of blocks B2 and B3 are comparable (within a factor of two) to the in situ hydraulic conductivity from the slug test (1.5 x 10^{-6} cm/s).

Blocks B2 and B3 and the slug test apparently captured a similar network of fractures. Inspection of Blocks B2 and B3 showed that they contained fine fractures that were coated with a tan oxide. In contrast, Block B1 contained no fractures, and had hydraulic conductivity (6.1×10^{-9} cm/s) comparable the geometric mean hydraulic conductivity of the specimens collected in tubes ($K_v=8.5\times10^{-9}$ cm/s). Apparently the fractures controlled flow in the field and in Blocks B2 and B3, whereas the micropores in the till matrix controlled flow in Block B1 and in the small specimens collected in sampling tubes.

The low hydraulic conductivity of Block B1 indicates that large-scale tests will not always yield hydraulic conductivity representative of the in situ condition. A low hydraulic conductivity might also have been obtained with the slug test if the screen been installed at another location. Thus, to obtain representative hydraulic conductivities, tests should be made at several locations to increase the likelihood of adequately capturing the fractures that control flow at field scale.

Influence of Overburden Stress

The effect of overburden pressure on hydraulic conductivity of the till is shown in Figure 3. For the slug test, the effective stress was assumed to equal that at mid-depth of the aquitard where the screen was placed (≈35 kPa). The hydraulic conductivity of block B3 (with fractures) is particularly sensitive to effective stress, decreasing by a factor of 15 as the stress is increased by 145 kPa. This sensitivity to effective stress is typical of specimens containing fractures (Othman and Benson 1993, Sims et al. 1996, Albrecht and Benson 2001). As the effective stress increases, the primary network of pores conducting flow switches from the fracture network to the microscale pores in the matrix, and consequently the hydraulic conductivity decreases significantly.

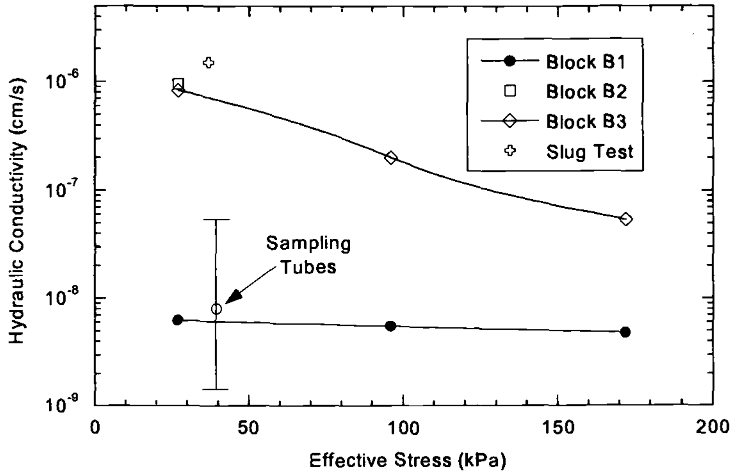

Figure 3 -- *Hydraulic conductivity of till at different effective stresses.*

In contrast, the hydraulic conductivity of Block B1, which did not have fractures, is much less sensitive to effective stress (a 1.3 fold reduction over a 145 kPa increment in stress). The primary network of pores conducting flow in this specimen is comprised of the microscale pores in the matrix. These pores do become smaller as the specimen is consolidated to higher effective stress. However, the hydraulic conductivity does not change dramatically because the network of pores is not switching from fractures to micropores.

Practical Applications

A comparison of hydraulic conductivities for this aquitard and those from other similar sites is shown in Table 2. The in situ hydraulic conductivities fall between 5×10^{-7} and 2×10^{-4} cm/s, and have a geometric mean of 7×10^{-6} cm/s. The matrix hydraulic conductivities fall between 3.5×10^{-9} and 5×10^{-7} cm/s. Their geometric mean is 2×10^{-8} cm/s.

Table 2 -- *Hydraulic conductivities of fractured clay till aquitards.*

Reference	Location	In Situ Hydraulic Conductivity (cm/s)	Matrix Hydraulic Conductivity (cm/s)
Hendry (1982)	Southern Alberta	2.2×10^{-5} to 5.1×10^{-5}	1×10^{-8}
Keller et al. (1986)	Saskatoon, Saskatchewan	5×10^{-7}	3.5×10^{-9}
McKay et al. (1986)	Sarnia, Ontario	1×10^{-5} to 3×10^{-5}	5.0×10^{-7}
Bradbury & Muldoon (1990) – Eastern Wisconsin	Eastern Wisconsin	1×10^{-6}	1×10^{-8}
Bradbury & Muldoon (1990) – Central Wisconsin	Central Wisconsin	6×10^{-6} to 2×10^{-4}	1×10^{-8} to 1×10^{-7}
Bruner & Lutenegger (1994)	Linn County, Iowa	3×10^{-6} to 2×10^{-5}	1.2×10^{-8}
This Study	Central Illinois	8×10^{-7} to 2×10^{-6}	6.9×10^{-9} (h) 8.5×10^{-9} (v)

Note: h = horizontal, v = vertical.

The geometric mean in situ hydraulic conductivity (7×10^{-6} cm/s) can be used as a preliminary estimate of the hydraulic conductivity of fractured clay till aquitards in the upper midwestern United States and Canada. The geometric mean matrix hydraulic conductivity can be used as a preliminary estimate of the hydraulic conductivity of similar aquitards after significant stress ($\geq$ 200 kPa) has been added that closes the fractures. These estimates can be used for preliminary calculations (e.g., in feasibility studies), but should not be used as a substitute for field and laboratory testing.

The data shown in Figure 3 for Block B3 are shown in Figure 4 in terms of the ratio of the hydraulic conductivity at a given effective stress ($K_{\sigma'}$) to the hydraulic conductivity at an effective stress of 20 kPa (K_{20}). An effective stress of 20 kPa was selected for normalization because it corresponds approximately to a depth of 1 m. Data for fractured clays from Othman and Benson (1993), Sims et al. (1996), and Albrecht and Benson (2001) are also shown in Figure 4. All of these data are for clays from midwestern sites.

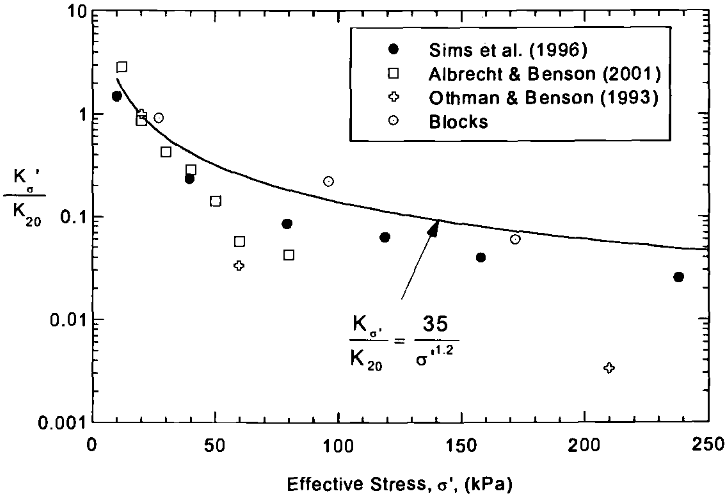

Figure 4 -- *Relative hydraulic conductivity as a function of effective stress.*

The data follow a similar trend, indicating that increasing the effective stress has a similar effect on the hydraulic conductivity of fractured clays. The line in Figure 4 corresponds to:

$$\frac{K_{\sigma'}}{K_{20}} = \frac{35}{\sigma'^{1.2}} \qquad (2)$$

where σ' is in kPa. Equation 2 can be used to provide a conservative estimate of the hydraulic conductivity of fractured aquitards as the overburden pressure is increased. However, as mentioned previously, site-specific testing ultimately should be conducted to more accurately define the relationship between hydraulic conductivity and effective stress.

Summary and Conclusions

An investigation was conducted to characterize the in situ hydraulic conductivity of a shallow glacial till aquitard and to assess how the hydraulic conductivity would change as additional stress was imposed by a landfill. A slug test was used to measure the in situ hydraulic conductivity of the aquitard at the existing effective stress. Laboratory measurements of hydraulic conductivity at the existing effective stress and higher effective stresses were conducted on undisturbed specimens obtained using thin-wall sampling tubes (71 mm diameter) and as large hand-carved blocks (460 mm diameter). The blocks were collected from an excavation in the aquitard.

Results of the hydraulic conductivity tests show that the hydraulic conductivity is a function of the scale of the tests. The slug test and tests on two of the large blocks yielded similar hydraulic conductivities ($\approx 10^{-6}$ cm/s). Much lower hydraulic conductivities ($\approx 10^{-9}$ to 10^{-8} cm/s) were obtained from tests on the small specimens removed in thin-walled sampling tubes and one of the blocks. The difference in these hydraulic conductivities is attributed to different networks of pores controlling flow. Hydraulic conductivities near 10^{-6} cm/s were obtained when flow occurred primarily through the fractures, which were adequately represented in the slug test and in two of the block specimens. Much lower hydraulic conductivities were obtained when flow occurred only in micro pores (i.e., in the specimens obtained with sampling tubes and one of the blocks). Tests conducted at higher effective stresses showed that the hydraulic conductivity of the fractured till is sensitive to the effective stress, and decreases as the effective stress increases due to closure of fractures. The hydraulic conductivity of specimens without fractures was less sensitive to effective stress because the primary pathways for flow in these specimens did not change as the effective stress increased.

Comparison of the data from the site in this study with data from similar midwestern sites indicates that a reasonable preliminary estimate of the hydraulic conductivity of near surface fractured clay till aquitards in the upper midwestern United States and Canada is 7×10^{-6} cm/s. Decreases in hydraulic conductivity caused by increases in effective stress can also be estimated using an empirical equation based on the data collected from this site and for other clays. However, these estimates of hydraulic conductivity should only be used for preliminary assessments such as feasibility studies. Site-specific testing should be conducted prior to final design.

References

Albrecht, B. and Benson, C., 2001, "Effect of Desiccation on Compacted Natural Clays," *Journal of Geotechnical and Geoenvironmental Engineering*," Vol. 127, No. 1, pp. 67-75.

Benson, C., Hardianto, F., and Motan, E., 1994, "Representative Specimen Size for Hydraulic Conductivity of Compacted Soil Liners," *Hydraulic Conductivity and Waste Contaminant Transport in Soils, STP 1142*, American Society for Testing and Materials, West Conshohocken, PA, S. Trautwein and D. Daniel, Eds., pp. 3-29.

Bosscher, P. and Connell, D., 1988, "Measurement and Analysis of Jointing Properties in Fine-Grained Soils," *Journal of Geotechnical Engineering*, Vol. 114, No. 7, pp. 826-843.

Bosscher, P., Bruxvoort, G., and Kelley, T., 1988, "Influence of Discontinuous Joints on Permeability," *Journal of Geotechnical Engineering*, Vol. 114, No. 7, pp. 826-843.

Boulton, G., 1976, "The Development of Geotechnical Properties in Glacial Tills," *The Royal Society of Canada, Special Publication No. 12*, Ottawa, pp. 292-303.

Bouwer, H., 1989, "The Bouwer and Rice Slug Test-an Update," *Groundwater*, Vol. 27, No. 3, pp. 304-309.

Bouwer, H. and Rice, R., 1976, "A Slug Test for Determining Hydraulic Conductivity of Unconfined Aquifers with Completely or Partially Penetrating Wells," *Water Resources Research*, Vol. 12, No. 3, pp. 423-428.

Bradbury, K., and Muldoon, M., 1990, "Hydraulic Conductivity Determinations in Unlithified Glacial and Fluvial Materials," *Groundwater and Vadose Zone Monitoring, STP 1053*, American Society for Testing and Materials, West Conshohocken, PA,, D. Nielsen and A. Johnson, Eds., pp. 138-151.

Bruner, D., and Lutenegger, J., 1994, "Measurement of Saturated Hydraulic Conductivity in Fine-Grained Glacial Tills in Iowa: Comparison of In situ and Laboratory Methods," *Hydraulic Conductivity and Waste Contaminant Transport in Soil, STP 1142*, American Society for Testing and Materials, West Conshohocken, PA,, S. Trautwein and D. Daniel, Eds., pp. 255-265.

D'Astous, A., Ruland, W., Bruce, J., Cherry, J., and Gillham, R., 1989, "Fracture Effects in the Shallow Groundwater Zone in Weathered Sarnia-Area Clay," *Canadian Geotechnical Journal*, No. 26, pp. 43-56.

Hendry, M., 1982, "Hydraulic Conductivity of a Glacial Till in Alberta," *Ground Water*, Vol. 20, No. 2. pp. 162-169.

Herzog, B. and Morse, W., 1984, "A Comparison of Laboratory and Field Measured Values of Hydraulic Conductivity at a Waste Disposal Site," *Proceeding 7th Annual Madison Waste Conference*, Dept. of Engineering Prof. Development, University of Wisconsin-Madison, pp. 30-52.

Herzog, B., 1994, "Slug Tests for Determining Hydraulic Conductivity of Natural Geologic Deposits," *Hydraulic Conductivity and Waste Contaminant Transport in Soil, STP 1142*, American Society for Testing and Materials, West Conshohocken, PA,, S. Trautwein and D. Daniel, Eds., pp. 95-110.

Keller, C., Van der Kamp, G., and Cherry, J., 1986, "Fracture Permeability and Groundwater Flow in a Clayey Till near Saskatoon, Saskatchewan," *Canadian Geotechnical Journal*, Vol. 23, pp. 229-240.

Kirkaldie, L., and Talbot J., 1992, "The Effects of Soil Joints on Soil Mass Properties," *Bulletin of the Association of Engineering Geologists*, Vol. 29, No. 4, pp. 415-420.

McKay, L., Cherry, J., and Gillham, R., 1993, "Field Experiments in a Fractured Clay Till-Hydraulic Conductivity and Fracture Aperture," *Water Resources Research*, Vol. 29, No. 4, pp. 1149-1162.

Othman, M. and Benson, C., 1993, "Effect of Freeze-Thaw on the Hydraulic Conductivity of Three Compacted Clays from Wisconsin," *Transportation Research Record*, No. 1369, pp. 118-125.

Othman, M., Benson, C., Chamberlain, E., and Zimmie, T., 1994, Laboratory Testing to Evaluate Changes in Hydraulic Conductivity Caused by Freeze-Thaw: State-of-the-Art, *Hydraulic Conductivity and Waste Containment Transport in Soils, STP 1142*, American Society for Testing and Materials, West Conshohocken, PA, S. Trautwein and D. Daniel, eds., pp. 227-254.

Sims, J., Elsworth, D., and Cherry, J., 1996, Stress Dependent Flow Through Fractured Clay Till: A Laboratory Study, *Canadian Geotechnical Journal*, Vol. 33, pp. 449-457.

J. M. Hubbell,[1] E. D. Mattson,[1] J. B. Sisson,[2] and D.L. McElroy[3]

Water Potential Response in Fractured Basalt from Infiltration Events

---

Reference: Hubbell, J.M., Mattson, E. D., Sisson, J. B., and McElroy, D.L., **"Water Potential Response in a Fractured Basalt From Infiltration Events,"** *Evaluation and Remediation of Low Permeability and Dual Porosity Environments, ASTM STP 1415,* M.N. Sara and L.G. Everett, Eds., ASTM International, West Conshohocken, PA, 2002.

Abstract: The detection of moisture movement in the vadose zone beneath hazardous waste disposal sites is important for monitoring and predicting contaminant transport in the subsurface. This study was conducted to determine if moisture movement could be detected from natural water infiltration in a dual porosity, fractured basalt at the Idaho National Engineering and Environmental Laboratory (INEEL). Episodic infiltration events were determined by examining long-term water potential over three and a half years. Water potential measurements were collected from 2 to over 30 m below land surface. Instruments were placed in both fractured and unfractured basalt media. Water potential measurements were within the tensiometric range, from approximately +100 to -250 cm of water. Typically, water potentials within the fractured basalt exhibited a near steady-state unit-gradient downward flux. However, episodic snowmelt infiltration events at land surface produced detectable changes in water potentials at depths to 15.5 m, in some cases within a few days of the infiltration events. Smaller infiltration events were difficult to distinguish due to fluctuations in water potential resulting from changes in barometric pressure. Water potential responses in boreholes varied both temporally and spatially during episodic infiltration events indicating preferential flow pathways through the fractured basalt. The results of this study indicate that water potential measurements can be used to detect and monitor deep infiltration events at waste disposal sites using tensiometers.

KEYWORDS: water potential, vadose zone, fractured rock, tensiometer, infiltration, percolation, recharge

---

[1] Advisory Scientist, [2] Consulting Scientist, and [3] Staff Scientist, Geosciences Research Department, Idaho National Engineering and Environmental Laboratory, PO Box 1625, Idaho Falls, ID 83415-2107. E-mail: **jmh@inel.gov**

Waste flow and contaminant transport in unsaturated fractured rock has become a topic of concern in the past few decades. Vadose zone monitoring at disposal sites is gaining acceptance as a means to avoid the high cost of remediating contaminants in aquifers (Beckman 1999). Nevertheless, long-standing attempts to monitor the vadose zone at disposal sites have been hampered by difficulties involving suitable instrumentation, suitable installation techniques, interpretation of results and spatial variability. Natural infiltration through fractured rock in deep vadose zone profiles is difficult to detect and quantify. Instrumentation has not been available to detect and characterize water movement in the deep subsurface accurately. Most vadose monitoring instruments evolved from agronomy/soil physics. As such, they were developed for shallow applications (less than 2 meters). Fortunately, instruments are now being adapted for deeper applications for monitoring at disposal sites including some at fractured rock sites (Evans and Nicholson 1986, Montazer 1987, Hubbell and Sisson 1998).

Infiltration through fractured vadose zones is more difficult to quantify than infiltration through porous media vadose zones. Although water can move through either the fractures or the material's matrix, most researchers agree that localized partially saturated infiltration through a fractured vadose zone occurs primarily through the fractures and not through the porous medium (Walton et al. 1989; Nativ et al. 1995; Dunnivant et. al. 1998). Infiltration at arid sites is highly variable and is dependent on both local topography and plant cover (Gee and Hillel 1988). Field and modeling results from a large-scale infiltration test conducted at Idaho National Engineering and Environmental Laboratory (INEEL) suggest that infiltration is primarily through the fractures, with the matrix flow having a minor influence on the advance of the wetting front (Magnuson 1995). The matrix storage may act to slow moisture flow within the vadose zone by retaining fluids within slower flow paths (Wang and Narasimham 1985). The infiltration pathway becomes more difficult to conceptualize when the fractures become filled with porous material.

The present paper examines long-term measurement of water potentials in fractured-dual porosity basalt and sedimentary interbeds to document episodic and steady state infiltration, as well as estimating moisture flux. Flux is defined as the mass of material moving through a cross-sectional area in a unit time period.

Methods and Materials

Water potential data from advanced tensiometers were used to monitor and estimate the amount of infiltration at these sites. Water potential measurements were collected from depths of 3 to 31 m below land surface (bls) in three boreholes at two locations. Tensiometers were placed in both fractured and unfractured basalt.

The advanced tensiometer consists of a porous cup connected to a permanently installed outer casing by a specially machined adapter. The porous cup/adapter contains about 60 mL of fluid. The porous cup material is a one bar air entry ceramic with either a high or low flow rate (Soil Moisture Equipment Corp., Santa Barbara, CA). A small volume of water is added inside the outer casing to fill the porous cup to a level above the adapter. The adapter is designed to connect to a pressure transducer immediately above the adapter thereby minimizing the amount of entrapped air and the height of the standing water column. A ±15 psid transducer (Electronic Engineering Innovations, Las Cruces, NM) was connected to a data logger (Tumult Gadara, Las Cruces, NM or 21X by Campbell Scientific, Inc., Logan, UT) and sampled hourly. This design and method of construction allows the measurement of water potential at depths exceeding those capable by conventional tensiometers. The advanced tensiometer represents an improvement in measuring the water potential within the soil profile for determining flux (Hubbell and Sisson 1998). This tensiometer design offers three advantages.

(a) The net water potential measured is almost the entire tensiometric range since the hydrostatic pressure head effect of the water column is removed from the potential measurement.
(b) Water potential measurements can be obtained at any depth, since the pressure transducer is located adjacent to the porous cup.
(c) The pressure transducer can be serviced or replaced, as required for most applications.

Three boreholes were instrumented with multiple advanced tensiometers to a depth of 31 m and monitored for periods of 1.5 to 3.5 years. The boreholes are located in southeast Idaho, on the Eastern Snake River Plain, which is a 90 km by 70 km arcuate plain (1500 m elevation) surrounded by mountains that rise to about 3300 m (Figure 1). The geology at the boreholes is comprised of a thin (2 to 4 m) cover of loess underlain by quaternary volcanics (olivine basalt). The basalt profile is intercalated with thin sedimentary interbeds at the INEEL location. Depth to groundwater is approximately 170 m at the INEEL and 40 m at the two boreholes in Idaho Falls.

Borehole 76-5 is located at the INEEL, a Department of Energy site 80 km west of Idaho Falls (Figure 1). This site receives about 250 mm/y precipitation (Clawson et. al 1989). The average summer temperature is 28 °C and the average winter temperature is -0.6 °C. The surface topography is located on a slight rise at about 1520 m elevation and is sparsely covered with crested wheat grass (*Agropyron cristatum*). Borehole 76-5 was air rotary drilled with a 14.9 cm diameter bit to a depth of 73 m to sample deep interbeds and subsequently instrumented with tensiometers from a depth of 6.7 to 31.4 m bls. The locations of the instruments, backfill, and more detailed lithology of the instrumented depths for borehole 76-5 is presented in Figure 2. The geology is obtained from the geologic core description, television (TV), and geophysical logs.

The borehole annular space was back-filled using the method described by Cassel and Klute (1986). A 0.3 to 1 meter layer of dry silt loam (-400 cm water potential from surficial sediments) was placed adjacent to the porous cups on the tensiometers to hydraulically connect the porous cup to the fractured basalt. Granular bentonite layers 0.3 m thick were placed above and beneath the loam-filled monitoring depths to isolate the monitoring intervals. Coarse sand, with a mean diameter of 2.8 mm, filled the remainder of the borehole annulus, except for thin layers of bentonite placed about every 2 m to inhibit channeling.

Two boreholes are located near the Idaho Research Center (IRC). These boreholes, IRC-3 and IRC-5 are located in Idaho Falls (Figure 1). This site receives about 300 mm/y precipitation. These boreholes are located at a flat location that experiences little to no additional run-on and is vegetated predominately with cheat grass (*bromus tectorum*). The boreholes are located 10 m from one another, and were air-rotary drilled with a 14.9 cm diameter bit to a depth of about 15 m in September 1995. The boreholes are located in a similar geologic formation as borehole 76-5 with loam and alluvial

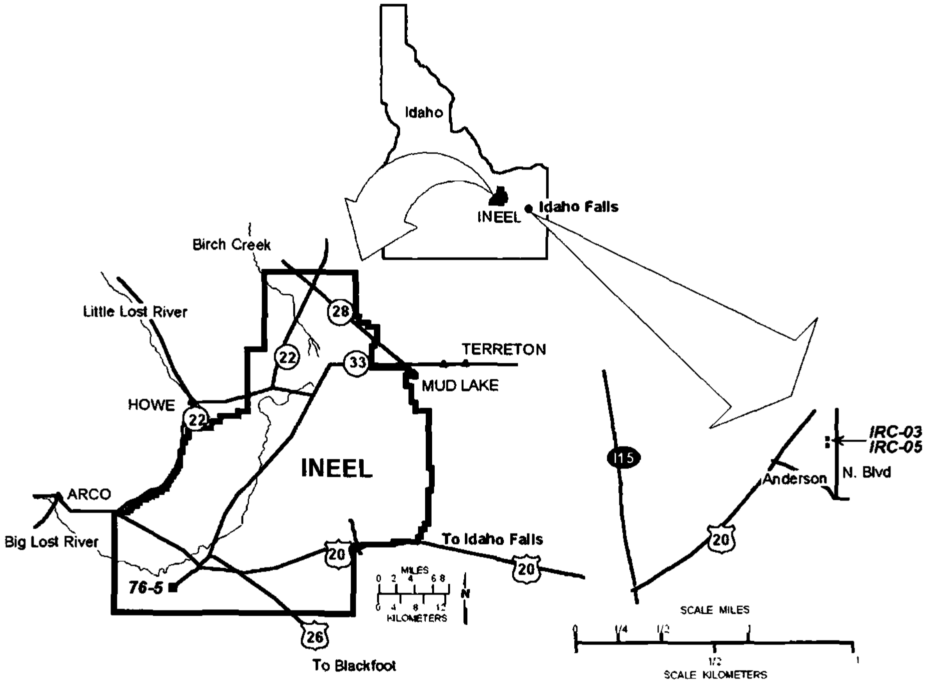

Figure 1-*Location of wells 76-5, IRC-3, and IRC-5.*

sediments from land surface to 2.7 m and basalt from 2.7 to 15.5 m (Figure 3a). Sedimentary interbeds are not present in the IRC boreholes. The borehole completion of IRC-3 varied from borehole 76-5 in that loam was used to backfill most of the borehole with 0.3 to 0.6 m layers of bentonite placed between the monitored intervals (Figure 3b).

Sediment and basalt samples were obtained from these sites and tested in the laboratory for hydrological and physical properties. Unsaturated hydraulic conductivity was calculated as a function of pressure head and moisture content for basalt and sediment samples using a closed-form analytical solution (van Genuchten 1980) based on Maulem's (1976) theoretical model.

Tensiometers were installed in IRC-5 in January 1998 at seven depths (Figure 3c). IRC-5 was backfilled primarily with granular bentonite with 0.3 to 1 m layers of loam adjacent to the porous cups of the tensiometers to isolate the measurement depth to small intervals.

Results and Discussion

Water Potential Measurements in Basalt and Sediment

Water potential measurements collected from the tensiometers for each of the three boreholes are illustrated in Figures 4, 5 and 6. Data was collected on an hourly basis with data from 12-hour intervals plotted. Missing data from these figures are due to transducer failure or air entry and loss of water from the tensiometers. Data are affected

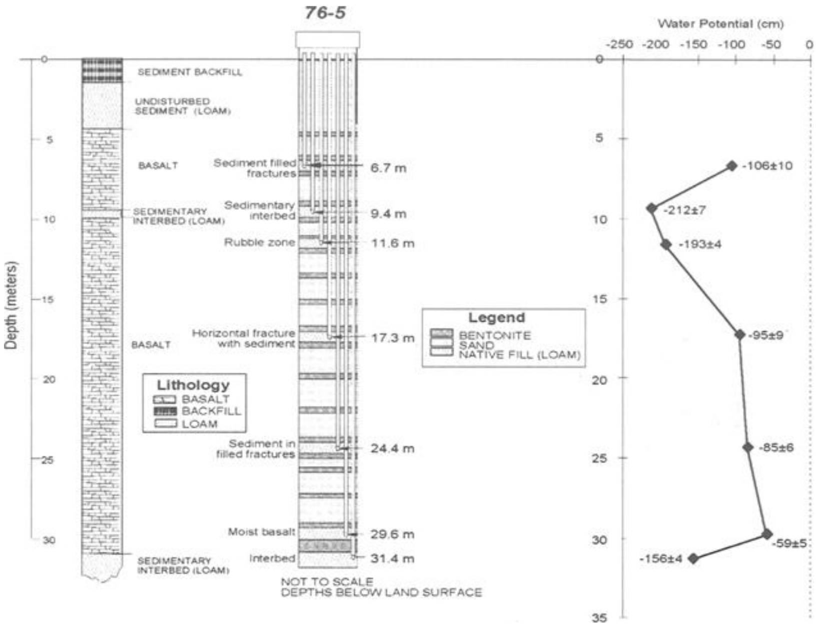

Figure 2-*Well completion, geology and water potential for well 76-5.*

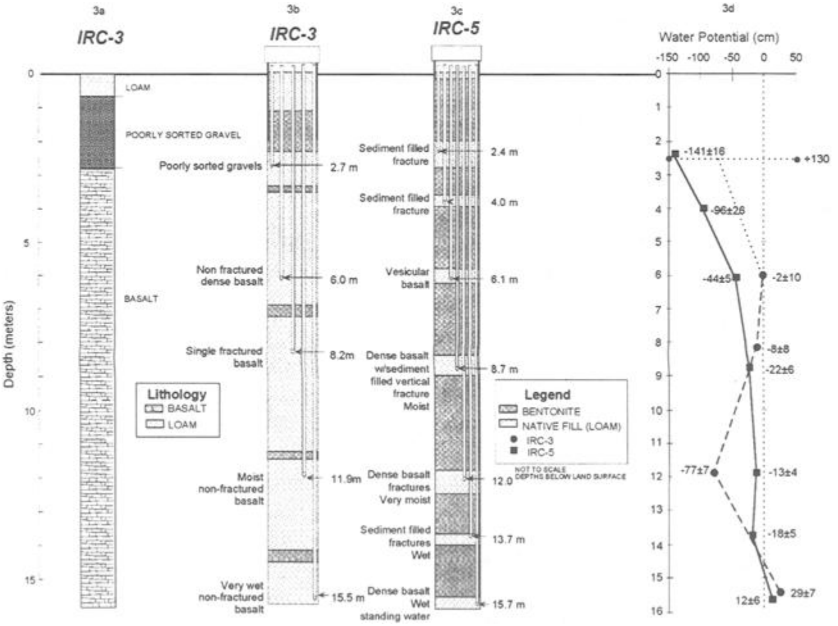

Figure 3-*Well completion, geology and water potential for wells IRC-3 and IRC-5.*

by initial equilibration with backfill, changes in barometric pressure, infiltration events and air entry into the tensiometer (Sisson and Hubbell 1999).

Borehole 76-5 was monitored from July 1996 through September 2000 (Figure 4). The data set can be viewed as three distinct intervals. During the first interval that lasted approximately two months, water potentials were initially in the range of –100 to –375 cm of water and increased to water potential values of –50 to –250 cm of water. During this initial 2-month period, we believe the backfill material was equilibrating with the surrounding bulk matrix as indicated by the rise in the water potential values. The second section of the data set illustrates fairly stable water potential values for a period of 2.5 years until January 1999. The last section of the data set in spring 1999 has an increase in water potential in the shallow tensiometers, indicating an infiltration event occurred. Snow depth data from a NOAA weather station located 8 km northeast of well 76-5 is included in Figures 4, 5 and 6 and indicates a relationship between snowmelt and infiltration events.

Borehole IRC-03 was monitored from November 1995 through September 2000 (Figure 5). Measured water potentials illustrate an initial equilibrium period, and long-term stable periods (10 to 12 month periods) interrupted by near annual infiltration events in the winter/spring. The most pronounced infiltration event occurred from snowmelt in late December 1996.

Borehole IRC-05 was monitored from January 1998 through May 1999 (Figure 6). Large fluctuations in water potentials (over 100 cm) occurred in the shallow surficial sediments and shallow basalt (2.4 and 4.0 m). Water potentials from 6.1 to 15.7 m were fairly stable for the first year of monitoring. An episodic infiltration event occurred in March 1999 that was reflected at the near surface monitored depths.

In general, the soil water potential measurements in all boreholes range from +100 to –250 cm water for the monitored period. Mean water potentials were calculated for the nearly steady state period from March 1998 to February 1999 for each tensiometer (Table 1). The shallowest tensiometers in surficial sediment show the greatest annual variation of water potential over time while tensiometers below 4 m show little variation, except during episodic infiltration.

In the IRC boreholes, episodic infiltration events tend to move rapidly through the basalt. One of the most pronounced and easily traced wetting events occurred as a result of a snowmelt event in late December 1996, and was monitored in borehole IRC-03 (Figure 5). The wetting front passed from the 2.7 to the 15.5 m depth in two days (2/15/96 to 2/17/96). Table 2 presents a list of dates where there was noticeable change in water potential in response to infiltration events. Although all of the tensiometers in this borehole responded to this infiltration event, the sequence of first arrival indicated preferential flow paths within the basalt. Following formation of perched water at 2.7 m at the basalt/sediment interface, the water potential responded first at the 8.2, 11.9 and 15.5 m depths on January 1, 1997 and then at the 6 m depth on January 6, 1997.

The velocity of this water pressure pulse ranges from 1 to 3 meters/day (m/d) through the basalt (Table 2). In comparison, this wetting front velocity range is close to the 5 m/d (range of 38 measurements was 1.4 - 17.7 m/d) averaged vertical wetting front velocity through basalt during a large-scale infiltration test (LSIT) at the INEEL (Porro and Bishop 1995, Dunnivant et al. 1998). At the LSIT water was ponded to several meters depth and the water movement monitored using neutron logging. The test was conducted

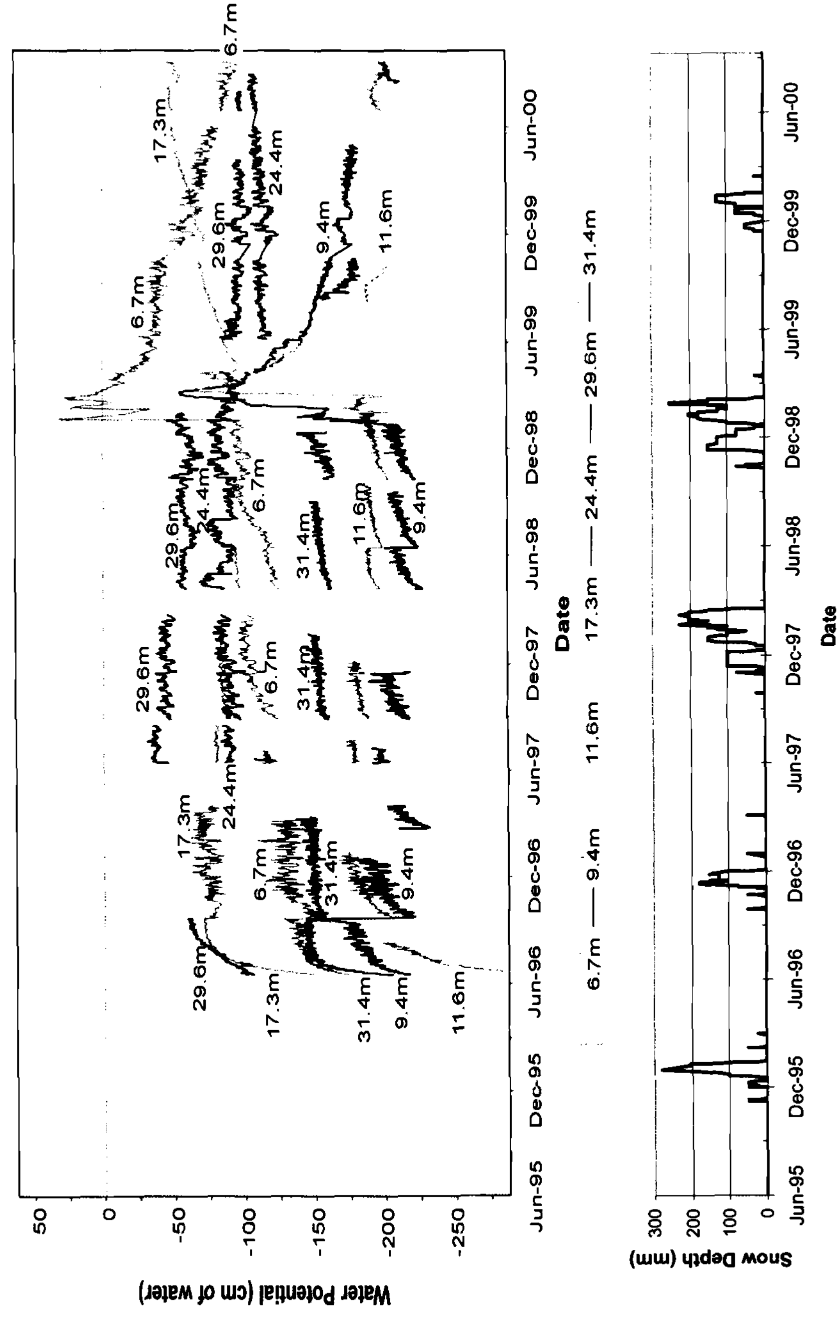

Figure 4-*Water potential in well 76-5 and snow depth.*

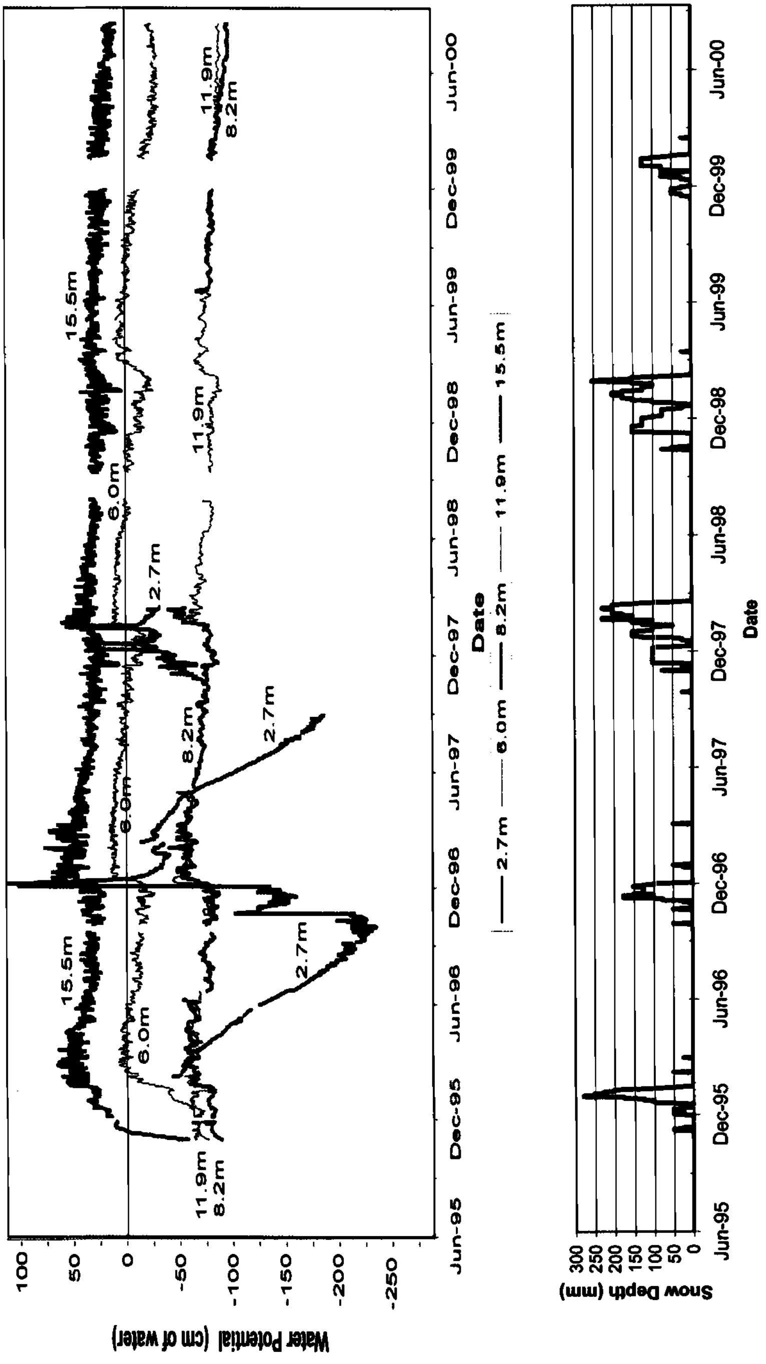

Figure 5-*Water potential in well IRC-3 and snow depth.*

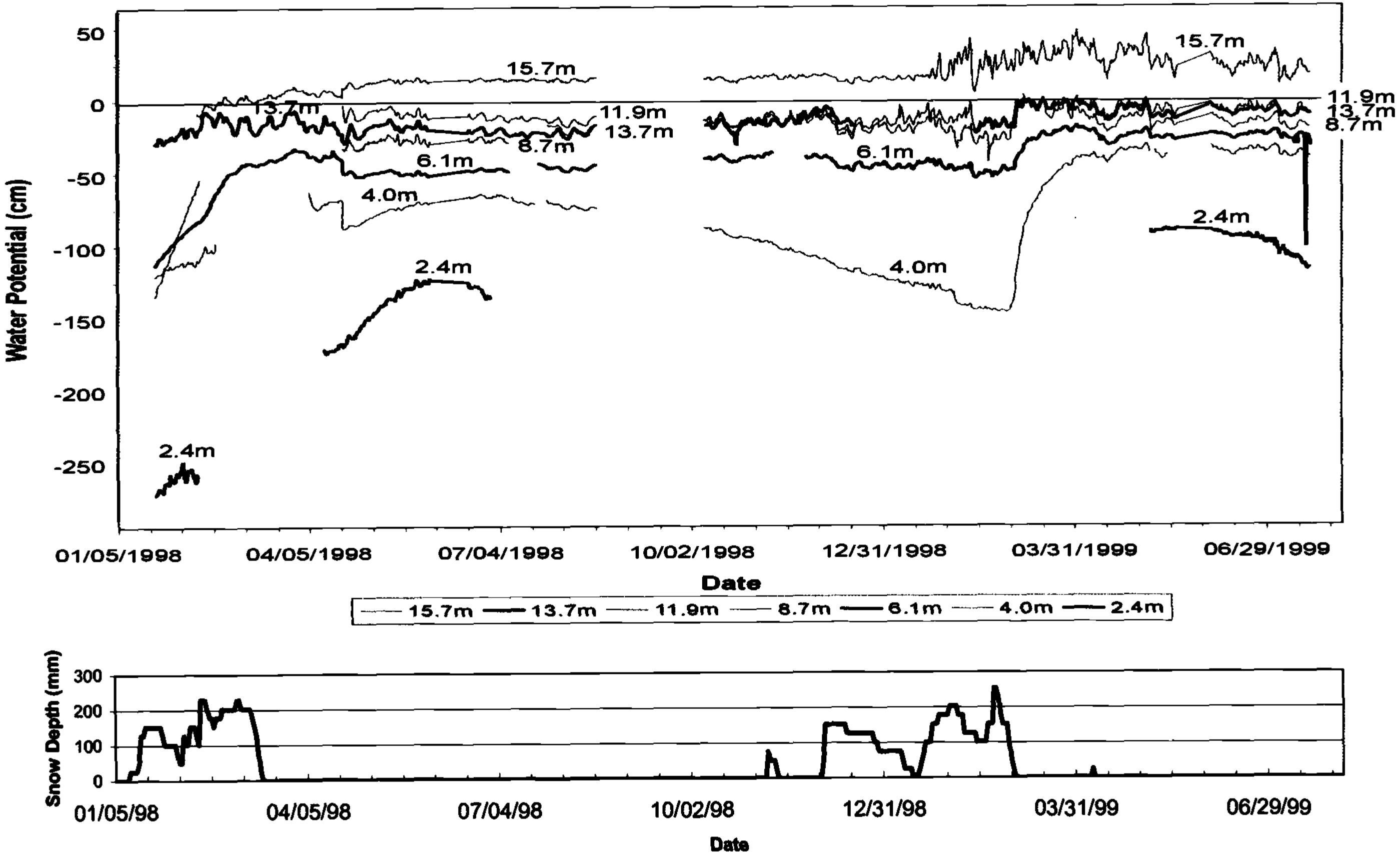

Figure 6-*Water potential in IRC-5 and snow depth.*

Table 1 - *Mean water potential March 1998 to February 1999.*

76-5			**IRC-3**			**IRC-5**		
Depth (m)	**Mean (cm)**	**Std. Dev. (cm)**	**Depth (m)**	**Mean (cm)**	**Std. Dev. (cm)**	**Depth (m)**	**Mean (cm)**	**Std. Dev. (cm)**
--	--	--	**2.7**	##	##	**2.4**	-141*	16
--	--	--	--	--	--	**4.0**	-96	26
6.7	-106	10	**6**	-2	10	**6.1**	-44	5
9.4	-212	7	**8.2**	-8**	15	**8.7**	-22	6
11.6	-193	4	**11.9**	-77	6	**11.9**	-13	4
--	--	--	--	--	--	**13.7**	-18	5
17.3	-95	9	**15.5**	29	7	**15.6**	12	6
24.4	-85	6	--	--	--	--	--	--
29.9	-59	5	--	--	--	--	--	--
31.4	-156	4	--	--	--	--	--	--

Data fluctuates
* Data collected April to June 1999
** Data collected January to December 1997
-- No instrumentation

about 2 km south of borehole 76-5 in similar geologic materials.

Episodic infiltration through the basalt fractures is time spatial dependent. Arrival dates listed in Table 2 for borehole IRC-03 suggests that the sequence of the infiltration front arrival varies according to the infiltration event. For example, at depth 6.0 m, the arrival of the infiltration front is recorded as the first arrival in the springs of 1996 and 1998, but shows the infiltration front arriving last during the winter 1996-1997 event. This may indicate that the magnitude of the formation of preferential infiltration pathways is related to infiltration flux. As illustrated by the 2.7 m water potential measurements in (Figure 5), the magnitude of the winter 96 - 97 infiltration event was the largest infiltration event recorded during the four year monitoring period as indicated by the depth of perched water. Saturated channel flow during this infiltration event may have created preferential flow channels in fractured basalt effectively bypassing the shallower tensiometers. During subsequent infiltration events, the magnitudes of the infiltration events were less than the winter 96-97 event, and the infiltration preferential flow pattern appears to have changed to a more sequentially travel time with respect to depth.

The presence of a sedimentary interbed appears to be an important control in the geologic profile by slowing the infiltration process. The infiltration front moved through the fractured basalt profile at the IRC boreholes at a rate of meters per day. Figures 5 and 6 show that steady-state background conditions are interrupted in spring 1999 by an infiltration event. A sharp increase in water potential from an infiltration event was measured down to 11.9 m bls at borehole IRC-03 and 13.7 m bls at borehole IRC-05. The wetting front moved from 6 to 11.9 m within two days (3 m/d), at both locations. In contrast, infiltration through borehole 76-5 (Figure 4), containing a sedimentary interbed

Table 2-*Date of "first arrival" of pressure wave in response to infiltration events.*

76-5		**IRC-3**					**IRC-5**	
Depth (m)	**Spring 1999**	**Depth**	**Spring 1996**	**Winter 96-97**	**Spring 1998**	**Spring 1999**	**Depth**	**Spring 1999**
--	--	**2.7 m**	No data	12-29-96	2-5-98	--	**2.4 m**	--
--	--	--	--	--	--	--	**4.0 m**	3-1-99
6.7	2-11-99	**6.0 m**	2-15-96	1-6-97	2-10-98	3-6-99	**6.1**	3-2-99
9.4	3-3-99	**8.2 m**	2-18-96	1-1-97	2-13-98	--	**8.7 m**	2-28-99
11.6	3-26-99	**11.9 m**	2-17-96	1-1-97	2-13-98	3-6-99	**11.9 m**	3-3-99
--	--	--	--	--	--	--	**13.7 m**	3-3-99
--	--	**15.5 m**	2-17-96	1-1-97	**	**	**15.6 m**	**
17.3 m	5-99	--	--	--	--	--	--	--
24.4 m	**	--	--	--	--	--	--	--
29.9 m	**	--	--	--	--	--	--	--
31.4 m	**	--	--	--	--	--	--	--

-- No instrumentation or instrument inoperative
** No response in tensiometer

at 9.4 m bls, occurred more slowly. The wetting front at borehole 76-5 infiltrated from a depth of 6.7 to 11.6 m in 43 days (0.1 m/d). The sedimentary interbed may have behaved as a capillary barrier retarding the advance of the infiltration front through the profile. This hypothesis is supported by the higher (-100 cm) water potential readings above the sedimentary interbed as compared to the -200 cm water potential steady state readings in the sedimentary interbeds (Figure 2).

The water potential response indicates that the sediment backfill adjacent to the tensiometer wets over the period of a few days to weeks but then drains back to original values over several months to years (Figure 5). It is suggested that rapid flow occurs in the fractures during wetting events and this water movement is transmitted into the sediment/tensiometer. The basalt matrix has probably not been fully wetted due to the low hydraulic conductivity of the basalt, but rather just a rind adjacent to the fracture has been wetted. The moisture retained in storage in the sediment backfill then drains, if a conduit (fracture) is available, or is temporarily retained in the sediment backfill by the surrounding low permeability basalt. Alternately, moisture may be retained in the sediment backfill adjacent to the tensiometer due to a capillary barrier formed by fractures in the basalt.

Water potential data indicates that the wetting fronts may cause either saturated and unsaturated flow conditions in the basalt fractures during infiltration events. Water potentials increased about 30 cm throughout the basalt profile in the December 1996 infiltration event at IRC-3 (Figure 5). During this infiltration event, the 2.7 and 6.0 m depths indicated the formation of perched water while the other tensiometers did not indicate the formation of saturated conditions. The 15.5 m tensiometer indicated saturated conditions over the monitoring period with increased water pressure in response to infiltration events.

Flux Estimates using Tensiometer Measurements

Steady State Flux Estimates in Basalt Matrix, Sedimentary Interbeds and Fractured Basalt

Flux rates can be estimated using Darcy's law with the measured hydraulic gradients and the unsaturated hydraulic conductivity at field water potential values. If the hydraulic gradient is unity, (i.e., water potentials do not change significantly with depth) the unsaturated hydraulic conductivity at that water potential is equal to the flux rate. Flux is generally defined as the mass of material moving though a unit cross-sectional area over a unit time period.

Figure 7 presents the hydraulic gradient with depth from the tensiometers in the three wells. A near unit-gradient exists below 4 m through the basalt profile during the steady state portion of the year in all the boreholes (when infiltration events are not occurring). Figure 7 is calculated using the mean water potentials for each tensiometer within the profile from Table 1. Mean water potential values are all within the tensiometric range and exhibit a relatively small standard deviation. At boreholes IRC-3 and IRC-5, the variation in mean water potential is less than 1.1 m (110 cm) beneath the surficial sediment tensiometer. At borehole 76-5, the maximum variation is 1.6 m (160 cm) over the 31.4 m profile.

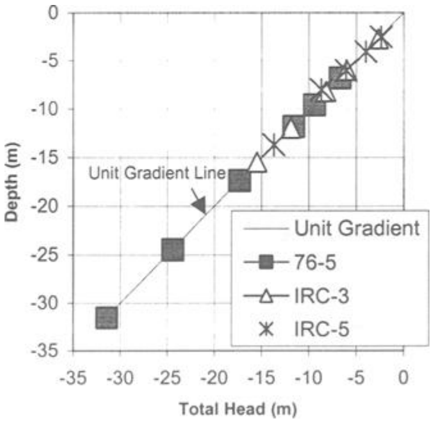

Figure 7-*Total head, calculated using mean water potential, versus depth for tensiometers showing a unit hydraulic gradient in these boreholes.*

The hydraulic properties for the basalt matrix and sedimentary interbeds at these sites have been determined from laboratory analysis of representative samples. Figure 8 shows the hydraulic conductivity characteristic curves for representative basalt matrix and sedimentary interbed material. The basalt curve was obtained from hydrologic characterization of a near surface basalt block located near well 76-5 (Bishop 1991). The sedimentary interbed curve comes from a sample of the 10-m sedimentary interbed from a well adjacent to 76-5 (Magnuson and McElroy 1993).

Boreholes IRC-3 and IRC-5 at Idaho Falls have water potentials in the −80 to 0 cm (saturated) range at depths below the 4 m monitoring depth. These water potentials in the basalt matrix correspond to a hydraulic conductivity (flux rate) of 2×10^{-9} to 1×10^{-6} cm/ s (0.7 to 30 cm/y). If the mean water potential from each borehole (below 4 m depth) of −14 cm is used, the corresponding hydraulic conductivity (flux) is estimated to be 9×10^{-8} cm/s (3 cm/y) for the basalt matrix.

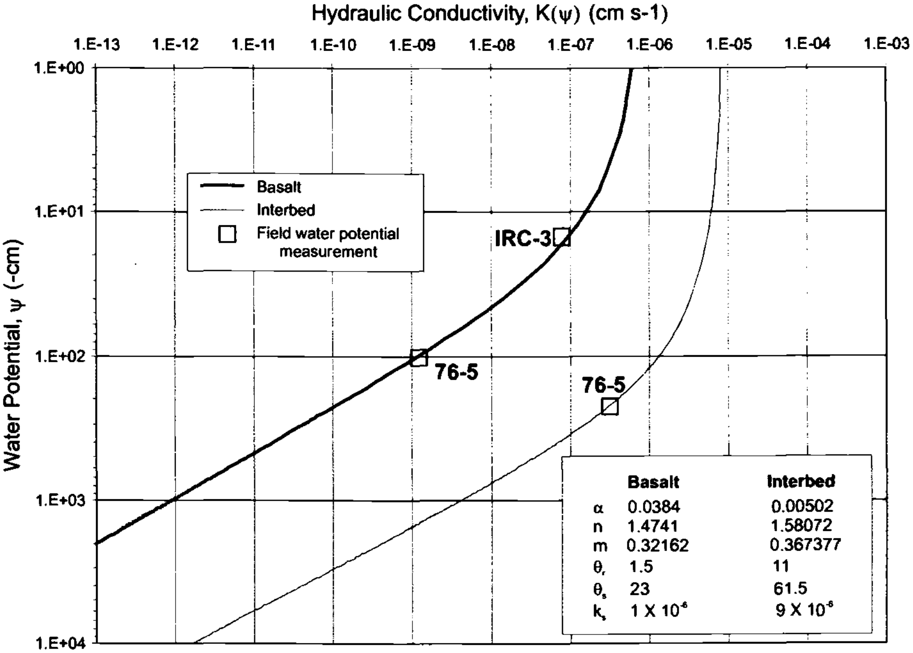

	Basalt	Interbed
α	0.0384	0.00502
n	1.4741	1.58072
m	0.32162	0.367377
θ_r	1.5	11
θ_s	23	61.5
k_s	1×10^{-6}	9×10^{-6}

Figure 8- *Water potential versus hydraulic conductivity for basalt and sedimentary interbed.*

Borehole 76-5 at the INEEL contains tensiometers adjacent to both the sedimentary interbeds and basalt. The average water potential of the basalt matrix is about −60 cm lower than in the sedimentary interbeds (Figure 2). The mean water potential in the basalt matrix is −107 cm, which corresponds to an unsaturated hydraulic conductivity (flux) of 1×10^{-9} cm/s (0.03 cm/y). The average water potential in the sedimentary interbeds is −168 cm, which corresponds to a hydraulic conductivity (flux) of about 5×10^{-7} cm/s (15 cm/y). Comparing these estimates, the steady state flux through the sedimentary interbeds is about three orders of magnitude larger than the flux through the basalt matrix. These estimates assume one-dimensional flow and a unit hydraulic gradient while ignoring fracture flow.

It is suggested that unsaturated film flow along the fracture walls combines with the matrix flow to equal the flux through the interbed. Assuming there is continuity of water flux at the basalt-interbed under steady-state conditions (assuming lateral flow is not dominant) the sediments are transmitting about three orders of magnitude more water (500 times) through the interbeds than is transported in the basalt matrix. The fractures would then be transmitting the remaining moisture through saturated or film flow. Thus the tensiometric data and the unsaturated hydraulic properties from the basalt matrix and sedimentary interbeds suggest significant unsaturated water flux is transported through the fractures during the bulk of the year at borehole 76-5.

Calculation of Flux for Episodic Infiltration Events

The volume of water moving through a geologic profile can be estimated by measuring the change in thickness of the perched water layer over time and calculating the equivalent mass of water. This calculation assumes vertical flow. The volume of water per unit area (extrapolating the tensiometer point measurement to three dimensions) is calculated using the change in the moisture content from saturation to the residual water content. The flux rate is then estimated using the change in volume of water over time from the water level recession data.

Episodic infiltration events caused the formation of perched water several times in IRC-3 and once in 76-5 (Figures 4 and 5). Hourly tensiometric data have been used in the following calculations instead of the twice a day measurements shown in these figures. Water level responses in basalt from well IRC-5 were not analyzed due to indistinct response from barometric pressure induced water level fluctuations that decrease the accuracy of the water level depths.

Episodic Infiltration Estimates from Surficial Sediments into Basalt- The volume of water that perched within surficial sediments overlying basalt is calculated for the two infiltration events in December 1996 and January 1998 in well IRC-3. A water-filled effective porosity of about 25% is based upon laboratory-derived values from similar sediments (sandy gravel) (Ansley et. al. 1988, McElroy and Hubbell 1990). The volumetric water content (field capacity) was 9%. A 1 cm rise or decline in measured water level in a porous media then corresponds to a 0.16 cm volume of water per unit area (0.25-0.9). This assumes vertical flow and the formation is completely wetted.

Flux from the surficial sedimentary material overlying basalt at IRC-3 is estimated using the slope of the water level recession line (decline per unit time) and time of perched water (Figure 9). Evaluation of the water level recession line indicated that the water level decline varied from –2.6 to -0.66 cm water/hr. The water level recession lines appear to be relatively linear and repeatable from the perched water drainage events. The greatest negative slope should correspond with the effective hydraulic conductivity of the material limiting drainage of the perched water (assuming vertical flow). Slopes more positive than –2.6 cm/hr then correspond with time periods where water is being added to the perched water body from infiltration (Figure 9). Since the change in head over time is nearly linear, the time that perched water is present can be used to estimate the volume of infiltrating into the underlying basalt. This –2.6 cm/hr slope combined with a field

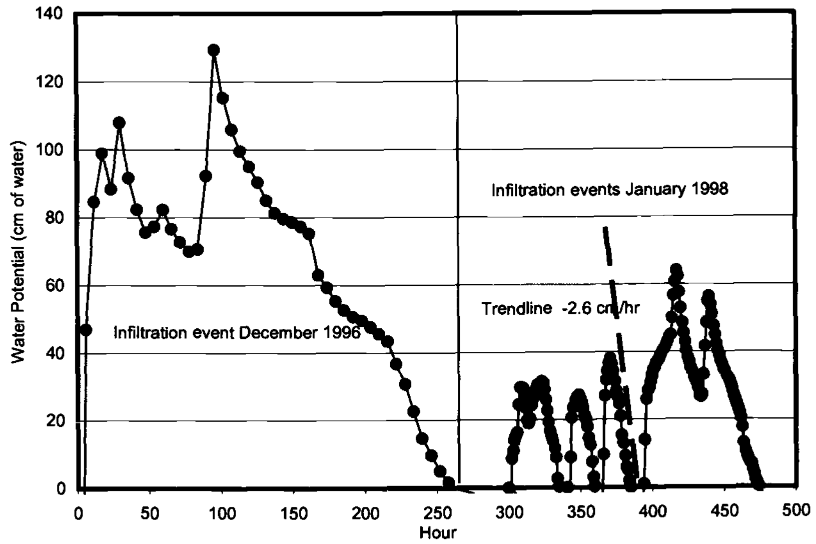

Figure 9-*Water level in IRC-3 showing trend line of maximum recession slope.*

capacity of 0.16 (-2.6 x 0.16), yields an infiltration rate (flux) of 0.42 cm/hr (1.2×10^{-4} cm/sec) from the sediment into the basalt. Perched water was present at this tensiometer for 250 hrs in December 1996, which suggests that there was about 104 cm equivalent depth of water of infiltration into the underlying basalt. In January 1998 the perched water was present for about 150 hours corresponding to an estimate of 62 cm equivalent depth of water. These flux estimates exceed the saturated hydraulic conductivity of the basalt matrix and so indicate that flow is primarily through the fractures. Table 3 presents a summary of the flux estimates.

The infiltration estimates exceed the annual precipitation by a factor of nearly five times. This suggests the borehole is monitoring a site with preferential infiltration that is draining the local area, however evidence of this is not evident by visual inspection of the site, even during the infiltration events. The infiltration mechanisms could include localized accumulation of water at land surface from surface runoff or lateral movement of water in the sediment above the basalt due to a topographic low at the sediment/basalt contact. Alternately, there are mice borrows around the boreholes that may allow enhanced infiltration at this site. Most of this volume of water is assumed to have infiltrated into the underlying basalt since the perching occurs a several meters below land surface and there is no possibility for evapotranspiration.

Episodic Infiltration Estimates Through Basalt- The same technique to estimate the volume of infiltration can be applied to changes in water level of perched water within basalt. An effective porosity of 3%, determined from modeling of the Snake River Plain aquifer (Magnuson 1995), is used to estimate the effective volume of water per unit change of water level in the basalt. Perched water has been present continuously in

Table 3. *Summary of estimated flux rates derived from tensiometer measurements.*

Borehole	**Comment**	**Flux Rate (cm/sec)**	**Recharge-Depth of Water**
*Steady State flow**			
IRC-3, IRC-5	Basalt matrix (range of ψ's)	2×10^{-9} to 1×10^{-6}	0.06 to 31 cm/yr
IRC-3, IRC-5	Basalt matrix (mean ψ)	9×10^{-8}	2.8 cm/yr
76-5	Basalt matrix (mean ψ)	1×10^{-9}	0.03 cm/yr
76-5	Sediment interbed (mean ψ)	5×10^{-7}	16 cm/yr
76-5	Basalt fractures (difference)	4.99×10^{-7}	16 cm/yr
*Episodic flow***			
IRC-3 Dec 96	Sediment into basalt	1.2×10^{-4}	104 cm
IRC-3 Jan 98	Sediment into basalt	1.2×10^{-4}	62 cm
IRC-3 Jan 97	Within basalt-15.5 m	3×10^{-8}	1.1 cm
IRC-3 Jan 98	Within basalt-15.5 m	3×10^{-8}	1.0 cm
76-5 Jan 99	Within basalt-6.7m	3×10^{-8}	0.96 cm

* Assuming vertical flow and a unit hydraulic gradient
** Assuming vertical flow

IRC-3 at 15.5 m depth following well installation. The tensiometer at this depth has indicated several water level increases and declines in response to annual infiltration events. The water level rose 38 cm and 32 cm in response to infiltration (January 1997 and January 1998, respectively). These depths of water correspond to an equivalent depth of water of 1.1 and 1.0 cm (0.03 x 38 cm and 0.03 x 32 cm). These estimates are only 0.8 to 5% of the estimates of the volume of water that accumulated at the surficial sediment basalt contact. This difference may be due to preferential flow past the perching layer, or more likely, the depth of perched water at the surficial sediment basalt contact was not representative of infiltration over this area. The larger scale or regional infiltration at this site may be better represented by the estimates from deeper perched water layers. The flux rate through the underlying basalt is calculated by dividing the volume of water by the time. The water level in the perched water declined over the course of a year indicating a flux rate through the basalt of about 3×10^{-8} cm/ sec.

Borehole 76-5 showed the formation of perched water at the 6.7 m depth adjacent to fractured basalt with sediment-filled fractures. The tensiometers detected three pulses of water, each forming perched water 12 to 20 cm depth (Figure 4). Using an assumed effective porosity of 3% corresponds to an equivalent depth of water of about 0.96 cm. The water level rose rapidly in 76-5 at 15.5 m and then declined slowly indicating very slow drainage through the basalt. The volume of flow that drains over these time periods corresponds to a vertical hydraulic conductivity of about 3×10^{-8} cm/sec, similar to the saturated hydraulic conductivity of the basalt matrix. This may indicate that the water is draining through the basalt matrix.

Variations of the alluvial sediment texture, local topography, evaporation, the moisture available in the snow, existing moisture in the sediments, and alluvial cover depth between the INEEL and IRC sites are likely responsible for the difference in observed frequency of episodic infiltration into the underlying fractured basalt. Both alluvial texture and topography contribute to the amount of snowmelt that could infiltrate into the alluvium material. Hydraulic conductivity less than the infiltration rate will result in surface ponding conditions. In a situation where the surface topography is completely level, the ponded water would eventually infiltrate into the soil profile but may also loose water to evaporation. However, when the surface exhibits a slope in the topography, the ponded water may run off to local surface depressions. At borehole 76-5, the surface alluvium exhibits fine texture but subsidence in the cover materials has formed a localized depression that allows ponding near the well during the spring snowmelt. The local effect is episodic infiltration at the 76-5 site from melting snow. In contrast, the alluvial texture at the IRC site is slightly coarser and the local topography is flatter than the INEEL site, allowing a greater percentage of the snowmelt to infiltrate initially into the overlying alluvial sediments.

Estimates of infiltration using the change in the depth of perched ground water allow point measurements of infiltration. Many fractured rock sites have surficial sediments that may allow the determination of local infiltration and subsequent drainage into the fractured media. Measurement of water level changes at greater depths may allow more representative estimates over larger areas, dependant on the spatial characteristics of the perched water.

Conclusions

Advanced tensiometers were installed in a dual-porosity fractured basalt matrix and sediments to monitor moisture movement from natural water infiltration at the INEEL. This data was used to infer infiltration mechanisms. Water potential measurements for all the instruments were in the tensiometric range from +130 to -250 cm of water at these arid and semi-arid sites (250-300 mm precipitation/yr). Water potential measurements were primarily constant with a variation of less than 10 cm and exhibited a near steady-state unit-gradient downward flux, except during periods of episodic infiltration/drainage. Spring snowmelt created episodic infiltration that moved rapidly through the fractured basalt. These infiltration events produced detectable changes in the water potential to depths up to 15.5 m, in some cases within a few days of the infiltration events. During high magnitude infiltration events, preferential saturated channeling of the moisture occurs, bypassing zones within the vadose zone. Sedimentary interbeds may have substantially reduced the percolation, acting as either a hydraulic or capillary barrier. Unit gradient analysis of the steady-state infiltration flux indicates that unsaturated fracture flow is the major infiltration mechanism through the fractured basalt during much of the year. Flux estimates were determined for the basalt matrix and sedimentary interbeds using steady state calculations as well as using the change in depth of perched water from episodic infiltration within overlying surficial sediments and the basalt matrix. The estimates suggest moisture moves primarily in the fractures during episodic infiltration events and that the episodic events transport significantly more moisture than steady state flow through the basalt matrix. Results from this study indicate that advanced tensiometers can be used to measure water potentials in deep vadose zones, detect and monitor infiltration events and estimate the contributions of episodic and steady state infiltration flux. Thus instrumentation exists for monitoring water movement below waste disposal sites.

Acknowledgments

Work was supported by the Laboratory Directed Research and Development (LDRD) program and EM-50 of the U.S. Department of Energy, Assistant Secretary of Environmental Management, under DOE Idaho Operations Office Contract DE-AC07-99ID13727 at the Idaho National Engineering and Environmental Laboratory.

References

Ansley, S. L., Hull, L. C. and Burns, S. M., 1988, *Shallow Drilling Report for CFA Landfills II and III- FY-1988*, Report no. EGG-ER-8291, EG&G Idaho, Inc., Idaho Falls, Idaho.

Beckman, M., 1999, "Journey to the Center of the.....Vadose Zone", July/August, *Radwaste Magazine*, Vol. 6, No. 4, pp. 55-57.

Bishop, C. W., 1991, "Hydraulic Properties of Vesicular Basalt", M. S. Thesis, Dept. of Hydrology and Water Resources, University of Arizona, Tucson, Arizona.

Cassel, D. K., and Klute, A., 1986, "Water Potential: Tensiometry", in *Methods of Soil Analysis, Part One. Physical and Mineralogical Methods*. A Klute. (ed.), Agronomy Monograph #9, second edition, American Society of Agronomy, Inc. Madison, WI, pp. 563-596.

Clawson K. L., Start, G. E. and Ricks, N. R., 1989, *Climatology of the Idaho National Engineering Laboratory*, Report no. DOE/ID-12118, U.S. Department of Commerce, National Oceanic and Atmospheric Administration, Environmental Research Laboratories, Air Resources Laboratory, Field Research Division, U.S. Department of Energy Idaho Operation Office, Idaho Falls, ID.

Dunnivant, F. M., Newman, M. E., Bishop, C. W., Burgess, D., Giles, J. R., Higgs, B. D., Hubbell, J. M., Neher, E., Norrell, G. T., Pfiefer, M. C., Porro, I., Starr, R. S. and Wylie, A. H., 1998, "Water and Radioactive Tracer Flow in a Heterogeneous Field-scale System", *Ground Water*, Vol. 36, No. 6, pp. 949-958

Evans D.D. and Nicholson T.J., 1987, "Flow and Transport Through Unsaturated Fractured Rock: An Overview", *Flow and Transport Through Unsaturated Fractured Rock*, Eds. D.D. Evans and T.H. Nicholson, Geophysical Monograph 42, American Geophysical Union, Washington, D.C, USA, pp. 1-10.

Gee G.W. and Hillel, D., 1988, Groundwater Recharge in Arid Regions: Review and Critique of Estimation Methods, *Hydrological Processes*; Vol. 2, No. 3, pp. 255-266.

Hubbell, J. M. and Sisson, J. B., 1998, "Advanced Tensiometer for Shallow or Deep Soil-Water Potential Measurements", *Soil Science*, Vol. 163, No. 4, pp. 271-277.

Magnuson, S. M. 1995, *Inverse Modeling for Field-Scale Hydrologic and Transport*

Parameters of Fractured Basalt, Report no. INEEL-95/0637, Idaho Falls, Idaho: U.S. Department of Energy, Idaho Operations Office, p. 41.

Magnuson, S. O., and McElroy, D. L., 1993, *Estimation of Infiltration from In Situ Moisture Contents and Representative Moisture Characteristic Curves for the 30', 110' and 240' Interbeds,* Report no. RWM-93-001, EG&G Idaho, Inc., Idaho Falls, Idaho.

Maulem, Y., 1976, "A New Model for Predicting the Hydraulic Conductivity of Unsaturated Porous Media," *Water Resources Research,* Vol. 12, No. 3, pp. 513-522.

McElroy, D. L. and Hubbell, J. M., 1990, *Hydrologic and Physical Properties of Sediments at the Radioactive Waste Management Complex,* Report no. EGG-BG-9147, EG&G Idaho, Inc., Idaho Falls, Idaho.

Montazer P., 1987, Monitoring Hydrologic Conditions in the Vadose Zone in Fractured Rock, Yucca Mountain, Nevada, in *Flow and Transport Through Unsaturated Fractured Rock,* Eds. D.D. Evans and T.H. Nicholson, Geophysical Monograph 42, American Geophysical Union, Washington, D.C. USA, pp. 31-42.

Nativ R., Adar, E., Dahan, O. and Geyh, M., 1995, "Water Recharge and Solute Transport Through the Vadose Zone of Fractured Chalk Under Desert Conditions", *Water Resources Research,* Vol. 31, No. 2, pp. 253-261.

Porro, I. and Bishop, C. W., 1995, *Large Scale Infiltration Test CPN Data Analysis,* Engineering Design File No. WAG7-58, INEL-ER-040.

Sisson, J.B. and Hubbell, J.M., 1999, "Water Potential to Depths of 30 Meters in Fractured Basalt and Sedimentary Interbeds," in *Characterization and Measurement of Hydraulic Properties of Unsaturated Porous Media,* ed. by M.Th. van Genuchten and F.J. Leij, U.S. Salinity Laboratory, Riverside, Calif., pp. 855-865.

van Genuchten, M. T., 1980, "A Closed-Form Equation for Predicting the Hydraulic Conductivity of Unsaturated Soils", *Soil Science Society America Journal,* Vol. 44, No. 5, pp. 892-898.

Wang J. S. Y. and Narasimham, T. N., 1985, "Hydrologic Mechanisms Governing Fluid Flow in a Partially Saturated, Fractured, Porous Media", *Water Resources Research,* Vol. 21, No. 12, pp. 1861-1874.

Walton, J. C., Baca, R. G., and Rasmussen, T. L., 1989, "Flow and Transport of Radionuclides in Unsaturated Fractured Basalt", Presented at Waste Management 89, University of Arizona, March.

LABORATORY TO FIELD EVALUATIONS

Sam S. Gordji,[1] and Leili Pirouzian[2]

On The Measurement Of The Hydraulic Properties Of The Environmental Medium

Reference: Sam S. Gordji, and Leili Pirouzian, "**On The Measurement Of The Hydraulic Properties Of The Environmental Medium,**" ***Evaluation and Remediation of Low Permeability and Dual Porosity Environments, ASTMSTP 1415,*** M. N. Sara and L. G. Everett, Eds., ASTM International, West Conshohocken, PA, 2002.

Abstract

Contaminates behave differently in the vadose zone than they do in the saturated zone and the governing equations for them are more involved. The hydraulic conductivity and porosity are the most important parameters affecting water and contaminates movements in the vadose and the saturated zones. To estimate these parameters certain methods are examined for measuring the hydraulic properties where the soil permeability is low and, where possible, the results are compared with measured data. Unsaturated hydraulic conductivity (UHC), unlike saturated hydraulic conductivity (SHC), is difficult to obtain especially for clayey soils and fractured rocks. Most available studies either overestimate or underestimate the UHC, especially for values close to the surface where the UHC values are several orders less than their corresponding values for SHC. The goal of this paper is to adjust and modify some empirical equations for obtaining UHC and compare the results with those already available in the literature. This is achieved through the use of non-linear least squares. Values that represent parameter b, in the Campbell's power function is allowed to vary in a given range instead of having a single value. For every value in this range the non-linear least squares equations is calculated and the b value with the smallest error term is picked to represent the empirical parameter for the Campbell's power function. Results indicate adjustment to the reported empirical parameter b is needed to minimize the sums of squares and to obtain a closer match between the measured and the experimental data. That is the sum of errors for the non-linear least squares between measured and empirical data is minimum somewhere near the values that they suggested. Therefore, for the clayey soil and fractured rocks the empirical parameters for the power function are modified to reflect the minimum sums of squares for non-linear least squares equation. To fine tune b further, non-linear least squares are used to find the best fitted value of b using the empirical equation that relates depth (h) to water content. We are in the process of classifying fractured rocks and are testing them to see

---

[1] Statistical Consultant & Assistant Professor, 120 Powers Hall, University of Mississippi , University, MS 38677, E-mail: ccsam@olemiss.edu.

[2] Graduate Student, Chemical Engineering Department, University of Mississippi, University, MS 38677. P. O. Box 2958, University, MS 38677

how their hydraulic conductivity compares with clayey, sandy and silty soils. This is done through the application of fractal geometry and use of Sierpinski carpet. The empirical and the theoretical relationships used here are simple and practical and may directly be applied to obtain corresponding UHC. The equations that are utilized here are based on the theory or have their roots in statistical modeling. Results obtained from this investigation should be compared with the field data before they are applied toward solving Richards' equation.

Keywords: vadose zone; saturated zone; permeability, hydraulic conductivity, least squares

Introduction

Numerous empirical, theoretical, and statistical models exist for obtaining soil water retention and saturated hydraulic conductivity (SHC) data. This number reduces as researchers focus on obtaining hydraulic conductivity for the unsaturated dual porosity soils and rocks. Knowledge of the exact shape and texture of the matrix and macropore is critical in describing and obtaining flow process and the hydraulic conductivity. Implementation of a mathematical model to investigate the unsaturated flow of fluid in a porous medium requires the knowledge of the hydraulic properties of the medium. The availability of the numerical method to solve Richards' equation far surpasses the availability of measured data and the available hydraulic conductivity for fractured rocks and clayey soils needed to solve Richards' equation. All the methods purposed by researchers for obtaining unsaturated hydraulic conductivity (UHC) may be put in one of three categories: direct measurement, inverse method, and prediction method. Although direct method is preferred over the other two, it has its deficiencies. Soil measurement is costly, time consuming, and is at best approximate because soil texture is hysteretic in nature and soil classification is not exact. Many of the above deficiencies also apply to the inverse method. If more than one parameter is introduced in setting up the formulation for the inverse problem, the uniqueness of the result may be questioned. That leads to the empirical method suggested by some researchers. Parameters for empirical equations are determined by several methods, curve fitting, least squares, and other techniques.

Theoretical and measured data for SHC are abundant in the literature and are relatively simple to obtain for variety of soils and fractured rocks. Several authors have developed empirical models containing one or two parameters, not including those that have real physical meanings such as UHC, water content, pressure head, and other parameters. Among them are Brooks and Corey (1964). Alexander and Skaggs (1987) examined fourteen methods to predict the unsaturated hydraulic conductivity function K(h) from the volumetric water content, $\theta(h)$. Their results showed that the best method of predicting K(h) for sandy and clayey soils was the closed form of Campbell (1974).

Theory

In the vertical one-dimensional (x) coordinates, Richards' equation for unsaturated flow can be written as

$$C(h)\frac{\partial h}{\partial t} = \frac{\partial}{\partial x}\left[K(h)\left({\partial h}/{\partial x} - 1\right)\right] \tag{1}$$

$$\begin{array}{ll} h = h_{o}(x) & t = 0, \quad 0 \le x \le L \\ {\partial h}/{\partial x} = 1 & t > 0, \quad x = 0 \\ h = h_{L} & t > 0, \quad x = L \end{array} \tag{2a-2c}$$

Where $C(h)=\partial\theta/\partial h$ is the water capacity, h is the pressure head, θ the volumetric water content, x is the depth, and K the unsaturated hydraulic conductivity, (UHC), which is the function of h or θ. x=0 is assumed to be the top of the plate and x=L is the bottom of the plate. h_L is the pressure head at the bottom of the plate; and t is time. The unsaturated hydraulic properties of $\theta(h)$ and $K(h)$ are strongly non-linear functions of the pressure head. The exact form of the functions $\theta(h)$ and $K(h)$ are unknown because of the varied nature of the soils. To solve the above equation (1) with the boundary conditions (2a-2c), numerical values for $K(h)$ is needed.

Any solution of Richards' equation requires the knowledge of the hydraulic properties. There are three distinct methods to obtain hydraulic conductivity: prediction models, inverse methods, and field measurement. In this study we concentrate on the empirical method for obtaining UHC as a function of θ or h.

Some authors have suggested various empirical and theoretical forms for obtaining $K(h)$ from effective saturation Θ . The soil hydraulic properties that are reported by Van Genuchten's (1980) equations are

$$\Theta = \begin{cases} \dfrac{1}{\left[1 + |a\,h|^{n}\right]^{1-1/n}} & h < 0 \\ 1 & h \ge 0 \end{cases}$$

$$K = K_s \Theta^{1/2}\left[1 - \left(1 - \Theta^{n/(n-1)}\right)^{1-1/n}\right]^2 \qquad (n > 1) \tag{3}$$

where

$$\Theta = (\theta - \theta_r)/(\theta_s - \theta_r) \tag{4}$$

Brooks and Corey's model is

$$\theta(h) = \begin{cases} \theta_r + (\phi - \theta_r)\left(\dfrac{h_b}{h}\right)^{\lambda} & h < h_b \\ \phi & h \ge h_b \end{cases} \tag{5}$$

$$C(h) = \begin{cases} \dfrac{-\lambda(\phi - \theta_r)}{h}\left(\dfrac{h_b}{h}\right)^{\lambda} & h < h_b \\ 0 & h \geq h_b \end{cases} \tag{6}$$

and

$$K(h) = \begin{cases} K_0\left(\dfrac{h_b}{h}\right)^{\gamma} & h < h_b \\ K_0 & h \geq h_b \end{cases} \tag{7}$$

where $\gamma = 2+3/b$.

Later Campbell (1974) used essentially the same prediction equation

$$k = k_s(\theta / \theta_s)^{2b+2} \tag{8}$$

The above three power functions are similar since λ, n, b, γ are related by simple linear functions and $b=1/\lambda$.

The above two equations (7-8) are relatively simple and contain only one empirical parameter b or γ. Generally, b is related to pore sizes and is small for medium having a large and varied pore size and becomes large for medium with rather uniform pore sizes. Several authors have utilized pore sizes to obtain UHC for variety of soils and varied parameter b to obtain UHC for various soil textures. The range reported by Poulsen et al (1998) for b is from (2.8 to 30). This range was reported by several authors and collected, and reported by Poulsen et al (1998). Campbell (1974) set b=12.5 for Cecil B3 soil; he arrived at this value using a least squares fit of a straight line on the data. These values are empirical in nature without any theoretical basis or any relation to a particular soil that is under study. The justification for utilizations seems to be that they yield a good approximation for UHC. These empirical models lack the physical significance and extensive field measurement, and data analysis is needed to justify their implementations. Theoretical relations should be derived to justify the physical significance and proper applications of these empirical relations. Employing fractal geometry and the application of Sierpinski carpet (1994), Tyler and Wheatcraft (1990) derived expressions similar to Equations (7-8) above and established theoretical basis for those empirical equations. In their work they showed that higher fractal dimensions are related to higher values of b or clayey type soil and lower fractal dimensions correspond to lower b values reported by Campbell (1974) for sandy type soil.

Discussion

To estimate UHC at least two physical parameters, saturated hydraulic conductivity K_s, θ and an empirical parameter b in Equations (7-8) are needed. K_s the saturates hydraulic conductivity is rather simple to obtain and numerous authors have calculated and reported K_s, among them are Zachmann et al. (1982), and especially McKeague

(1982). Campbell's power functions may then be used to obtain a relationship between water content and the UHC.

Through the use of non-linear least squares we fine tune the empirical value of b. After simulating b, the resulting b is closer to the measured values with the minimum of sums of squares.

In the soil and fractured rocks K is directly proportional to the surface area in the vertical z-direction where the cracks occupy the smallest area. We are in the process of testing certain fractured rocks where the surface contains varying number of cracks. The UHC of these fractured rocks are then compared with several different soil textures such as sand, sandy loam etc. to establish a relationship among the several types of soils and fractured rocks. In this manner the existing hydraulic conductivity from soil may be applied to fractured rocks to obtain unsaturated hydraulic conductivity. Compared with K_S, unsaturated hydraulic conductivity (K) as a function of soil-water retention is time-consuming and difficult to obtain. A single equation used by Brooks and Cory (1966), Campbell (1974) and other authors does not seem to yield good answer for various types of soil. Correct estimation of UHC for vadose zones are necessary if the investigators are interested in the movement of the contaminates and clean up. The relationship between relative hydraulic conductivity and soil-water content is typically hysteretic and non-linear as illustrated by several authors, among them Gardner (1958).

It is often difficult to obtain an accurate estimate of the relative hydraulic conductivity and water movement throughout the unsaturated zone. This gets even more difficult when one tries to obtain a single expression that covers various soils. One-parameter models are preferred because more parameters make the stochastic analysis of the models more complicated and the results are about the same. Examples of one-parameter K models are given by Campbell (1974), Yeh et al. (1982), Dagan and Bresler (1983), Protopapas and Bras (1990), and some others.

Estimation of soil saturated hydraulic conductivities are available from many sources. Several authors have theoretically estimated saturated hydraulic conductivity and have checked their results with available measured data. Temperature also affects the UHC but because the effect is rather small most investigators have ignored it. Some have reported that UHC increases with temperature. The objective of this study is to modify present empirical relations to better estimate the measured values.

Numerical Example

One parameter empirical expression relating water content to water potential is: $\psi = \psi_e(\theta / \theta_s)^{-b}$. Values for θ_s, and ψ_e are available from literature. A few values for θ, the unsaturated water content, are needed to obtain water content from water potential ψ. This may be found from the literature or by measurement. Then, the above equation is simulated using non-linear least squares until the optimal value for b is obtained. The optimal value of b is then substituted into empirical expressions given by Campbell (1974) or others to obtain UHC. Following is the step-by-step instruction of how to obtain UHC.

1. Solve $\psi = \psi_e(\theta / \theta_s)^{-b}$ using non-linear least squares method to obtain the optimal value for b. Values for ψ, ψ_e, θ, θ_s for a particular soil may be found from literature, Brooks and Corey, Campbell and some others.

2. After the optimal value for b is obtained for a particular soil it should be inserted into: $k = k_s(\theta / \theta_s)^{2+2/b}$ introduced by Brooks and Corey and others to obtain an estimate for UHC or K_r, the relative hydraulic conductivity. The refined "b" obtained from non-linear-least squares then should be used for prediction of UHC for similar soil. Several empirical values reported by other investigators were tested using this method. Reported value by Zachmann et al. (1982). is b= 3.7, obtained value using non-linear least squares is b= 3.2.

Summary

Measured data for testing and simulations seems to be scarce. A few authors, Brooks and Corey among others have done extensive field measurement and data collecting. Our own results indicate that empirical methods deviate from the field measurements when soil is fine with a low UHC away from the saturated zone near the surface. This occurs when the parameter b takes on high values, b=14 or higher. It is recommended that especially in these cases non-linear least squares should be performed to obtain the optimal value for b or other similar parameters used to estimate UHC. Our results show that for some soils the simulated value of b does not converge and is different from the starting value for b. This happens when non-linear least squares are utilized to optimize the value of b. In a subsequent paper this discrepancy is investigated. Also the similarities and differences between varieties of soils and fractured rocks are compared to see if there are any similarities between the two groups as far as the behavior of hydraulic conductivity is concerned.

References

Alexander, L. and Skaggs, R. W. "Predicting unsaturated hydraulic conductivity from soil texture," *Journal of Irrigation and drainage Engineering, ASCE*, Vol. 113, No. 2, 1987, pp.184-197.

Brooks, R.H., Corey, A. T. "Hydraulics properties of porous medium," *Hydrology Paper No. 3, Colorado State University, Fort Collins, CO.*, 1964a.

Brooks, R.H., Corey, A. T. " Properties of porous media affecting fluid flow," *Journal of Irrigation and Drainage Division. ASCE*, Vol. 92, No. IR2, 1966, pp. 61-68.

Campbell, G. S. "A simple method for determining unsaturated conductivity from moisture retention data," *Soil Science*, Vol. 117, No. 6., 1974, pp. 311-314.

Dagan, E.C., Bresler. "Unsaturated Flow in Spatially Variable Field. Water Resources Research," Vol. 19, 1983, pp.413-420.

Engelking, R. and K. Sieklucki., " Introduction to Topology," Amsterdam: North-Holland, 1994.

Gardner, W. R. "Some Steady State Solutions of the Unsaturated Moisture flow Equation with Application to Evaporation from a Water Table," *Soil Science*, Vol. 85, 1958, pp. 228-232.

Kool, J.B., Parker, J.C., Van Genuchten, M.T. " Determining Soil Hydraulic Properties from One-step Outflow Experiments by Parameter Estimations: I. Theory and Numerical Studies," *Soil Science Society of America Journal*, Vol. 49, 1985, pp. 1348-1359.

McKeague, J.A., Wang, C., Topp, G.C. "Estimating saturated Hydraulic Conductivity from Soil Morphology," *Soil Science society of America Journal*, Vol. 46, 1982, pp. 1239-1244.

Poulsen, T. G., Moldrup, P., Jacobsen, O.H. " One-parameter Models for Unsaturated Hydraulic Conductivity," *Soil Science.* Vol. 163,No. 6, 1998, pp. 425-435.

Protopapas, A.L., Bras, R.L. "Uncertainty Propagation with numerical models for flow and transport in the Unsaturated Zone," *Water Resources Research.* Vol. 26, pp. 1990, 2463-2474.

Tyler S.C., Wheatcraft, S. W. 1990. "Fractal Processes in Soil Water Retention," *Water Resources Research*, Vol. 26, No. 5, 1990, pp. 1047-1054.

Van Genuchten, M. T. "A closed-form equation for predicting the hydraulic conductivity of saturated soils," *Soil Science society of America Journal*, Vol. 44, 1980, pp. 892-898.

Yeh, T.-C.J., Gelher, L.W., Gutjahr, A.L. "Stochastic Analysis of Unsaturated Flow in Heterogeneous Soil: 1-staistically isotropic media," *Water Resources Research.* Vol. 21, 1985a, pp.447-457.

Zachmann, D.W., Chateau, P.C., Klute, A. "Simultaneous Approximation of Water Capacity and Soil Hydraulic Conductivity by Parameter Identification," *Soil Science*, Vol. 134, No. 3, 1982, pp. 157-163.

Robert P. Chapuis[1] and David Cazaux[2]

Pressure-Pulse Test for Field Hydraulic Conductivity of Soils: Is the Common Interpretation Method Adequate?

REFERENCE: Chapuis, R. P. and Cazaux, D., "**Pressure-Pulse Test for Field Hydraulic Conductivity of Soils: Is the Usual Interpretation Method Adequate?**", *Evaluation and Remediation of Low Permeability and Dual Porosity Environments, ASTM STP1415,* M. N. Sara and L. G. Everett, Eds., ASTM International, West Conshohocken, PA, 2002.

Abstract: Pressure-pulse tests are performed in boreholes in either impervious rock or clayey formations. According to the usual theory, they give the hydraulic conductivity, *k*, and the storativity, *S*, of the tested material. However, comparative testing programs have shown that the usual interpretation method may give *k* values that are quite different from those given by other methods. It gives also unrepresentative (much too low) values of *S* for the tested formations. Several reasons for the discrepancies are examined. First, the theory came from a heat conduction problem but the mass and energy transfers in a pulse test are quite different from those in the heat conduction problem. Thus the usual interpretation method is derived from equations that do not represent correctly the physical phenomena involved in a pulse test. A correct theory should use equations that consider medium deformation to be partly instantaneous (undrained) and partly delayed (drained) during and after the pulse. This is not the case in the commonly used theory. It should also consider that both the testing system and the formation wall are deformed during the pulse, which is ignored by the usual theory. Besides this theoretical inadequacy, the usual interpretation method is frequently affected by an inaccurate knowledge of the local piezometric level for the test. This level is frequently guessed prior to testing, and this estimate may be incorrect. However, a velocity graph technique can be used to analyze the test data and establish the real piezometric level for the test. Considering the inadequacy of the usual equations and interpretation method, it is proposed to interpret the test data as those of a slug test after having determined the local piezometric level using the velocity graph method. Hvorslev's method is used after introducing an imaginary open tube with an inside diameter that is defined by the volume of injected water associated with the initial pulse. A detailed example is treated where this interpretation method yielded a *k*-value close to that obtained from a constant-head test in the same injection cavity, both values being 50 times lower than the *k*-value derived from the usual superposition method.

Key words: permeability, field, borehole, pulse test, piezometric level

---

[1] Professor, Department CGM, École Polytechnique, P.O. Box 6079, Station CV, Montreal, Quebec, Canada, H3C 3A7

[2] Research Scientist, BRGM, 3 avenue Claude Guillemin, BP 6119 Orleans F, 45061 Orleans, France

Introduction

The pressure pulse test is used to determine the field transmissivity T and field storativity S of impervious formations. According to the standard ASTM D4631 for "Determining Transmissivity and Storativity of Low Permeability Rocks by In Situ Measurements Using Pressure Pulse Technique", this test can be used in a formation having a hydraulic conductivity, k, lower than 10^{-3} Darcy (approximately 10^{-8} m/s). A borehole is drilled into the formation. Sealing plugs or inflatable rubber packers seal each interval of formation to be tested. The packed-off interval is totally filled with water between the two inflated packers (or between the bottom of the hole and a sealing plug). A time delay must be allowed for reaching initial equilibrium of hydraulic head in the soil or rock around the cavity before testing. When the water circuit is closed, a positive or negative pressure pulse is applied to the water confined between the packers, and the water circuit is closed again to register the pressure decay with time. The data of the pressure decay curve are interpreted to calculate the values of T and S.

The pulse test is used for impervious rock formations and for clay deposits that are considered as barriers for waste disposal. Recent results have questioned the capability of the usual equations to give realistic values of T and S. Cazaux (1998) compared 11 different field techniques (constant head, variable head and pulse test) to determine the k value of a homogeneous clay deposit at Montré (France). Ten methods gave values between 10^{-10} and 10^{-9} m/s whereas the pulse test method gave k values lower than 10^{-11} m/s. Chapuis (1998) theoretically examined the commonly accepted equations and questioned their adequacy for slug tests and pulse tests.

In this paper, the two authors have pooled their experience to better assess the capability of the common equations to yield correct estimates of T, S and k for the tested formation.

Usual Solution

The geometry of the problem is shown in Figure 1. It is assumed that the packed-off interval represents the total thickness b of the layer to be tested ($T = kb$) and that the upper and lower horizontal boundaries are fully impervious. The resulting radial symmetry implies that the hydraulic head h depends only on the radial distance r and time t: $h = h(r,t)$ within the ideal material. The inside diameter of the hole is $D = 2\,r_w$. Cooper et al. (1967) proposed a solution after assuming that the unsteady-state problem is described by Fourier's equation

$$\partial^2 h/\partial r^2 + (1/r)\,(\partial h/\partial r) = (S/T)\,(\partial h/\partial t) \qquad \text{for } r > D/2 \tag{1}$$

that has been used extensively to solve pumping test problems in confined aquifers.

The natural hydraulic head in the tested zone, or local piezometric level, is supposed to be known before the test. It may be measured in the small diameter open pipe (Figure 1). However, in formations having a low k value, it may take several weeks to measure it by this method and this is assuming it not to vary during the observation time (Hvorslev 1951). It is faster to obtain it with a data acquisition system when the valves are closed. The pore water pressure in the packed-off interval is registered and the curve of h vs. t is usually extrapolated to estimate the at-rest value of h and thus the local piezometric level.

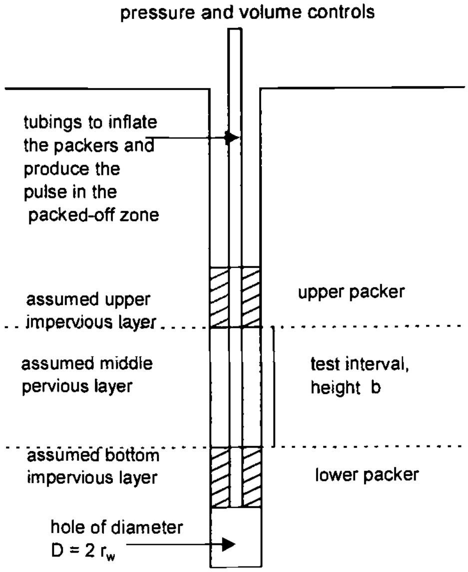

Figure 1 - *Cross-section of the pulse-test problem.*

Using Eq. 1 supposes that the tested formation is fully saturated and linearly elastic. It means also that a change in pore water pressure, Δu_w, is immediately (fraction of a second) and fully transformed into an effective stress transfer, which induces a strain of the solid matrix, without delayed deformation. Thus Eq. 1 does not adequately represent a low-*k* medium. To better represent a low *k*-medium, Eq. 1 should be modified and several terms would no longer be constant as in Eq. 1. For the pulse test, the boundary conditions are

$$h(\infty,t) = 0 \qquad \text{for } t > 0 \tag{2}$$

$$h\,(r_w+0,\,t) = H(t) \qquad \text{for } t > 0 \text{ and } H(t{=}0{+}) = H_i \tag{3}$$

$$h\,(r,t{=}0) = 0 \qquad \text{for } r > r_w \tag{4}$$

where $H(t)$ is the difference in total head between the packed-off cylinder and the tested formation in equilibrium conditions (local piezometric level) at time t, and H_i is the initial H-value at time t=0+, immediately after the pressure pulse.

Between the tested zone and the packed-off interval, the flux continuity was written as (Bredehoeft and Papadopulos,1980)

$$\pi Dbk\,[\partial h(r_w+0,\,t)]/\partial r = V_w C_w \rho_w g\,[\partial h(t)]/\partial t] \tag{5}$$

where V_w is the volume of water in the packed-off interval, C_w is the compressibility of water ($4.4\text{x}10^{10}$ Pa^{-1}), ρ_w is the density of water and g the gravitational acceleration. Here the compressibility of the testing system and the undrained deformation of the medium are ignored. Bredehoeft and Papadopulos (1980) proposed for the pulse test the same type of solution that Cooper et al. (1967) previously proposed for the slug test, namely

$$H(t) / H_i = F(\alpha,\beta) = (8\,\alpha / \pi^2) \int_0^\infty \exp(-\beta u^2/\alpha)\, du / u\, \Delta(u) \tag{6}$$

with:

$$\Delta(u) = [uY_0(u)-2\alpha Y_1(u)]^2 + [uJ_0(u)-2\alpha J_1(u)]^2 \tag{7}$$

$$\alpha = \pi r_w^2 S / V_w C_w \rho_w g \tag{8}$$

$$\beta = \pi k b t / V_w C_w \rho_w g \tag{9}$$

where J_0, J_1, Y_0 and Y_1 are Bessel's functions. Cooper et al. (1967) and Papadopulos et al. (1973) tabulated $F(\alpha,\beta)$ against β for ten values of α from 10^{-1} to 10^{-10} and provided type curves to be matched with experimental data (Figure 2). Bredehoeft and Papadopulos (1980) provided additional values and master curves for α between 0.1 and 10.

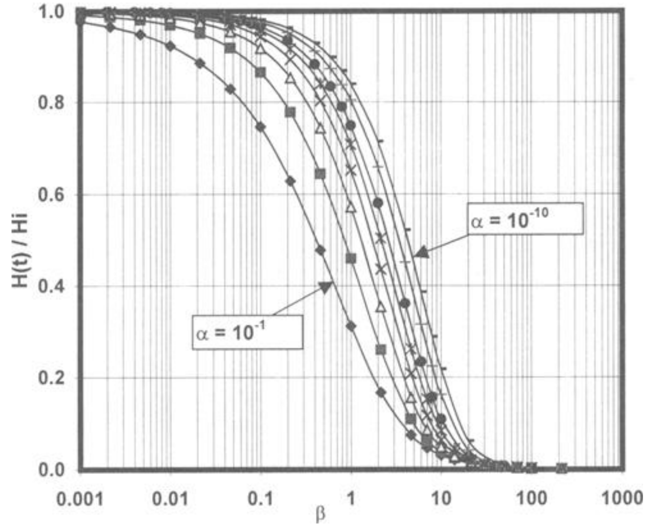

Figure 2 - *Graphs of type curves as proposed by Cooper et al. (1967), Papadopulos et al. (1973), and Bredehoeft and Papadopulos (1980).*

Comparison with the Heat Conduction Problem

Bredehoeft and Papadopulos (1980) derived their solution from an analogy with a heat conduction problem for which Carslaw and Jaeger (1959, pp. 341-342) provided a solution. The heat conduction problem involved "*a cylinder of a metallic conductor surrounded by an infinite medium such as soil or rock of much lower thermal conductivity*" for no contact thermal resistance between the cylinder and the medium. The metal was considered a perfect conductor of heat (i.e. the temperature is uniform within the metallic cylinder). The interest of the problem was then centered on the temperature of the metallic cylinder.

This seems similar to the ideal pulse test case in which the pipe acts as a perfect conductor of water, and it is assumed that there are no skin effects at the contact between the injection zone and the formation. The pulse test problem is also centered on the hydraulic head difference between the injection zone and the formation (at equilibrium).

However, the similarity between the two problems is not total. The pulse test involves a mechanical energy transfer in the formation (initial energy is stored in the packed-off interval and in the deformed formation) coupled to a small mass transfer through the injection zone-formation interface. The heat conduction problem of Carslaw and Jaeger (1959) involves only a thermal energy transfer (initial energy is stored only in the conductive cylinder) and does not involve mass exchange between the hot conductor and the surrounding medium. Thus there are two differences between the heat conduction problem and the pulse test problem. Consequently, by ignoring the deformation of the testing system and that of the medium, by confusing a pure energy transfer with an energy-and-mass transfer, and by using an inadequate Eq. 1, the usual equations of the pulse test do not represent adequately the physical phenomena during the test. This will be demonstrated through an example later.

In addition, Chapuis (1998) noted that Carslaw and Jaeger (1959) defined α as "twice the ratio of the heat capacity of an equivalent volume of the medium to that of the perfect conductor" and used a factor 4 instead of 8 in their equation equivalent to Eq. 6. As a result, the use of Eq. 6 with its coefficient 8 implies that the real α is the ratio of the storativity of an equivalent volume of the medium to that of the (pipe+packer) system

$$\text{real } \alpha = S\, r_w^2 \,/\, b\, r_w^2 S_{\text{system}} = bS_s r_w^2 \,/\, b r_w^2 S_{\text{system}} = S_s \,/\, S_{\text{system}} \tag{10}$$

where S_s is the specific storativity of the tested material ($S_s = S/b$) and S_{system} is the storativity of the complete test system. This definition of α (Eq. 10) differs from that of Eq. 8 proposed by Bredehoeft and Papadopulos (1980) on two counts. First, the total volume of the cavity including that of any pipe or transducer should be used instead of the parameter V_w for the volume of pulsed water. Second, the compressibility of the complete test system, S_{system}, must replace that of water in Eq. 8, as already pointed out by Neuzil (1982). Similarly, the real value of β (according to the solution of Carslaw and Jaeger, 1959) is

$$\text{real } \beta = \pi k b t \,/\, b\, r_w^2 S_{\text{system}} \tag{11}$$

and consequently

$$\text{real } k = k\alpha \text{ (from curve fitting of Eqs. 8-9)} \,/\, (\text{real } \alpha) \tag{12}$$

The value of S_{system} is derived from the compressibility of the packers, that of air trapped below and that of the inside tubing and equipment. The system compressibility is usually higher than that of water alone as considered in Eqs. 8-9. As a result, the real values of α and β (Eqs. 10-11) are usually higher than those calculated using Eqs. 8-9. A practical consequence is that the usual Eq. 9 produces a k value that is smaller than the real k value of the tested formation. Consequently, a correct evaluation of the system compressibility is mandatory to get a fair estimate of α and β, and thus of k and S.

The storativity, S_{system}, or compressibility, C_{system}, of the (pipe+packer) system, must be established before testing. An approximation would be to neglect the pipe (and screen if one is used) compressibility, and to consider only the packer compressibility as measured after installation in a closed thick-wall (rigid) pipe in laboratory conditions. A refinement would be to use elasticity equations to calculate the volumetric deformation due to the pipe and the screen, and to take it into account. This approximation is deemed acceptable for field conditions when a device is provided to purge any air bubble that may be trapped below the upper packer.

In the field, the amount of water dV_w entering the packed-off cavity during a pressure pulse, dp, may be registered. It yields an observed compressibility, C_{obs}

$$C_{obs} = (dV_w / V_w) / dp \qquad (13)$$

It has been suggested that C_{obs} replace C_w in Eqs. 8-9 (e.g. D4631). This suggestion does not consider that dV_w includes the undrained (but not totally instantaneous) deformation of the medium (soil or rock), dV_m. Only a small portion of dV_w is due to the testing system deformation, dV_{system}. Thus, C_{obs}, as provided by Eq. 13, overestimates S_{system}, because

$$C_{obs} = (dV_m + dV_{system}) / V_w\, dp = C_m + C_{system} \qquad (14)$$

The medium compressibility, C_m, may be determined from the mechanical interpretation of the test in terms of deformation vs. storativity and/or compressibility, as shown below.

Storativity and Compressibility

The specific storativity, S_s, is related to the compressibilities of water and solid matrix

$$S_s = S/b = \gamma_w(nE_w^{-1} + E_s^{-1}) = n(4.7\text{x}10^{-6}) + \gamma_w E_s^{-1} \approx \gamma_w/E_s \qquad (15)$$

where n is the material porosity, γ_w is the unit weight of water ($\gamma_w = g\rho_w$, kN/m^3), E_w and E_s (kN/m^2 or kPa) are the elastic moduli of water and solid matrix respectively (Jacob 1950). Frequently, E_w^{-1} (or C_w) is negligible before E_s^{-1}.

During the pressure pulse, it is assumed that there is no dissipation of pore water pressure. As a result, dV_w is measured by a procedure similar to an undrained pressuremeter test in an impervious soil. The portion due to the volumetric undrained deformation of the medium, dV_m, may be evaluated from the solutions to the problem of radial expansion of a cylindrical cavity in an infinite medium. Since the usual pulse test equations assume linear and instantaneous elasticity, the expansion solution to be used is that of Lamé (1852). It relates the dilation or contraction dV_m of the medium to the initial volume V_w of the packed-off interval, the stress increase, $\Delta\sigma$, and the medium (undrained) elastic modulus, E_u

$$dV_m = 2(1+\nu)\, V_w\, \Delta\sigma / E_u \qquad (16)$$

with

$$V_w = b\, \pi D^2/4 = b\, \pi r_w^2 \qquad (17)$$

It is assumed that the Poisson's ratio $\nu = 0.5$ in undrained soils. Values of E_u range from 2.5 to 25 MPa for clayey soils and exceed 100 MPa for rocks (Baguelin et al. 1978). For the test data that will be analyzed in detail, the influence of the medium deformability, C_m, will be assessed and compared to the measured value of C_{obs}.

Be Sure to Know the Local Piezometric Level

The usual Equations 1-7 assume that the piezometric level for the test is known before testing. Considering the long time it takes for hydraulic heads to come back to equilibrium in an impervious formation around a borehole, it is likely that the piezometric level is not known for sure. If this is the case, then the interpretation of the test data will be done with an estimated piezometric level, which in turn will yield unreliable estimates of T and S.

The usual way to interpret the data of a pulse test is to superimpose them on the type curves of Figure 2. However, such type curves cannot be used to detect whether or not the assumed piezometric level is correct. Chapuis (1998) proposed to redraw the common type curves as velocity graphs before the superimposition in order to get the right interpretation including the determination of the local piezometric level from the test data. A normalized total head difference, H^*, is defined as

$$H^* = H / H_i = H(t) / H(t{=}0+) = \Delta u_w(t) / \Delta u_w\,(t{=}0+) \tag{18}$$

where $\Delta u_w\,(t)$ is the difference in total head between the packed-off cylinder and the tested ground in equilibrium conditions (local piezometric level) at time t, and $\Delta u_w\,(t{=}0+)$ is its value at time $t{=}0+$, immediately after pressure application. Then a normalized head drop or pressure drop velocity, v^*, is defined as

$$v^* = (\Delta H/\Delta t) / (\Delta H/\Delta t)_{95} \tag{19}$$

where $(\Delta H/\Delta t)_{95}$ is the head drop velocity at a time corresponding to $H^* = 0.95$. Taking 0.95 instead of 1.00 is preferred for practical reasons because initial readings are frequently affected by inaccuracy in initial time and phenomena such as irreversible wall deformation. The velocity graphs of pulse test data that would follow the common theory (Eqs. 1-7), and its assumptions, are shown in Figure 3. The limiting straight line corresponds to Hvorslev's method ($\alpha < 10^{-10}$ or $S \approx 0$) in which the influence of aquifer deformation is neglected and Laplace's equation is used to solve the problem instead of Fourier's equation (Eq. 1).

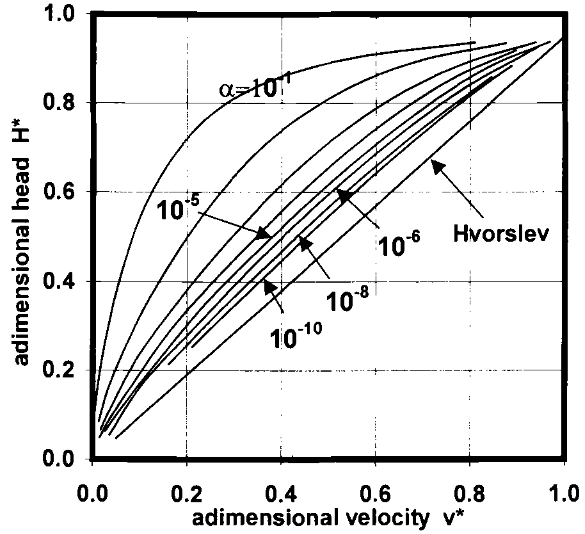

Figure 3 - *Velocity type graphs (Chapuis 1998).*

The interpretation of pulse test data proceeds as follows using Figure 3 (Chapuis 1998):

(a) Draw the experimental velocity graph of the test where $y = H(t)$ and $x = \Delta H/\Delta t$.

(b) The extrapolation of the experimental data towards the H-axis gives an H_0 value for a null velocity ($\Delta H/\Delta t = 0$). According to Darcy's law the H_0-value is zero when the piezometric level is correctly evaluated. If the experimental H_0 value is not zero, then the assumed piezometric level is incorrect and the H_0-value corresponds to the difference between the incorrect and correct piezometric levels.

(c) Compute the actual head differences as being the measured test values minus the correction H_0 and estimate the velocity $(\Delta H/\Delta t)_{95}$ that corresponds to 95% of the actual initial head (or pressure) difference.

(d) Compute the normalized values H^* and v^* with Eqs. 18-19.

(e) Superimpose the experimental graph over the theoretical graphs of Figure 3.

(f) The best match provides the α-value and then the values of k and S can be obtained using Eqs. 10-11 instead of erroneous Eqs. 8-9.

Interpretation of Field Data - Example

A pulse test was performed at the bottom of a deep excavation in overconsolidated clay at Vaivre (France). It is used here to compare several interpretation methods. The tested interval had a diameter $D = 2r_w = 6.3$ cm and a length $L = b = 1.00$ m. A small pulse $\Delta h = 0.23$ m ($\Delta u_w = 2.25$ kPa) corresponded to an injected volume $dV_w = 0.4\ \text{cm}^3$ that deformed the testing system and the walls of the injection cavity during the pulse duration (1-2 s). Consequently, the real value of S_{system} is unknown for this test. The local piezometric level was evaluated by registering and extrapolating the curve of the pore water pressure versus time. For the test, the pressure pulse lasted 1 to 2 seconds and produced an initial increase in hydraulic head of 156 cm (pore water pressure increase of 15.56 kPa).

First Estimate of Clay Compressibility

According to Baguelin et al. (1978) the usual values of undrained modulus for clays, E_u, range between 2.5 to 25 MPa. Thus a first estimate for the cavity deformation dV_m during the pulse of $\Delta u_w = 2.25$ kPa is $dV_m = 0.84$ to $8.4\ \text{cm}^3$ using Eq. 16. Since the registered dV_w is only $0.4\ \text{cm}^3$, it is confirmed that dV_{system} is small before dV_m in Eq. 14. Then dV_m is close to $0.4\ \text{cm}^3$, which gives for the tested clay an undrained modulus $E_u = 52.6$ MPa. This value is above the usual range and it may be explained by the clay overconsolidation. Then the value of E_s (drained modulus) to be used in Eq. 15 is lower than 52.6 MPa, which means that S_s for this clay (Eq. 15) is estimated as higher than $1.86 \times 10^{-4}\ \text{m}^{-1}$.

The value of C_{obs} for this test is higher than C_w. From Eq. 13, $C_{\text{obs}} = (0.4\ \text{cm}^3) / [(100 \times 3.14 \times 3.15^2\ \text{cm}^3) \times 2250\ \text{Pa}] = 5.7 \times 10^{-8}\ \text{Pa}^{-1}$ whereas $C_w = 4.7 \times 10^{-10}\ \text{Pa}^{-1}$. Consequently, after replacing C_w by C_{obs} in Eq. 8, one gets $\alpha = S \times 1.79 \times 10^3$, thus α is expected to be in the range 0.1-1.0 since $b = 1$ m and S_s is in the range of 10^{-3} to 10^{-4} as usually for most clays.

Common Interpretation

The conventional curve of the ratio $H(t)/H_i$ versus time is superimposed over the common type curves in Figure 4. The test data appear in Table 1. The best visual fit is obtained for $\alpha = 10^{-3}$, which is fairly low when compared to the previous estimate of α. A common point of the superposed graphs is taken as $\beta = 1$ or $t = 0.05$ min $= 3$ s, which gives from the curve fitting (and C_{obs} instead of C_w): $k = 1.85 \times 10^{-7}$ m/s and $S = 5.6 \times 10^{-7}$. Consequently, the usual interpretation method, using C_{obs} instead of C_w, yields $S_s = 5.6 \times 10^{-7}$, which is significantly lower than 10^{-4} to 10^{-3} as derived from usual mechanical tests for measuring clay compressibility. The discrepancy between these S_s values may be viewed as a result of confusing C_{obs} with C_{system} (see Eq. 14).

Table 1 – *Data of the presented example where* $H^*_{95} = 148$ *cm and* $v^*_{95} = 5.5$ *cm/min.*

time *t* min	assumed *H* cm	*H / Hi* -------	*dH/dt* cm/min	*v** --
0	156.0	1.000	-----	------
0.5	152.3	0.976	7.40	------
1	149.5	0.958	5.60	1.018
2	144.2	0.924	5.30	0.964
4	135.1	0.866	4.55	0.827
8	119.9	0.769	3.80	0.691
12	108.0	0.692	2.98	0.541
16	96.7	0.620	2.83	0.514
20	87.9	0.563	2.20	0.400
25	78.3	0.502	1.92	0.349
30	71.0	0.455	1.46	0.265
35	64.9	0.416	1.22	0.222

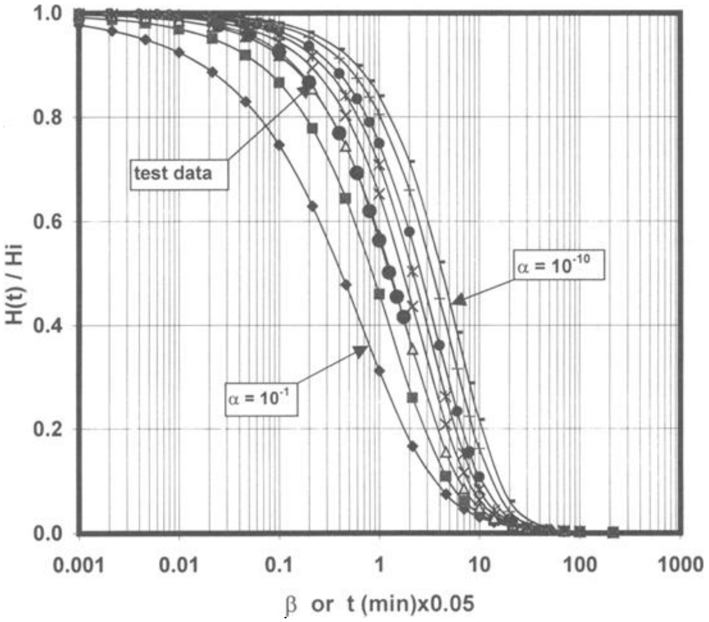

Figure 4 - *Field data of test SK7 (Vaivre, France) superimposed on common type curves. It is assumed that the piezometric level for the test was correctly assessed. The best visual fit gives an α-value close to* 10^{-3}*, and then k =* 1.85×10^{-7} *m/s and S =* 5.6×10^{-7}.

Proposed Interpretation with the Velocity Graph

The velocity graph of this test (Figure 5) is close to a straight-line: it means that α has a much lower value than 10^{-3} as derived from Figure 4. In addition, the extrapolated curved graph indicates that the estimated piezometric level was wrong by $H^*_0 = 0.20$ or $H_0 = 31.2$ cm. This error was used to get the real values of $H = H_{assumed} - H_0$, draw the adimensional velocity graph and superimpose it on the type graphs (Figure 6). The value of α is now close to 10^{-9} instead of the 10^{-3} obtained using the common interpretation method. When superimposed over the usual type graphs (Figure 7), the data fall on the type curve of $\alpha = 10^{-9}$. A common point of the superposed graphs is $\beta = 1$ or $t = 0.23$ min = 13.8 s, which gives from the curve fitting (and using C_{obs} instead of C_w): $k = 4.0 \times 10^{-8}$ m/s and $S = S_s = 5.6 \times 10^{-13}$. This S_s value is much lower than the usual S_s values for clays (10^{-4} to 10^{-3}). Here again, the large discrepancy between these S_s values may be viewed as a result of the confusion of C_{obs} with C_{system} (see Eq. 14) and as a result of the inadequacy of the usual equations to represent the physical phenomena of the pulse test.

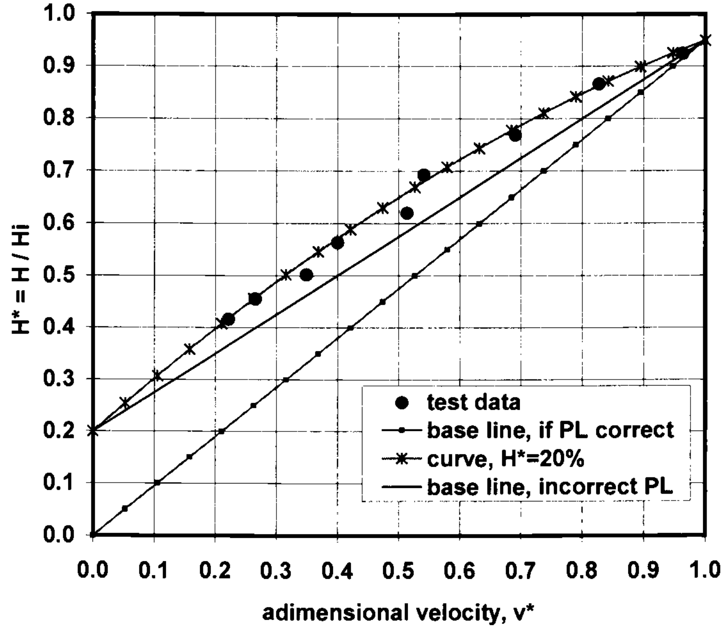

Figure 5 - *Velocity graph of field data of test SK7 (PL = piezometric level).*

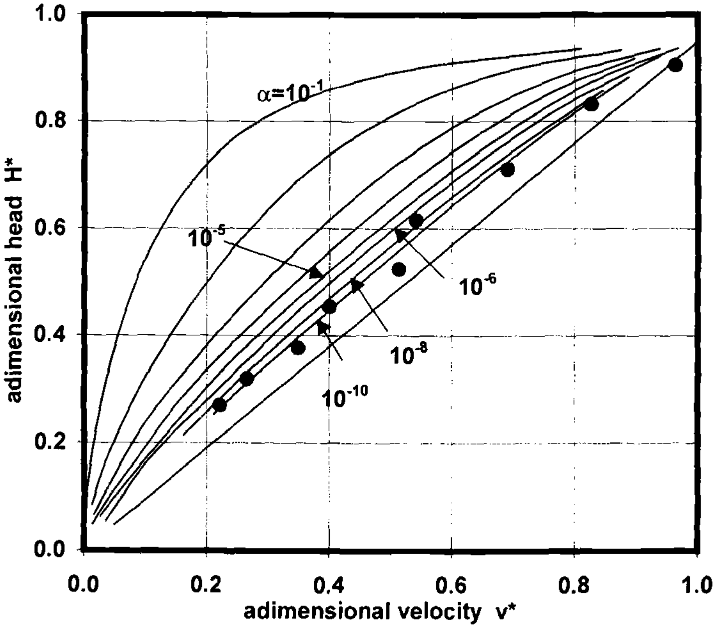

Figure 6 - *Superposition of the field data to the adimensional velocity type graphs.*

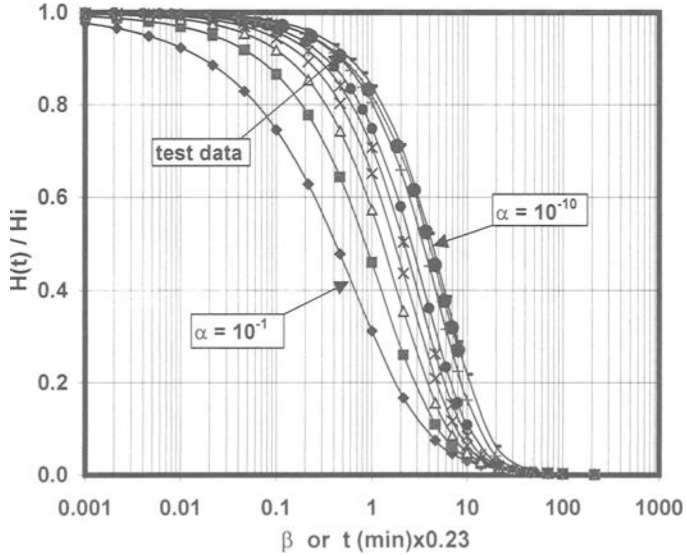

Figure 7 - *Field data of test SK7 (Vaivre, France) superimposed on common type curves after correction for the wrong estimate of the piezometric level. The best visual fit is for* α *close to* 10^{-9}*, and then* $k = 4.0 \times 10^{-8}$ *m/s and* $S = 5.6 \times 10^{-13}$.

Using directly the original solution with Eqs. 8-9 with C_w would have given $k = 3.3\times10^{-10}$ m/s and $S = 4.6 \times 10^{-15}$. Thus, the suggestion to use C_{obs} instead of C_w makes a large difference for k and S. However, if the usual equations are supposed to be correct, then from a mechanical point of view, instead of C_{obs} one should use the value of C_{system} that is lower than C_{obs} (Eq. 14). As a result, using Eq. 9 with C_{system} gives a k value that is lower than that derived from using Eq. 9 with C_{obs}. For example, if $C_{system} = 0.01\ C_{obs}$ then the superposition would give a k value of 4×10^{-10} m/s instead of 4.0×10^{-8} m/s. Thus, there is a serious margin of ignorance about the k value derived from the usual equations. Such an approximation for k simply confirms the theoretical conclusion that the usual equations for the pulse test do not represent adequately the physical phenomena.

In addition, Eq. 8 with C_{obs} provided for the tested clay an S_s value that is unrealistic by several orders of magnitude. Replacing C_{obs} with C_{system} would yield an even more unrealistic S_s value. To get a realistic S_s value, according to Eq. 8, C_{system} should be higher than C_{obs} by several orders of magnitude, but this is mechanically impossible. Such a dead end for S_s is another confirmation that the usual equations for the pulse test are not an adequate representation of the physical phenomena.

Alternative Interpretation Method

In the previous sections it has been shown that the usual test equations have theoretical and practical limitations. For interpreting the pulse test data, an alternative method may be used. The pulse corresponds to an increase of hydraulic head Δh and an increase of volume of water dV_w that becomes available for injection into the packed-off interval. The volume dV_w corresponds to the volume of water rising by Δh inside an imaginary small pipe of diameter d (radius r_c) such as

$$dV_w = \Delta h\ S_{inj} = \Delta h\ \pi d^2 / 4 = \Delta h\ \pi r_c^2 \tag{20}$$

Consequently, the test data may be analyzed as those of a slug test performed with a small pipe of diameter d. This suggestion is similar to that of Bredehoeft and Papadopulos (1980) who used C_w to calculate this diameter d, instead of using C_{obs} as proposed here.

Three independent proofs (mathematical, physical and numerical analyses) were recently provided that the medium storativity has a negligible influence during a slug test (Chapuis, 1998). Consequently, it is proposed to treat the data as those of a Hvorslev's problem after having determined the real piezometric level for the test (Chapuis et al., 1981; Chapuis, 1988; Chapuis and Sabourin, 1989) using the method of the velocity graph.

In Hvorslev's solution (the equivalent of Newton's cooling law, Chapuis 1998) the flow obeys Laplace's equation (Eq. 1 without second member). The mass conservation equation, at the interface between the soil and the packed-off interval, relates the flow into the soil (Q_{soil}, Darcy's law) to the flowrate in the pipe (Q_{inj}). It is written

$$Q_{inj} = -S_{inj}\ (dH/dt) = Q_{soil} = ckH \tag{21}$$

where c is the shape factor of the injection zone, H is the applied difference in hydraulic head. In the test, Q_{inj} is the product of the internal cross-section, S_{inj} of the injection pipe by the water velocity, dH/dt, in this pipe. Rearranging Eq. 21 gives

$$dH/dt = -kcH / S_{inj} \tag{22}$$

in which the variables may be separated

$$dH/H = -(kc/S_{inj})\,dt \tag{23}$$

Integration of Eq. 23 yields the general equation of Hvorslev (1951)

$$\ln(H_1/H_2) = -(kc/S_{inj})(t_1-t_2) = -kC(t_1-t_2) \tag{24}$$

where H_1 and H_2 are the differences in total heads at times t_1 and t_2 respectively and $C=c/S_{inj}$. Here the velocity graph method corresponds to Eq. 22 and graphically to the limiting straight line of Figure 3.

In the case of the previously analyzed test, Eq. 20 gives $d = 0.149$ cm which corresponds to a small tube of internal diameter close to 1.5 mm. The injection zone of diameter $D = 6.3$ cm and length $L = 100$ cm has a shape factor $c = 181.71$ cm that is given by the so-called ellipsoid approximation (Chapuis 1998)

$$c = 2\pi L / \ln[(L/D) + (1 + L^2/D^2)^{1/2}] \approx 2\pi L / \ln(2L/D) \quad \text{when } L/D \geq 4 \tag{25}$$

For assumed H values between 156 and 140 cm, the velocity graph (Figure 9) is curved. Its curvature lasts only a few minutes and may be due to either incomplete saturation (e.g. Chapuis 1999) or delayed (partly undrained and partly drained) wall deformation. For assumed H values lower than 140 cm the velocity graph becomes a straight line and indicates a piezometric error $H_0 = 42.5$ cm. With a poorly estimated piezometric level, all H values were erroneous and the graph of $\ln H$ versus time t was curved (Figure 8). After correcting the H values for the piezometric error, the graph of $\ln(H-H_0)$ becomes a straight line (Figure 10). The velocity graph and the semi-log graph give the same k value of 7.3×10^{-10} m/s, which is 50 times lower than that derived with the superposition method using C_{obs} in Eqs. 8-9.

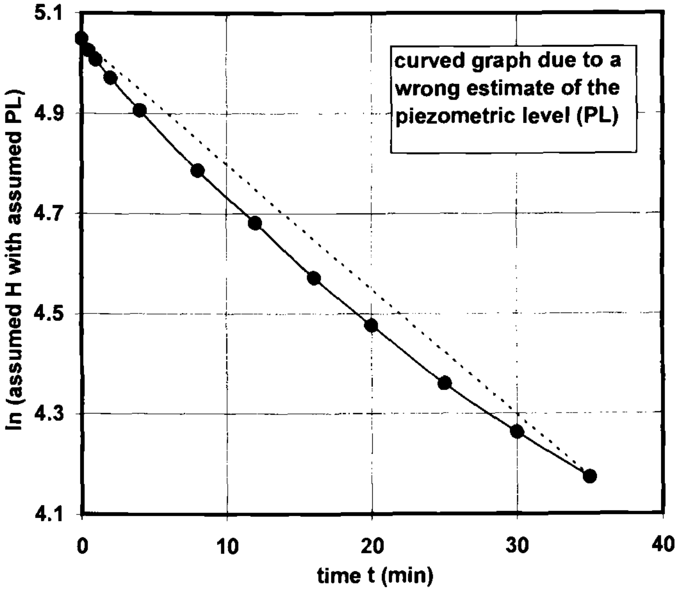

Figure 8 - *Graph of assumed H versus time t.*

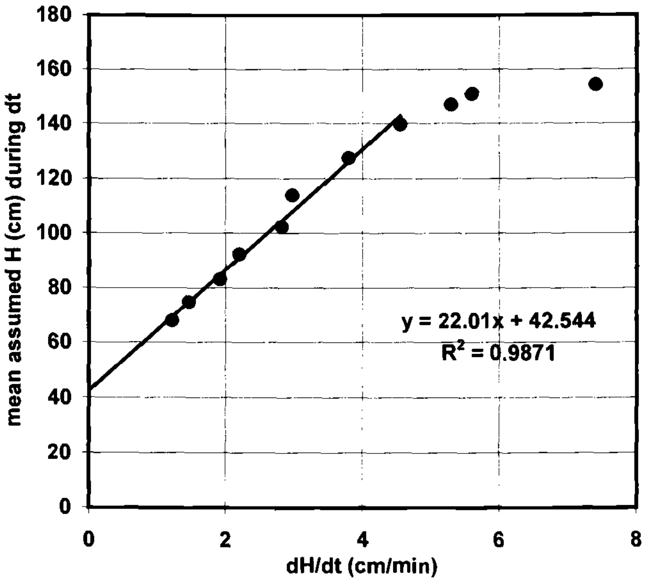

Figure 9 – *Velocity graph indicating that the estimated piezometric level is wrong by H_0 =42.5 cm.*

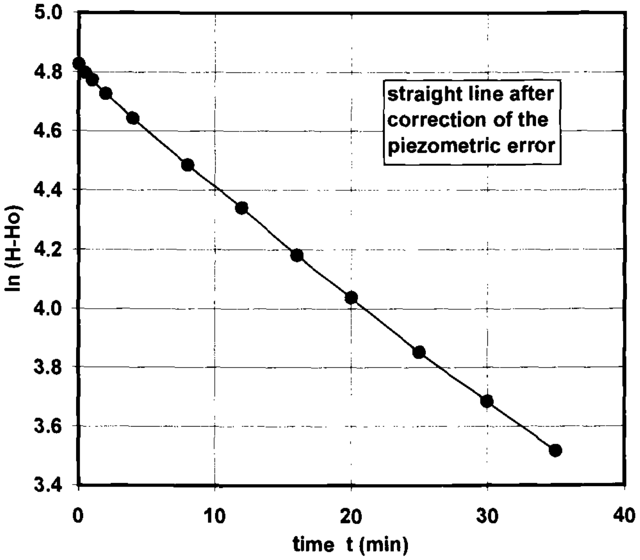

Figure 10 - *Graph of real H = assumed H - H_0 versus t after correction for the wrongly estimated piezometric level.*

In the same hole, a constant-head permeability test was performed. This test had a much longer duration, three days, and the injected flowrate slowly declined. The k value given by this test was 6.5 x 10^{-10} m/s. This is very close to the value of 7.3 x 10^{-10} m/s obtained from the pulse test data interpreted as a slug test. Again, these values are approximately 50 times lower than the k value derived with the usual superposition method using C_{obs}.

Discussion and Conclusion

It was shown that the pulse test solution started with Eq. 1, in which terms should be added or modified to correctly represent the behavior of a low-permeability medium. Then it was shown that the usual pulse test solution was copied from the solution for a heat-conduction problem although the two problems differ in many respects. As a result, by ignoring the deformation of the testing system and that of the medium, by confusing a pure energy transfer with an energy-and-mass transfer, and by using a too simplified Eq. 1, the usual equations for the pulse test do not represent adequately the physical phenomena during the pulse test.

The consequences of this poor representation can be seen in the results of the accompanying superposition method. First, it gives a k value that may be very different from the k values given by other testing methods (Cazaux, 1998). Second, it gives a S_s value that is much lower (by several orders of magnitude) than the S_s values obtained from purely mechanical tests.

The data of a pulse test in an overconsolidated clay deposit have been used to illustrate the inadequacy of the usual method (Table 2). It was also shown that the small water volume intake due to the pulse can be used to obtain the modulus of the tested clay and then its S_s value. This procedure provided a realistic S_s value as compared to the usual values derived from mechanical tests in geotechnical engineering. For comparison, the usual equations for the pulse test gave for S_s a value that was too low by up to eight orders of magnitude.

Table 2 – *Calculated k and S by the different methods used for the example data set*

method of interpretation	pressure-pulse test		independent references	
	k (m/s)	S (--)	k (m/s)[1]	S (--)[2]
common method				
with C_{obs}	1.85×10^{-7}	5.6×10^{-7}	6.5×10^{-10}	$\approx1.0\times10^{-4}$
common method plus velocity graph for piezometric level				
with C_{obs}	4.0×10^{-8}	5.6×10^{-13}	6.5×10^{-10}	$\approx1.0\times10^{-4}$
with C_w	3.3×10^{-8}	4.6×10^{-15}	6.5×10^{-10}	$\approx1.0\times10^{-4}$
proposed method with velocity graph				
with C_{obs}	7.3×10^{-10}	1.86×10^{-4}	6.5×10^{-10}	$\approx1.0\times10^{-4}$

[1] constant-head permeability test in the same piezometer
[2] estimate from pressuremeter tests in stiff clay

In addition, the usual superposition method to interpret the test data cannot be used to check whether the assumed piezometric level for the test is the correct one. A reliable graphical method is provided here: it uses the test data to plot a "velocity graph" and obtain the correct piezometric level for the tested formation interval.

During a pulse test, it is usually observed that the experimental velocity-graph is curved at the beginning of the test and perfectly straight afterwards. However, the graph of $ln\ H$ vs. t is always close to a straight line when the correct H values are used (after the piezometric level has been correctly assessed using the velocity graph method). The initial curvature of the velocity graph is due physically to partial saturation and delayed deformation (partly undrained and partly drained) of the wall of the cavity after the initial pulse. Frequently, after drilling and cleaning the borehole some time is allowed for any induced pore water pressure to dissipate. The return to pore water pressure equilibrium, however, may be a very long (several weeks) process in a low-permeability medium. In addition, after drilling and before testing, the wall of the hole in low-k soils moves inward. During testing, it moves outwards, mainly at the beginning of the test. Such (mostly) undrained movement is not considered in the usual equations. However, its effect is to curve the initial part of the velocity graph in the same way as observed. Similarly, if the tested medium is somewhat unsaturated before testing (e.g. compacted clay liner), the effect of unsaturation is also to curve the initial part of the velocity graph in the same way (Chapuis 1999).

Considering the inadequacy of the usual equations, it was proposed to interpret the pulse test using Hvorslev's method, after having determined the real piezometric level using the velocity graph method. For the example of this paper, the proposed interpretation method gave a k value close to that obtained by a constant-head test in the same injection cavity, both values being 50 times lower than the k value derived from the usual interpretation method for a slug-test. This confirmed that this usual interpretation method is highly questionable since it provided both an erroneous k value and an unrealistic S value.

Acknowledgments

This paper is a result of a research program to improve the reliability of permeability tests and aquifer tests. The Natural Sciences and Engineering Council of Canada and the French Environmental Agency (ADEME) sponsored these studies. Their financial assistance are gratefully acknowledged.

References

Baguelin, F., Jézéquel, J.F., and Shields, D.H., 1978, *The Pressuremeter and Foundation Engineering,* Trans-Tech. Publications, 617 p.

Bredehoeft, J.D., and Papadopulos, S.S., 1980, "A Method for Determining the Hydraulic Properties of Tight Formations", *Water Resources Research,* 16, pp. 233-238.

Carslaw, H.S., and Jaeger, J.C., 1959, *Conduction of Heat in Solids,* 2nd Edition, Oxford University Press, Amen House, London, U.K.

Cazaux, D. 1998. *In Situ Measurement and Control of Permeability of Materials Used in Hydraulic Barriers for Environmental Protection. State-of-the-Art and Developments (in French),* Ph.D. Thesis, INSA, Lyon, France, 335 p.

Chapuis, R.P., 1988, "Determining whether Wells and Piezometers Give Water Levels or Piezometric Levels", *In Ground Water Contamination, Field Methods*, STP 963, pp.162-171, American Society for Testing and Materials, Philadelphia, Pa.

Chapuis, R.P., 1998, "Overdamped Slug Test in Monitoring Wells: Review of Interpretation Methods with Mathematical, Physical and Numerical Analysis of Storativity Influence", *Canadian Geotechnical Journal*, 35(5), pp. 697-719.

Chapuis, R.P., 1999, "Borehole Variable-Head Permeability Tests in Compacted Clay Liners and Covers", *Canadian Geotechnical Journal*, 36(1), pp. 39-51.

Chapuis, R.P., and Sabourin, L., 1989, "Effects of Installation of Piezometers and Wells on Groundwater Characteristics and Measurements", *Canadian Geotechnical Journal*, 26(4), pp. 604-613.

Chapuis, R.P., Paré, J.J., and Lavallée, J.G.,1981, "In Situ Variable Head Permeability Tests (in French)", *Proceedings, Xth International Conference on Soil Mechanics and Foundation Engineering*, Stockholm, vol.1, pp.401-406.

Cooper H.H. Jr., Bredehoeft, J.D., and Papadopulos, I.S., 1967, "Response of a Finite-Diameter Well to an Instantaneous Change of Water", *Water Resources Research*, 3(1), pp. 263-269.

Hvorslev, M.J., 1951, *Time-Lag and Soil Permeability in Ground Water Observations, Bulletin 36*, U.S. Army Engineering Waterways Experimental Station, Vicksburg, Miss.

Jacob, C.E., 1950, "Flow of Ground Water", *In Engineering Hydraulics*, Proceedings of the 4th Hydraulic Conference, John Wiley & Sons, New York, N.Y.

Lamé, G., 1852, *Leçons sur la théorie mathématique d'élasticité des corps solides (in French)*. Bachelier, Paris.

Neuzil, C.E., 1982, "On Conducting the Modified "Slug Test" in Tight Formations", *Water Resources Research*, 18, pp. 439-441.

Papadopulos, I.S., Bredehoeft, J.D., and Cooper, H.H.,1973, "On the Analysis of Slug Test Data", *Water Resources Research*, 9(4), pp.1087-1089.

Ming Zhang,[1] Manabu Takahashi,[1] Roger H. Morin,[2] Hidenori Endo,[1] and Tetsuro Esaki[3]

Determining the Hydraulic Properties of Saturated, Low-Permeability Geological Materials in the Laboratory: Advances in Theory and Practice

Reference: Zhang, M., Takahashi, M., Morin, R. H., Endo, H., and Esaki, T., **"Determining the Hydraulic Properties of Saturated, Low-Permeability Geological Materials in the Laboratory: Advances in Theory and Practice,"** *Evaluation and Remediation of Low Permeability and Dual Porosity Environments, ASTM STP 1415,* M. N. Sara and L. G. Everett, Eds., ASTM International, West Conshohocken, PA, 2002.

Abstract: The accurate hydraulic characterization of low-permeability subsurface environments has important practical significance. In order to examine this issue from the perspective of laboratory-based approaches, we review some recent advancements in the theoretical analyses of three different laboratory techniques specifically applied to low-permeability geologic materials: constant-head, constant flow-rate and transient-pulse permeability tests. Some potential strategies for effectively decreasing the time required to confidently estimate the permeability of these materials are presented. In addition, a new and versatile laboratory system is introduced that can implement any of these three test methods while simultaneously subjecting a specimen to high confining pressures and pore pressures, thereby simulating *in situ* conditions at great depths. The capabilities and advantages of this innovative system are demonstrated using experimental data derived from Shirahama sandstone and Inada granite, two rock types widely encountered in Japan.

Keywords: low-permeability, specific storage, hydraulic gradient, constant head, constant flow rate, transient pulse, laboratory permeability tests, geologic materials

Introduction

Laboratory testing of representative specimens has been a very useful and widely adopted approach for characterizing the physical properties of geological materials. One of the particular challenges in geotechnical/geoenvironmental laboratory testing is the accurate determination of the hydraulic properties of low-permeability geological materials such as clays and intact crystalline rocks. These materials are now being

---

[1] Senior Researcher, Research Center for Deep Geological Environments, AIST, Higashi 1-1-1, Tsukuba, Ibaraki 305-8567, Japan.

[2] Geophysicist, United States Geological Survey, Mail Stop 403, Denver Federal Center, Denver, Colorado 80225, U. S. A.

[3] Professor, Faculty of Engineering, Kyushu University, Hakozaki 6-10-1, Higashi-ku, Fukuoka 812-8581, Japan.

scrutinized in increasing detail because of their importance in retarding the transport of hazardous wastes (e.g., Hanor 1993), including radioactive nuclear wastes that are disposed or stored underground (e.g., Moore et al. 1986). The hydraulic properties of low-permeability geological media also have implications in the recovery of natural gas from tight gas sands (Lin et al. 1986), the storage of oil and LP gas, compressed air energy storage (Lien et al. 1987), the generation of abnormal subsurface fluid pressures (Neuzil 1995, Ge and Garven 1992), and the propagation of seismic energy (Rojstaczer et al. 1994, Roeloffs 1998).

In general, any of four types of laboratory techniques are commonly employed for measuring the permeability of geological materials: the constant-head, falling-head (D 5084, JSF T 311-1990), constant flow-rate (Olsen 1966, Olsen et al. 1988), and transient-pulse permeability tests (Brace et al. 1968, Hsieh et al. 1981, Neuzil et al. 1981). The first two of these conventional methods estimate the permeability of a saturated specimen by directly measuring induced flow rates under a constant or quasi-constant hydraulic gradient. However, these flow rates are too slow to monitor reliably with common fluid-volume measurement devices when permeabilities are very low (Zhang et al. 1998a). The latter two methods estimate the permeability of a saturated specimen by measuring time-dependent variations of differential hydraulic head across the entire length of the specimen. Although these latter techniques are thought to be much faster for testing low-permeability specimens, a substantial period of time, perhaps up to several tens of hours, can still be required for testing specimens having very low permeabilities (Zhang et al. 1997, Trimmer 1982).

In order to determine low permeabilities both rapidly and reliably in the laboratory, a systematic evaluation of both theories and experimental approaches has been performed (Esaki et al. 1996, Zhang et al. 1997, 1998a, 2000a, 2000b). In this paper, we review some recent advancements in the theoretical analyses of three laboratory techniques: constant-head, constant flow-rate and transient-pulse permeability tests. Discussions concerning falling-head permeability tests are not considered because these may be regarded as a special case of a transient-pulse permeability test (Zhang et al. 1998b). Some potential strategies for effectively decreasing the time required to confidently measure the permeability of hydraulically-tight specimens are also presented. Finally, a new and versatile laboratory system is introduced that can implement any of these three test methods while simultaneously exposing the specimen to high confining pressures and pore pressures, thereby simulating *in situ* conditions at great depths. The capabilities and advantages of this new system are demonstrated using experimental data derived from Shirahama sandstone and Inada granite, two rock types widely encountered in Japan.

Laboratory Permeability Tests and Theories

Theoretical Formulations

Schematic diagrams summarizing initial and boundary conditions for the constant-head, the constant flow-rate, and the transient-pulse permeability tests are depicted in (Table 1). One-dimensional transient flow of a compressible fluid through a saturated porous and compressive medium can be described by the following Equation (1), which combines the principle of conservation of fluid mass in a deformable medium and Darcy's law for laminar flow through a hydraulically isotropic matrix. The validity of applying these principles to these laboratory analyses has been theoretically verified by Fox and Zhu (1999).

Table 1-*Schematic diagrams, initial and boundary conditions for laboratory permeability tests.*

Test method	Constant-head	Constant flow-rate	Transient-pulse
Schematic diagrams	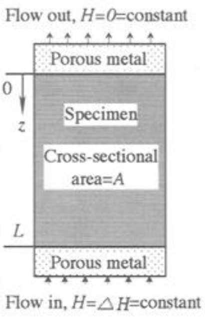	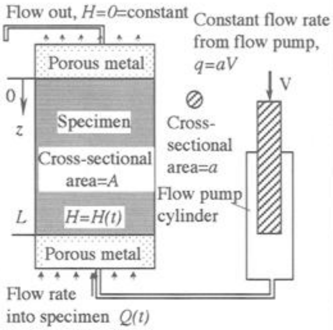	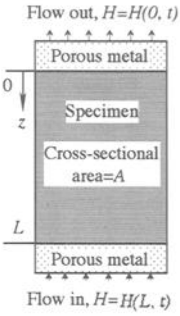
Initial condition	$H(z,0)=0$ at $0<z\le L$	$H(z,0)=0$ at $0<z\le L$	$H(z,0)=0$ at $0<z\le L$
Boundary condition	$H=0$ at $z=0$ $H=\Delta H$ at $z=L$	$H=0$ at $z=0$ $\frac{\partial H}{\partial z}=\frac{1}{KA}\left(q-C_e\frac{\partial H}{\partial t}\right)$ at $z=L$	$\frac{S_d}{KA}\frac{\partial H}{\partial t}-\frac{\partial H}{\partial z}=0$ at $z=0$ $\frac{S_u}{KA}\frac{\partial H}{\partial t}+\frac{\partial H}{\partial z}=0$ at $z=L$

H = hydraulic head, L; A = cross-sectional area of specimen, $L2$; z = vertical distance along the specimen, L;
K = permeability, L/T; L = the length of specimen, L; ΔH = the constant-head, L; q = the constant flow rate, $L3/T$;
$Q(t)$ = flow rate to the specimen at time t, $L3/T$; Ce = Storage capacity of the flow pump system, $L2$;
t = time, T; Su, Sd = the compressive storages of the upstream and downstream reservoirs, respectively, $L2$

$$\frac{\partial^2 H}{\partial z^2}-\frac{S_s}{K}\cdot\frac{\partial H}{\partial t}=0 \qquad (1)$$

where S_s is the specific storage of the specimen, L^{-1}, and the other parameters are defined in (Table 1).

A theoretical expression representing each individual permeability test can be obtained from the solution of Equation (1) together with the particular initial and boundary conditions described in Table 1. The hydraulic gradient distribution, *i(z,t)*, within the specimen can be obtained by differentiating the expression for hydraulic head with respect to the variable *z*. These rigorous analytical solutions for both hydraulic head and hydraulic gradient are summarized in Table 2; conventional, steady-state expressions corresponding to each laboratory method are also listed.

Simulations and Discussion

The permeability of a geologic material depends upon its porosity and the connectivity between pores. Its specific storage is a function of the interconnected porosity, the bulk and matrix compressibilities, and also the compressibility of the saturating pore fluid. Accordingly, the hydraulic properties of geologic materials may vary dramatically. For example, values of permeability may range from several tens of cm/s for a gravel to less than 10^{-11} m/s for a clay or intact rock. Even for the same type of

Table 2-*Solutions to the constant-head, constand flow-rate and transient-pulse permeability tests*[1].

Test Method	Steady state expression	Rigorous analytical solution: Hydraulic head	Rigorous analytical solution: Hydraulic gradient
Constant head	$K=-\frac{q}{K\cdot i}=-\frac{qL}{A\cdot\Delta H}$	$H(z,t)=\Delta H\left\{\frac{z}{L}+\frac{2}{\pi}\cdot\sum_{n=1}^{\infty}\frac{\cos(n\pi)}{n}\cdot\sin\frac{n\pi z}{L}\cdot\exp\left(-\frac{K}{S_s}\cdot\frac{n^2\pi^2}{L^2}t\right)\right\}$ *Zhang et al., 1998, Geotechnical Testing J., 21(1), 52-57.*	$i(z,t)=\frac{\Delta H}{L}\left\{1+2\sum_{n=1}^{\infty}\cos(n\pi)\cdot\cos\left(\frac{n\pi z}{L}\right)\cdot\exp\left(-\frac{K}{S_s}\cdot\frac{n^2\pi^2}{L^2}t\right)\right\}$
Constant flow-rate	$K=-\frac{q}{K\cdot i}=-\frac{qL}{A\cdot\Delta H}$ *Olsen, 1966 Water Resources Research, 2(6), 287-295.*	$H(z,t)=\frac{qL}{AK}\left\{\frac{z}{L}-2\cdot\sum_{n=0}^{\infty}\frac{\exp\left(-\frac{K}{S_s}\beta_n^2t\right)\sin(\beta_nz)}{L\delta\beta_n\cos(\beta_nL)\left[L\left(\beta_n^2+\frac{1}{\delta^2}\right)+\frac{1}{\delta}\right]}\right\}$ $\delta=\frac{C_e}{A\cdot S_s}$ $\tan(\beta L)=\frac{1}{\beta\delta}$ *Esaki and Zhang et al., 1996, Geotech. Testing J., 19(3), 241-246.* *Zhang et al., 1998, Geotechnical Testing J., 21(1), 52-57.*	$i(z,t)=\frac{qL}{AK}\left\{\frac{1}{L}-2\cdot\sum_{n=0}^{\infty}\frac{\exp\left(-\frac{K}{S_s}\beta_n^2t\right)\cos(\beta_nz)}{L\delta\cdot\cos(\beta_nL)\left[L\left(\beta_n^2+\frac{1}{\delta^2}\right)+\frac{1}{\delta}\right]}\right\}$
Transient pulse	$h_u-h_f=H\cdot\frac{V_d}{V_u+V_d}\cdot e^{-\theta t}$ $K=\frac{\theta\rho\lambda lV_uV_d}{A(V_u+V_d)}$ *Brace et al., 1968, J. Geoph. Res., 73(6), 2225-2236.*	$\frac{H(z,t)}{H}=\frac{1}{1+\beta+\gamma}+2\sum_{m=0}^{\infty}\times\frac{\exp(-\alpha\phi_m^2)\left[\cos\phi_m\xi-(\gamma\phi_m/\beta)\sin\phi_m\xi\right]}{\left(1+\beta+\gamma-\gamma\phi_m^2/\beta\right)\cos\phi_m-\phi_m(1+\gamma+2\gamma/\beta)\sin\phi_m}$ $\xi=\frac{z}{L}$, $\alpha=\frac{Kt}{L^2S_s}$, $\beta=\frac{S_sAL}{S_u}$, $\gamma=\frac{S_d}{S_u}$, $\tan\phi=\frac{(\gamma+1)}{\gamma\phi^2/\beta-\beta}$ *Hsieh, et al. 1981, Int. J. Rock Mech. Min. Sci., 18(3), 245-252.*	$\frac{i(z,t)}{H}=-2\sum_{m=0}^{\infty}\frac{\phi_m}{L}\times\frac{\exp\left(-\frac{Kt}{L^2S_s}\phi_m^2\right)\left[\sin\left(\phi_m\frac{z}{L}\right)-\left(\frac{\gamma\phi_m}{\beta}\right)\cos\left(\phi_m\frac{z}{L}\right)\right]}{\left(1+\beta+\gamma-\frac{\gamma\phi_m^2}{\beta}\right)\cos\phi_m-\phi_m\left(1+\gamma+\frac{2\gamma}{\beta}\right)\sin\phi_m}$ *Zhang et al. 2000, Geotechnical Testing J., 23(1), 83-90.*

---

[1] The symbols used in this table are different from those used by Brace et al. (1968).

geologic material, permeabilities may range over nearly three orders of magnitude because of microstructural differences (Neuzil 1994; Nelson 1994). Compared to the wealth of permeability data available in the literature, reports on the specific storage of geologic materials are relatively scarce. Laboratory measurements of storage are complicated by equipment compliance or the compressive storage of reservoir tanks which depend upon the combined compressibilities of the equipment and the permeating fluid. Compliance is also a function of the applied pressure.

In this paper, the permeability and specific storage of a hypothetical test specimen are assumed to be 5E-9 cm/s and 2E-7 1/cm, respectively. The equipment compliance for the constant flow-rate permeability test is assumed to be 2E-5 cm^2, with a flow rate of 0.1microliter/min. The fluid compressibility and the reservoir volumes for the transient-pulse permeability test are assumed to be 1E-6 1/cm H_2O and 100 cm^3, respectively. These values are based on estimates derived from a series of permeability tests performed on Inada granite to be presented later in this paper. In addition, the constant-head pressure is assumed to be 170 cm H_2O. The specimen dimensions are assumed to be 50 mm in diameter by 100 mm in length, a standard size typically used in laboratory triaxial compression tests.

With the above conditions and the expressions introduced in (Table 2), the particular response characteristics of each laboratory technique can be simulated and evaluated. For ease of comparison, all of the simulated results demonstrating the time-dependent changes in hydraulic head and hydraulic gradient within the specimen during a constant-head, a constant flow-rate and a transient-pulse test are depicted in (Table 3). Additional simulations may be produced by systematically changing the values of

Table 3-*Transient variations of simulated hydraulic head and hydraulic gradient within the specimen during laboratory permeability tests.*

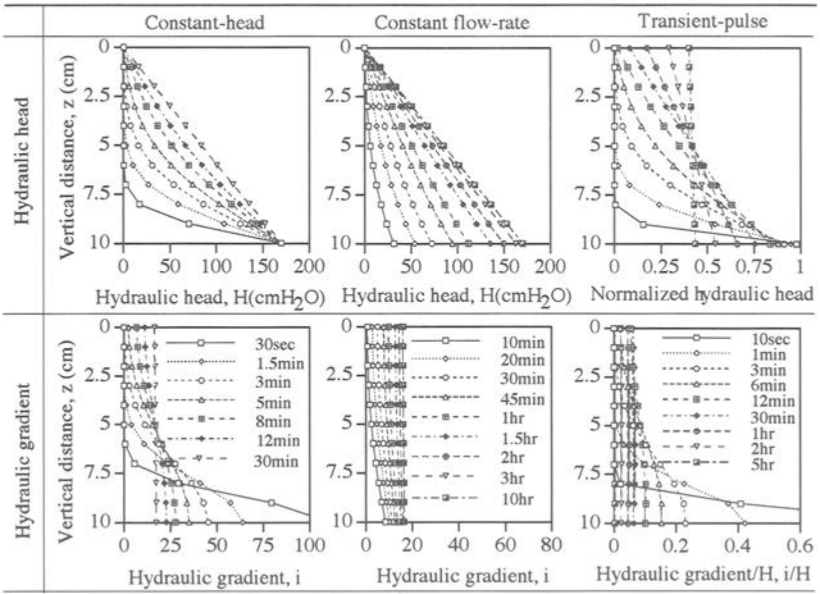

Conditions used for simulation: A=19.625 cm^2; L=10 cm; ΔH=170 cmH $_2$O; q=0.1 μL/min; C_e=2E-5 cm ^{2}; C_{ew}=1E-6 1/cmH $_2$O (1cmH$_2$O=98.1Pa); V_u=V_d=100 cm ^{3}

selected parameters and evaluating their effects on the responses associated with any individual laboratory test. This was done for the transient-pulse permeability test by Zhang et al (2000a).

From the results depicted in (Table 3) as well as in (Table 2), the following general observations can be made:

1. When testing low-permeability geological materials, all three laboratory techniques require relatively long times to approach steady or quasi-steady state conditions where conventional expressions (see Table 2) can be used to calculate the value of permeability. A series of simulations (not shown in this paper) for the hydraulic head distribution within the specimen show that the lower the permeability and/or the larger the specific storage of the specimen, the longer will be the time required to establish steady or quasi-steady state for each test. Transient conditions will also persist for a longer time if the specimen length is increased. Therefore, when testing a specimen having a relatively low permeability, it is advisable to use a shorter specimen having a larger cross-sectional area. In practice, a right cylindrical specimen with dimensions measuring 50 mm in diameter by 100 mm in length is typically chosen for permeability tests on rock, but we think that this standard size is not efficient for testing low-permeability materials. We suggest that new criteria be adopted for determining the optimum specimen size for permeability tests based upon the maximum grain size and/or the maximum length of microcracks in the specimen. For example, both the diameter and length of a test specimen should be larger than 5 to 10 times the maximum grain size and/or the maximum length of microcracks within the specimen.

2. At the onset of an experiment, the increase in hydraulic head at the base of the specimen is gradual in the constant flow-rate permeability test and relatively abrupt in the other two tests. Consequently, the patterns of changes in hydraulic gradients within the specimen induced by the constant flow-rate test and by the other two tests are markedly different. During the constant flow-rate test, the gradients are established slowly across the entire specimen until a steady-state bound is reached that is also the maximum gradient. This maximum value is still comparatively small and can be controlled by the flow rate, q, of the pump (see expression in Table 2). In the constant-head and transient-pulse tests, the magnitude of the imposed hydraulic gradient can be substantial (note that the values of hydraulic gradient during the pulse test are normalized with respect to H). At early time, hydraulic gradients induced near the base of the specimen are also significantly greater than the final steady or quasi-steady state magnitude. Thus, from the perspective of subjecting a specimen to controlled hydraulic gradients similar to those existing *in situ*, the constant flow-rate test has its intrinsic advantage over the other tests. Relatively small differential hydraulic heads and relatively small step increases in pressure are recommended when conducting the constant-head and transient-pulse permeability tests, respectively.

Parameter Identification Technique

The theoretical solutions to the laboratory permeability tests are rigorous (Table 2) and it is difficult to determine analytically the permeability, K and the specific storage, S_s, of a specimen from the experimental measurements. Several investigators used graphical methods to quantify these parameters for a particular test (e.g., Neuzil et al. 1981, Morin et al. 1989), but the attendant procedures are relatively cumbersome and their accuracy is limited. To address this problem, we have proposed a numerical inverse method to back-calculate the hydraulic properties of a test specimen as well as other parameters associated with the experimental system, specifically, the equipment compliance, C_e, of the flow-pump permeating system or the compressive storage of reservoirs used in a pulse test. This method is based on a parameter identification theory developed previously in the general context of system engineering; it has been successfully applied to both mechanical (Zhang and Weng 1994) and hydraulic problems (Esaki et al. 1996, Zhang et al. 1997, Zhang et al. 2000b) encountered in laboratory testing. The basic premise of the method is to back-calculate values of specific parameters by minimizing a properly defined error function which represents a least-squares reduction of the discrepancy between the measured and the theoretically calculated hydraulic differences across the specimen. Detailed descriptions of this Parameter Identification Technique and of error-function analysis are presented by Zhang et al. (2000b).

Versatile Laboratory Permeability Test System

Test Apparatus

A newly-developed experimental system for measuring the permeability of rocks in the laboratory is shown in (Figure 1). It consists primarily of a pressure vessel for hydrostatic testing, three syringe pumps with a controlling unit, a data logger and personal computer (PC) connected to several sensors (a differential-pressure transducer (DPT) and thermocouples) for data acquisition and monitoring, the necessary plumbing (valves and stainless-steel tubing), and ancillary reservoirs and heat insulated chambers.

The pressure vessel can support hydrostatic pressures up to 100MPa and can accommodate a right cylindrical specimen with a diameter ranging from 3 to 12 cm and a length from 1 to 16 cm through the use of adjustable end caps. The syringe pumps have a

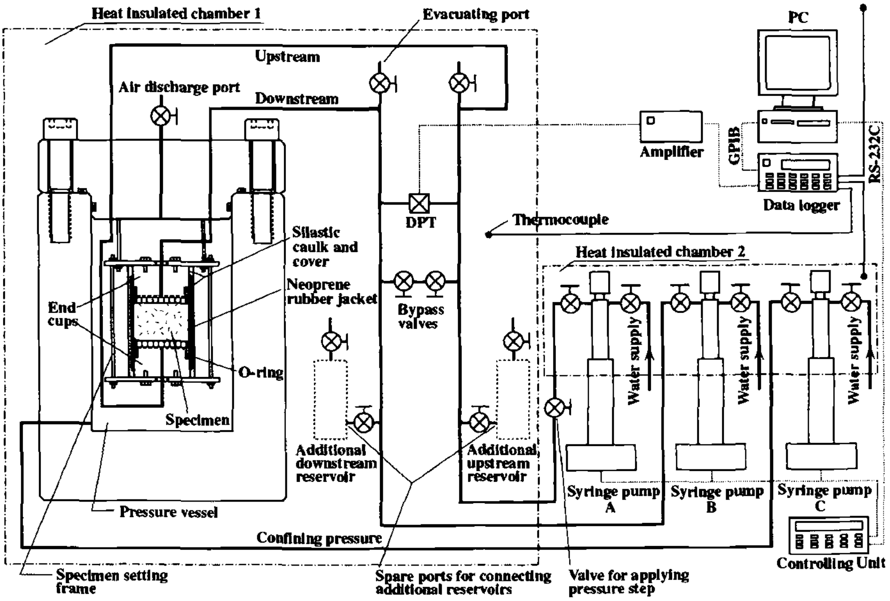

Figure 1-*Schematic of the versatile laboratory permeability test system for rocks.*

volumetric capacity of 103 mL, can support hydrostatic pressures up to 69MPa, and can generate the same pore and confining pressures. They can deliver and monitor a constant flow of permeating fluid at rates from 25 mL/min to 0.01 microliter/min (about one thousand times lower than the resolution of common fluid-volume measurement devices) with an accuracy of +/- 3%. These devices can also produce and monitor a constant pressure with a resolution of 1 psi (6.9kPa). All three pumps can be manipulated by the same controlling unit. A high-linearity DPT is used to monitor the induced hydraulic head difference across the entire length of the specimen during a permeability test and sensitive pressure transducers built into the syringe-pump cylinders are used to monitor the pore and confining pressures. The computer-based data-acquisition and monitoring system records all of the physical parameters at any specified time interval during the test. Run by a specially developed software package, the system can simultaneously display the measured parameters graphically and/or digitally to facilitate real-time evaluation of a test in progress. A detailed description of the system components as well as their technical features is provided by Zhang et al. (2000b).

Procedures for Individual Permeability Tests

Test Preparation Procedure - The specimen is loaded into the pressure vessel and the confining pressure is slowly increased up to a desired level and subsequently maintained constant with syringe pump C. The specimen and permeating system are then thoroughly evacuated through the evacuating port and saturated with pure water. The fluid volumes in syringe pumps A and B are adjusted to the appropriate size for testing. At this stage, the pore pressure is slowly increased up to a desired level and maintained constant by means of syringe pump A (syringe pump B is stopped). The variations in the temperatures of the heat-insulated chambers and in the flow rate of syringe pump A are monitored and the actual permeability tests are started only when fluctuations remain negligible for more than 2 hours.

Constant-Head Permeability Test – One of the bypass valves is slowly closed and syringe pump A is stopped. If the differential pressure induced by closing this valve is relatively large, another bypass valve is adjusted to return the differential pressure to approximately zero. A constant differential hydraulic head across the specimen is then applied by setting syringe pumps A and B to constant but different pressure levels; values of this differential head are continuously monitored by the DPT. The permeability of the specimen is calculated by means of the recorded volume changes in the syringe pump cylinders over a certain time span when flow was known to be steady (see examples in this section).

This improved constant-head permeability test has the following advantages over a conventional constant-head test: 1) The specimen can be tested under relatively high confining and pore pressures; 2) the permeating system is closed so that errors due to evaporation are eliminated in measurements of flow rate; and 3) the fluid volumes in the syringe pump cylinders can be measured with a higher precision compared to commonly used fluid-volume measurement devices. Consequently, the time required for testing a low-permeability specimen can be significantly reduced.

Constant Flow-Rate Permeability Test - This test is performed by injecting a small, constant flow-rate into the base of the specimen using syringe pump A. Syringe pump B is stopped and a large-volume (1000 mL) reservoir is connected to the downstream end of the specimen to dampen any pressure fluctuations. The permeability and specific storage are calculated from the time-dependent variations of differential hydraulic head across the specimen by means of the Parameter-Identification Technique (Esaki et al. 1996, Zhang et al. 1997). The value of permeability can also be determined analytically once conditions have reached steady state (Olsen 1966, Olsen et al. 1988).

Transient-Pulse Permeability Test - Syringe pumps A and B are stopped and used as upstream and downstream reservoirs, respectively. A small pressure pulse is then applied to the upstream reservoir with the valve typically used for applying pressure steps. The permeability and specific storage are calculated from the recorded pulse decay across the specimen, again by means of the Parameter-Identification Technique (Zhang et al. 2000b). The advantages of using high-pressure syringe pumps as fluid reservoirs for this pulse test are discussed by Zhang et al. (2000b).

Application of the New Laboratory System

Test Specimen

Two types of rock commonly available in Japan were used for the experiments. Shirahama sandstone (with grain size of about 0.1mm) and Inada granite (with grain size of about 2 to 4 mm) were chosen as typical examples of sedimentary and igneous rocks, respectively.

In general, sedimentary rocks have anisotropic properties known to vary relative to bedding orientations (Morin et al. 1997). Also, granite contains many small defects which are preferentially oriented along three mutually perpendicular planes, defined as Rife Plane, Grain Plane and Hardway Plane (Osborne 1935). To investigate the effects of heterogeneity on rock permeability, specimens were cored parallel to and perpendicular to bedding for sandstone, and in the directions perpendicular to Rift, Grain and Hardway Planes for granite, as shown in Figures 2a and b, respectively. Based upon the observations listed in the previous section, we used disc-shaped cylindrical specimens (see dimensions shown in Figure 2) to reduce the time required for a test.

Testing Strategies

In order to evaluate the capabilities of this innovative laboratory system and to cross-check the results obtained from the three complementary test methods, a sandstone specimen cored perpendicular to bedding (named SVS) and a granite specimen cored perpendicular to the Hardway Plane (named GHL) were tested under a series of confining and pore pressure conditions shown in (Table 4). To investigate the effects of confining pressure and rock heterogeneity on hydraulic properties, a series of permeability tests was performed on specimens cored in different orientations for both sandstone and granite. The confining pressure was increased stepwise up to 60 MPa and a transient-pulse test was conducted at each step.

Results

Figures 3a and 4a show the laboratory data generated during the constant-head

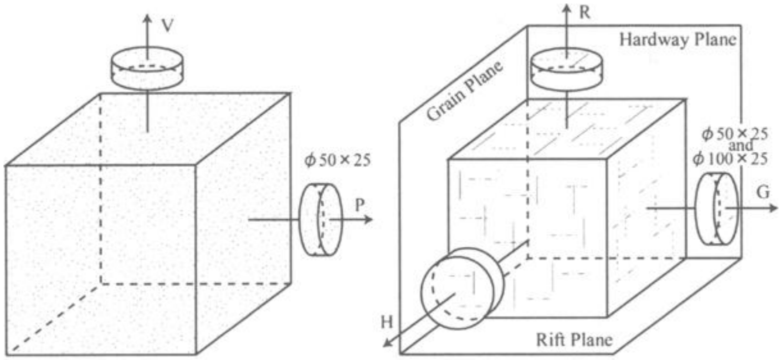

a) Shirahama sandstone b) Inada granite

Figure 2-*Specimens cored parallel to and perpendicular to bedding for sandstone, and specimens cored perpendicular to Rift, Grain and Hardway Planes for granite.*

Table 4-*Conditions for cross-check permeability tests on Shirahama sandstone and Inada granite.*

Shirahama sandstone				Inada granite			
Test No.	Confining pressure (MPa)	Pore pressure (MPa)	Other conditions*	Test No.	Confining pressure (MPa)	Pore pressure (MPa)	Other conditions*
SVS21CH	2	1	29.1	GHL1.5CH	1	0.5	29.4
SVS21FP			0.005	GHL1.5FP			0.002
SVS21TP			68.4	GHL1.5TP			34.9
SVS41CH	4	1	38.5	GHL21CH	2	1	42.7
SVS41FP			0.002	GHL21FP			0.0005
SVS41TP			65.6	GHL21TP			36.4
SVS101CH	10	1	31.7	GHL42CH	4	2	47.5
SVS101FP			0.001	GHL42FP			0.0005
SVS101TP			82.9	GHL42TP			113.3
SVS105CH	10	5	44.3	GHL102FP	10	2	0.0003
SVS105TP			65.8	GHL102TP			141.8
SVS2010CH	20	10	32.5	GHL202FP	20	2	0.0003
SVS2010TP			61.4	GHL202TP			89.12
SVS3015CH	30	15	20.9	GHL302FP	30	2	0.0002
SVS3015TP			56.5	GHL302TP			117.7
SVS4020CH	40	20	31.4				
SVS4020TP			76.2				

*Other conditions illustrate the hydraulic head in cmH_2O, the constant flow-rate in cm^3/min and the step increase in pressure in cmH_2O ($1cmH_2O$=98.1Pa) for the constant-head, the constant flow-rate and the transient-pulse tests, respectively.

permeability tests for Shirahama sandstone and Inada granite, respectively. Each curve illustrates the variations in differential hydraulic head across the specimen as a function of time; after a certain period of time, this head difference approaches a quasi-steady state. The changes in fluid volumes in both the upstream (inflow) and downstream (outflow) reservoirs are measured over a certain time span (solid horizontal line). As can be observed from the curves, all of the tests were performed under hydraulic gradients less

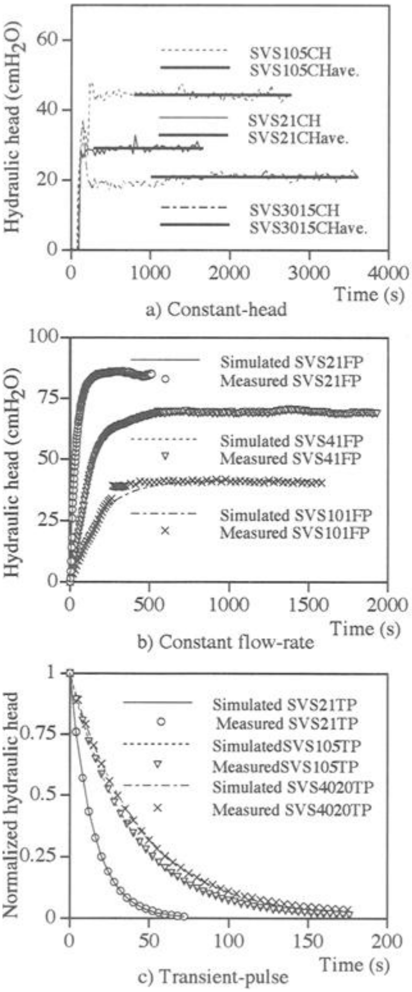

Figure 3-*Examples of the results obtained from the cross-check testing on Shirahama sandstone.*

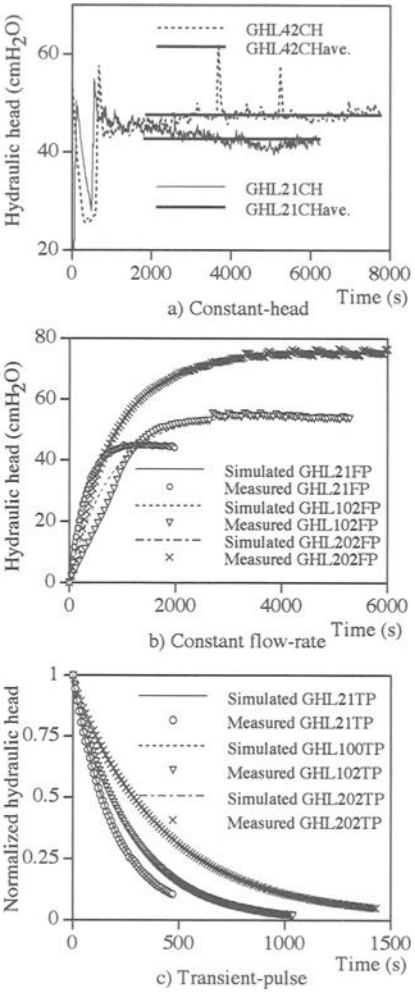

Figure 4-*Examples of the results obtained from the cross-check testing on Inada granite.*

than 20. Permeability estimates are derived from inflow and outflow rates (changes in fluid volumes divided by the time period) using the expression for steady-state flow (see Table 2). These values and their averages are listed in (Table 5).

Figures 3b and 4b show examples of the results obtained from constant flow-rate permeability tests for Shirahama sandstone and Inada granite, respectively. These curves illustrate the time-dependent rise in differential hydraulic head across the specimen induced by an externally imposed constant flow-rate from the syringe pump. The permeability and specific storage of each specimen are calculated from the data obtained over the whole-test and the half-test times by means of the Parameter-Identification

Table 5-*Results obtained from the cross-check tests on Shirahama sandstone and Inada granite.*

	Test No.	Constant-head (CH)				Constant-flow rate (FP)						Transient-pulse (TP)		
		K_i	K_o	K_{ave}	Time	K_h	K_w	K_s	Ss_h	Ss_w	Time	K	S_s	Time
Shirahama Sandstone	SVS21	0.86	0.85	0.86	540	1.04	1.04	1.04	1.40	1.41	510	3.69	0.0059*	72
	SVS41	0.44	0.48	0.46	1 440	0.51	0.51	0.51	2.51	2.62	1 930	1.51	0.0999*	140
	SVS101	0.39	0.39	0.39	1 020	0.40	0.43	0.43	2.76	2.62	1 580	1.32	0.0070*	170
	SVS105	0.42	0.40	0.41	1 920							1.43	0.0993*	176
	SVS2010	0.38	0.39	0.39	1 860							1.37	0.0697*	170
	SVS3015	0.36	0.38	0.37	2 580							1.32	0.0200*	165
	SVS4020	0.33	0.35	0.34	1 920							1.22	0.1860*	175
Inada granite	GHL1.5	3.06	4.29	3.68	3 240	4.57	4.51	4.53	7.00	4.85	2 970	5.91	29.4	792
	GHL21	4.14	3.10	3.62	5 775	4.28	4.77	4.85	36.0	61.3	1 980	6.61	7.07	470
	GHL42	3.51	3.28	3.40	5 788	3.88	4.10	4.11	19.7	12.1	2 790	7.12	4.92	940
	GHL102					2.23	2.40	2.43	60.0	40.3	5 280	5.13	5.53	1 040
	GHL202					1.71	1.76	1.75	30.8	23.7	6 360	3.09	16.90	1 428
	GHL302					0.81	0.87	0.91	19.6	12.8	7 680	2.13	10.20	2 070

Units of K for sandstone and granite are ($\times 10^{-7}$ cm/s) and ($\times 10^{-9}$ cm/s), respectively; Units of Ss for sandstone and granite are ($\times 10^{-6}$ 1/cm) and ($\times 10^{-8}$ 1/cm), respectively; Unit for the time is second; K_i and K_o indicate the values of K obtained from the inflow and outflow fluid volumes, respectively; Subscripts h, w and s for the FP tests mean the estimations from the half-time, whole-time and steady-state experimental data, respectively; All the values of K are converted at the temperature of 15 ℃.

Technique (Zhang et al. 1997) and these are tabulated in (Table 5). Permeability values derived from only the steady-state measurements are also listed.

Figures 3c and 4c depict the decay of the normalized differential hydraulic head across the entire length of the specimen generated during transient-pulse permeability tests on Shirahama sandstone and Inada granite, respectively. The permeability and specific storage of each specimen are calculated from these response curves by means of the Parameter-Identification Technique and are tabulated in (Table 5). For comparison with these laboratory data, simulated curves developed from the constant flow-rate and the transient-pulse permeability tests are also shown in the above figures. These simulated curves were produced by substituting the back-calculated values of associated parameters into the expression (Table 2) for each individual test. Finally, the effects of confining pressure and specimen heterogeneity on the hydraulic properties of Shirahama sandstone and Inada granite are illustrated in (Figures 5a and b), respectively.

Discussion

The simulated curves representing both the constant flow-rate and the transient-pulse tests are in close agreement with the experimental data (Figures 3, 4b and c). These results demonstrate the accuracy of the rigorous theoretical analyses for individual tests. Although the permeability values obtained from the three different permeability tests are on the same order, there is some notable variability among tests, particularly in the case of sandstone (Table 5). These differences may reflect the errors arising from measuring substantial changes in hydraulic pressure at very early times during the pulse test. They may also be related to very small plumbing leaks or slight temperature variations that may affect long-term test response. The test durations for the constant-head and the

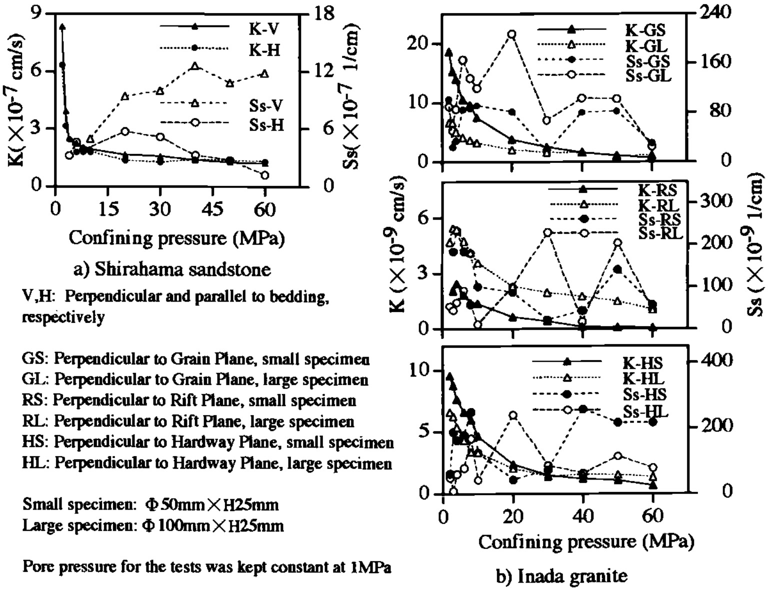

a) Shirahama sandstone

V,H: Perpendicular and parallel to bedding, respectively

GS: Perpendicular to Grain Plane, small specimen
GL: Perpendicular to Grain Plane, large specimen
RS: Perpendicular to Rift Plane, small specimen
RL: Perpendicular to Rift Plane, large specimen
HS: Perpendicular to Hardway Plane, small specimen
HL: Perpendicular to Hardway Plane, large specimen

Small specimen: Φ50mm×H25mm
Large specimen: Φ100mm×H25mm

Pore pressure for the tests was kept constant at 1MPa

b) Inada granite

Figure 5-*Effects of confining pressure and heterogeneity on permeability and specific storage of rocks (Permeabilities are converted into the values at the temperature of 15 ℃).*

constant flow-rate tests are roughly the same and so are the resulting permeability values (Table 5). Since a "real" or "reference" value for permeability is unknown, we cannot assess which technique is the best. However, this comparison among techniques does increase our confidence in our ability to test low-permeability specimens and achieve consistent results. The agreement among test results was better for the granite specimen, which is the sample with the lower permeability.

The values of specific storage obtained from the constant flow-rate and transient-pulse tests for granite vary over an order of magnitude (Table 5). However, estimates of specific storage for sandstone derived from the pulse tests are extremely low and unrealistic. The reasons why such low experimental values are obtained for this specimen are discussed by Zhang et al. (2000b).

The values for both the permeability and the specific storage back-calculated from the half-time experimental data are in close agreement with those back-calculated from the whole-time experimental data (Table 5, middle column). These permeability values are also similar to those calculated from the steady-state measurements. Thus, results indicate that using the Parameter-Identification Technique based on rigorous theoretical analysis not only reduces the time required for testing low-permeability specimens, but also permits the specific storage to be determined as well.

Under the test conditions summarized in (Figure 5), the permeability and specific storage of Shirahama sandstone ranged from 8.3E-7 to 1.2E-7 cm/s and from 1.3E-6 to 1.2E-7 1/cm, respectively. Likewise, the permeability and specific storage of Inada granite ranged from 1.9E-8 to 0.7E-10 cm/s and from 2.5E-7 to 8.3E-9 1/cm, respectively. In general, the permeabilities of both rock types decreased monotonically with increasing confining pressure, but the rate of this decrease diminished at higher confining pressures. This reduction in permeability is attributed to the closure of microcracks at low confining pressure that control fluid flow (Walsh and Brace 1984). The variation in specific storage for both rocks displayed no systematic pattern or trend as a function of increasing confining pressures. This variability may be due to a cyclical generation and closure of secondary microcracks that are formed between grains and perpendicular to the contacting surface during hydrostatic crushing (Zhang et al. 1990; Berge and Berryman 1995).

The permeabilities of the specimens cored perpendicular and parallel to bedding for sandstone are almost the same (Figure 5a). This implies that Shirahama sandstone is relatively isotropic in a hydraulic sense. For the granite specimen, changes in permeability perpendicular to the Rift Plane are larger than those perpendicular to the Grain and Hardway Planes (Figure 5b). Thus, the hydraulic properties of this rock type are affected by its physical and mechanical heterogeneities.

Summary and Conclusions

The accurate hydraulic characterization of low-permeability environments has important practical implications. In order to examine this issue from the perspective of laboratory-based investigations, we review some recent advancements in theoretical analyses associated with three laboratory techniques applied to low-permeability geologic materials: constant-head, constant flow-rate and transient-pulse permeability tests. A versatile laboratory system is then introduced that can implement any of these three test methods while subjecting a specimen to high confining pressures and pore pressures, thereby simulating *in situ* conditions at great depths. The capabilities and advantages of this new system are illustrated with experimental data from Shirahama sandstone and Inada granite, two rock types widely encountered in Japan. Primary conclusions drawn from this present study are as follows.

1. To reduce the time required to satisfactorily measure low permeability, it is advisable to use a shorter specimen having a larger cross-sectional area, i.e., a disk-shaped specimen. Physical characteristics related to maximum grain size and/or the maximum length of microcracks in a specimen should be incorporated into developing a new standard for determining optimum specimen dimensions when testing low-permeability geological materials.

2. The rigorous theoretical analysis of the transient-phase data obtained during a constant flow-rate test permits the test duration to be significantly shortened without sacrificing accuracy in estimating both the permeability and the specific storage of a test specimen.

3. The permeabilities derived from the three complementary laboratory methods and the specific storages obtained from the constant flow-rate and transient-pulse tests are in general agreement. The consistency of these results illustrates the effectiveness and versatility of this innovative laboratory system for testing low-permeability geologic materials.

4. The permeabilities of Shirahama sandstone and Inada granite range from about 8.3E-7 to 1.2E-7 cm/s and from 1.9E-8 to 0.7E-10 cm/s, respectively. Both the permeability and the specific storage of either specimen are found to vary with confining pressure; permeability decreases monotonically with increasing stress, whereas specific storage varies circularly. Inada granite in particular appears to exhibit hydraulic anisotropy and demonstrates significant changes in permeability perpendicular to the Rift Plane.

References

Berge, P. A., and Berryman, J. G., 1995, Realizability of Negative Pore Compressibility in Poroelastic Composites, *Journal of Applied Mechanics*, Vol. 62, pp. 1053-1062.

Brace, W. F., Walsh, J. B., and Frangos, W. T., 1968, Permeability of Granite under High Pressure, *Journal of Geophysical Research*, Vol. 73, No. 6, pp. 2225-2236.

Esaki, T., Zhang, M., Takeshita, A., and Mitani, Y., 1996, Rigorous Theoretical Analysis of a Flow Pump Permeability Test, *Geotechnical Testing Journal*, Vol. 19, No. 3, pp. 241-246.

Fox, P. J., and Zhu, Y., 1999, Discussion on Theoretical Evaluation of the Transient Response of Constant Head and Constant Flow-Rate Permeability Tests by M. Zhang, M. Takahashi, R. H. Morin, and T. Esaki, *Geotechnical Testing Journal*, Vol. 22, No. 4, pp. 356-357.

Ge, S., and Garven, G., 1992, Hydromechanical Modeling of Tectonically Driven Groundwater Flow With Application to the Arkoma Foreland Basin, *Journal of Geophysical Research*, Vol. 97, No. B6, pp. 9119-9144.

Hanor, J. S., 1993, Effective Hydraulic Conductivity of Fractured Clay Beds at a Hazardous Waste Landfill, Louisiana Gulf Coast, *Water Resources Research*, Vol. 29, No. 11, pp. 3691-3698.

Hsieh, P. A., Tracy, J. V., Neuzil, C. E., Bredehoeft, J. D., and Silliman, S. E., 1981, A Transient Laboratory Method for Determining the Hydraulic Properties of Tight Rocks - I. Theory, *International Journal of Rock Mechanics and Mining Sciences & Geomechanics Abstracts*, Vol. 18, No. 3, pp. 245-252.

Lien, R., Loset , F., and Saarai, K. H. O., 1987, Updated Review of Norwegian Rock Caverns Storing Liquids, Oil Products or Gas under High Pressure or Low Temperature, *Proceedings*, International Symposium on Large Rock Caverns, Pergamon Press, Oxford, pp. 517-522.

Lin, C., Pirie, G., and Trimmer, D. A., 1986, Low Permeability Rocks: Laboratory Measurement and Three-Dimensional Microstructural Analysis, *Journal of Geophysical Research*, Vol. 91, No. B2, pp. 2173-2181.

Moore, D. E., Morrow, C. A., and Byerlee, J. D., 1986, High-Temperature Permeability and Groundwater Chemistry of Some Nevada Test Site Tuffs, *Journal of Geophysical Research*, Vol. 91, No. B2, pp. 2163-2171.

Morin, R. H., Carleton, G. B., and Poirier, S., 1997, Fractured-Aquifer Hydrogeology from Geophysical Logs; the Passaic Formation, New Jersey, *Ground Water*, Vol. 35, No. 2, pp. 328-338.

Morin, R. H., Olsen, H. W., Nelson, K. R., and Gill, J. D., 1989, Graphical Method for Determining the Coefficient of Consolidation, Cv, from A Flow-Pump Permeability Test, *Geotechnical Testing Journal*, Vol. 12, No. 4, pp. 302-307.

Nelson, P. H., 1994, Permeability-Porosity Relationships in Sedimentary Rocks, *The Log Analyst*, Vol. 35, No. 3, pp. 38-62.

Neuzil, C. E., 1995, Abnormal Pressures as Hydrodynamic Phenomena, *American Journal of Science*, Vol. 285, No.6, pp. 742-786.

Neuzil, C. E., 1994, How Permeable are Clays and Shales?, *Water Resources Research*, Vol. 30, No. 2, pp. 145-450.

Neuzil, C. E., Cooley, C., Silliman, S. E., Bredehoeft, J. D., and Hsieh, P. A., 1981, A Transient Laboratory Method for Determining the Hydraulic Properties of Tight Rocks - II. Application, *International Journal of Rock Mechanics and Mining Sciences & Geomechanics Abstracts*, Vol. 18, No. 3, pp. 253-258.

Olsen, H. W., 1966, Darcy′s Law in Saturated Kaolinite, *Water Resources Research*, Vol. 2, No.6, pp. 287-295.

Olsen, H. W., Morin, R. H., and Nichols, R. W., 1988, Flow Pump Application in Triaxial Testing, *Advanced Triaxial Testing of Soil and Rock, STP977*, R. T. Donaghe, R. C. Chaney, and M. L. Silver, Eds, ASTM, West Conhohocken, PA, pp. 68-81.

Osborne, F. F., 1935, Rift, Grain and Hardway in Some Pre-Cambrian Granites, Quebec, *Economic Geology*, Vol. 30, No. 5, pp. 540-551.

Roeloffs, E.A., 1998, Persistent Water Level Changes in a Well Near Parkfield, California, due to Local and Distant Earthquakes, *Journal of Geophysical Research*, Vol. 103, No. B1, pp. 869-889.

Rojstaczer, S. A., Wolf, S. C., Michel, R. L., Hickman, S. H., Sibson, R. H., Bruhn, R. L., and Jacobson, M. L., 1994, Long-Lived Permeability Changes in the Shallow Crust Associated with Earthquakes, *Proceedings*, Workshop LXIII, USGS Red-Book Conference on the Mechanical Involvement of Fluids in Faulting, U.S. Geological Survey, VA, pp. 476-481.

Trimmer, D., 1982, Laboratory Measurements of Ultralow Permeability of Geologic Materials, *Review of Scientific Instruments*, Vol. 53, No. 8, pp. 1246-1254.

Walsh, J. B. and Brace, W. F., 1984, The Effects of Pressure on Porosity and the Transport Properties of Rock, *Journal of Geophysical Research*, Vol. 89, No. B11, pp. 9425-9431.

Zhang, M., Esaki, T., Olsen, H. W., and Mitani, Y., 1997, Integrated Shear and Flow Parameter Measurement, *Geotechnical Testing Journal*, Vol. 20, No.3, pp. 296-303.

Zhang, M., Takahashi, M., Morin, R. H., and Esaki, T., 1998a, Theoretical Evaluation of the Transient Response of Constant Head and Constant Flow-Rate Permeability Tests, *Geotechnical Testing Journal*, Vol. 21, No.1, pp. 52-57.

Zhang, M., Takahashi, M., Esaki, T., and Sakai, K., 1998b, Theoretical Evaluation of the Falling-Head Permeability Test Method, *Hokkaido Geotechnics '98*, pp. 15-20 (in Japanese with English Abstract).

Zhang, M., Takahashi, M., Morin, R. H., and Esaki, T., 2000a, Evaluation and Application of the Transient-Pulse Technique for Determining the Hydraulic Properties of Low-Permeability Rocks - Part 1: Theoretical Evaluation, *Geotechnical Testing Journal*, Vol. 23, No. 1, pp. 83-90.

Zhang, M., Takahashi, M., Morin, R. H., and Esaki, T., 2000b, Evaluation and Application of the Transient-Pulse Technique for Determining the Hydraulic Properties of Low-Permeability Rocks - Part 2: Experimental Application, *Geotechnical Testing Journal*, Vol. 23, No. 1, pp. 91-99.

Zhang, M., and Weng, J. J., 1994, Elasto-Plastic Back Analysis of Frozen Soil Wall, *Journal of China University of Mining and Technology*, Vol. 4, No. 1, pp. 52-61.

Zhang, J., Wong, T. F., Yanagidani, T., and Davis, D. M., 1990, Pressure-Induced Microcracking and Grain Crushing in Berea and Boise Sandstones: Acoustic Emission and Quantitative Microscopy Measurements, *Mechanics of Materials*, Vol. 9, pp. 1-15.

LOW PERMEABILITY ENVIRONMENTS AND REMEDIATION ISSUES

David Cazaux[1]

Evaluation of Constant Head Infiltration Test Analysis Methods for Field Estimation of Saturated Hydraulic Conductivity of Compacted Clay Liners

Reference: Cazaux, D., "**Evaluation of Constant Head Infiltration Test Analysis Methods for Field Estimation of Saturated Hydraulic Conductivity of Compacted Clay Liners**", *Evaluation and Remediation of Low Permeability and Dual Porosity Environments, ASTM STP 1415,* M.N. Sara and L.G. Everett, Eds., ASTM International, West Conshohocken, PA, 2002.

Abstract: Field infiltration tests are commonly used to assess the hydraulic conductivity of low permeability materials such as natural clay barriers and compacted clay liners. The soils used for compacted clay liners are always partially saturated and require very long testing times to reach steady-state flow conditions. Consequently, because they are less time consuming, laboratory tests are usually preferred for construction quality control. Nevertheless, it is well-known that field tests are more representative of the clay liner because of the scale effect. This is why, since the 1980s, the main issues associated with field procedures have been studied and several methods proposed for testing low-permeability materials within short time periods. The proposed methods are based on early-time flow analysis in unsaturated conditions and have been applied to various compacted soils under field and laboratory conditions. To evaluate these methods, we carried out a comprehensive testing program using a hydraulic field infiltrometer method (sealed single-ring infiltrometer) and a laboratory rigid-wall permeameter method that reproduces surface field test conditions. The laboratory tests were continued until saturated hydraulic conductivity was obtained so that this value could be compared against the hydraulic conductivity estimated from early-time analysis on the same specimen. The obtained results show the influence of (a) the initial moisture content, (b) the sorptivity and hydraulic head on the early-time infiltration rate, and (c) the final estimated hydraulic conductivity. A comparison of analysis methods shows the limitations of some and tries to explain the reasons for such inadequacies in the description of early-time unsaturated flows. Nevertheless, the conclusions of our study show that conventional early-time analyses give a good estimation of saturated hydraulic conductivity within a short time period compatible with construction quality-control procedures.

Keywords: infiltration, hydraulic conductivity, clay liner, constant head, infiltrometer, pressure, suction.

---

[1] Research Engineer, BRGM, Environment and Process Division, BP6009, 45060 Orléans, France, d.cazaux@brgm.fr. Former Project Manager at INSA Lyon (France)

Introduction

Permeability tests are not often interpreted under unsaturated conditions. They are generally continued until steady-state conditions are reached, following which Darcy's law is applied assuming that the water potential at the wetting front is at atmospheric pressure (Olson and Daniel 1981, Purdy and Ramey 1995). The hydraulic conductivity in the vertical direction k_v, is then expressed by the following equation:

$$v = k_v \cdot \frac{h + z_w}{z_w} \tag{1}$$

where v is the infiltration rate, z_w is the thickness of the saturated profile and h is the hydraulic head at the soil surface.

The conventional interpretation of tests on low-permeability materials is based on the value of z_w determined at the end of the test. Here Darcy's law is applied by computing the steady-state infiltration rate with the hydraulic gradient. As the moisture profile in the soil generally shows an increase in moisture content in the topmost centimeters of the flow zone, z_w is determined in practice by sampling and determining the moisture content θ at various depths of the topmost centimeters of the soil (Figure 1a). The Green and Ampt (1911) model, assuming the profile to have a perfect piston shape (Figure 1b), can also estimate z_w. In reality, the shape of the profile shows that the distribution of the wetting front is not a perfect piston shape because it includes a diffusion term characterizing the capillary flow. A transmission zone and a moistening zone fed by capillarity can be observed between the initial moisture content of the soil, θ_i, and the saturation moisture content, θ_{sat}. The separation of these two zones is determined formally to the inflection point depth of the profile, which is z_w.

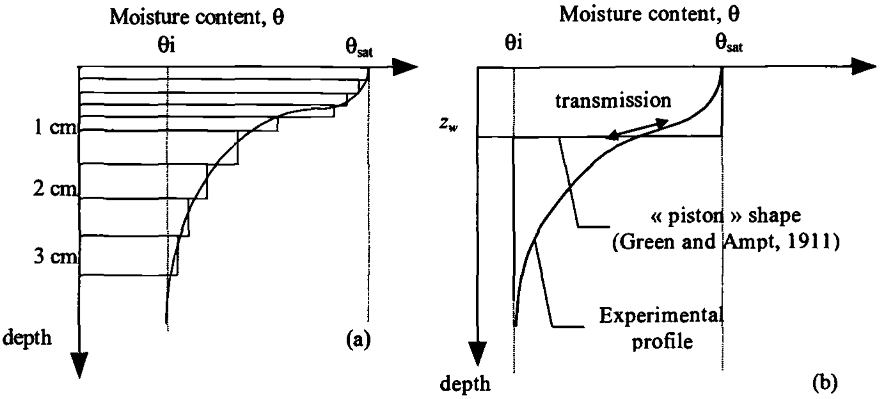

Figure 1 - *(a) Experimental saturation profile determined from actual moisture content, and (b)* z_w *estimated using the Green and Ampt (1911) model.*

The hydraulic conductivity, k, is determined at time t when the infiltration rate is $v(t)$

in a saturated profile of thickness equal to $z_w(t)$, supposing that the pressure of the water is equal to the atmospheric pressure at the wetting front and the flow is vertical. Equation 2 describes this condition.

$$k = \frac{z_w(t)}{h + z_w(t)} \cdot v(t) \qquad (2)$$

Here, for a given hydraulic head, h, we can calculate the hydraulic conductivity at any time t by computing the hydraulic head to the saturated thickness. We determine the hydraulic conductivity from (a) the infiltration rate at the end of the test, and (b) the wetting front deduced from the analysis. The results are generally satisfactory, but if the soil is initially very far from saturation, they slightly overestimate the hydraulic conductivity because suction at the wetting front is not considered. Consideration of the actual suction at the wetting front, h_f, leads to the more general relationship of Green and Ampt (1911):

$$k = \frac{z_w(t)}{h - h_f + z_w(t)} \cdot v(t) \qquad (3)$$

Here the hydraulic conductivity is calculated assuming that the wetting front progressing through the soil is a plane separating a nearly saturated transmission zone located between the soil surface and this plane, and a zone where the soil retains its initial degree of moisture content. The suction at the wetting front, h_f, is assumed to be constant throughout the infiltration. The applied hydraulic head, h, is constant and referenced to the soil surface.

Determining the infiltration rate, the saturation profile, and the suction h_f at the wetting front in this equation is difficult. In this paper, we present the main available methods for estimating the parameters of Equation 3 (Philip 1969, Green and Ampt 1911, Cazaux 1998). We compare the obtained hydraulic conductivity values, estimate hydraulic conductivity by analytical methods in unsaturated conditions (Fallow et al. 1994, Elrick and Reynolds, 1992) and compare them to the conventional methods. Our testing program was carried out in both the laboratory and the field on several soils used for hydraulic barrier construction. The soils were tested in the field with ring infiltrometers and in the laboratory with a rigid-wall permeameter and an oedo-permeameter.

Test Procedure

Hydraulic Conductivity Measurement in the Field

The field tests in our program were realized with a sealed single-ring infiltrometer (SSRI) of 200-mm diameter. The laboratory tests were realized with a rigid-wall permeameter and an oedo-permeameter, both of 101,6-mm diameter (4 inches), which reproduce the conditions of the field surface test with infiltrometers.

Sealed-Ring Infiltrometers – The single- or double-ring infiltrometer method is based on measuring infiltration rate under a given constant hydraulic head. In the case of the double ring, the outer ring allows vertical flow in the inner ring. Application of the hydraulic head and monitoring of the infiltration is done through a pressure volume controller (PVC). The infiltrometer, with one or two concentric rings closed by a lid, is pushed into the soil and filled with water (Figure 2). Several PVC types can be used for applying the hydraulic head, such as Mariotte bottle, pressurized reservoir, piston syringe, or horizontal capillary. A confining system can be used to apply a normal load to the soil surface.

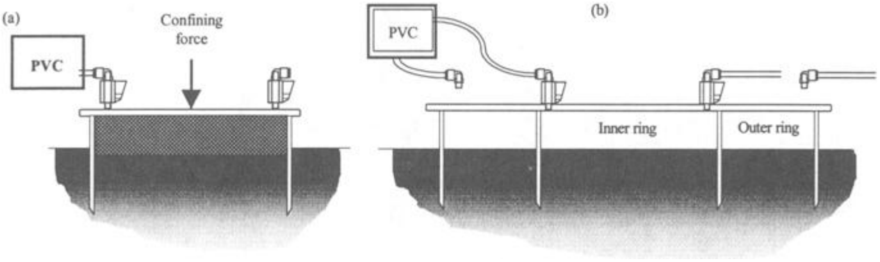

Figure 2 - *Diagram of the sealed single-ring infiltrometer (SSRI) used in this program (a) and of a sealed double-ring infiltrometer (b).*

Hydraulic Conductivity Measurement in the Laboratory

Rigid-Wall Permeameter (RWP)- The RWP isolates a soil specimen between two porous stones embedded in caps and enables the test to be realized at constant volume; it keeps the specimen from swelling. The RWP can only be used for fine-grained soils with a low swelling potential. Being side and surface confining, the test conditions are close to those applied in situ.

Oedo-Permeameter (ODP) - With the ODP the soil specimen is placed between two porous stones. The top of the cell consists of a piston that allows vertical swelling of the specimen, as well as the application of normal stress to the specimen. Monitoring of infiltration and swelling can be done simultaneously. The ODP reproduces the conditions of field tests made without confinement of the soil surface.

Soil Characteristics

Four soil types were tested in our program:

Silt A (SA) – a very homogeneous low-plasticity silt that gives a good reproducibility of laboratory hydraulic conductivity tests. All the tests made on this soil were performed in the laboratory on compacted specimens in the RWP mould according to the Standard Proctor procedure.

Silt B (SB) – a plastic silt with clayey nodules, approximately one centimeter in diameter. Laboratory tests made on this soil were performed on compacted specimens (Standard Proctor procedure) in the RWP mould, and a few field tests were made with the SSRI. In the field, the clay liner was built up in three layers of 30 cm each, compacted with a sheep-foot roller.

Sand Bentonite Mixture (SBM) – a fine-grained silty sand treated with 4% bentonite.

Laboratory tests made on this soil were performed on compacted specimens in the RWP and ODP moulds (Standard Proctor procedure); field tests were made with the SSRI. In the field, the liner was built with a fine factory-treated sand with 5% of Na-activated bentonite. The liner is made of two 50-cm layers, compacted with a heavy vibrating roller.

Clay (C) – a very plastic black silty clay. Tests made on this soil were performed in the laboratory on compacted specimens in the RWP mould (Standard Proctor procedure).

The characteristics of these soils, whose densities are of the order of 95-97% of the Proctor optimum value, are summarized in Table 1. Grain-size distributions of the four soils are resumed in Figure 3. The physical characteristics of each test, as well as the hydraulic head applied during infiltration, are summarized in Table 2. The initial soil saturation $\Delta\theta$ (difference between saturated volumetric moisture content and initial volumetric moisture content, i.e. $\theta_{sat} - \theta_i$) for the tests ranged between 40 and 95%. In addition, various hydraulic head values (from 10 and 150 cm) were applied to evaluate the influence of the initial saturation on the estimation of the saturated hydraulic conductivity.

Table 1 - *Soil characteristics.*

	SA	SB	C	SBM
Methylene blue value (g/100g)	-	2.6	3.3	1.7
Initial volumetric moisture content θ_i (%)	-	36.7	32.4	24.4
Optimum moisture content, θ_{OPT} (%)	28.2	26.3	31.0	20.0
Dry density, γ_d (kN/m^3)	-	16.7	15.8	17.4
Optimum Proctor dry density, $\gamma_{d\,OPN}$ (kN/m^3)	17.3	17.5	17.7	18.2
Atterberg Liquidity limit, W_L	33	-	40	-
Atterberg Plasticity Index, I_P	10	-	21	-

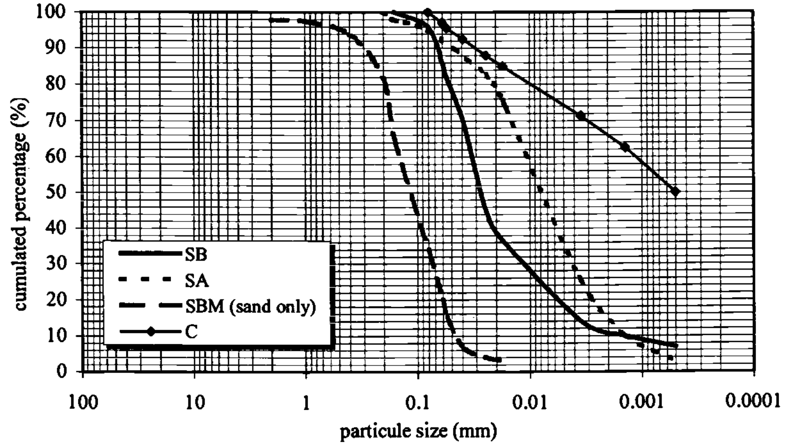

Figure 3 – *Grain-size distribution of the tested soils (sand only for SBM)*

Table 2 - *Test parameters for compacted (suffix R) and intact (I) specimens.*

Test	θ (%)	γ_d (kN/m^3)	$\Delta\theta$ (%)	h (cm)
SA 1R	15.1	15.9	24.9	50
SA 2R	15.3	15.9	24.7	100
SA 3R	10.4	16.2	24.4	150
SA 4R	16.8	17.1	15.8	30
C 1R	32.5	17.2	2.6	100
C 2I	32.4	15.8	8.0	30
SB 1R	22.0	16.4	2.0	10
SB 2R	36.1	16.6	0.6	10
SB 3I	33.2	16.2	5.7	10
SB 4I	31.8	16.2	7.1	40
SB 5I	33.1	16.7	3.9	140
SB 6I	32.3	16.0	7.3	135
SB 7I	32.2	16.1	7.0	60
SB 8I	32.1	16.3	6.4	30

Test	θ (%)	γ_d (kN/m^3)	$\Delta\theta$ (%)	h (cm)
SB 9I	32.2	16.7	4.8	135
SB 10I	34.1	16.9	2.1	47
SB 11I	18.2	16.8	6.0	20
SB 12I	30.6	16.5	3.9	10
SBM 1R	19.5	18.6	10.3	50
SBM 2R	19.7	18.8	9.3	10
SBM 3I	23.8	17.0	12.0	130
SBM 4I	23.4	17.6	10.2	140
SBM 5I	22.5	17.3	12.2	140
SBM 6I	23.8	17	12.0	30
SBM 7I	22.6	17.1	12.9	120
SBM 8I	25.0	17.5	8.9	120
SBM 9I	24.3	17.1	11.2	130
SBM 10I	23.7	17.2	11.4	10

Determination of Steady-State Infiltration Rate

Conventional Determination

A very long time is necessary to approach the exact value of the steady-state infiltration rate during an infiltration test, and theoretically it is not possible. The boundary conditions are those of a semi-infinite medium and the hydraulic gradient tends to 1. To achieve a pseudo-steady state requires several weeks in the case of low-saturation and low permeability soils (of the order of 1.10^{-10} m/s). Bentoumi (1995) showed that the variation in infiltration rate for hydraulic gradients higher than 10 becomes low at the assumed onset of steady-state conditions. The steady-state infiltration rate, v_{SS}, is determined graphically from the slope of the linear portion of the infiltration curve versus time. Figure 4 shows the typical evolution of the infiltration rate with two stages: a 'transient state' during which the infiltration rate decreases rapidly versus time, and a 'steady state' during which the infiltration rate decreases slowly as the wetting front deepens (Philip, 1969).

Low hydraulic heads (lower than 30 cm) are applied for tests performed with open-ring infiltrometers and for hydraulic conductivities higher than 1.10^{-9} m/s. With sealed infiltrometers, infiltration rate can be accelerated by applying higher hydraulic heads (50 to 200 cm) (Philip 1969, Bentoumi 1995, Groenevelt et al 1996). The 'transient state' phase reveals a gravitational force and a more-or-less important suction force when the test is made on an initially unsaturated material. The limit between these two states is called critical time, t_{cr}, which is the moment at which the 'transient state' gradually becomes steady (Philip 1969, Groenevelt et al.1996).

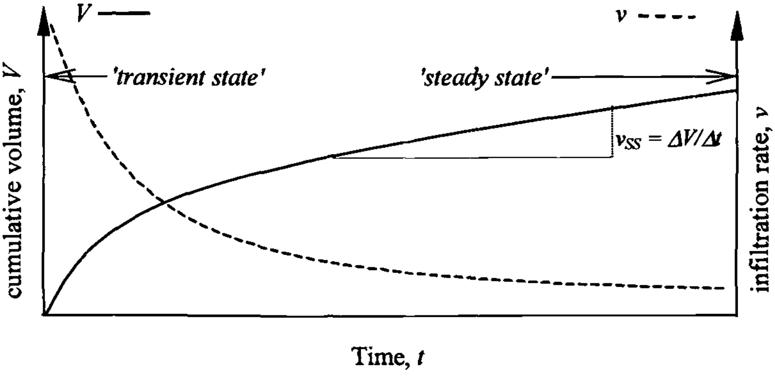

Figure 4 – *Typical relationship of cumulative infiltrated volume (V) and infiltration rate (v) versus time for an initially unsaturated soil.*

Philip's Model

Philip (1957) describes infiltration rate during the 'transient phase' as

$$v = \frac{S_h}{2 \cdot \sqrt{t}} + A \tag{4}$$

where S_h is the sorptivity for hydraulic head, *h*, and *A*, a parameter close to the hydraulic conductivity (among *k/2* and *2.k/3).*

Bentoumi (1995) showed in several tests that the hypothesis of the *A* parameter being among *k/2* and *2.k/3* is rarely verified experimentally. Using compacted SA soil with various initial moisture contents, he showed that the *A* to *k* ratio varies between 3 and 40. Parameter *A* seems to be dependent on the hydraulic head and is close to the state-steady infiltration rate, v_{SS}, for a given hydraulic head. By introducing hydraulic conductivity into the term *A* and considering it to be equal to *2.A*, Groenevelt et al. (1996) propose the equation

$$v = \frac{S_h}{2 \cdot \sqrt{t}} + \frac{k}{2} \tag{5}$$

S_h can be expressed from the White and Perroux (1987) equation

$$S_h^2 = \Delta\theta \left(2 \cdot k \cdot h + \frac{\varphi_m}{b} \right) \tag{6}$$

where *b* is a empirical parameter equal to 0.5 and φ_m, the matric potential at the wetting front.

The method of determining S_h and *A* consists in plotting the infiltration in a $(I/t^{1/2}, t^{1/2})$ graph and using linear regression to determine (a) the slope equal to *A*, and (b) the Y-axis intercept point S_h. In some cases the plot does not give a straight line whereupon S_h can be determined by linear regression in a I versus $t^{1/2}$ plot. Figure 5a presents a typical evolution of infiltration rate versus t, and Figure 5b shows the evolution of the same data versus $t^{-1/2}$. The curve decreases first in a linear pattern according to Philip's model, and then more slowly until it reaches a constant value equal to 'steady state' infiltration rate, v_{SS}. The intersection of these two lines occurs at the critical time t_{cr} (Groenevelt et al 1996).

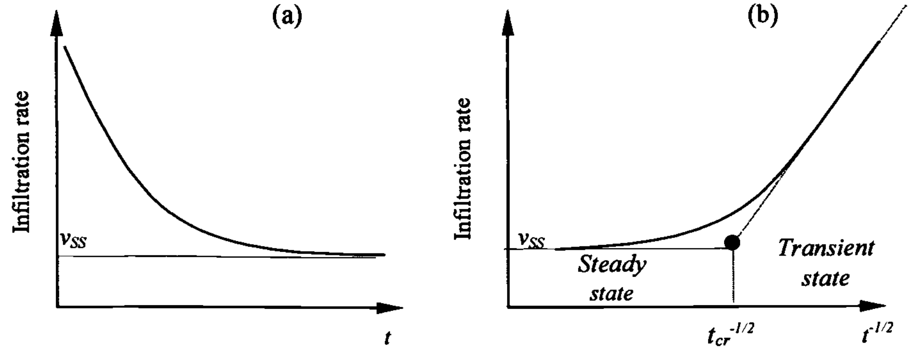

Figure 5 - *Determination of critical time (t_{cr}) and stead- state infiltration rate (v_{SS}) (after Groenevelt et al 1996).*

In the plot versus $t^{-1/2}$, the state steady v_{SS} is estimated by linear extrapolation of the state-steady line on the Y-axis; this value has no theoretical meaning because it decreases constantly to reach the value of the hydraulic conductivity (hypothesis of the semi-infinite medium). The method allows easy determination of the limit between the 'transient' and 'steady' states, but does not always enable easy estimation of the steady-state infiltration rate, v_{SS}. Moreover, for hydraulic conductivities lower than 1.10^{-9}m/s, the decrease of the infiltration rate beyond t_{cr} is not linear versus the square root of time and does not allow an accurate linear extrapolation.

Hyperbolic Law

The steady-state infiltration rate, v_{SS}, can also be determined by a hyperbolic law for a given hydraulic gradient during the transient phase. The tests realized on soils with different hydraulic heads and initial degrees of saturation show that the evolution of the infiltration rate can be described by a hyperbolic law from the first moments of the test. The relationship between infiltration rate and time with this method is postulated to adjust the hyperbolic curve given by the following equation

$$v = \frac{\alpha}{t} + v_{SS} \qquad (7)$$

where α is the model slope factor. At the infinite time

$$lim\left(\frac{\alpha}{t}+v_{SS}\right)=v_{hyp} \tag{8}$$

Equation 7 is that of a straight line in the graph $(v,1/t)$, and Equation 8 shows that the steady-state infiltration rate is given for a infinite time. Consequently, v_{SS} corresponds to the Y-axis intercept of the straight line of slope α. The infiltration rate at time t can be easily determined by Equation 7. Experience has shown that, in most cases, the first infiltration-rate values will be highly variable (Cazaux 1998) due to the very short period (a few minutes) when the infiltrated volumes are not recorded during the setting of the apparatus. Therefore one or several first abnormal points must be systematically deleted when applying this model. Figure 6a shows the SB 1R test data for Philip's model and the hyperbolic law. The infiltration rate versus the opposite of the square root of time shows that Philip's model fits on the first points, but that after about five hours, the infiltration rate drops out of the model and decreases gradually versus time. In this case, the steady-state infiltration rate is difficult to determine. Figure 6b plots the same infiltration-rate values but versus the opposite of time; here the hyperbolic law is linear from the first points and the linear regression can be made before the first five hours, enabling good accuracy in evaluating the infiltration rate. The steady-state infiltration rate computed by hyperbolic law is noted as v_{hyp} that is the infiltration rate determined by the Y-axis intercept of the regression made on the early-time test data.

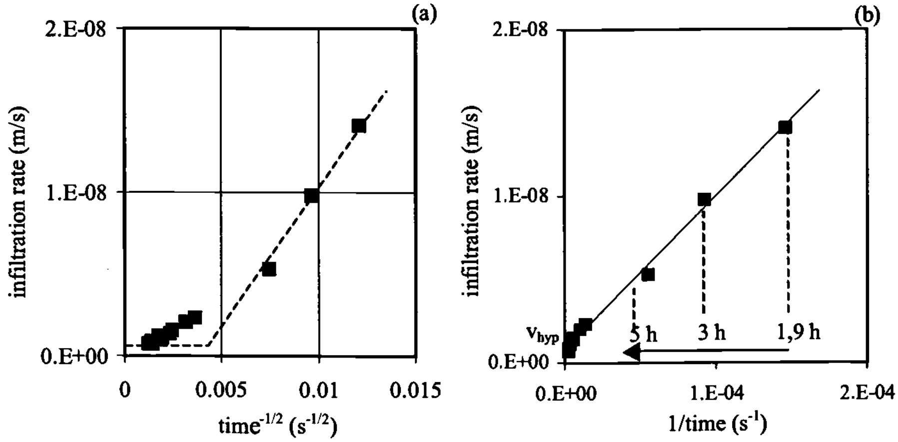

Figure 6 - *Plot of the infiltration rate for test SB 1R using Philip's model (a) and the hyperbolic law (b).*

Comments

For each test, we determined v_{SS} with all the methods described above. We also determined (a) the initial infiltration rate corresponding to the first moments of the test, noted v_{ini}, (b) the infiltration rate after 24 hours infiltration, corresponding to the time of a field test and noted v_{24}, (c) the saturation infiltration rate corresponding to the linear regression of the infiltration curve versus time at the end of test and noted v_{fin}, (Figure 7), (d) the parameters of Philip's model, which are the sorptivity S_h and parameter A, and (e) the infiltration rate obtained with the hyperbolic law, v_{hyp}. Table 3 gives the results for all the tests, along with the testing times to obtain the final infiltration rate v_{fin} and the hyperbolic rate v_{hyp}.

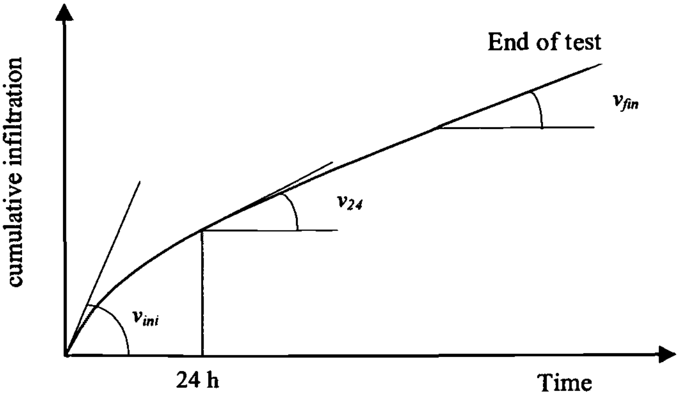

Figure 7 - *Graphical determination of infiltration rate at the beginning of the test* v_{ini}, *after 24 hours testing* v_{24}, *and at the end of test* v_{fin}.

The results show that, for all the tests, the ratio between the initial infiltration rate and the infiltration rate after 24 hours is between 1 and 10, as is the ratio between the final infiltration rate and the rate after 24 hours (Figure 8). This ratio is influenced by the initial soil saturation, $\Delta\theta$, and the hydraulic head, h; the more saturated the soil and the higher the hydraulic head, the lower this ratio, as illustrated by Figure 9. Figure 10 compares the infiltration rate estimated from the hyperbolic model v_{hyp} with that estimated after 24 hours v_{24} and that at the end of test v_{fin}. The ratio between v_{hyp} and v_{24} is between 1 and 10, which is comparable with that obtained initially for all the tests. It is also seen that v_{hyp} gives a good estimation of the final infiltration rate. Comparing the times for determining the final infiltration rate v_{fin} shows the interest of the hyperbolic extrapolation; apart from test C 1R, for which the measurement of the volumes was not made within the first hours of infiltration, this can be done within 24 hours. The average time for estimating v_{hyp} is 10 to 15 times lower than that needed for determining v_{fin}.

The hypothesis concerning parameter A of Philip's model tends to be verified, as shown by Figure 11 in which parameter A is plotted against the infiltration rate estimated from the hyperbolic law v_{hyp} and final test data v_{fin}. Considering these observations, we note that the evolution of the infiltration rate is a function of (a) the initial degree of soil saturation and (b) the applied hydraulic head —the more saturated the soil and the higher the hydraulic head, the more rapidly steady-state conditions are reached. A good estimation of v_{SS} can be obtained both by parameter A of the Philip's model, and by the hyperbolic method, although the latter is easier to use because Philip's model does not always give a good fit.

Table 3 - *Infiltration rates estimated using the various methods*

Test	*Test method*	h (cm)	S_h (m^2/s)	A (m/s)	v_{ini} (m/s)	v_{24} (m/s)	v_{fin} (m/s)	t *(hr)*	v_{hyp} (m/s)	t *(hr)*
SA 1R	RWP	50	$2.7.10^{-5}$	$5.8.10^{-8}$	$3.3.10^{-7}$	$1.2.10^{-7}$	$8.0.10^{-8}$	110	$8.4.10^{-8}$	7.5
SA 2R	RWP	100	$4.4.10^{-5}$	$7.2.10^{-8}$	$5.1.10^{-7}$	$1.2.10^{-7}$	$5.5.10^{-8}$	80	$8.0.10^{-8}$	7.5
SA 3R	RWP	150	9.10^{-5}	$1.1.10^{-7}$	$5.5.10^{-7}$	$1.7.10^{-7}$	$9.0.10^{-8}$	60	$1.2.10^{-7}$	7
SA 4R	RWP	30	$3.8.10^{-5}$	$6.1.10^{-8}$	$3.5.10^{-7}$	$8.7.10^{-8}$	$4.0.10^{-8}$	29	$4.2.10^{-8}$	3
C 1R	RWP	100	$1.7.10^{-6}$	$5.4.10^{-10}$	$6.1.10^{-9}$	-	$8.8.10^{-10}$	800	$6.5.10^{-10}$	100
C 2I	SSRI	30	$1.1.10^{-6}$	$2.5.10^{-9}$	$1.1.10^{-8}$	-	$3.3.10^{-9}$	11	$3.6.10^{-9}$	1.8
SB 1R	RWP	10	$2.1.10^{-6}$	-	$1.4.10^{-8}$	$2.7.10^{-9}$	$7.0.10^{-10}$	150	$6.6.10^{-10}$	5
SB 2R	RWP	10	$1.4.10^{-7}$	$1.1.10^{-9}$	$1.7.10^{-8}$	$2.0.10^{-9}$	$1.5.10^{-9}$	350	$1.3.10^{-9}$	18
SB 3I	RWP	10	$9.2.10^{-7}$	-	$1.8.10^{-8}$	$1.8.10^{-9}$	$3.0.10^{-10}$	170	$4.8.10^{-10}$	4
SB 4I	RWP	40	$4.6.10^{-7}$	$2.2.10^{-10}$	$5.8.10^{-9}$	$7.2.10^{-9}$	$5.0.10^{-10}$	120	$5.9.10^{-10}$	4
SB 5I	RWP	140	$3.0.10^{-6}$	$2.5.10^{-9}$	$2.5.10^{-8}$	$3.5.10^{-9}$	$2.2.10^{-9}$	170	$2.0.10^{-9}$	9
SB 6I	RWP	135	$3.7.10^{-6}$	-	$7.1.10^{-8}$	$1.1.10^{-8}$	-	24	$1.2.10^{-8}$	2
SB 7I	RWP	60	$2.5.10^{-7}$	$3.0.10^{-9}$	$8.1.10^{-9}$	$3.0.10^{-9}$	$2.5.10^{-9}$	40	$2.6.10^{-9}$	3.5
SB 8I	ODP	30	$2.8.10^{-7}$	-	$3.4.10^{-8}$	$1.0.10^{-8}$	$7.0.10^{-9}$	90	-	6
SB 9I	SSRI	135	$1.0.10^{-5}$	-	$3.2.10^{-7}$	$4.1.10^{-8}$	-	(24)	$4.1.10^{-8}$	1.6
SB 10I	SSRI	47	$1.9.10^{-6}$	$4.9.10^{-9}$-	$2.0.10^{-8}$	$7.6.10^{-9}$	-	(24)	$5.5.10^{-9}$	4.9
SB 11I	SSRI	20	$1.3.10^{-5}$	$6.1.10^{-9}$-	$3.3.10^{-8}$	$6.6.10^{-9}$	-	(24)	$7.2.10^{-9}$	2.4
SB 12I	SSRI	10	$1.0.10^{-6}$	$4.3.10^{-10}$	$1.9.10^{-8}$	$3.1.10^{-9}$	$1.5.10^{-9}$	70	$1.9.10^{-9}$	9
SBM 1R	RWP	50	$1.7.10^{-6}$	-	$4.3.10^{-8}$	$5.0.10^{-9}$	$4.4.10^{-10}$	480	$4.2.10^{-10}$	25
SBM 2R	RWP	10	$1.5.10^{-6}$	-	$3.3.10^{-8}$	$3.4.10^{-9}$	$4.0.10^{-10}$	560	$3.7.10^{-10}$	25
SBM 3I	RWP	130	-	$1.1.10^{-10}$	$9.7.10^{-10}$	$8.0.10^{-10}$	$1.2.10^{-9}$	280	$1.2.10^{-9}$	14
SBM 4I	RWP	140	$7.2.10^{-7}$	-	$6.7.10^{-9}$	$1.9.10^{-9}$	$3.8.10^{-10}$	190	$2.9.10^{-10}$	5
SBM 5I	RWP	140	$2.2.10^{-7}$	$2.8.10^{-9}$	$6.7.10^{-9}$	$3.3.10^{-9}$	$3.7.10^{-9}$	840	$3.2.10^{-9}$	29
SBM 6I	ODP	30	$9.9.10^{-7}$	$1.3.10^{-9}$	$5.3.10^{-9}$	$3.7.10^{-9}$	$5.5.10^{-10}$	16	-	16
SBM 7I	SSRI	120	$5.5.10^{-7}$	$1.5.10^{-9}$	$2.1.10^{-8}$	$3.1.10^{-9}$	-	(24)	$2.9.10^{-9}$	0.9
SBM 8I	SSRI	120	$6.9.10^{-7}$	-	$2.4.10^{-8}$	$4.1.10^{-8}$	-	(24)	$3.5.10^{-9}$	1.6
SBM 9I	SSRI	120	$1.2.10^{-6}$	$4.1.10^{-9}$	$3.0.10^{-8}$	$4.2.10^{-9}$	-	(24)	$5.3.10^{-9}$	0.8
SBM 10I	SSRI	10	$1.1.10^{-6}$	-	$1.9.10^{-8}$	$2.4.10^{-9}$	$1.3.10^{-9}$	40	$2.0.10^{-9}$	3

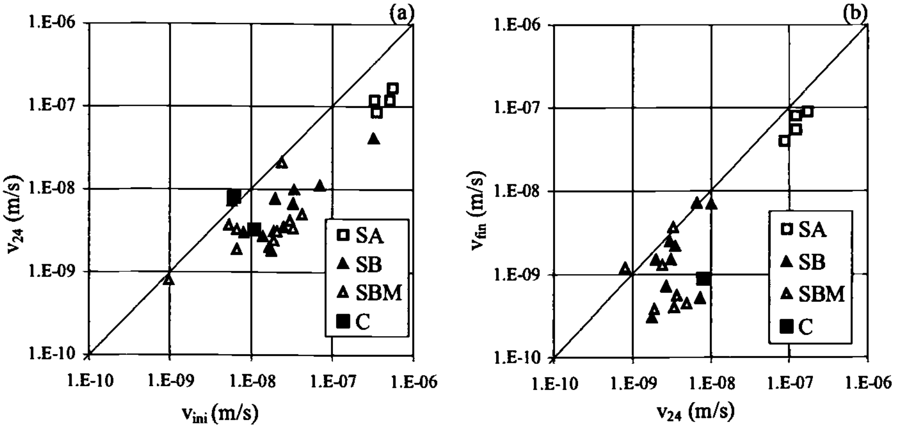

Figure 8 - *Plot of v_{24} versus v_{ini} (a) and of v_{fin} versus v_{24} (b).*

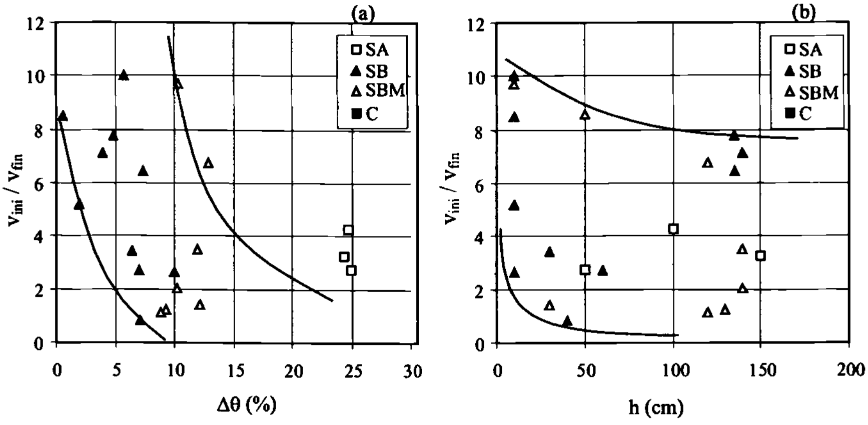

Figure 9 - *Ratio between v_{ini} and v_{fin} versus initial saturation (a) and hydraulic head (b).*

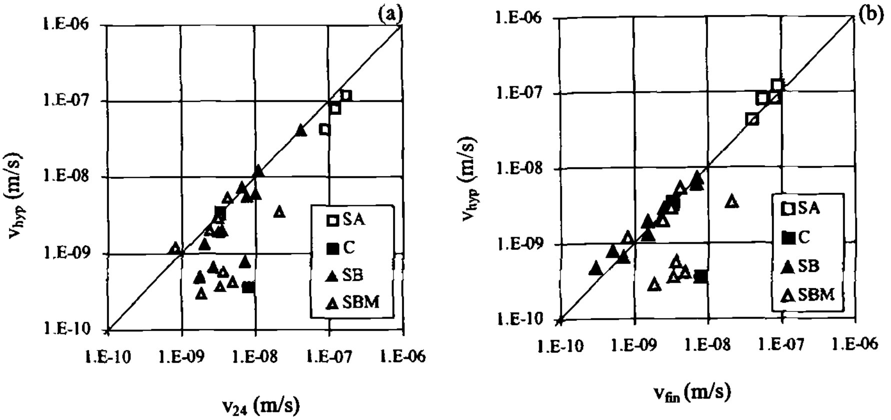

Figure 10 – *Plot of* v_{hyp} *versus* v_{24} *(a) and* v_{fin}*. (b).*

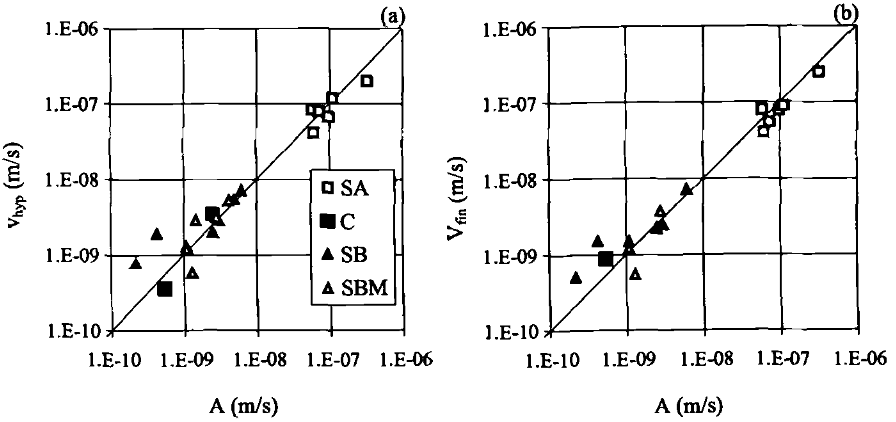

Figure 11 - *Plot of* v_{hyp} *(a) and* v_{fin} *(b) versus parameter A of Philip's model.*

Evaluation of the Hydraulic Gradient

Green and Ampt Model

The depth of the wetting front, z_w, is usually determined at the end of the test by sampling and laboratory water-content determination. It can also be estimated each time with Equation 9 (Green and Ampt 1911)

$$zw = \frac{I}{\Delta\theta} \qquad (9)$$

where I is the cumulative infiltration and $\Delta\theta$ the difference between initial and saturated volumetric water content $(\theta_{sat} - \theta_i)$.

We compared the experimental z_w observed on 22-cm soil columns at different times of infiltration against the estimated values calculated from Equation 9. Figure 12a shows the experimental and calculated curves versus time for test SA 1R with a hydraulic head of 50 cm. Of note is (a) a deviation at the beginning of infiltration, and (b) the similar shape of the experimental and calculated z_w curves after 20 hours testing. The ratio between the experimental and calculated depth is about 2 up to 20 hours and then decreases to 1.2 at 100 hours. The deviation between the two profiles stabilizes at 20 hours to a value of 5 cm; the model tends to underestimate the profile within first hours of testing. Figure 12b shows the same graph but for test SA 3R with a hydraulic head three times higher than in SA 1R. Here we note that the deviation is lower (3 cm) and is acquired within first 10 hours of infiltration. This initial deviation is due to several factors. For example, the shape of the moisture profile is very different from the theoretical piston-shape profile and, in the case of the low-saturation soils and low hydraulic heads, the suction provokes model inadequacy. The difference between the calculated and experimental depth is lessened with long a infiltration time, a high hydraulic head and soil initially close to saturation.

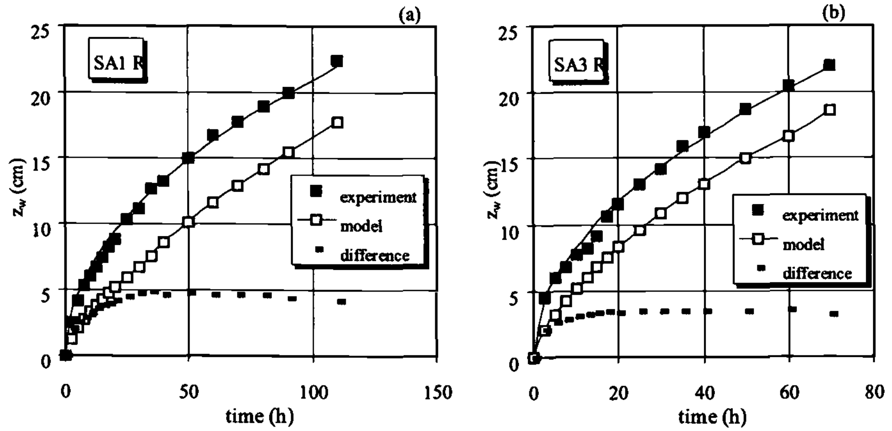

Figure 12 - *Deviation between calculated and experimental moisture profile for tests SA 1R with h = 50 cm (a) and SA 3R with h =150 cm (b).*

Hyperbolic Determination

The depth of the wetting front z_w corresponding to the infiltration rate determined by the hyperbolic law v_{hyp} is estimated according the same law in agreement with Darcy's law (Equation 3). The hydraulic gradient is infinite at the beginning of the infiltration and then decreases to 1 after an infinite testing time. If the infiltration rate follows a hyperbolic law in the first moments of test, the hydraulic gradient i will also follow a hyperbolic law. In these conditions, it can be described by the following relationship:

$$i = \frac{\alpha}{t} + i_{\infty} \qquad (10)$$

where α is the model slope factor and i_{∞} the hydraulic gradient at infinite time. At an infinite time

$$lim\left(\frac{\alpha}{t} + i_{\infty}\right) = i_{hyp} \qquad (11)$$

Equation 11 is a straight-line equation in *(i, 1/t)*, with i_{hyp} corresponding to the Y-axis intercept point of the straight line of slope α. The hydraulic gradient can be determined at any time *t*.

Figure 13 shows the plot for two tests performed on the sand bentonite mixture (SBM): SBM 1R and SBM 4I.

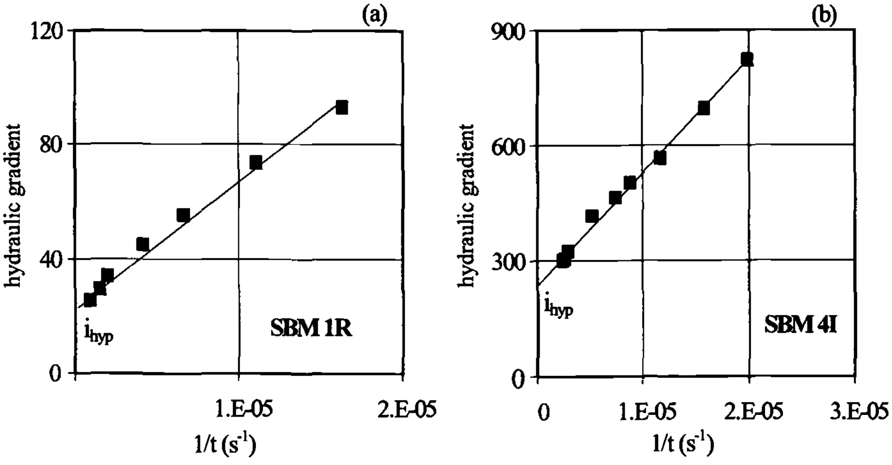

Figure 13 - *Hydraulic gradient versus 1/t for tests SBM 1R (a) and SBM 4I (b).*

Evaluation of Effective Hydraulic Head

In Equation 3, the suction at the wetting front h_f actually corresponds to the water-entry value and can be considered as being equal to 0.5 times the air-entry value (Bouwer 1966). The value of h_f is traditionally taken to be lower than or equal to 0.5 m (Green and Ampt 1911, Hillel and Gardner 1970). It can be determined experimentally by using a pressure transducer connected to the infiltrometer (Bouwer 1966, Topp and Binns 1976, Cazaux 1998) or with a Mariotte bottle and controlled suction (Fallow and Elrick, 1996).

The method consists in closing the water supply of the infiltrometer and recording the decrease in hydraulic head versus time at the soil surface. The hydraulic head shows an initial rapid decrease to a minimum negative value corresponding to the air-entry value Ψ_a (Figure 14), following which the hysteresis effect increases the hydraulic head to a value that allows water to enter the soil. The head then enters a decrease-increase cycle. Analysis of this phenomenon enables experimental determination of the air- and water-entry values respectively Ψ_a and Ψ_w.

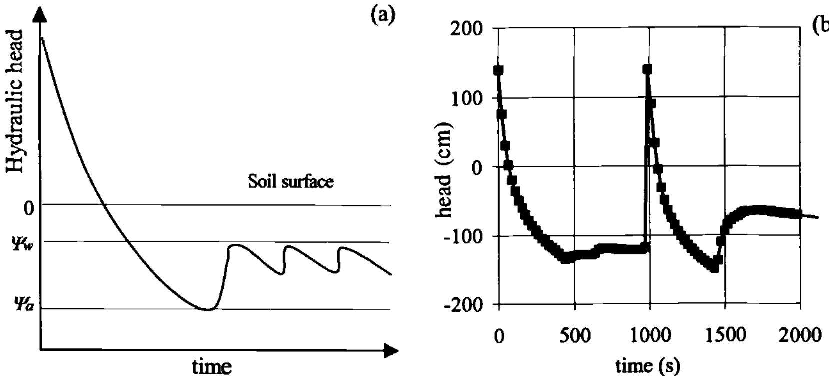

Figure 14 - *(a) Typical variation of hydraulic head versus time (after Fallow and Elrick, 1996), and (b) Hydraulic head versus time for test SA 7R.*

The air-entry value Ψ_a is the hydraulic head in the soil that allows air to escape from the soil pore network. The water-entry value Ψ_w is the head allowing the water to fill the pore network preventing the flow of air; it is very difficult to determine in the field. The air-entry value is only determined if it is assumed that the water-entry value is equal to half the air-entry value. Recently, Fallow and Elrick (1996) noted that the ratio between the water-entry and air-entry values is about 2/3 for a Ψ_w average value of 1 m. Equation (3) becomes

$$k_s = \frac{zf(t)}{h - \psi_w + zf(t)} \cdot v(t) \qquad (12)$$

Saturated Hydraulic Conductivity Calculation

In this section, we compare the hydraulic conductivity estimation from Darcy's law with the parameters estimated using the various available models (Hyperbolic Law, Philip 1969, Green and Ampt 1911, Cazaux 1998). Hydraulic conductivity can also be calculated by analytical methods in unsaturated conditions (Fallow et al. 1994, Elrick and Reynolds, 1992). Two further determinations of hydraulic conductivity are made: the first with Philip's model assumes that *k* is equal to *A/3*, and the second is an indirect method that is described below.

Estimation from Darcy's Law and the Green and Ampt Model

Calculation of hydraulic conductivity with Equation 12 was done for all the tests by computing the parameters estimated from the various analysis methods described above. k_{hyp} is the hydraulic conductivity calculated from v_{hyp} and the hydraulic gradient estimated from hyperbolic law i_{hyp}. k_{fin} is the hydraulic conductivity calculated from v_{fin} and the wetting-front depth z_w experimentally determined at the end of the test. k_{24} is the hydraulic conductivity calculated from v_{24} after 24 hours infiltration and the wetting front z_w calculated from the Green and Ampt model after 24 hours (Equation 9).

Estimation from the Indirect Method (IM)

If we consider the Green and Ampt model (Equation 9) assuming that the wetting front z_w is a perfect horizontal plan, the cumulative infiltration I is expressed as

$$I = z_w \cdot \Delta\theta \tag{13}$$

If we then inject in Equation 3, we obtain

$$v = \frac{dI}{dt} = k\left(\frac{ho - hf + \dfrac{I}{\Delta\theta}}{\dfrac{I}{\Delta\theta}}\right) \tag{14}$$

$$v = k\left(\frac{\Delta\theta \cdot (ho - hf)}{I} + 1\right)$$

$$v = \frac{k_{IM} \cdot \Delta\theta \cdot (ho - hf)}{I} + k_{IM} \tag{15}$$

In the plotting the infiltration rate v versus $1/I$, the slope is equal to $k_{IM}.\Delta\theta.(h-h_f)$ and the Y-axis intercept point to k_{IM}., which is the hydraulic conductivity determined by this indirect method. This procedure only requires the independent measurement of the initial degree of soil moisture and the flow data. The correlation is good from the first points of the test data and solving the hydraulic conductivity consists in finding the best k_{IM} value to obtain the best fit. The hydraulic head at the wetting front h_f may be adjusted to obtain a better fit for very low degrees of initial saturation $\Delta\theta$ (Figure 15). The indirect method nevertheless has the disadvantage of being directly dependent on $\Delta\theta$, and so a poor estimation of this parameter can lead to errors. Moreover, fitting of experimental data with the model can lead to potential error too and in that case, the method can lead to an estimated result with a major systematic error.

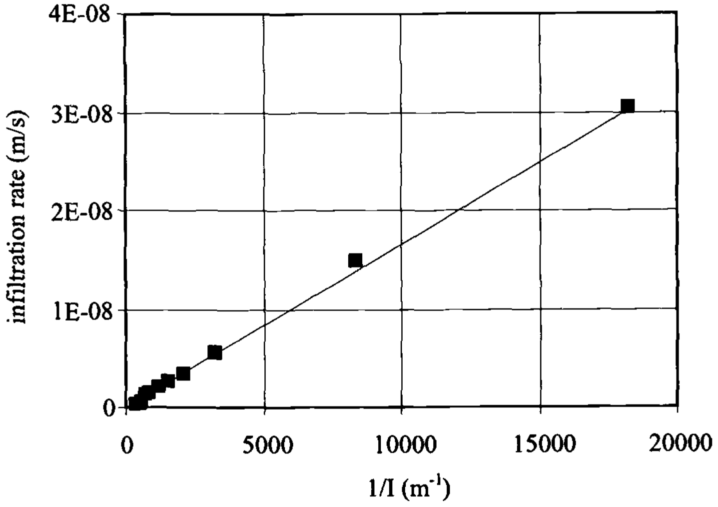

Figure 15 - *Solving hydraulic conductivity test SBM 2R by the indirect method (*$\Delta\theta = 9.3\%$*,* $h = 0.1$ *m, adjusted* $hf = 0.5$ *m);* $k_{IM} = 2.9.10^{-11}$ *m/s.*

Unsaturated Analysis

Basic Analysis - The procedure suggested by Elrick and Reynolds (1992) for interpreting hydraulic conductivity from infiltration tests is based on the calculation of k from the estimation of a empirical parameter α^*

$$k_{ER} = \frac{Q_{rp}}{\left(\frac{r}{C_2}h + \pi r^2 + \frac{r}{C_2}\frac{1}{\alpha^*}\right)} \qquad (17)$$

where Q_{rp}, is the steady-state flow, h is the hydraulic head, r is the radius of the infiltrometer and C_2 is a shape coefficient equal to 0.5 for the device used in this program.

Transient-state analysis - Fallow et al (1994) proposed estimating the saturated hydraulic conductivity from the early-time data obtained in the infiltration measurements. The validity domain of this analysis is limited to the transient state before the critical time, as defined earlier. The hydraulic conductivity k_{FAL} determined by this procedure is calculated with the relationship proposed by Reynolds and Elrick and (1990) between k and the matrix potential Φ_m

$$\alpha^* \equiv \frac{k_{FAL}}{\Phi_m} \qquad (19)$$

The first step of the method is to determine the sorptivity S_h from the representation of the infiltration versus the square root of time. The sorptivity S_0 is then determined from the relationship giving S_h (Fallow et al 1994)

$$S_h = S_0 \cdot \left[1 + 2b\alpha^* h\right]^{1/2} \tag{20}$$

α^* is chosen according to the structure of the soil; in the case of compacted clays it is equal to 1 m^{-1}. From Equation 21, Φ_m is calculated with the experimental value of $\Delta\theta$ and assuming b =0.55

$$S_0 = \left[\Delta\theta \cdot \Phi_m / b\right]^{1/2} \tag{21}$$

The hydraulic conductivity k_{FAL} is then determined from Equation 19. This analytical method requires only a short testing time, but is partially based on empirical parameters.

Results Analysis

We used all the methods (k_{24}, k_{fin}, k_{hyp}, $A/3$, k_{ER}, k_{FAL}, k_{IM}) to determine the hydraulic conductivity for each test so as to be able to compare the values both between each other and with the values of the saturated hydraulic conductivity determined for each test and noted k_S. The results are given in Table 4.

Here it can be seen that the indirect method based on an analysis of the first hours of testing gives a good estimation of the hydraulic conductivity k for most of the soils. The ratio k_{IM} / k_S varies from 0.3 to 5, with the exception of a few tests where it reaches 10 (Figure 16). Nevertheless, a tendency to underestimation is observed for a few tests performed on the SB silt and the SBM. The experimental determination of the initial saturation made on a small sample can also explain deviation of the model. Inaccurate fitting of the experimental data by the operator with indirect method can also amplify the error made on the estimation of initial saturation. Whereas many authors propose simple empirical relationships such as k equal to $A/2$, $A/3$ or $2A/3$ for estimating hydraulic conductivity, we propose estimating k from parameter A of Philip's model since we have shown that A is much closer to v_{fin} than to $2k$ or $3k$. As shown by the most favorable relationship, $A/3$ does not lead to a good estimation of the hydraulic conductivity. A could reasonably be used as a first estimation of k_S, because it is strictly a function of hydraulic head h. The three singular points giving $A/3$ lower than the hydraulic conductivity obtained on SA silt concern three tests with a very low hydraulic head (10 cm). In this case, the divisor 3 is higher than the actual hydraulic gradient.

The results from Elrick and Reynolds (1992) procedure, k_{ER}, show a tendency to overestimation (Figure 17). In the case of the SBM soil, the points that are the farthest from the equal line correspond to the four field tests and give a k_{ER}/k_S ratio of 4 to 10. The calculation was made by taking an α^* coefficient of 1, corresponding to a homogeneous fine-grained soil. Even though the SBM is originally a coarse-grained structure, we must take into account that the addition of bentonite confers the characteristics of a fine-grained soil. α^* was then calculated by an inverse method from the value of the actual saturated hydraulic conductivity k_S. We note that α^* varies between 0.2 and 2.6 for the laboratory tests and between 0.04 and 0.5 for the field tests that show an overestimation of the hydraulic conductivity. These results are in agreement with Elrick and Reynolds (1992) hypotheses, which assume that field material usually has greater macroporosity than soil tested in the laboratory because of the scale effect; in these conditions α^* should be higher.

Table 4: *Hydraulic conductivity values (m/s) obtained from the analysis methods*

Test	*method*	k_{24}	k_{fin}	k_{ER}	k_{FAL}	k_{IM}	*A/3*	k_{hyp}	k_S
SA 1R	RWP	$1.3.10^{-8}$		$1.8.10^{-8}$	$2.0.10^{-9}$	$1.1.10^{-8}$	$1.9.10^{-8}$	$2.3.10^{-8}$	$1.3.10^{-8}$
SA 2R	RWP	$8.4.10^{-9}$		$1.2.10^{-8}$	$3.2.10^{-9}$	$9.9.10^{-9}$	$2.4.10^{-8}$	$1.3.10^{-8}$	$1.1.10^{-8}$
SA 3R	RWP	$1.0.10^{-8}$		$1.7.10^{-8}$	$9.6.10^{-9}$	$1.4.10^{-8}$	$3.6.10^{-8}$	$1.5.10^{-8}$	$1.6.10^{-8}$
SA 4R	RWP	$2.1.10^{-8}$		$3.8.10^{-9}$	$8.7.10^{-9}$	$5.6.10^{-9}$	$2.0.10^{-8}$	$2.9.10^{-9}$	$4.8.10^{-9}$
C 1R	RWP	$1.2.10^{-10}$		$8.7.10^{-11}$	$2.9.10^{-11}$	$9.2.10^{-11}$	$1.8.10^{-10}$	$7.5.10^{-11}$	$4.0.10^{-11}$
C 2I	SSRI	$1.9.10^{-10}$		$1.5.10^{-10}$	$2.2.10^{-11}$	$8.0.10^{-11}$	$8.3.10^{-10}$	$1.5.10^{-10}$	$1.5.10^{-10}$
SB 1R	RWP	$3.9.10^{-10}$	$2.2.10^{-10}$	$4.1.10^{-9}$	$2.9.10^{-11}$	$9.6.10^{-11}$		$3.5.10^{-10}$	$7.0.10^{-10}$
SB 2R	RWP	$2.5.10^{-10}$	$7.9.10^{-10}$	$2.5.10^{-10}$	$1.9.10^{-11}$	$4.5.10^{-10}$	$3.7.10^{-10}$	$6.8.10^{-10}$	$6.0.10^{-10}$
SB 3I	RWP	$8.2.10^{-11}$	$2.5.10^{-11}$	$5.0.10^{-11}$	$7.4.10^{-11}$	$9.5.10^{-11}$		$3.7.10^{-11}$	$8.0.10^{-11}$
SB 4I	RWP	$3.6.10^{-11}$	$1.1.10^{-10}$	$5.7.10^{-11}$	$2.3.10^{-11}$	6.10^{-12}	$7.3.10^{-11}$	$9.3.10^{-12}$	$8.0.10^{-11}$
SB 5I	RWP	$4.4.10^{-11}$	$1.2.10^{-10}$	$8.8.10^{-11}$	$1.2.10^{-10}$	$5.8.10^{-11}$	$8.3.10^{-10}$	$7.4.10^{-11}$	$8.0.10^{-11}$
SB 6I	RWP	$1.1.10^{-11}$		$2.8.10^{-10}$	$1.2.10^{-11}$	$9.0.10^{-11}$		$6.3.10^{-11}$	$1.2.10^{-10}$
SB 7I	RWP	$3.5.10^{-11}$	$1.4.10^{-10}$	$1.0.10^{-10}$	$4.4.10^{-13}$	$1.5.10^{-11}$	$1.0.10^{-9}$	$8.1.10^{-11}$	$1.1.10^{-10}$
SB 8I	ODP	$4.6.10^{-10}$	$1.3.10^{-9}$	$7.7.10^{-10}$	$2.3.10^{-12}$	$4.5.10^{-10}$		$6.7.10^{-10}$	$8.0.10^{-10}$
SB 9I	SSRI	$2.1.10^{-9}$		$6.1.10^{-10}$	$1.4.10^{-10}$	$5.1.10^{-10}$		$3.9.10^{-10}$	$3.0.10^{-10}$
SB 10I	SSRI	$3.8.10^{-10}$		$4.4.10^{-10}$	$5.6.10^{-11}$	$1.5.10^{-10}$	$1.6.10^{-9}$	$2.0.10^{-10}$	$4.0.10^{-10}$
SB 11I	SSRI	$4.6.10^{-10}$		$6.9.10^{-10}$	$8.9.10^{-10}$	$6.7.10^{-10}$	$2.0.10^{-9}$	$4.8.10^{-10}$	$5.5.10^{-10}$
SB 12I	SSRI	$1.5.10^{-10}$	$1.5.10^{-10}$	$2.8.10^{-10}$	$8.9.10^{-12}$	$3.2.10^{-10}$	$1.5.10^{-10}$	$1.0.10^{-10}$	$7.0.10^{-10}$
SBM1R	RWP	$6.9.10^{-11}$	$2.4.10^{-11}$	$1.9.10^{-11}$	$1.0.10^{-11}$	$2.4.10^{-11}$		$1.8.10^{-11}$	$2.0.10^{-11}$
SBM2R	RWP	$1.6.10^{-10}$	$8.8.10^{-11}$	$2.4.10^{-11}$	$1.1.10^{-11}$	$2.9.10^{-11}$		$5.1.10^{-11}$	$2.0.10^{-11}$
SBM3I	RWP	$4.3.10^{-12}$	$2.1.10^{-11}$	$3.5.10^{-11}$	$1.6.10^{-14}$	-	$3.7.10^{-10}$	$3.2.10^{-11}$	$4.0.10^{-11}$
SBM4I	RWP	$3.1.10^{-12}$	2.10^{-12}	$8.3.10^{-12}$	$9.4.10^{-13}$	$4.6.10^{-12}$		$3.3.10^{-12}$	$1.0.10^{-11}$
SBM5I	RWP	$6.1.10^{-12}$		$8.3.10^{-11}$	$1.0.10^{-13}$	$4.2.10^{-11}$	$9.3.10^{-10}$	$2.3.10^{-11}$	$2.0.10^{-11}$
SBM6I	ODP	$3.9.10^{-11}$	$5.6.10^{-11}$	$2.8.10^{-11}$	$3.3.10^{-12}$	$4.9.10^{-11}$	$4.3.10^{-10}$	$4.4.10^{-11}$	$5.0.10^{-11}$
SBM7I	SSRI	$9.0.10^{-12}$		$1.7.10^{-10}$	$5.6.10^{-13}$	$3.9.10^{-12}$	$5.0.10^{-10}$	$1.3.10^{-11}$	$1.4.10^{-11}$
SBM8I	SSRI	$3.5.10^{-11}$		$9.3.10^{-11}$	$1.3.10^{-12}$	$5.0.10^{-12}$		$1.6.10^{-11}$	$2.3.10^{-11}$
SBM9I	SSRI	$4.5.10^{-11}$		$3.9.10^{-11}$	$3.3.10^{-12}$	$1.6.10^{-11}$	$1.4.10^{-10}$	$3.3.10^{-11}$	$3.3.10^{-11}$
SBM10I	SSRI	$7.0.10^{-11}$	$7.2.10^{-11}$	$7.0.10^{-11}$	$5.9.10^{-12}$	$7.4.10^{-11}$		$7.8.10^{-11}$	$3.0.10^{-11}$

We assume that the overestimation does not result from α^*, but from the shape factor of the flow, especially considering that all the SBM specimens had very homogeneous initial physical characteristics. With the other soils the model shows a better adaptation with the k_{ER}/k_S ratio varying between 0.5 and 3. Figure 17, which gives the values of α^* computed from the saturated hydraulic conductivity k_s, shows good homogeneity for this parameter with the clay C, silt SA, and silt-bentonite mixture SBM, although not in the field tests. For silt SB, the spatial dispersion reveals the heterogeneousness that was noted in the field and laboratory samples. The range of α^* from 0.2 to 20 can be explained by the macroporosity created by compaction process, that makes the barrier heterogeneous compared to the theoretical homogeneous soil matrix in the model.

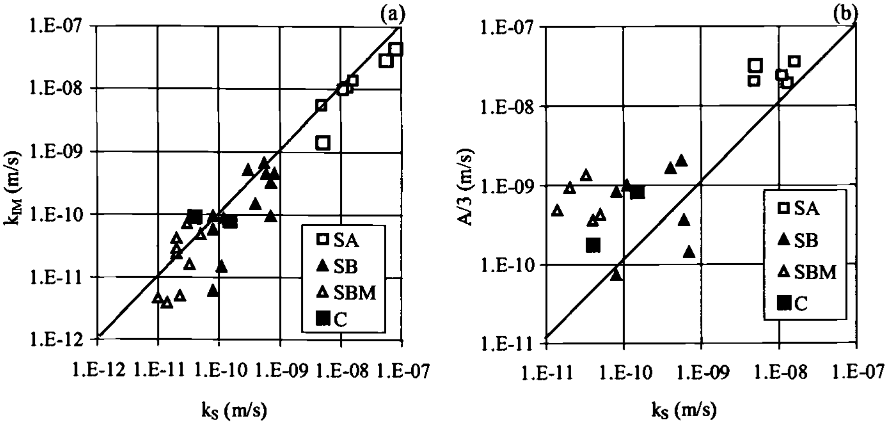

Figure 16 - *Hydraulic conductivity calculated using the indirect method (a) and parameter A of the Philip's model (b).*

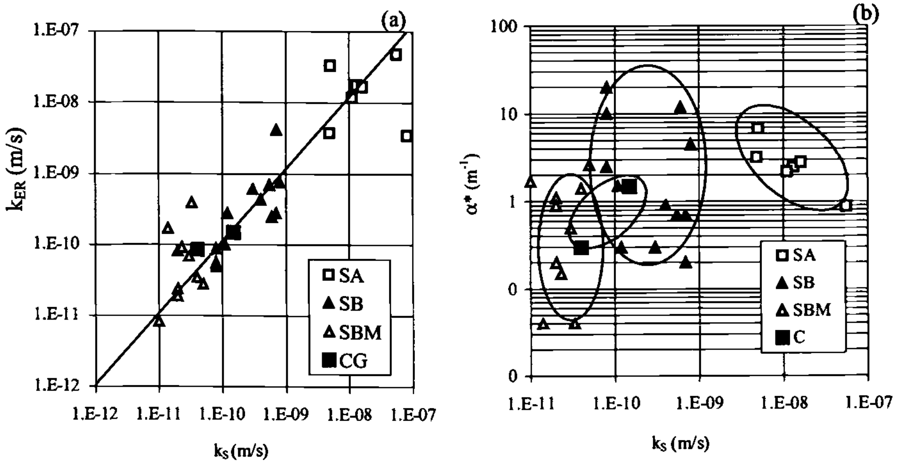

Figure 17 - *Hydraulic conductivity calculated using the Elrick and Reynolds (1992) procedure (a), and values of α^* computed from saturated hydraulic conductivity (b).*

Figure 18 shows the hydraulic conductivity calculated from (a) the data at 24 hours and (b) the final data. The k_{24} values deviate to both sides of the equal line with a ratio between 0.1 and 10. Unlike the previous two methods and k_{fin}, where points are closer to the line, a real dispersion is observed around the equal line and not only a few singular points. In the case of k_{fin}, the singular points correspond to specimens that had a lower initial degree of soil saturation $\Delta\theta$: SB 3I, SB 4I and SBM 4I. We must also admit that the overall time of testing has a real influence on the validity of the final result. Even though conventional analysis of the data after 24 hours gives a satisfactory estimation of the hydraulic conductivity, the application of longer testing times decreases the uncertainty.

Figure 19 shows the hydraulic conductivity k determined by the Fallow et al (1994) analysis and by the hyperbolic law method. The former, which is based on the sorptivity value, gives a few underestimated values. Those closest to the saturated hydraulic conductivity k_s correspond to the tests made on specimens with the lowest degree of initial soil saturation $\Delta\theta$. As the hydraulic conductivity calculation is directly related to the sorptivity S_h, the model gives important deviations when dealing with soils of very low sorptivity because initially close to saturation. When considering the relationship between k_{hyp} and k_S with this method, we note that the points are close to the equal line and that the ratios are the closest to 1 of all the methods. Only five tests give k_{hyp} distant from the equal line, with a maximum k_{hyp}/k_S ratio of 2 (SB 4I, SB 12I, SBM 4I, MA 1 and MA 3).

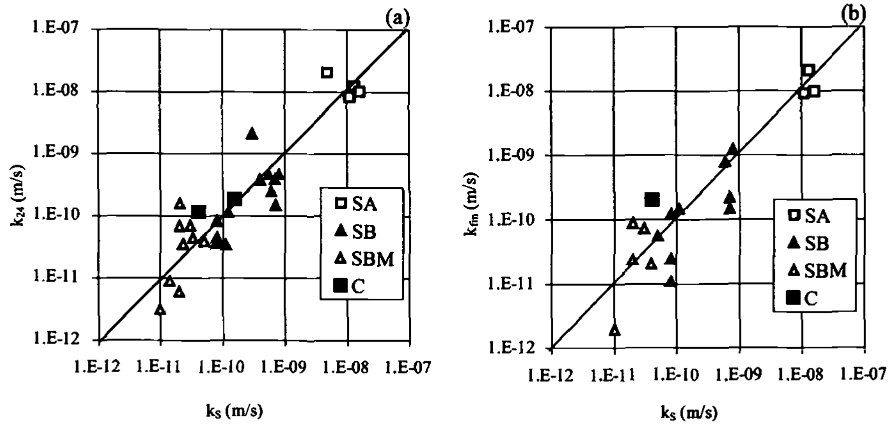

Figure 18 - *Hydraulic conductivity calculated from data after 24 hours (a) and from final data (b).*

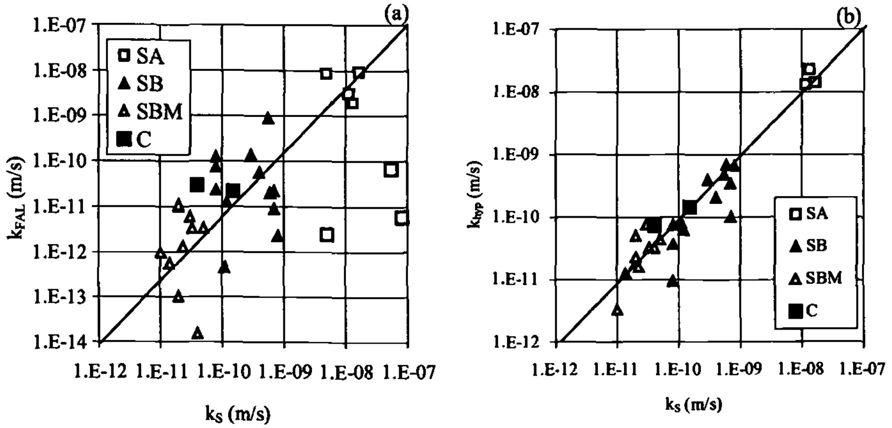

Figure 19 - *Hydraulic conductivity calculated from the Fallow et al (1994) method (a) and from the hyperbolic law (b).*

Conclusions

The results presented in this paper give very interesting information. First, it seems that the conventional methods for determining hydraulic conductivity, based on the Green and Ampt model and Darcy's law, are reliable if the testing times are sufficiently long. With short test times (generally a few hours), the indirect method and the hyperbolic method give estimations of the saturated hydraulic conductivity with lowest uncertainty. However, both methods are based on a best-fit analysis of experimental data that can lead to systematic error. This is particularly true for the indirect method where the value of hydraulic conductivity can be highly influenced by the unique determination of initial saturation of soil. Moreover, the practice shows that the first experimental infiltration data are always abnormal. The analysis proposed by Elrick and Reynolds (1992) gives satisfactory results, but leads to an overestimation of the hydraulic conductivity; it also requires the choice of the parameter α^*, which can increase uncertainties to more than magnitude 10. Assuming the typical value of α^* to 1, according to Elrick and Reynolds (1992) maybe non conservative with respect to landfill liners applications (Guyonnet et al., 2000). The estimation of the hydraulic conductivity from parameter A of Philip's model is also not satisfactory. Analysis using final data leads to the best centering on the equal line, similar to that determined from the hyperbolic law. The overestimation with the Philip's model and the Elrick and Reynolds (1994) method, and the underestimation noted with the indirect method are obvious. The hyperbolic law and the indirect method are able to give a good estimation of the saturated hydraulic conductivity with very short testing times. The hyperbolic law appears simple and fast to use and the indirect method needs very few data, but both require are source of important errors of interpretation. The conventional analytical method based on the final data of the infiltration tests remains the most commonly used in practice. We note that with both the analysis after 24 hours and the final analysis, the testing time is an essential parameter in the validity of the estimation of the saturated hydraulic conductivity using the conventional Darcy's method. The results of this testing program show that it is possible to use short-term field hydraulic conductivity tests with sufficient accuracy to assess the hydraulic performance of hydraulic barriers, especially since characterizing the real saturated hydraulic conductivity is not the main objective for site construction quality control program. If the soil has been previously well-defined in the laboratory (saturated hydraulic conductivity, compaction parameters, moisture content and density), short-term field testing can offer a very useful and representative tool for field control procedure of hydraulic performance. However, to assess the real saturated hydraulic conductivity of a fine-grained soil, long term tests should be performed in the laboratory until full saturation of specimen.

References

Bentoumi, O., 1995, "Transfert par infiltration de l'eau dans les sols fins compactés non saturés: Etude de la diffusivité et de la conductivité hydraulique," *Doctoral thesis, Institut National des Sciences Appliquées de Lyon, France,* No. D'ordre 95ISAL0100, 202 p.

Bouwer, H., 1966, "Rapid Field Measurement of Air Entry Value and Hydraulic Conductivity of Soil as Significant Parameters in Flow System Analysis," *Water Resources Research,* 4th quart. No. 4, pp. 729-738.

Cazaux, D., 1998, "Mesure et contrôle in situ de la perméabilité des matériaux utilisés dans les dispositifs d'étanchéité pour la protection de l'environnement, Etat de l'art et Développements," *Doctoral thesis, Institut National des Sciences Appliquées de Lyon, France,* 335 p.

Elrick, D.E. and Reynolds, W.D., 1992, "Infiltration from Constant-Head Well Permeameters and Infiltrometers," *Advances in Measurement of Soil Physical Properties: Bringing theory into practice,* Madison (WI), *Soil Science Society of America Journal,* SSSA Special Publication No. 30, pp. 1-24.

Fallow, D.J. and Elrick, D.E., 1996, "Field Measurement of air-entry and water entry soil water pressure head," Soil Sci. Soc. Am. J., No. 60, pp. 1036-1039.

Fallow, D.J., Elrick, D.E., Reynolds, W.D., Baumgartner, N. and Parkin, G.W., 1994, "Field Measurement of Hydraulic Conductivity in Slowly Permeable Materials Using Early-time Infiltration Measurements in Unsaturated Media," *Hydraulic Conductivity and Waste Contaminant Transport in Soil,* David E. Daniel and Stephen J. Trautwein, Eds., Philadelphia, American Society for Testing and Materials, pp 375-389, ASTM STP 1142.

Green, W.H. and Ampt, G.A., 1911, "Studies on Soil Physics: I. The Flow of Air and Water through Soils," *Journal Agric. Science,* Vol. 4, pp. 1-24.

Groenevelt, P.H., Odell, B.P. and Elrick, D.E., 1996, "Time domains for early-time and steady-state pressure infiltrometer data," *Soil Science Society of America Journal*, Vol. 60, pp. 1713-1717.

Guyonnet, D., Amraoui, N. and Kara, R., 2000, " An analysis of transient flow during ring infiltrometer tests in fine-grained soils, " *Ground Water*, Vol. 38, no. 3, pp. 396-402.

Hillel, D. and Gardner, W.R., 1970, "Measurement of unsaturated conductivity and diffusivity by infiltration through an impeding layer," *Soil Science.*, Vol. 109, No. 3, pp. 149-162.

Olson, R.E. and Daniel, D.E., 1981, "Measurement of the hydraulic conductivity of fine-grained soils," *Permeability and Groundwater Contaminant Transport, T.F. Zimmie and C.O. Riggs Eds., Philadelphia: American Society for Testing and Materials*, pp. 18-64, ASTM STP 746.

Philip, J.R., 1957, "The theory of infiltration: 1. The infiltration equation and its solution," *Soil Science*, Vol. 83, pp. 345-357.

Philip, J.R., 1969, "Theory of infiltration," *in Advances in Hydrosciences*, Ed. V.T. Chow, New York: Academic Press, Vol. 5,pp. 215-296.

Purdy, S.D. and Ramey, T.V., 1995, "Comparison of Hydraulic Conductivity test methods," *Proc. Sardinia 95, 5th Int. Landfill Symposium*, Cagliari, Italy, pp 321-329.

Reynolds, W. D., and Elrick, D.E., 1990, "Ponded infiltration from a single ring: I. Analysis of steady flow," *Soil Science Society of America Journal*, Vol. 54, pp 1233-1241.

Topp, G.C. and Binns, M.R., 1976, "Field Measurement of Hydraulic Conductivity with a Modified Air-Entry Permeameter," *Canadian Journal of Soil Science*, Vol. 56, pp. 139-147.

White, I. and Perroux, K.M., 1966, "Use of sorptivity to determine filed soil hydraulic properties," *Soil Science Society of America Journal,* 1987, Vol. 51, pp. 1093-1101.

Rosa Galvez-Cloutier[1] and Jean-Sèbastien Dubé[1]

Impact of Residual NAPL on Water Flow and Heavy Metal Transfer in a Multimodal Grain Size Soil under Saturation Conditions: Implications for Contaminant Mobility

---

Reference: Galvez-Cloutier, R. and Dubé, J.-S., "**Impact of Residual NAPL on Water Flow and Heavy Metal Transfer in a Multimodal Grain Size Soil under Saturation Conditions: Implications for Contaminant Mobility**", *Evaluation and Remediation of Low Permeability and Dual Porosity Environnements, ASTM STP 1415,* M.N. Sara and L.G. Everett, Eds., ASTM International, West Conshohocken, PA, 2002.

Abstract:

This paper presents the study of the influence of residual NAPL on the transport of various heavy metals trough a mixed contaminated soil under saturation conditions. The concepts of soil structure, preferential flow, heavy metal transfer: retention and transport and multiphase hydrodynamics are investigated for various conditions. Residual NAPL causes water to bypass regions it occupies towards regions having less flow resistance, hence creating preferential flow and transport. Residual NAPL can also obstruct small pore entries and mask active surface sites. Thus, it can influence heavy metal net transfer. Our results show that mobility of heavy metals is altered by the presence of NAPL. This behavior has important implications from both contamination assessment and remediation perspectives.

Keywords: contaminated soil, mixed contamination, heavy metals, NAPL, preferential flow, mobility

Introduction

Among the most commonly encountered soil contaminants are heavy metals, petroleum hydrocarbons, and halogenated organics. Many of them are highly toxic and/or potential carcinogens. In 80% of the 1384 Quebec polluted sites, heavy metals and NAPL (Non Aqueous Phase Liquids) are simultaneously found.

From a scientific and technical perspective, assessment of metal mobility, risk evaluation and remediation of mixed contaminated sites are often complicated by the lack of fundamental knowledge about interactions between metals and NAPLs. These interactions have yet to be identified and their impact on contaminant mobility and site remediation have to be assessed. Therefore, this study provides critical information on heavy metals-NAPL interactions in soil and addresses the following issues: 1) the relation between residual NAPL occupation of void space and modification of water flow and

---

[1] Associate Professor and Research Assistant, respectively, Civil Engineering Department Laval University, Faculty of Sciences and Engineering, Quebec, Canada, G1K 7P4.

heavy metal transport and 2) the implications of NAPL-induced water flow modifications on heavy metal retention and chemical interactions with the soil solid phase.

Objectives

The main goal of this study is to identify the processes by which residual NAPL influences heavy metal transfer in a water saturated soil.

Review of literature

Classic transport theory through porous media considers a homogeneous medium composed of identical particles generating a void network of identical pores, each pore having the same water conductivity as all others. In such ideal media, macroscopic parameters, such as hydraulic conductivity (*K*) and grain- or pore-size distributions, are constant in space. However, real soil formations show spatial variations in these parameters. A homogeneous soil can be described as having macroscopic parameters showing variations but maintaining constant average values through space (Freeze and Cherry 1979). Such parameters have monomodal probability density functions. In heterogeneous soils, however, the spatial variability of parameters is greater and hence their average values also vary in space. Parameters in these soils have multimodal probability density functions. For instance, in well-aggregated soils, the distribution of porosity is usually bimodal because of the discontinuity between macroporosity and matrix porosity.

When residual NAPL is present, it will occupy regions of the void network and hence decrease the relative permeability to water of those regions. In water-wet media, residual NAPL will form ganglia in the intermediate to large pores. The heads and tails of these ganglia will occupy the pores themselves whereas their body will occupy the pore necks (Conrad et al. 1992). This situation creates discontinuities in the void network and modifies the water flow pattern. Water will therefore bypass NAPL-regions of lower relative permeability to regions of higher relative permeability if available (Mayer and Miller 1993). In oil-wet media, this water bypassing phenomenon may be increased, because residual NAPL occupies the finer pores, forms non-miscible films at the surface of soil grains and aggregates, and water can then only flow through larger pores. The presence of residual NAPL causes water to flow preferentially through larger pores, thereby decreasing the surface area and time available for contact with the solid phase. Therefore, residual NAPL may shift the water flow pattern from matrix to preferential flow. If a preferential flow pattern was already present before the introduction of residual NAPL, it may be stabilized and even enhanced by the presence of residual NAPL.

Reactions between solutes and the solid surfaces are controlled by 1) the available surface area, 2) the contact time between the liquid and solid phases, and 3) the reactivity of the solid phase. The first two parameters are functions of the pore size distribution and pore water velocity, respectively, making reactions dependent on the water flow pattern. In homogeneous soils, because permeability and porosity distributions are constant through space, surface area and contact time are considered constant throughout the medium. In these soils, flow is homogeneous and called matrix flow. However, in heterogeneous soils, for example well-aggregated soils, bimodal porosity produces a heterogeneous flow pattern consisting of macroporous flow (i.e. very rapid flow through macropores also called inter-aggregate flow) and matrix flow (i.e. intra-aggregate flow).

Furthermore, surface area and contact time vary through space being high in micropores and decrease as the pore size increases.

The mechanisms by which residual NAPL is retained in the void network depend on the wettability of the solid surfaces. As mentioned before, if the soil is water-wet, NAPL will be retained as ganglia occupying pore bodies and pore throats and therefore creating discontinuities in the void network. If the soil is oil-wet, NAPL will be retained as films and pendular rings, and will occupy the smaller pores. However, in real surface soils, the wettability of the soil surface is mixed due to the presence of different mineral and organic surfaces. Hence, NAPL ganglia as well as surface films can occur. Therefore, in addition to decreasing the access of solutes to reaction sites by creating bypassing water flow, residual NAPL can also decrease available surface area by forming non-miscible film at the surface of solid particle, therefore masking solute reaction sites. Retention of solutes is possible once they can access reaction sites. In heterogeneous soils, solute reactions are usually limited by the rate of diffusion of the solutes from the larger pores to the smaller pores containing the reaction sites. The presence of non-miscible NAPL films at the surface of soil particles prevents the infiltrating solutes from diffusing into the smaller reactive pores by creating a physical barrier between the infiltrating solution and the resident matrix solution.

Materials and Methods

The soil was sampled from a stormwater runoff infiltration basin under construction in l'Isle d'Abeau (France). It is a quaternary fluvio-glacial deposit representative of the region of Lyon. Sampling was performed in the unsaturated zone at a depth of approximately 2 m. The soil was stored in plastic containers at 4°C. The physico-chemical characterization of the soil was performed during previous studies, namely Laboratoire de Sciences de l'Environnement (LES, 1997) and Plassard (1999). Major components of the soil, determined by X-ray diffraction, are, in decreasing order of abundance; quartz, calcite, muscovite, clinochlore ferrian, albite and a few iron oxides. The natural grain-size distribution of the soil (see Figure 1, reference) indicated a well-graded silty sand having a wide range of particle sizes, which is typical of a fluvio-glacial deposit. The curve 15W-40 shows the impact of NAPL in grain size distribution.

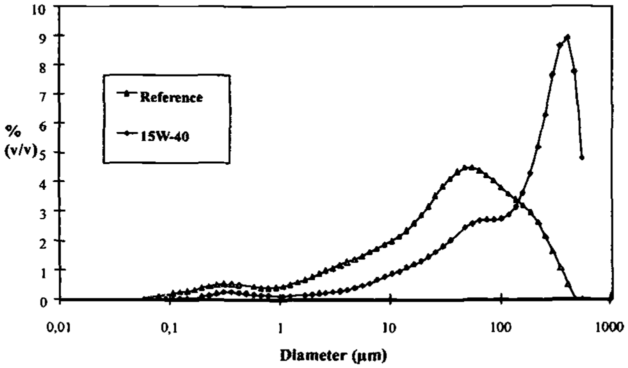

Figure 1 - *Grain size distribution*

The soil showed traces of copper (Cu), chromium (Cr), nickel (Ni), and zinc (Zn) in the range of natural levels reported for those metals. Lead (Pb) and cadmium (Cd) showed slightly detectable levels. Iron (Fe) and calcium (Ca) levels were high, these being constitutive elements of the soil. Soil pH was alkaline (8.0) and the insoluble carbonates content was high (23% w/w) indicating a high buffering capacity and the potential to retain heavy metal as (co-precipitates). The soil was poor in organic matter (1.75 % w/w) and had a low Cation Exchange Capacity (CEC = $2.75 \cdot 10^{-5}$ g/mol).

Laboratory Column Setup

Laboratory columns were composed of a central cell with end diffusers (see Figure 2). The central cell was made of clear PVC (10 cm I.D., 20 cm length) and end diffusers of perforated PVC plates placed between polypropylene screens. Soil was compacted in the silicone grease-lined cells at a water content (*%w*) of 11% (i.e. on the wet side of the modified Proctor curve) producing a dry density of 1.61 ± 0.06 g/cm^3. The total pore volume of columns was 258 ± 9 cm^3 and was measured gravimetrically. Soil columns were then saturated with a saline solution (10^{-2} M NaCl) to maintain an ionic equilibrium during soil column conditioning. The columns were saturated from the bottom at a constant head and kept under static saturation for 24 hours. Then, the resident solution was flushed with 3 pore volumes (PV) of fresh saline solution.

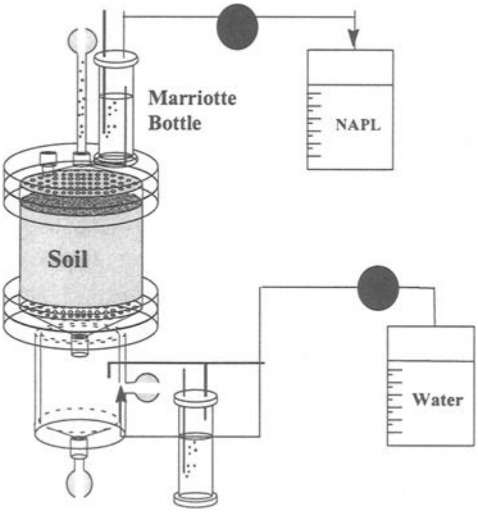

Figure 2- *Experimental setup*

Three series of columns were used with three different NAPL viscosities (O1, O2 and O3) while a fourth series was used as a blank (i.e. no NAPL, reference). Three different mineral oils (motor oils) were used as NAPLs. The density and dynamic viscosity of these oils were measured and are given in Table 1. NAPL was placed into columns similarly to the procedures described by Conrad et al. 1992, Pennell et al. 1993, Dawson and Roberts, 1997 and Fortin et al. 1998. Detailed description of the column setup can be found in Dubé (2001).

Table 1- *Density and viscosity of NAPLs*

NAPL	Density (g/cm^3)	Viscosity (cP)
O1	0.828	156.49
O2	0.856	161.12
O3	0.856	191.22

Columns were run in duplicates and average results were reported. Residual NAPL was determined by the difference between the volume of NAPL injected and that displaced by water. A residual concentration of approximate 12% was obtained for the three NAPL. Then, tracing was performed to characterize the flow pattern in soil columns by continuously injecting a bromide solution (2g Br^-/L) from the bottom at a constant flow rate of 5 mL/min. Samples were taken at each 0.1 PV for a total elution of 3 PV and Br concentration was determined using an ion selective electrode. Similarly, a nitrate solution of Cd, Cu, and Pb (200 mg/L each), was introduced in the soil columns. Effluent solution was sampled at each 0.5 PV for a total elution time of 5 PV. Samples were filtered on 0.45 μm ashless filters and acidified (< pH 2) using HNO_3. The Cd, Cu and Pb were analyzed using flame-AAS. Following the elution of 5 PV of metallic solution, the soil casts were extracted from the cells and fractionated into four layers of 5 cm each. Six samples were taken per layer, air-dried, and screened at 2-mm. In a first sample triplicate, total concentrations of Cd, Cu, and Pb were determined. On a second sample triplicate, the geochemical distributions of the three heavy metals were determined using a sequential chemical extraction method (Tessier et al. 1979). Some samples were also examined using Scanning Electron Microscopy (SEM) coupled with Energy Dispersive Spectrometry (EDS) in order to identify metal-mineral associations and oil pathways.

Results and Discussion

SEM results are presented in Figure 3a and b. Figure 3a shows a silicate particle covered by a mixed coating of NAPL and fine particles possibly of clay and calcite. Figure 3b is a detail of the first figure, which clearly shows the mixed nature of the coatings. Even though silicate surfaces are water-wet, the presence of constitutive elements of calcite at the surface of silicate particles is an indication that calcite has precipitated at the surface of silicates, therefore shifting the wettability of a fraction of the surfaces to oil-wet. Furthermore, the coating of fine reactive particles (clay, carbonate precipitates) by non-miscible films is also evidence that NAPL decreased the reaction potential of the soil and the access to micro-pores.

Water flow is characterized by the elution profiles obtained for Br^- tracer (see Figure 4). The blank series showed preferential tracer elution with a BT (breaktrough) of 0.4 PV and tailing. It could be assumed that the soil columns presented distinctive water fluxes, namely a rapid flux conducted through preferential flow channels and a slower flux through the soil matrix. This preferential flow pattern produced early tracer breakthrough. The remaining fraction of the tracer solution infiltrated the soil matrix and was eluted more slowly, hence producing the tailing of the elution profile. The presence of residual NAPL influenced water flow in comparison to the blank series. Residual NAPL enhanced flow bypassing through preferential channels. Respective BTs for the three NAPL conditions were 0.4, 0.3 and 0.17 PV. The presence of NAPL increased preferential channeling and decreased matrix flow, hence reducing the residence time and the possibility of exchanges between the soil and aqueous phases.

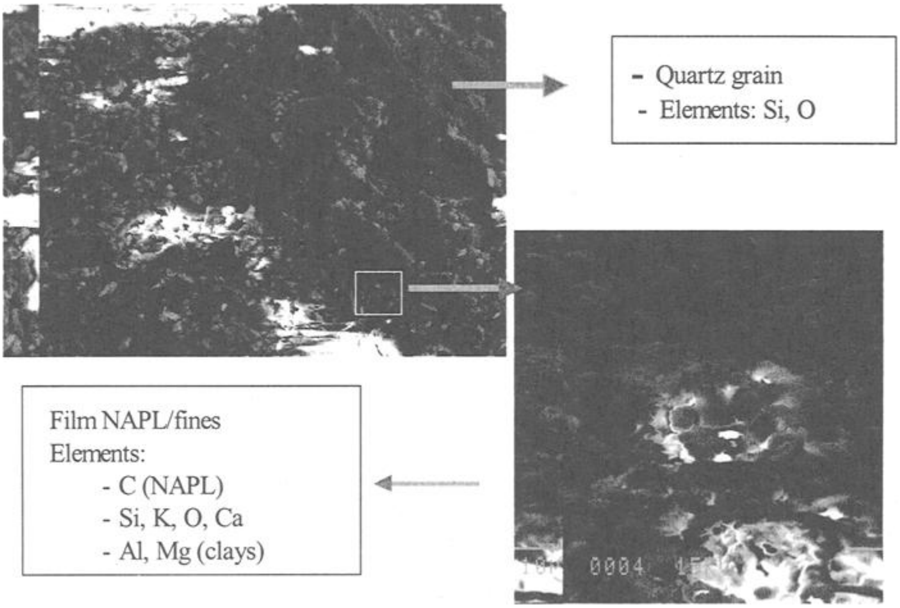

Figure 3 - *SEM photographs of a typical soil-NAPL system.*

Physical properties of the NAPLs influence water flow. The denser and more viscous NAPL (O3) clearly had the greater influence on flow bypassing, followed in order of decreasing viscosity and density by O2 and O1. This shows that, even though macroscopic concentrations of residual NAPL are the same, the microscopic arrangement of NAPL ganglia in the pore network can generate different effects on flow pattern. In the present case, as NAPL viscosity and density increase, the size of the largest stable NAPL ganglia also increases (Hunt et al., 1988). Larger ganglia can more effectively disconnect the network of voids occupied by water because they tend to occupy multi-pore domains (Conrad et al., 1992). This then creates a more significant bypassing of water flow towards more conductive pore sequences and hence increases the velocity of flow and solute breakthrough. In essence, this process decreases the size of the pore volume to water flow and to metal transport.

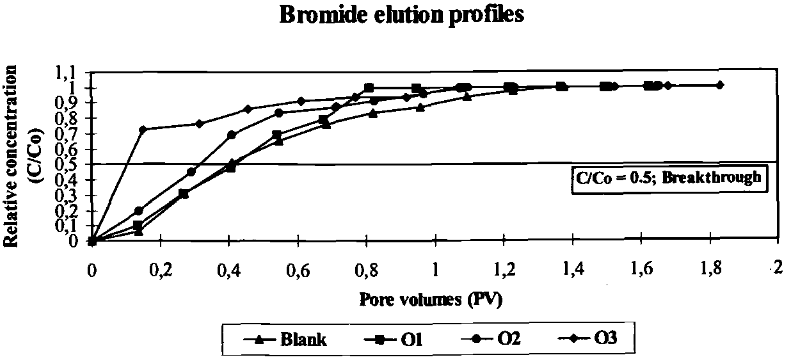

Figure 4 - *Tracer elution profiles*

It is not possible to use a tracer to differentiate between bypassing due to NAPL ganglia and films. Being the soil water-wetted initially, the presence of residual NAPL ganglia is safely assumed. Other than enhancing water flow bypassing, oil films also prevent solute diffusion towards micro-pores and reactive sites and reduce the surface area available for reaction.

Heavy Metal Transfer

Figures 5a to 5c below show elution profiles of the metallic solutions for each column series. All heavy metals were retarded with respect to the tracer for each column series. Hence, even though the presence residual NAPL reduced the contact between the aqueous solution and the solid phase, retention of heavy metals occurred.

For the blank series, no Pb or Cu were eluted after 5 PV indicating the complete retention of these metals in the soil column. Conversely, Cd was eluted from the blank columns, starting at 3 PV, and reaching a relative concentration (C/Co) of 0.13 after 5 PV. The elution of Cd may indicate a competition with the other heavy metals for the same retention sites and/or competitive precipitation.

If reaction sites had not been present in preferential channels, elution of heavy metals would have occurred earlier, concurrently with tracer breakthrough. Nevertheless, the surface available for contact between the solid and liquid phases is lower in preferential channels than in matrix pores. A lower surface area leads to a lower total amount of reactive sites and therefore a lower retention capacity in preferential channels. This difference in retention capacity between preferential and matrix flow regions may become important as preferential retention sites may rapidly become saturated as a result of longer infiltration times and/or increasing bypassing of flow through these channels.

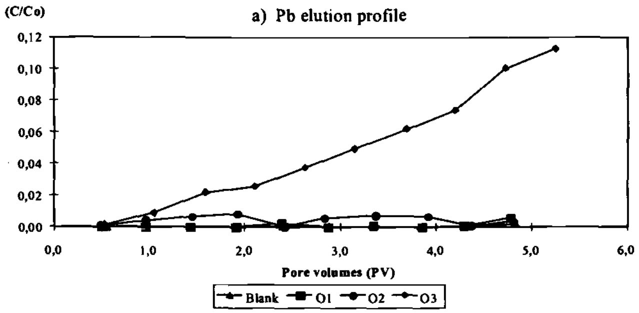

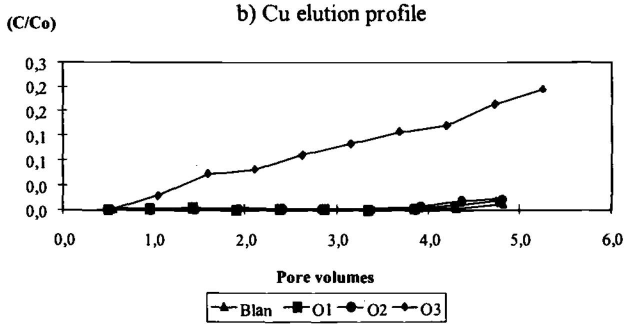

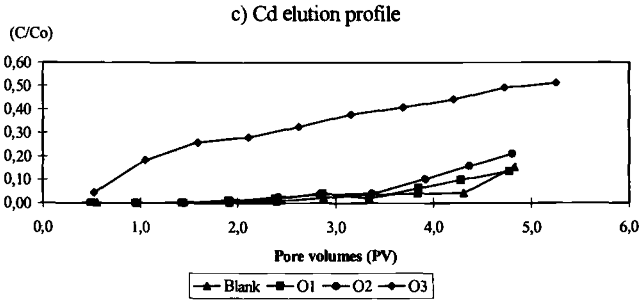

Figures 5a to 5c - *Heavy metal elution profiles*

The results for the O3 columns clearly show an effect on heavy metal elution. For these columns, elution was noticeable at 1 PV. The elution reached the following C/Co values after 5 PV : Cd (0.50, breakthrough) > Cu (0.24) > Pb (0.12). As for the tracer experiments, the relative influence of the different NAPLs on water flow and metal transfer depended on their physical properties. The O3 NAPL, because of its higher density and viscosity, may have produced larger ganglia and/or wetted larger areas of oil-wet surfaces, hence having the largest effect on heavy metal elution. On the other hand, the effect of the O1 and O2 NAPLs on water flow was not sufficient to significantly affect heavy metal elution. The results obtained, particularly those for the O3 columns, demonstrate that residual NAPL did not occupy the largest pores, as would be the case according to theory in a water-wet saturated soil. If this would have been the case, preferential flow would have been reduced. Hence, residual NAPL seemed to have occupied pore sequences of intermediate sizes, i.e., probably overlapping the boundary between preferential channels and matrix pores. Such pores may have been smaller preferential pores and/or large matrix pores. Moreover, films of residual NAPL may have occupied this boundary where oil-wet surfaces were located. Both forms of residual NAPL increased flow bypassing and decreased the available surface area.

Heavy metal migration profiles are shown for column O3 and are presented in Figure 6. They give the distribution of total Pb, Cu and Cd (after digestion) in the soil column depth following the elution of 5 PV.

As it can be seen in Figure 6, upper layers retained higher concentrations than lower layers. This was true for the 3 metals under study. Gloabally, more Pb than Cu than Cd was retained. Given the fact that total soil retention capacity was not exceeded, the lower concentrations found in deeper layers may have resulted from slower retention kinetics, hydrodynamic dispersion, and preferential flow.

In the presence of residual NAPL, it was first observed that the retention of heavy metals in the first layer is invariably reduced. However, in deeper layers, retention is increased. As for the elution profiles, the degree to which the behavior observed for the blank columns is modified is related to the physical characteristics of the NAPLs.

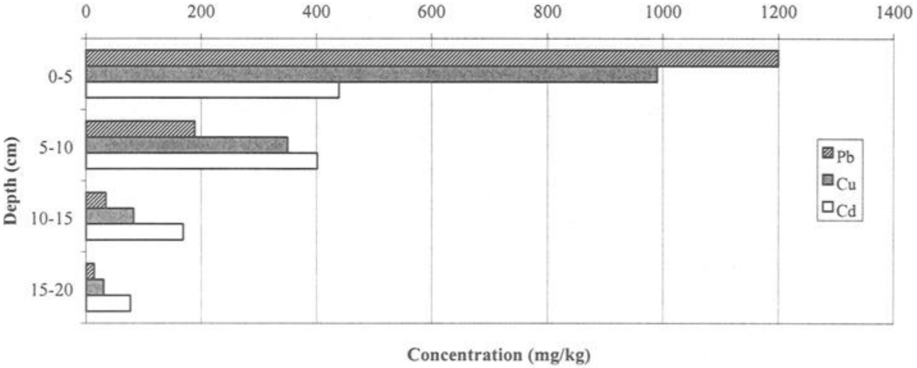

Figure 6 - *Heavy metal migration profiles for column O3*

The more viscous and denser O3 NAPL induced to most significant effect on heavy metal migration. Table 3 presents the differences in retention versus depth between the blank and O3 columns.

Table 3 - *Difference in heavy metal retention w/r to blank for O3 columns.*

Depth (cm)	Pb	Cu	Cd
0-5	-45%	-52%	-43%
5-10	+92%	-19%	-57%
10-15	+838%	+197%	-1%
15-20	+839%	+437%	+73%

+ = increase in heavy metal retention; - = decrease in heavy metal retention

The decrease in heavy metal retention in the first layer can be explained by a decreased access of the metallic solution to the soil matrix produced by the combination of flow bypassing and formation of NAPL films. This in turn enhanced transport of heavy metals further down the soil column along a network of preferential paths stabilized by the presence of residual NAPL. The retention capacity of every layer was effectively reduced but at the same time the metallic load imposed on the deeper layers was increased. Hence, for an infiltration time under 5 PV, while heavy metal retention in the first layer was less than the blank, it was higher in the deeper layers. If longer infiltration times would have been used, heavy metal retention in the deeper layers would have been greater in the blank because of their higher retention capacity. On the other hand, in the presence of residual NAPL, retained concentrations of heavy metals would have been lower, the soil columns would have saturated more rapidly, and heavy metal elution would have been considerably increased.

Heavy Metal Geochemical Distribution

The geochemical distribution of heavy metals in the solid phase was evaluated as a function of depth. As an example, Pb results are presented in Figure 7. The distribution patterns for the blank columns show that Pb and Cd were mainly retained in the acid-soluble and reducible fractions. Cadmium presented an lower affinity for the exchangeable fraction in the first layer where the competition with Pb and/or Cu was likely most significant. Copper was also mainly retained in the acid-soluble and reducible fractions and showed a low affinity for the oxidizable fraction (1%). Hence, all metals mainly (co-)precipitated as carbonates and/or (hydr-)oxides. Despite the variations in the concentration of each metal with depth and variation of the concentration ratios between metals, the percent distribution pattern of each metal among the geochemical fractions remained very similar.

In the presence of residual NAPL, the percent distribution patterns also stayed similar with depth. More importantly, the percent distribution patterns of each metal stayed similar to the blank independently of the NAPL used. Variations observed between percent distributions are within the precision of the method of sequential chemical extractions. Hence, it seemed that while preferential channeling and NAPL films affected the overall quantity of chemical exchanges between the aqueous and solid phases, they did not alter the quality of these exchanges. For example, NAPL films may have reduced the availability of the retention sites but the proportions of each type of site (i.e. proportions of each geochemical constituent active in heavy metal retention) with respect to the total number of sites still available remained the same.

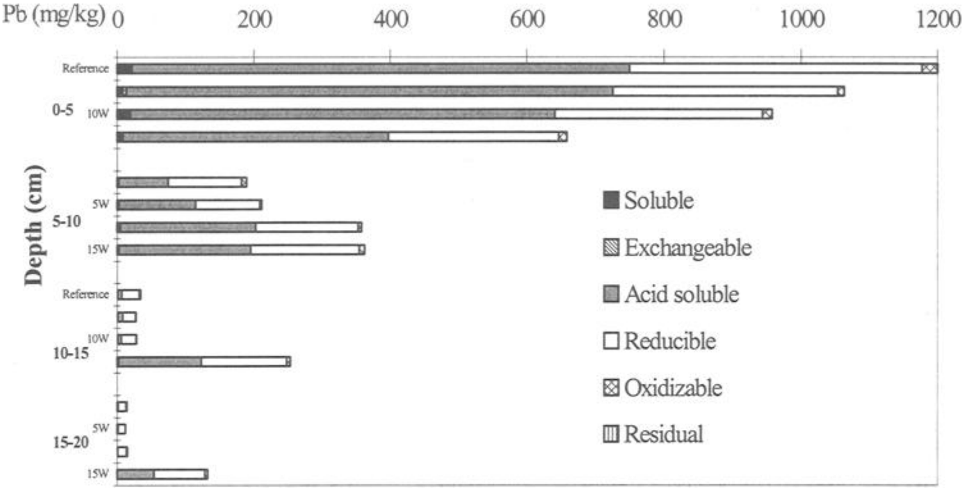

Figure 7 - *Lead geochemical distribution pattern*

Concluding remarks

The results presented allow us to conclude that residual NAPL has an effect on heavy metal transfer in an initially water-saturated carbonated alkaline soil. This effect is expressed globally as a decrease in the heavy metal retention potential of the soil and therefore an increase in heavy metal mobility. This increased mobility is characterized by an earlier elution of the aqueous heavy metals out of the flow domain as well as a greater depth of migration.

This increased heavy metal mobility mainly results from two alterations of the soil by residual NAPL. First, the water flow pattern is affected by NAPL ganglia and films occupying void regions located at the boundary between preferential channels and soil matrix. As a result, infiltrating water is forced to bypass matrix regions of high retention potential towards highly conductive pore sequences of low retention potential. Secondly, NAPL films mask retention sites by coating active geochemical constituents and prevent diffusion of dissolved heavy metals into the soil matrix. However, residual NAPL does not influence the modes of retention of heavy metals.

Therefore, residual NAPL induces changes in soil structure which translate into higher heavy metal mobility through an alteration of water flow pattern. These interactions seem to be physical in nature, emphasizing the importance of accounting for hydrodynamics when studying heavy metal transfer in soils.

Acknowledgement
This paper summarizes research work conducted thanks to funds from the Natural Sciences and Engineering Research Council of Canada, the French Ministry of Public Works and the Quebec and French Ministries of International Affaires.

References

Conrad S.H., Wilson, J.L., Mason, W.R., and Peplinski, W.J., 1992. "Visualization of Residual Organic Liquid Trapped in Aquifers", *Water Resources Research Journal* Vol 28 No 2 pp. 467-478.

Dubé, J.-S. 2001 'Modifications Hydrodynamiques du Comportement des Métaux Lourds dans un Sol Hétérogène Présentant une ContamAUthors Responsination Résiduelle en NAPL' Ph.D. Thesis. Laval University, Québec, Canada. 235pp.

Dawson, H.E. and Roberts, P.V. 1997, 'Influence of viscous, gravitational, and capillary forces on DNAPL saturation', *Groundwater*. Vol. 35 No 2 pp. 261-269.

Fortin, J., Jury, W.A. and Anderson, M.A., 1998, 'Dissolution of trapped nonaqueous phase liquids in sand columns'. *Journal of Environmental Quality* vol. 27 pp. 38-45.

Freeze, R.A. and Cherry, J.A, 1979, Groundwater, Prentice-Hall, Inc., Englewood Cliffs, N.J.

Hunt, J.R., Sitar, N. and Udell, K.S., 1988, "Nonaqueous Phase Transport and Cleanup, 1. Analysis of Mechanisms", *Water Resources Research Journal*. Vol 28 pp. 1247-1258.

Laboratoire des Sciences de l'Environnement (LSE), Ecole Nationale des Travaux Publiques de l'État, 1997. "Les ouvrages d'infiltration d'eau pluviale, Impact sur les eaux souterraines, Action C: Interaction entre les métaux lourds et la zone non saturée". 11^e Plan État-Région. Programme « L'eau dans la Ville ». Lyon, France.

Mayer A.S. and Miller, C.T., 1993. "An Experimental Investigation of Pore-Scale Distributions of Non-Aqueous Phase Liquids at Residual Saturation" *Transport in porous media*. Vol 10 pp. 57-80.

Pennell, K.D., Abriola, L.M. and Weber J. 1993. 'Surfactant-Enhanced Solubilisation of Residual Dodecane in Soil Columns. 1. Experimental Investigation', *Environmental Sciences and Technology* vol. 27 pp. 2332-2340.

Plassard, F. 1999. "Influence de la Complexation sur la Rétention de Trois Cations Métalliques par un Sol Alcalin: Application à un Bassin d'Infiltration d'Eaux Pluviales". Doctorate thesis. Université Claude Bernard – Lyon, France 1140p.

Tessier, A., Campbell, P.G.C. and Bisson, M. 1979. "Sequential Extraction Procedure for the Speciation of Particulate Metals". *Analytical Chemistry Journal* Vol 51 pp. 844-850.

Krishna R. Reddy[1] and Richard E. Saichek[1]

Electrokinetic Removal of Phenanthrene from Kaolin Using Different Surfactants and Cosolvents

Reference: Reddy, K.R., and Saichek, R.E., **"Electrokinetic Removal of Phenanthrene from Kaolin Using Different Surfactants and Cosolvents,"** *Evaluation and Remediation of Low Permeability and Dual Porosity Environments, ASTM STP 1415,* M.N. Sara and L.G. Everett, Eds., ASTM International, West Conshohocken, PA, 2002.

Abstract: In this study, an experimental program was conducted to determine electrokinetic remedial efficiency of PAHs in low permeability soils. Kaolin was selected as a representative low permeability soil, and phenanthrene was selected as a representative PAH. Several surfactants/cosolvents were evaluated to enhance desorption/solubilization of PAHs in soils, and bench-scale electrokinetic experiments were performed to investigate the enhanced removal of PAHs using surfactants/cosolvents. Electric current, cumulative electroosmotic flow, and cumulative contaminant mass removal were measured during the application of electric potential, and pH and residual contaminant concentration in the soil were measured after electrokinetic treatment. The results showed that the extent of contaminant desorption/solubilzation as well as the amount of electroosmotic flow both affected PAH removal efficiency. Furthermore, significantly different results were obtained due to the chemical and electrical characteristics of the surfactants/cosolvents. Generally, electroosmotic flow behaved according to Helmholz-Smoluchowski (H-S) theory and advective transport of the contaminant occurred from the anode towards the cathode. Electrokinetic treatment caused slightly acidic conditions throughout the soil because of the electrolysis reaction at the anode and the electroosmotic flow towards the cathode. Although contaminant mass removal was low in all the tests, the results showed significant PAH migration towards the cathode. Reaction kinetics or a change in solution and/or surface chemistry under electric potential, however, seems to have caused sorption or precipitation of the contaminant to the soil and hindered complete PAH removal from the soil. Thus, further evaluation needs to be performed to determine the cause of low contaminant removal, but enhanced electrokinetic remediation appears to be a promising technique for the removal of PAHs from low permeability soils.

Keywords: electrokinetics, electrokinetic remediation, low-permeability soils, clays, organics, surfactants, cosolvents, PAHs, phenanthrene, remediation

---

[1] Associate Professor and Graduate Research Assistant, respectively, Department of Civil and Materials Engineering, University of Illinois at Chicago, 842 West Taylor Street, Chicago, Illinois 60607

Introduction

Toxic polycyclic aromatic hydrocarbons (PAHs), such as phenanthrene, anthracene, and pyrene, are persistent and difficult to remove from low permeability clayey soils because these contaminants have low aqueous solubilities and a tendency to strongly bind with the clay minerals and organic matter present in these soils (Connell 1997, Luthy et al. 1997). Generally, conventional remediation techniques such as *in-situ* flushing or soil washing require enhanced solutions containing surfactants/cosolvents to achieve adequate PAH desorption and solubilization (Roote 1998, Sabatini et al. 1996). Basically, the surfactants/cosovlents increase contaminant desorption by reducing the interfacial tension between the PAH and the soil. However, when low permeability soils are present, *in-situ* flushing or soil washing remediation is not effective because the low hydraulic conductivity of the soils severely limits the flow and the contaminant and surfactant/cosolvent interaction. Ultimately, with these types of remediation techniques, it is the hydrogeology of the site that largely governs the amount of PAH removal and the degree of contaminant tailing (Fountain et al. 1995). Therefore, it is important to develop innovative remediation technologies that are applicable for PAH-contaminated sites where low permeability soils are present, and the electrokinetic remediation process offers great promise under such conditions. Electrokinetics essentially involves the installation of wells/drains, the insertion of electrodes into the soil, and the application of a low electric potential. The applied voltage gradient induces electroosmotic flow that is capable of transporting surfactants/cosolvents through low permeable soils at rates magnitudes higher than flow rates generated under typical hydraulic gradients (Casagrande 1949).

This paper presents the results of a laboratory investigation that was performed to evaluate different surfactants/cosolvents for enhancing electrokinetic remediation. In particular, surfactants/cosolvents were selected based on their ability to cleanup a low permeability clayey soil, kaolin, spiked with a typical PAH contaminant, phenanthrene. The surfactant/cosolvent screening process was primarily based on (1) a literature review and the results from previous studies, (2) applicability for *in-situ* electrokinetic remediation and the enhancement of electroosmotic flow, and (3) ability to desorb and solubilize phenanthrene in batch tests. The soil type and other electrokinetic variables were kept constant in order to compare the relative performance of the surfactants and/or cosolvents. The parameters that were evaluated for surfactant/cosolvent performance included the electric current, cumulative electroosmotic flow, and cumulative mass removal during the electric potential application as well as the soil pH and residual contaminant concentrations after the electric potential application.

Background

Electrokinetics and Electroosmotic Flow

At the electrodes, electrolysis reactions occur and generate oxygen gas and hydrogen ions at the anode and hydrogen gas and hydroxide ions at the cathode.

$2H_2O \Rightarrow 4e^- + O_2\,(g) + 4H^+$ oxidation (anode)

$2H_2O + 2e^- \Rightarrow H_2\,(g) + OH^-$ reduction (cathode)

Electrokinetic remediation is accomplished through various contaminant transport processes such as *electromigration*, *electroosmosis*, *electrophoresis*, and *diffusion*. *Electromigration* describes the transport of ionic species present in the pore fluid. This mechanism is largely responsible for generating the electrical current through the soil, and it includes the migration of H^+ and OH^- generated due to electrolysis towards the oppositely charged electrode. Moreover, under an electric potential, *electroosmosis*, which refers to the bulk movement of pore fluid, occurs because the locally existing excess ions migrate in a plane parallel to the particle surface towards the oppositely charged electrode, and, as they migrate, they transfer momentum to the surrounding fluid molecules via viscous forces (Eykholt 1992). *Electrophoresis*, which describes the transport of charged colloidal-sized particles through the pore fluid as well as *diffusion*, which describes the transport of species due to concentration gradients also contribute to contaminant transport.

PAHs such as phenanthrene are electrically neutral, and, thus, they basically do not electromigrate towards an electrode due to electromigration or electrophoresis. Diffusion usually is a very slow process, so it was also not expected to contribute substantially to PAH removal. Therefore, electroosmosis is the controlling mechanism for PAH removal because the electroosmotic flow should greatly enhance flow and soil-solution-contaminant interaction through low permeability soils. If the PAHs are desorbed from the soil and solubilized into solution, electroosmosis should facilitate the advective transport of them towards the electrode well(s)/drain(s) where they can be extracted. Finally, after removal, the contaminant-laden effluent can be treated using established wastewater treatment technologies (Abdul et al. 1992, Pinto and Moore 2000, Lee et al. 2001).

Generally, the surfaces of clay particles are negatively charged primarily due to isomorphic substitution or to broken bonds around the edges of composite silica-alumina units (Grim 1968). As a result, cations that are dissolved in the solution surrounding clay particles are attracted to the negative electric field originating from the mineral surface. Initially, the amount of cations attracted to the surface outnumbers the amount necessary to balance the negative charges, and, since the concentration of cations near the mineral surface is high, due to thermal motion energy they diffuse away from the surface in the direction of decreasing concentration gradient (Dukhin and Derjaguin 1974). Consequently, the charges become distributed in a diffuse double layer configuration (Mitchell 1993). Under an electric potential, the solubilized ions electromigrate, and, as they move, they transfer momentum to surrounding fluid molecules. If the cations and anions are evenly distributed, equal and opposite flow results and the net flow is zero. However, when the momentum transferred to the fluid in one direction exceeds the momentum of the fluid traveling in the other direction, electroosmotic flow is generated (Gray and Mitchell 1967).

Helmholz developed one of the first theories concerning electroosmosis in 1879, and Smoluchowski modified it in 1914 (Mitchell 1993). Helmholz-Smoluchowski theory (H-S theory) is still widely accepted, although it is more applicable for soils with fairly large pores (Gray and Mitchell 1967). The theory states that electroosmotic flow velocity is directly proportional to the applied voltage gradient (E_z), zeta potential (ζ), and dielectric constant (D) of the fluid and inversely proportional to the fluid viscosity (η) (Gray and Mitchell 1967).

$$v_e = -\frac{D \zeta E_z}{\eta} \qquad (1)$$

The zeta potential is basically a complex function of the interfacial chemistry between the liquid and solid phases (Eykholt and Daniel 1994), and West and Stewart (1995) define it as the electric potential at the junction between the fixed and mobile parts in the double layer. The zeta potential is a function of many parameters including the types of clay minerals and ionic species that are present as well as the pH, ionic strength, and temperature (Vane and Zang 1997). At a unique pH, called the point of zero charge (pH_{pzc}), the net charge on the mineral surface and the zeta potential equal zero, and, according to H-S theory, the electroosmotic flow ceases.

It has been reported that the pH_{pzc} of kaolin soil is approximately 4.5 (Evangelou 1998), so, when the pH is greater than this value, the soil has negative surface charge and negative zeta potential, and, under these conditions, the electroosmotic flow is directed from the anode towards the cathode. The electrolysis reaction at the anode, however, generates an acidic solution that causes the pH to drop. Consequently, as the flow of low pH solution enters the soil from the anode, the zeta potential might become more positive, and this could cause the electroosmotic flow to cease or possibly reverse and be directed from the cathode towards the anode (Vane and Zang 1997, Eykholt and Daniel 1994). It is important to note that there are many additional factors, such as ionic strength and the voltage gradient, that affect the electroosmotic flow, so a low pH and positive zeta potential in one region does not necessarily cause the flow to reverse throughout the soil sample.

Although soil conductivity is largely a function of the pore fluid conductivity, the surface charge of the clay minerals might produce substantial effects. Mitchell (1993) notes that the mineralogy plays a crucial role because of mineral dissolution as well as other mineral-solution interactions such as hydrogen bonding, van der Waals forces, osmosis, or surface-dipole attraction. Furthermore, besides mineralogy, the conductivity depends on other soil properties, such as the particle size and shape, porosity, fabric and cementation, and degree of saturation (Mitchell 1993).

Besides the H^+ and OH^- ions generated by the electrolysis reactions, there are many ions that might be associated with clays (Greenland and Hayes 1978). In particular, kaolin soil, which is frequently used in electrokinetic experiments, has been characterized extensively for its physical and chemical properties (Eykholt 1992). Kaolinite has the chemical formula of $Al_2Si_2O_5(OH)_4$, and it has a low cation exchange capacity (CEC), implying a low tendency to substitute different cations such as Mg^{2+} or Fe^{2+} for Al^{3+}. However, impurities such as titanium and iron oxides, and smectite have been found to exist in kaolin soil (Eykholt 1992). Although these impurities are small and difficult to determine with x-ray diffraction, they can affect the surface charge of kaolin soil (Eykholt 1992).

When the pH is low, the H^+ ions balance the negatively charged clay particles, and, consequently, aluminum dissolution from the clay may take place, increasing the aluminum ions in solution (Carrol-Webb and Walther 1988). Depending on the pH, different chemical reactions occur as kaolinite dissolves and the products are hydrolyzed species of aluminum and silicon (Eykholt 1992).

Surfactants/Cosolvents

The current carrying capacity of an electrolyte, or its conductivity, mainly depends on the viscosity of the solution and the concentration, charge, radii, and mobility of the dissolved ions (Hamann et al. 1998). Solutions that possess high conductivities are generally ones that have high concentrations of ions that are able to easily dissociate. If the ion concentration becomes too high however, ionic interaction may decrease conductivity. Generally, pure solvents such as benzene, methanol, or distilled water are poor conductors because the electrolyte molecules only slightly dissociate (Hamann et al. 1998). They also may contain stronger conducting impurities that cannot be removed. The dielectric constant, or permittivity, of a fluid is closely related to the dipole moment of the fluid molecule, and it is a measure of the ability of the liquid to resist the presence of an electrical field (Mitchell 1993). Non-aqueous liquids are generally composed of molecules with low polarities, so non-polar organic compounds, such as PAHs, are usually more soluble in non-aqueous solvents. The low polarity of non-aqueous solvents commonly means that they have lower dielectric constants, and, for example, the dielectric constant of ethanol is less than one-third the dielectric constant of water (Weast et al. 1984).

In addition to solvents, surfactants have been used extensively for enhancing the aqueous solubility of organic contaminants (Lowe et al. 1999). Basically, surfactant molecules, or monomers, are composed of two separate groups or moieties. The head group is lypophilic (attracted to the bulk phase) and the tail group is lypophobic (repelled from the bulk phase). Furthermore, when the bulk phase is water, the corresponding terminology becomes hydrophilic and hydrophobic. The presence of the characteristically divergent (amphiphilic) monomers in the bulk phase causes an increase in the overall free energy of the system. Thus, to lower the free energy, the monomers concentrate at surfaces and interfaces and lower the surface tension (Myers 1988).

At a specific concentration, termed the critical micelle concentration (CMC), the monomers have sufficiently saturated the interface locations and they begin to aggregate into structures called micelles. For micelles in dilute aqueous surfactant solutions, the hydrophilic head moieties are directed towards the aqueous phase and the hydrophobic tails are directed towards the interior region. The interior of the micelle becomes a hydrophobic region suitable for PAHs, and, as a result, PAH solubility is greatly enhanced above the CMC (Ganeshalingam et al. 1994).

Surfactants reduce interfacial tension and enhance PAH desorption and solubilization, but it has been determined that micellar solubilization is a rate-limited process (Grimberg et al. 1995, Yeom et al. 1996, Patterson et al. 1999, Farrell et al. 1999). The rates at which micelles are created and dissipate are considered to be very rapid (Attwood and Florence 1983), and the partitioning of the PAH between the aqueous and micellar phases is also generally assumed to be a fast process (Grimberg et al. 1995). However, Patterson et al. (1999) and Yeom et al. (1996) suggest that the mass transfer is limited due to the diffusion of the PAH from the soil matrix.

Water-miscible organic cosolvents such as ethanol or other alcohols do not form micelles, but, as mentioned earlier, their molecules are less polar than water and more chemically similar to PAH molecules. Therefore, when cosolvents are present, PAH-water interfacial tension is usually reduced and PAH desorption and solubility is enhanced (Li et al. 2000). The effect of cosolvents on PAH removal can be estimated by using the ratio of the soil-cosolvent and soil-water partitioning coefficients, and this ratio largely depends on the cosolvent concentration as well as the relationship of the cosolvent with the soil and contaminant (Li et al. 2000). Generally, the higher the cosolvent concentration, the greater the PAH desorption/solubilization, but many factors are involved so it is commonly a nonlinear relationship (Yalkowsky and Banerjee 1992).

Experimental Methodology

Materials

The soil chosen for this research was kaolin, and Table 1 shows its mineralogy and properties. As seen in the table, kaolin basically consists of the mineral kaolinite and has a hydraulic conductivity of around 10^{-8} cm/s, which is significantly lower than the 10^{-5} cm/s value that is generally required for *in-situ* soil flushing. Kaolin has been previously used in many electrokinetic research studies (Eykholt 1992, Reddy and Parupudi 1997, Reddy et al. 1997, Reddy and Chinthamreddy 1999, Saichek 2002).

Phenanthrene (molecular formula = $C_{14}H_{10}$; molecular weight = 178.2; aqueous solubility = 7.25×10^{-6} mol/L; Log K_{ow} = 4.57) was chosen as the representative PAH in this study (Connell 1997). Phenanthrene is a common PAH found at numerous contaminated sites and it has environmental properties such as aqueous solubility, K_{ow}, and vapor pressure that are comparable to other PAHs, such as acenaphthene, fluoranthene, and fluorene (Schwarzenbach et al. 1993, Connell 1997). Although higher molecular weight and more carcinogenic PAHs, such as benzo (a) pyrene, often have higher K_{ow} values and lower aqueous solubilities, it was hypothesized that since the parent structures are similar, phenanthrene would be an adequate representative compound that would give a general indication of PAH behavior. The kaolin was spiked with phenanthrene with a target concentration of 500 mg/kg (based on the dry mass of soil).

Four surfactant/cosolvent solutions, namely 1% Witconol 2722, 3% Tween 80, 40% ethanol, and 4% Witco 207 in 40% ethanol were investigated as flushing solutions and their properties are presented in Table 2. Additionally, testing was performed using deionized water for baseline comparison purposes. These surfactants/cosolvents are non-ionic and have been used previously by researchers to enhance PAH solubility (Yeom et al. 1995, Ko et al. 1998a). Ethanol was purchased from Fisher Scientific, Pittsburgh, Pennsylvania, Tween 80 was obtained from Aldrich Chemical Company, and the Witco surfactants were obtained from Witco Corporation, Houston, Texas. Ethanol was selected as a cosolvent because of its relatively high solvency properties (phenanthrene solubility in pure ethanol = 7.63×10^{-2} mol/L) (Li et al. 2000), its fairly good results at a 40% concentration in batch tests, and its low toxicity as compared to other cosolvents. The surfactant/cosolvent concentrations were selected based on the results of the batch experiments (Saichek 2002).

Table 1 - *Summary of soil properties.*

Property	Value
Mineralogy	Kaolinite: 100% Muscovite: trace Illite: trace
Particle Size Distribution (%) (ASTM D 422)	
Gravel	0
Sand	0
Silt	10
Clay	90
Atterberg Limits (ASTM D 4318)	
Liquid Limit	44
Plastic Limit	29
Plasticity Index	15
Specific Gravity (ASTM D 854)	2.61
Compaction (ASTM D 698)	
Maximum Dry Density	14
Optimum Moisture Content	30
Hydraulic Conductivity [cm/s] (ASTM D 2434)	1.0×10^{-8}
Cation Exchange Capacity [meq/100g] (ASTM D 9081)	1.0 – 1.6
pH (ASTM D 4972)	4.5 – 5.0
USCS Classification (ASTM D 2487)	CL

Table 2 - *Selected properties of surfactants/cosolvents.*

Name	Chemical Formula	Molecular Weight	CMC [M]
Tween 80	$C_{64}H_{124}O_{26}$	1310	1.2×10^{-5}
Ethanol	C_2H_5OH	46	Not Applicable
Witconol 2722	$C_{64}H_{124}O_{26}$	1310	1.2×10^{-5}
Witco 207	Not Available	Not Available	Not Available

Electrokinetic Test Set-up

An electrokinetic test set-up similar to that used in previous electrokinetic research was used in this study (Reddy and Shirani 1997, Reddy et al. 1997, Reddy and Parupudi 1997). A schematic diagram of the entire test set-up and the electrokinetic cell is shown in Figure 1.

The test set-up consisted of a cell, two electrode compartments, an anode reservoir and cathode sample bottle, a power supply, a multimeter, and peripherals such as tubing, wiring, and support stands. The cell was made of Plexiglas and measured 6.2 cm in diameter and 19.1 cm in length. Each electrode compartment was also made of Plexiglas, and consisted of an electrode and a porous stone as shown in Figure 1. The slotted graphite electrodes were placed in the electrode compartments, and filter paper was used at the end of the sample to prevent particulate matter from entering into the porous stones, reservoir, or sample bottle. A porous stone was then placed next to the filter paper between the end of the sample and the graphite electrode. Gas vents were provided in the electrode compartments to allow the gases generated from the electrolysis reactions to escape.

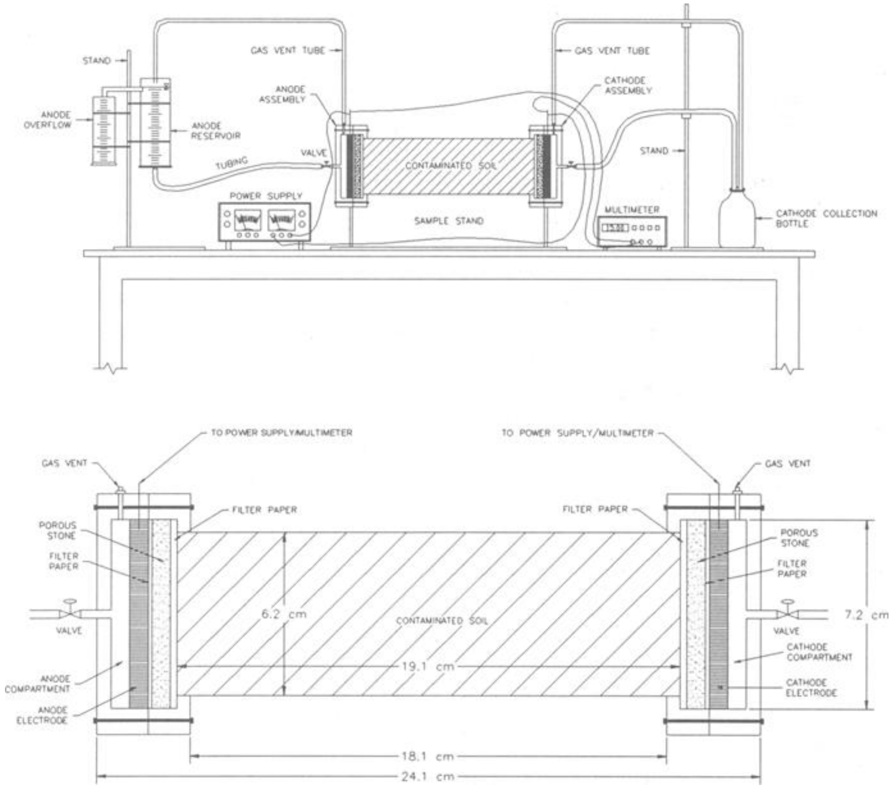

Figure 1 – *Electrokinetic test setup.*

Testing Procedure

For each experiment, approximately 1.0 kg of kaolin was used. Since phenanthrene is relatively insoluble in deionized water, hexane was used to solubilize the contaminant. The hexane-phenanthrene mixture was added to the kaolin and mixed thoroughly using a stainless steel spoon. Additional hexane was added to ease mixing and aid in homogeneous contaminant distribution throughout the soil. The hexane-phenanthrene-kaolin mixture was then placed in a ventilation hood for 4-5 days, where the hexane evaporated, leaving the kaolin dry. A sample of the contaminated dry soil was saved for chemical analysis. Deionized water was added and thoroughly mixed with the soil to yield the initial water content of approximately 35%. The prepared moist soil was then tamped into the cell in uniform layers using a hand-held aluminum alloy pestle for compacting and eliminating voids.

The electrode compartments, the anode reservoir, and the cathode sample bottle were connected to either ends of the electrokinetic cell. The anode reservoir was filled with the surfactant/cosolvent solution and the cathode compartment was initially filled with deionized water. The kaolin in the cell was then subjected to a voltage gradient of 1.0 VDC/cm for the required duration. During testing, the current and cumulative electroosmotic flow was measured, and aliquots of effluent were collected to determine phenanthrene concentrations.

After each experiment was completed, the soil was removed from the cell using a mechanical extruder and then sectioned into five parts from the anode to cathode as 0-4, 4-8, 8-12, 12-16, 16-19.1 cm. Each section was mixed and representative soil samples were collected to measure water content, pH, and phenanthrene concentration. Moisture content was measured by the standard test method for laboratory determination of water (moisture) content of soil and rock by mass (ASTM D 2216). The pH measurements were made using a digital pH meter.

Quantitative measurement of the phenanthrene concentration in the initial and sectioned soil samples was accomplished by conducting Soxhlet extraction and high-performance liquid chromatograph (HPLC) analysis (Saichek 2002). The phenanthrene from the effluent samples was extracted using a triple liquid-liquid extraction procedure using a total volume of about 50 mL of dichloromethane. The volume of the extract was then reduced using a Kuderna-Danish concentrator, and the solvent was exchanged to methanol for subsequent injection into the HPLC.

The HPLC that was used was a Hewlett Packard Model 1100 equipped with an Alltech Econosphere reverse-phase C18 column (250 x 4.6, 5 μm particle size) and a diode array UV detector, and the samples were filtered through a 0.22 Cameo 13F PTFE membrane prior to injecting. The samples were injected manually using a 20 μL sample loop, and a mixture of water and methanol, 25:75 was used as the mobile phase with a constant flow rate of 1.0 mL/min. The detector wavelength was set at 254 nm. Calibration of the HPLC was performed using four external standard solutions (phenanthrene) and two concentration ranges, and linearity was determined on a daily basis. The system was determined to be free of contamination by running blank samples regularly, and recovery of the spiked phenanthrene samples was about 101 and 99.5% for the soil and liquid samples, respectively.

After the electrokinetic tests were completed, a mass balance analysis was performed for the phenanthrene in each test. The mass balance was reasonably good for most of the tests, with all the final phenanthrene mass results within plus or minus 21% of the initial mass, and most of them within 15% (Table 3). The mass balance differences were primarily attributed to uneven contaminant distribution in the soil samples. Although the soil samples were thoroughly mixed, the phenanthrene distribution was probably still somewhat heterogeneous, and only a representative portion of the soil (10 g) was used for the Soxhlet extraction procedure. The chemical analysis of the phenanthrene concentration in the effluent samples was much more consistent and accurate because the contaminant was evenly distributed through the liquid. In addition, the liquid-liquid extraction and concentration procedure allowed the detection of very low (0.01 mg) phenanthrene concentrations in the effluent.

Table 3 - *Mass balance.*

Flushing Solution	**Initial Mass in Soil [mg]**	**Mass Removed by Solution [mg]**	**Mass Remaining in Soil [mg]**	**Final Mass Removed and Remaining/Initial Mass [%]**
Deionized water	386.4	0.00	386.2	100.0
1% Witconol 2722	335.9	0.01	371.3	110.5
3% Tween 80	377.5	0.04	365.0	96.7
40% Ethanol	398.6	0.44	349.3	87.7
4% Witco 207 in 40% ethanol	486.5	0.48	382.8	78.8

Results and Analysis

Current

Figure 2 shows the current measured during electric potential application in all tests. These current measurements exhibit a similar basic pattern. Generally, at the beginning of the test the current starts near or at its peak value and then begins to decrease fairly rapidly. Initially, the decrease may be drastic, as in the 4% Witco 207 in 40% ethanol and 1% Witconol 2722 tests, but after a few weeks, the decrease became gradual, and, after around 50 days all the tests reached a nearly constant long-term current value. The long-term current values are indicative of the electrical characteristics of the surfactants and cosolvents used. The long-term current values ranged from a low 0.1 mA in the 40% ethanol test to a high of 0.7 mA in the test using 4% Witco 207 in 40% ethanol. The current value in the 40% ethanol test was only slightly below the 0.2 mA baseline value measured in the deionized water test, whereas the 4% Witco 207 in 40% ethanol test showed over three times that current. The 1% Witconol 2722 solution was dilute and similar to deionized water, so it was not surprising that it had a similar 0.2 mA current value. Lastly, the 3% Tween 80 was a bit more concentrated than 1% Witconol 2722 surfactant, and the resulting 0.3 mA current value is slightly above that measured in the deionized water test.

The pattern of a decreasing current over time in tests using kaolin soil correlates well to the findings of other investigators (Eykholt 1992, Pamukcu 1994, Grundl and Michalski 1996), but these other studies report somewhat higher initial current values. The initial current value is largely a reflection of the amount of sorbed or associated ions in the soil, or of the amount of mineral dissolution that occurs, so the kaolin soils in the other studies may have simply contained a larger amount of impurities or salt precipitates. As time passes, the current decreases and stabilizes because the amount of initial excess ions is depleted as they electromigrate to the electrode chamber, where they may concentrate and precipitate (Pamukcu 1994). The long-term current value is more difficult to understand. Although H^+ and OH^- ions are generated at the electrodes due to the electrolysis of water, when these ions migrate towards the opposite electrode, they meet and react to form water, so they may not significantly contribute to the current (Dzenitis 1997). However, the adsorption of these ions to the soil and the slow dissolution of minerals and/or salt precipitates may have led to the stable, long-term, supply of charge carriers (Eykholt 1992).

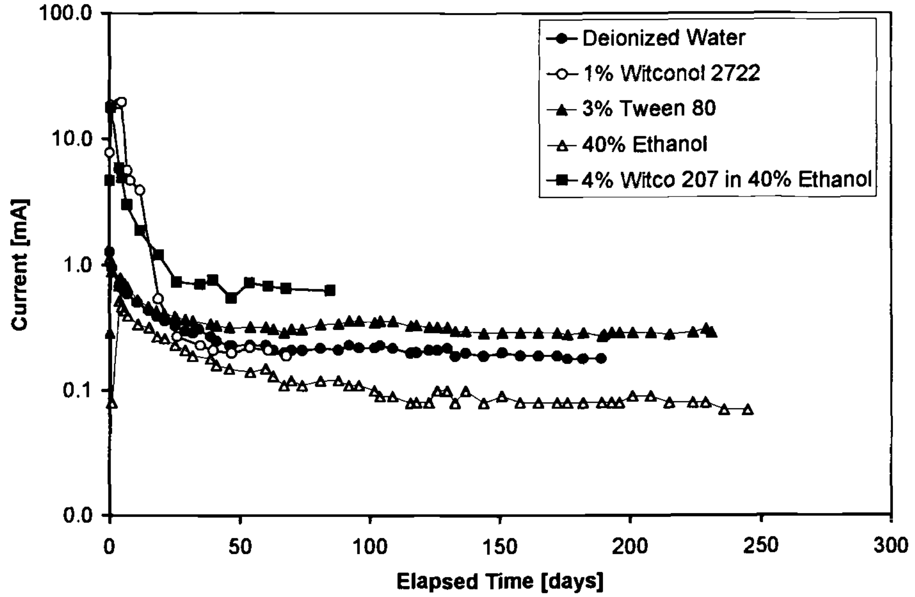

Figure 2 – *Current measured in the soil during electrokinetic remediation.*

It appears that the presence of a nonionic surfactant, as well as an increase in surfactant concentration, generally has the effect of slightly increasing the current. Although nonionic surfactants are neutrally charged compared to anionic or cationic surfactants, several researchers have shown evidence that surfactant sorption may occur due to hydrogen bonding with an oxyethylene group (Edwards et al. 1994, Rosen 1989, Ko et al. 1998b). Moreover, a nonionic surfactant also showed weak adsorption to positively charged alumina, and, at low pH, it was found that the ether linkages of oxyethylene chains could be protonated, giving the molecules a positive charge (Rosen 1989). Therefore, nonionic surfactants may possibly acquire ionic charges, and the sorption or presence of nonionic surfactant molecules may change the soil surface or solution chemistry so that additional ions can become solubilized.

Ethanol has a much lower dielectric constant than water so there may be less ion dissociation when this solution is present, and, thus, it is reasonable that the 40% ethanol solution had a smaller long-term current value than deionized water. Furthermore, since the 40% ethanol solution had a relatively low long-term current, it was probably the micellization and solution chemistry effects of the surfactant that were responsible for raising the current in the test using the combination of 4% Witco 207 in 40% ethanol. It is also obvious that the 4% Witco 207 in 40% ethanol and 1% Witconol 2722 tests had much higher initial current values than the 3% Tween 80 test, and this is most likely due to the differences in the chemistry of these surfactants.

Cumulative Electroosmotic Flow

Figure 3 shows the cumulative electroosmotic flow measured in all tests using the different flushing solutions. Similar to the current measurements, the basic pattern of flow was relatively consistent for each test. Near the beginning, when the current was high, the flow rate was high, then, within a few weeks, as the current started to decrease, the flow rate decreased. After approximately 50 days, the current reached a nearly constant value and the flow rate stabilized. The initial flow for all the tests was substantial, and within the first few weeks each test reached a cumulative volume of approximately 100 mL. However, it was the long-term stable flow acquired after nearly 50 days that determined which test produced the overall greatest cumulative flow.

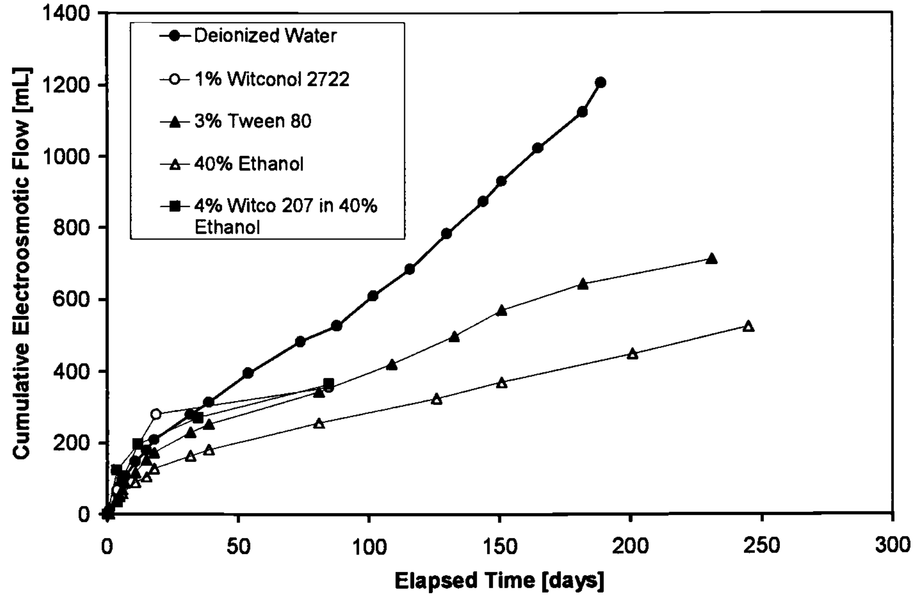

Figure 3 – *Cumulative electroosmotic flow measured during electrokinetic remediation.*

The basic patterns of flow and current behavior were similar, but the magnitudes of the flow and current differed. For example, the test with the highest current was 4% Witco 207 in 40% ethanol, and this does not correspond to the test with the highest flow, which was deionized water. This is because there are many additional factors that affect electroosmosis besides the electric current. According to H-S theory, the electroosmotic flow velocity is a function of the viscosity and dielectric constant of the fluid, the zeta potential, as well as the electrical field strength. Furthermore, pH changes occur as a result of the electrolysis reactions, and these reactions tend to decrease the electroosmotic flow (Shapiro and Probstein 1993). The electrolysis reactions change the pH thereby affecting the surface charge on the soil and the zeta potential, and, as a consequence, non-uniform electroosmotic flow and significant positive and/or negative pore pressures may be produced (Eykholt and Daniel 1994, Eykholt 1997). The pH and solution chemistry changes and the development of pore pressures can further result in the flocculation or dispersion of the soil particles, and these effects can cause smaller or clogged void spaces, compaction, lower permeability, and a reduction or cessation of electroosmotic flow.

The flow rate in the 1% Witconol 2722 and the 4% Witco 207 in 40% ethanol tests started high but it reduced substantially after a few weeks. For the 4% Witco 207 in 40% ethanol test, the average flow rate was 15 mL/day for the first 19 days, but it dropped to just over 1 mL/day during the last 65 days. Similarly, the 1% Witconol 2722 test had an average flow rate of nearly 8 mL/day during the first 35 days, but it reduced to less than 2 mL/day for the last 50 days. The 3% Tween 80 test had a lower initial average flow rate of around 7 mL/day for the first 40 days, but it maintained a rate of over 2 mL/day for the next 70 days. The 40% ethanol test had an even lower initial average flow rate of about 5 mL/day for the first 40 days, and it dropped to less than 2 mL/day for the next 90 days. The highest cumulative flow rate was seen in the deionized water test that began with an initial average rate of around 8 mL/day for the first 40 days, and maintained over a 5 mL/day average for the next 90 days.

According to H-S theory, it is logical that the baseline test employing deionized water probably possessed the highest dielectric constant and the lowest viscosity, resulting in the greatest amount of cumulative electroosmotic flow. Moreover, since ethanol has a dielectric constant that is about a third of the dielectric constant of water at 25 °C, it makes sense that the test using 40% ethanol had a much lower cumulative flow than the baseline test. The dielectric constants and viscosities of the surfactant solutions were not measured or found in the literature, but it is assumed that due to the organic nature of these solutions the viscosities were most likely greater and the dielectric constants were less than deionized water (Attwood and Florence 1983).

The results of the three tests using surfactant solutions are difficult to interpret due to the amphiphilic nature of the surfactant molecules. Since the surfactant concentration in the 1% Witconol 2722 test was dilute and the long-term current value was similar to the baseline deionized water test, it was expected that the 1% Witconol 2722 test and the baseline test would have comparable cumulative flows, but the flow in the dilute surfactant test was much lower. Surfactant monomers congregate at interfaces, and it appears that even at low surfactant concentrations the long-term electroosmotic flow was reduced compared to the baseline test. Based on electroosmotic theory, it is possible that the aggregation of surfactant monomers at interfaces affects the diffuse double layer region and interferes with ionic movement, which, consequently, reduces the transfer of momentum to the bulk water molecules. Furthermore, the increased viscosity in the diffuse double layer region as well as the presence of micelles could also decrease the amount of pore space and the flow velocity.

The 1% Witconol 2722 and 4% Witco 207 in 40% ethanol tests were conducted for a shorter duration than the other tests, but it is interesting that all three of the surfactant solutions had around 350 mL of cumulative electroosmotic flow after about 80 days. The

CMC of 4% Witco 207 in 40% ethanol was not measured, but the lower concentration, 1% Witconol 2722, solution was at a concentration which was approximately 600 times its CMC, and the 3% Tween 80 solution was about 1800 times the CMC, so all three surfactants were at concentrations that far exceeded their CMCs (Table 2). Thus, the surfactant solutions should have been under the conditions where the surfactant monomers had saturated the soil particle surfaces, a sufficient number of micelles were present, and the micellar solubilization of phenanthrene was occurring. At the interfacial regions near the soil particle surface, there should have been similar conditions for surfactant adsorption, and this might be the reason for the comparable electroosmotic flow between the different surfactant solutions.

Cumulative Mass Removal

Figure 4 shows the cumulative mass removal in all tests using different flushing solutions. Overall, considering the initial mass of contaminant in the soil, none of the flushing solutions removed significant amounts of phenanthrene. It should be noted that the largest amount of phenanthrene was detected in the solution drained from the cathode reservoir at the conclusion of testing. Since phenanthrene has such a low aqueous solubility, it was expected that the baseline deionized water test would show a negligible amount of mass removal, and this was verified by the results. Similarly, the solution most resembling deionized water, the dilute surfactant (1% Witconol 2722), did not produce any phenanthrene removal, and this may have been due to a large amount of surfactant sorption and/or a low amount of micellization. Although the 1% Witconol 2722 concentration was much higher than its CMC, several investigators have determined that surfactant sorption might continue until the concentration is well above the CMC

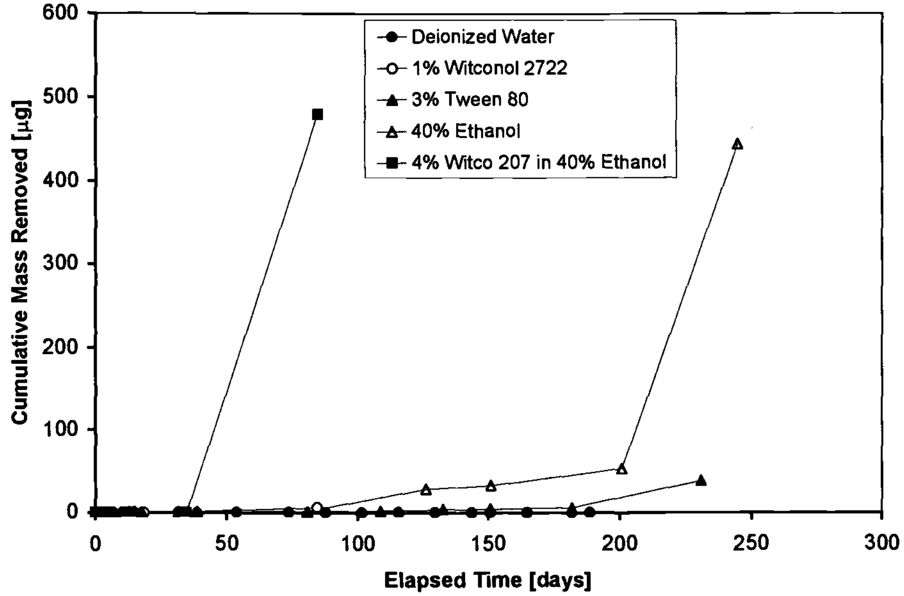

Figure 4 – *Cumulative mass removed during electrokinetic remediation.*

(Pennell et al. 1993, Adeel and Luthy 1995, Ko et al. 1998a). The more concentrated surfactant, 3% Tween 80, showed a slight amount of removal of 38 μg, but this was minor compared to the 4% Witco 207 in 40% ethanol and the 40% ethanol solutions, that removed over 400 μg. However, even this amount of phenanthrene mass (400 μg) corresponds to less than 0.1% of the initial mass present in the soil. Clearly, for all five tests, the results show that most of the phenanthrene remained within the soil.

Profile of pH in the Soil

Figure 5 shows the pH profile in the soil after conducting the electrokinetic remediation experiments with different flushing solutions. These results show that acidic conditions, which ranged from a pH of approximately 5.5 to 2.5, existed throughout the soil, and the pH at the anode was often much lower than the pH at the cathode as a result of the electrolysis reaction at the anode. It should be noted that for all the tests, electroosmotic flow was directed from the anode towards the cathode. The H^+ ions generated at the anode are about twice as mobile as the OH^- ions generated at the cathode so they generally dominate in electrokinetics, and both H^+ and OH^- ions have a high rate of transport because they easily associate and/or dissociate with water (Acar et al. 1995). In kaolin, the combined transport mechanisms of electroosmosis and electromigration are largely responsible for causing the acidic solution generated by the electrolysis reaction at the anode to migrate faster into the soil and move towards the cathode, and this explains the acidic conditions that existed in all the tests (Acar et al. 1995). However, if the electroosmotic flow reduces, a substantial amount of electromigration of OH^- into the soil from the cathode electrolysis reaction could raise the pH near the cathode, and this

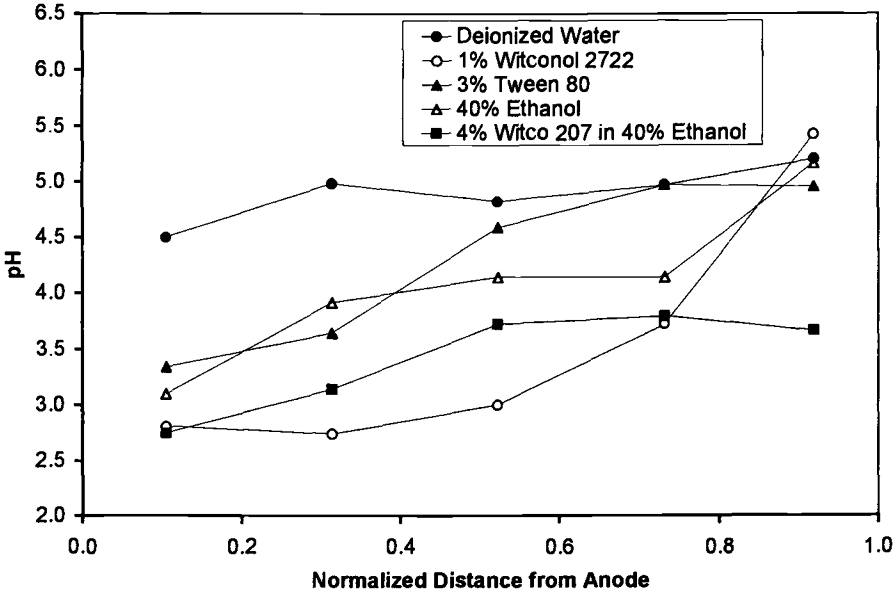

Figure 5 – *pH in the soil after electrokinetic remediation.*

accounts for the higher pH that is seen in the soil section closest to the cathode in the 1% Witconol 2722 and the 40% ethanol tests. In addition, a decrease in electroosmotic flow means that less solution is flowing in from the anode reservoir, and, thus, the electrolysis reaction occurring at the anode causes the H^+ ions to become more concentrated, thereby lowering the pH further in the anode region.

The baseline deionized water test was the only test where the pH remained above 4 near the anode, and this is probably due to the higher electroosmotic flow in this test. The consistent inflow of relatively high pH water from the anode reservoir helped to dilute the H^+ ion concentration that was being generated by the electrolysis reaction in the anode compartment. Moreover, since the deionized water solution was migrating more quickly from the anode towards the cathode than in other tests, the soil pH remained relatively constant at a pH of about 4.5 to 5.5. The baseline test is also of interest because the point of zero surface charge (pH_{pzc}) for kaolin is reported to be near pH = 4.5 (Evangelou 1998, Eykholt and Daniel, 1994), and Figure 5 shows that all the tests, with the exception of the baseline test, had a pH near the anode that was below 4 near the anode. As mentioned earlier, when the pH is below the pH_{pzc}, by H-S theory, the flow rate should substantially decrease towards the cathode, or possibly reverse, due the reduction and/or transformation of net charge on the mineral surface and the resulting effect on the zeta potential (Eykholt and Daniel 1994, Acar et al. 1995, Vane and Zang 1997). Therefore, from the pH analysis, it is evident that it may be beneficial to raise the pH at the anode to counteract the electrolysis reaction, and this may maintain the pH above the pH_{pzc} and result in a high electroosmotic flow. Typically, for kaolin, buffering solutions as well as recycling the solution in the anode compartment have been shown to generate additional electroosmotic flow (Shapiro and Probstein 1993, Ko et al. 2000).

The lowest pH values occurred in the 1% Witconol 2722 and 4% Witco in 40% ethanol tests, and Figures 2 and 3 show that both of these experiments started with high current and flow rates, where, for both tests, about 270 mL of flow was collected in the cathode bottle within the first 40 days. During the following 40 days, however, the flow substantially decreased in these tests, and only around 95 mL, or a third of the initial flow, was collected. In these surfactant tests, it appears that the electrolysis reaction at the anode and surfactant adsorption to the mineral surface affected the diffuse double layer, and this might have led to the development of negative pore pressures or a reduction in void space that resulted in a lower electroosmotic flow. Furthermore, the low electroosmotic flow allowed the H^+ ions to concentrate in the anode compartment, and this acidic front began electromigrating towards the cathode, thereby lowering the pH along soil profile. The tests using 40% ethanol and 3% Tween 80 had a more gradual initial current and electroosmotic flow, and they both resulted in a more sustained flow and slightly higher pH values along the soil samples.

Residual Phenanthrene Distribution in Soil

Figure 6 shows the phenanthrene concentration in the soil at the completion of the electrokinetic remediation experiments with the different flushing solutions. Since phenanthrene has such a low aqueous solubility, it is not surprising that the contaminant concentration remained essentially unchanged throughout the soil in the deionized water test. The dilute surfactant test using 1% Witconol 2722 also showed contaminant concentrations along the soil column that were close to the initial concentration. It is likely that the low concentration of this surfactant as well as surfactant adsorption to the soil surface caused the amount of phenanthrene desorption and solubilization to be limited when the 1% Witconol 2722 solution was used.

For the 40% ethanol test, Figure 6 exhibits a clean soil section near the anode and slightly elevated phenanthrene levels through the remainder of the soil specimen. It is possible that a greater amount of electroosmotic flow and soil-solution-contaminant interaction occurred near the anode since this is where the solution enters the soil. The greater interaction might have been capable of causing phenanthrene desorption and solubilization or mobilization from the anode region, but as it traveled farther along the soil profile towards the cathode, changes in the soil or solution chemistry caused the contaminant to sorb, become trapped or precipitate back on the soil particles. Lambe and Whitman (1969) state that decreasing the pH tends to cause the flocculation of clay particles, and, due to the electrostatic attractions between the face of one particle and the edge of another, the particles form a loose array. Conversely, the dispersed clay particles tend to stack tightly together and form in an efficient parallel array. Therefore, the low pH region near the anode could have led to particle flocculation and a more open structure so that the phenanthrene was accessible to the solution and/or micelles. Moreover, the loose array structure would have caused the phenanthrene to be more easily desorbed and solubilized or possibly flushed towards the cathode. In the higher pH region, the clay may have been more disperse and tightly packed, and these conditions could have contributed to phenanthrene sorption or to the contaminant becoming entrapped and lodged in the smaller void spaces.

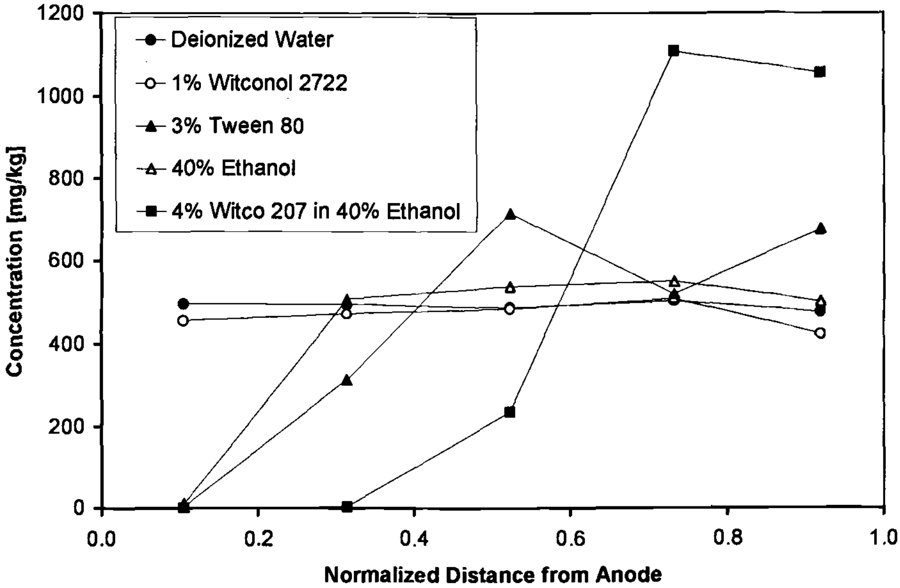

Figure 6 – *Phenanthrene concentration in soil after electrokinetic remediation.*

Figure 6 also shows that the 3% Tween 80 solution cleaned the soil section near the anode, and migration is more evident because in the middle region and further towards the cathode, the contaminant concentration is substantially higher than the initial concentration. Phenanthrene migration is also clearly observed in the 4% Witco 207 in 40% ethanol test, because the soil sections near the anode are clean, whereas the soil sections near the cathode have concentrations that are much higher than the initial concentration. When used alone, the 40% ethanol solution had a much lower amount of phenanthrene migration, so it appears that the greater amount of contaminant migration in the 4% Witco 207 in 40% ethanol test is a result of the surfactant or a synergistic effect produced by combining the surfactant and the cosolvent.

As shown in Figure 4, the cumulative mass removal was high in the 40% ethanol test, and the same amount of removal was observed in the test using the combined 4% Witco 207 in 40% ethanol. The 3% Tween 80 test had a comparatively low amount of cumulative mass removal, so it appeared as though using a surfactant without a cosolvent was ineffective. However, the residual phenanthrene concentration profiles shown in Figure 6 reveal that a large amount of phenanthrene migration occurred in the test using the 3% Tween 80 solution. Thus, although there was a low amount of phenanthrene removal, it is evident that under the right conditions surfactants may be quite effective at PAH desorption and solubilization during the electrokinetic remediation process.

Conclusions

The objective of this laboratory investigation was to evaluate different surfactants and cosolvents for enhancing the electrokinetic remediation of PAH-contaminated low permeability clayey soils. Phenanthrene was used as a representative PAH and kaolin soil was used as a representative low permeability clayey soil. Five different electrokinetic experiments were conducted under the electric potential of 1.0 VDC/cm using deionized water, 1% Witconol 2722, 3% Tween 80, 40 % ethanol, and 4% Witco 207 in 40% ethanol. The parameters that were measured included the electric current, cumulative electroosmotic flow, and cumulative mass removal. At the conclusion of testing, the treated soil was extruded and examined to assess the pH and residual contaminant concentration along the soil profile.

The main conclusions drawn from the results of this investigation were as follows:

1. The electrical current measurements showed that the presence of a surfactant and/or cosolvent solution affects the electrical current, and the long-term current appears to correlate to the chemical properties, such as the viscosity and/or dielectric constant, of the flushing solution. The higher current observed in the surfactant tests was attributed to the nonionic surfactant molecules, which may possibly acquire ionic charges, and the sorption or presence these molecules may change the soil surface or solution chemistry so that additional ions can become mobilized.

2. The highest cumulative electroosmotic flow was produced by the baseline deionized water test, and, according to H-S theory, this flow was because of the higher dielectric constant and lower viscosity of water. Although the electroosmotic flow in this baseline

test greatly increased soil-solution-contaminant interaction, this interaction alone was not effective for accomplishing contaminant mass removal, and it is evident that the flushing solution must be capable of producing adequate phenanthrene desorption and solubilization. The only tests that generated phenanthrene removal and/or migration used surfactant/cosolvent solutions that had at least a 3% surfactant concentration and/or a 40% cosolvent concentration.

3. The pH profiles were helpful for assessing the relationship between the electrolysis reaction at the anode and the reduction in electroosmotic flow. The test with the highest cumulative electroosmotic flow, the baseline deionized water test, provided a greater inflow that contributed to diluting the H^+ ions generated by the electrolysis reaction at the anode. In the other tests, with lower electroosmotic flows, the electrolysis reaction at the anode dominated, and this caused the H^+ concentration to increase and the pH in the soil nearest the anode to fall below the pH_{pzc}.

4. For the three tests using at least a 3% concentration of surfactant/cosolvent, namely, 3% Tween 80, 40% ethanol, and 4% Witco 207 in 40% ethanol, the region closest to the anode was found to be free of phenanthrene. In these tests, the low pH in the anode region could have caused the clay particles to flocculate, thereby producing a more open mineral structure. Thus, near the anode, the phenanthrene may have been more accessible to the surfactant/cosolvent solution, and it may have been more easily desorbed and solubilized or possibly flushed or mobilized towards the cathode. Conversely, in the higher pH region, the clay may have been more tightly packed, and/or the pore spaces became clogged, and these conditions could have contributed to micelle dissolution, phenanthrene sorption, or to the contaminant becoming entrapped and lodged in the smaller void spaces.

5. Although contaminant mass removal was limited in all the tests, with 3% Tween 80, 40% ethanol, and 4% Witco 207 in 40% ethanol, substantial phenanthrene desorption and solubilization apparently occurred near the anode, but removal was hindered because the contaminant sorbed back onto the soil further along the cell, towards the middle and cathode regions. The results from this investigation are very promising, but further testing needs to be performed to gain a greater understanding of the electrokinetically enhanced *in-situ* flushing process for PAHs.

Acknowledgements

This research was partly funded by the National Science Foundation (Grant # CMS 0100073), and the support of this agency is gratefully acknowledged. The authors were also grateful to the reviewers for their useful comments.

References

Abdul, A. S., Gibson, T. L., Ang, C. C., Smith, J. C., and Sobczynski, R. E., 1992, "*In-situ* surfactant washing of polychlorinated biphenyls and oils from a contaminated site," *Ground Water*, Vol. 30, No. 2, pp. 219-231.

Acar, Y. B., Gale, R. J., Alshawabkeh, A. N., Marks, R. E., 1995, Puppula, S., Bricka, M., and Parker, R., "Electrokinetic remediation: Basics and technology status," *Journal of Hazardous Materials*, Vol. 40, pp. 117-137.

Adeel, Z., and Luthy, R. G., 1995, "Concentration-dependent regimes in sorption and transport of a nonionic surfactant in sand-aqueous systems," Chapter 4 in Surfactant Enhanced Subsurface Remediation - Emerging Technologies, Sabatini, D. A., Knox, R. C., and Harwell, J. H., Eds. ACS Symposium Series 594, American Chemical Society, Washington, DC, pp. 39-53.

Attwood, D. and Florence, A. T., 1983, Surfactant Systems, Their chemistry, pharmacy and biology, Chapman and Hall, New York, NY.

Carrol-Webb, S. A. and Walther, J. V., 1988, "A surface complex reaction model for the pH-dependence of corundum and kaolinite dissolution rates," *Geochimica et Cosmochimica Acta*, Vol. 52, pp. 2609-2623.

Casagrande, I. L., 1949, "Electro-osmosis in soils," *Geotechnique*, Vol. 1, No. 3, pp. 159-177.

Connell, D. W., 1997, Basic Concepts of Environmental Chemistry, Lewis Publishers, New York, N. Y.

Duhkin, S. S. and Derjaguin, B. V., 1974, Electrokinetic Phenomena, Volume 7 in Surface and Colloid Science, Egon Matijevic, Editor, John Wiley and Sons, New York, NY.

Dzenitis, J. M., 1997, "Steady state and limiting current in electroremediation of soil," *Journal of the Electrochemical Society*, Vol. 144, No. 4, pp. 1317-1322.

Edwards, D. A., Adeel, Z., and Luthy, R. G., 1994, "Distribution of nonionic surfactant and phenanthrene in a sediment/aqueous system," *Environmental Science and Technology*, Vol. 28, No. 8, pp. 1550-1560.

Evangelou, V. P., 1998, Environmental Soil and Water Chemistry, Principles and Applications, John Wiley and Sons, Inc. New York, N. Y.

Eykholt, G. R., 1997, "Development of pore pressures by nonuniform electroosmosis in clays," *Journal of Hazardous Materials*, Vol. 55, pp. 171-186.

Eykholt, G. R., 1992, "Driving and complicating features of the electrokinetic treatment of contaminated soils," Ph. D. Dissertation, Dept. of Civil Engineering, University of Texas at Austin.

Eykholt, G. R. and Daniel, D. E., 1994, "Impact of system chemistry on electroosmosis in contaminated soil", *Journal of Geotechnical Engineering*, Vol. 120, No. 5, pp. 797-815.

Farrell, J., Grassian, D., and Jones, M., 1999, "Investigation of mechanisms contributing to slow desorption of hydrophobic organic compounds from mineral solids," *Environmental Science and Technology*, Vol. 33, No. 8., pp. 1237-1243.

Fountain, J. C., Waddell-Sheets, C., Lagowski, A., Taylor, C., Frazier, D. and Byrne, M., 1995, "Enhanced removal of dense non-aqueous phase liquids using surfactants; Capabilities and limitations from field trials," Chapter 13 in Surfactant Enhanced Subsurface Remediation - Emerging Technologies, Sabatini, D. A., Knox, R. C., and Harwell, J. H., Eds. ACS Symposium Series 594, American Chemical Society, Washington, D. C.

Ganeshalingam, S., Legge, R. L., and Anderson, W. A., 1994, "Surfactant-enhanced leaching of polycyclic aromatic hydrocarbons from soil," *Transactions – Institution of Chemical Engineers*, Vol. 72, Part B, pp. 247-251.

Gray, D. H. and Mitchell, J. K., 1967, "Fundamental aspects of electro-osmosis in soils," *Journal of the Soil Mechanics and Foundations Division*, ASCE, Vol. 93, No. SM 6, pp. 209-236.

Greenland, D. J. and Hayes, M. H. B., 1978, The Chemistry of Soil Constituents, John Wiley and Sons, New York, NY.

Grim, R. E. 1968, Clay Mineralogy, McGraw-Hill, New York, NY.

Grimberg, S. J., Nagel, J., and Aitken, M. D., 1995, "Kinetics of phenanthrene dissolution into water in the presence of nonionic surfactants," *Environmental Science and Technology*, Vol. 29, No. 6, pp. 1480-1487.

Grundl, T. and Michalski, P, 1996, "Electroosmotically driven water flow in sediments," *Water Research*, Vol. 30, No. 4, pp. 811-818.

Hamann, C. H., Hamnett, A., and Vielstich, W., 1998, Electrochemistry, Wiley-VCH, New York, N. Y.

Ko, S., Schlautman, M. A., and Carraway, E. R., 2000, "Cyclodextrin-enhanced electrokinetic removal of phenanthrene from a model clay soil," *Environmental Science and Technology*, Vol. 34, No. 8, pp. 1535-1541.

Ko, S., Schlautman, M. A., and Carraway, E. R., 1998a, "Partitioning of hydrophobic organic compounds to sorbed surfactants. 1. Experimental studies," *Environmental Science and Technology*, Vol. 32, No. 18, pp. 2769-2775.

Ko, S., Schlautman, M. A., and Carraway, E. R., 1998b, "Effects of solution chemistry on the partitioning of phenanthrene to sorbed surfactants," *Environmental Science and Technology*, Vol. 32, No. 22, pp. 3542-3548.

Lambe, W. T., and Whitman, R. V., 1969, Soil Mechanics, John Wiley and Sons, New York, NY.

Lee, D., Cody, R. D., and Hoyle, B. L., 2001, "Laboratory evaluation of the use of surfactants for ground water remediation and the potential for recycling them," *Ground Water Monitoring and Remediation*, Vol. 21, No. 1, pp. 49-57.

Lowe, D. F., Oubre, C. L., Ward, C. H., and others, 1999, Surfactants and Cosolvents for NAPL Remediation: A Technology Practices Manual, Lewis Publishers, Boca Raton, FL.

Li, A., Cheung, K. A., and Reddy, K. R., 2000, "Cosolvent-enhanced electrokinetic remediation of soils contaminated with phenanthrene," *Journal of Environmental Engineering*, Vol. 126, No. 6, pp. 527-533.

Luthy, R. G., Aiken, G.R., Brusseau, M.L., Cunningham, S.D., Gschwend, P.M., Pignatello, P.M., Reinhard, M., Traina, S.J., Weber, W.J., JR., and Westall, J.C., 1997, "Sequestration of hydrophobic organic contaminants by geosorbents," *Environmental Science and Technology*, Vol. 31, No. 12, pp. 3341-3347.

Myers, D., 1988, Surfactant Science and Technology, VCH Publishers Inc., New York, N.Y.

Mitchell, J. K., 1993, Fundamentals of Soil Behavior, John Wiley and Sons, Inc., New York, N. Y.

Pamukcu, S., 1994, "Electrokinetic removal of coal tar constituents from contaminated soils," Electrical Power Research Institute, Report TR-103320.

Patterson, I. F., Chowdhry, B. Z., and Leharne, S. A., 1999, "Polycyclic aromatic hydrocarbon extraction from a coal tar-contaminated soil using aqueous solutions of nonionic surfactants," *Chemosphere*, Vol. 38, No. 13, pp. 3095-3017.

Pennell, K. D., Abriola, L. M., and Weber, W. J. Jr., "Surfactant-enhanced solubilization of residual dodecane in soil columns. 1. Experimental investigation, " *Environmental Science and Technology*, Vol. 27, No. 12, 1993, pp. 2332-2340.

Pinto, L. J. and Moore, M. M., 2000, "Release of polycyclic aromatic hydrocarbons from contaminated soils by surfactant and remediation of this effluent by *Penicillium* spp.," *Experimental Toxicology and Chemistry*, Vol. 19, No. 7, pp. 1741-1748.

Reddy, K.R. and Chinthamreddy, S., 1999, "Electrokinetic remediation of heavy metal contaminated soils under reducing environments", *Waste Management*, Vol.19, No.4, pp. 269-282.

Reddy, K. R. and Shirani, A. B., 1997, "Electrokinetic remediation of metal contaminated glacial tills," *Geotechnical and Geological Engineering Journal*, Vol. 15, No. 1, pp. 3-29.

Reddy, K. R. and Parupudi, U. S., 1997, "Removal of chromium, nickel, and cadmium from clays by *in-situ* electrokinetic remediation," *Journal of Soil Contamination*, Vol. 6, No. 4, pp. 391-407.

Reddy, K. R., Parupudi, U. S., Devulapalli, S. N., and Xu, C. Y., 1997, "Effects of soil composition on removal of chromium by electrokinetics," *Journal of Hazardous Materials*, Vol. 55, No. 1-3, pp. 135-158.

Roote, D.S., Nov. 1998, Technology Status Report: *In-situ* Flushing, Ground-Water Remediation Technologies Analysis Center, Pittsburgh, PA.

Rosen, M. J., 1989, Surfactants and Interfacial Phenomena, second edition, John Wiley and Sons, New York, NY.

Sabatini, D. A., Knox, R. C., and Harwell, J. H., August, 1996, "Surfactant-enhanced DNAPL remediation: Surfactant selection, hydraulic efficiency, and economic factors," *Environmental Research Brief*, EPA/600/S-96/002.

Saichek, R. E., 2002, "Electrokinetically Enhanced In-Situ Flushing for HOC-Contaminated Soils", Ph. D. Thesis, University of Illinois at Chicago, Chicago, IL.

Schwarzenbach, R. P., Gschwend, P. M., and Imboden, D. M., 1993, Environmental Organic Chemistry, John Wiley and Sons, Inc., New York, NY.

Shapiro, A. P. and Probstein, R. F., 1993, "Removal of contaminants from saturated clay by electroosmosis," *Environmental Science and Technology*, Vol. 27, No. 2, pp. 283-291.

Vane, L. M. and Zang, G. M., 1997, "Effect of aqueous phase properties on clay particle zeta potential and electro-osmotic permeability: Implications for electro-kinetic soil remediation processes," *Journal of Hazardous Materials*, Vol. 55, pp. 1-22.

Weast, R. C., Astle, M. J., and Beyer, W. H., 1984, CRC Handbook of Chemistry and Physics, 65th Edition, CRC Press, Boca Raton, FL.

West, J. L. and Stewart, D. I., 1995, "Effect of zeta potential on soil electrokinesis," *Geoenvironment 2000*, ASCE, Geotechnical Special Publication Vol. 2, No. 46, pp. 1535-1549.

Yalkowsky, S. H. and Banerjee, S., 1992, Aqueous Solubility: Methods of Estimation for Organic Compounds, Marcel Dekker, Inc., New York, NY.

Yeom, I. T., Ghosh, M. M., and Cox, C. D., 1996, "Kinetic aspects of surfactant solubilization of soil-bound polycyclic aromatic hydrocarbons," *Environmental Science and Technology*, Vol. 30, No. 5, pp. 1589-1595.

Yeom, I., Ghosh, M. M., Cox, C. D., and Robinson, K. G., "Micellar solubilization of polynuclear aromatic hydrocarbons in coal tar-contaminated soils," *Environmental Science and Technology*, Vol. 29, No. 12, 1995, pp. 3015-3021.

Laurent Lassabatere,[1] Thierry Winiarski,[2] and Rosa Galvez Cloutier[3]

Transfer of Heavy Metals in a Soil Amended with Geotextiles

Reference: Lassabatere, L., Winiarski, T., and Galvez Cloutier, R., "**Transfer of Heavy Metals in a Soil Amended with Geotextiles**", Evaluation and Remediation of Low Permeability and Dual Porosity Environments, *ASTM STP 1415*, M. N. Sara and L. G. Everett, Eds., ASTM International, West Conshohocken, PA, 2002.

Abstract: Although geotextiles are increasingly employed in environmental engineering works for their hydraulic and mechanical properties, their influence on the flow and transfer of solutes, such as heavy metals, has not been fully investigated. This article considers the transfer of a tracer to characterize the flow, and three heavy metals (zinc, lead and cadmium) in a calcareous soil from a fluvio-glacial deposit with and without geotextiles, under steady state flow and saturated conditions. Leaching column experiments were conducted. Results showed that in some cases, geotextiles can homogenize the flow and reduce heavy metals elution, while in others, the flow was heterogenized and the heavy metals were more eluted. The influence on both flow and heavy metals elution depends on the injection rate, the initial water content of the geotextile, and its properties (resistance to water penetration).

Keywords: Transfer, heavy metals, calcareous fluvio-glacial deposit, geotextile, flow.

Introduction

Geotextiles Increasingly Used in Geoenvironmental Engineering

Geosynthetics are increasingly used today in civil, geotechnical and geoenvironmental engineering, mostly in environmental works like waste dumps and infiltration basins.

---

[1] Civil engineer, Laboratoire des Sciences de l'Environnement, Ecole Nationale des Travaux Publics de l'Etat, Rue Maurice Audin, 69518 Vaulx-en-Velin, France, lassabatere@entpe.fr.

[2] Research associate, Laboratoire des Sciences de l'Environnement, Ecole Nationale des Travaux Publics de l'Etat, Rue Maurice Audin, 69518 Vaulx-en-Velin, France, winiarski@entpe.fr.

[3] Associate Professor, Environmental laboratory, Department of Civil Engineering, Faculty of Sciences and Engineering, Laval University, Sainte Foy, Quebec, Canada, rosa.cloutier@gci.ulaval.ca.

These fibrous materials have specific mechanical properties - high shear strength, high resistance to puncture, etc.- and hydraulic properties - high porosity, high permeability and a small filtration opening size (parameter linked to filtration capacity) (Bidim Geosynthetics 1996). Their mechanical properties are exploited to protect other components (geomembranes, clay, pipes, etc.), and reinforce the soil. Their hydraulic properties are exploited to drain and filter water. In particular, they are used to filter leachates in collection systems and drainage layers, thereby preventing drainage equipment from clogging (Artières et al. 1993, Koerner and Koerner 1990).

Infiltration basins are used for runoff water management in the Lyon region (France). Stormwater and runoff water is collected over a wide area and injected in a small area, allowing high concentration of some pollutants (Mikkelsen et al. 1994). Thus groundwater quality depends on proper monitoring of these geoenvironmental works. In some of these infiltration basins, geotextiles have been placed to separate the upper soil-reactive layer from the groundwater underneath. Geotextiles make it easy to remove the upper layer if it is too contaminated.

Despite their growing use in infiltration basins, the influence of geotextiles on flow and on dissolved contaminants has not been fully investigated. And yet a literature review suggests that geotextiles could significantly influence the flow and the transfer of pollutants such as heavy metals.

How Do They Influence the Flow and Transfer of Heavy Metals?

Geotextiles are not presumed to interact directly with these pollutants, due to the low chemical reactivity of their fibers. But they may interact with the soil to produce a new soil-geotextile system with new characteristics.

When geotextiles are put into the soil, they constitute a particular layer with a particular structure. This structural heterogeneity could modify the soil around the geotextile due to soil particle movement and other physical and chemical processes (precipitation, biological clogging; Farkhouh 1994, Koerner and Koerner 1990). When steady state conditions are reached, the soil-geotextile system consists of a layer comprising (1) the original soil, (2) a layer including the modified soil plus the geotextile, and (3) a layer consisting of the original soil underneath. As a rule, the layer including the modified soil and the geotextile displays a different structure (high porosity), different physical and biological properties, and different hydraulic properties (high hydraulic conductivity). This modification of hydraulic properties can be expected to modify the flow. Thus the process of heavy metals transport by water as well as the retention mechanisms could be modified. Actually, these mechanisms can be affected by the volume of soil in contact with the heavy metals and the contact time, both of which are flow dependent.

This study aims at characterizing the influence of different geotextiles on the transfer and the retention of three heavy metals (Zn, Pb, and Cd) in a calcareous soil. Their influence is studied for saturated and steady state flow conditions. The comparison between flow and transfer in the soil system and flow and transfer in the soil-geotextile system is studied for different hydraulic conditions (pore water velocity), different geotextile installation conditions (water content) and two geotextiles with different resistance to water penetration (wetting capacity when subjected to water and initially dry).

Experimental

The experimental method is based on column leaching experiments. The properties of the materials i.e., soil and geotextiles, experimental setup and transport models are successively presented.

Materials

Soil – the soil was collected and sieved through a 1-cm sieve from a calcareous fluvio-glacial deposit in an infiltration basin near Lyon in the Rhône Alpes Region. It is characterized by a coarse texture (Figure 1), low CEC (Cationic Exchange Capacity), low organic matter content and high carbonate content and pH (Table 1). This soil was selected for its retention property for heavy metals (Plassard et al. 2000).

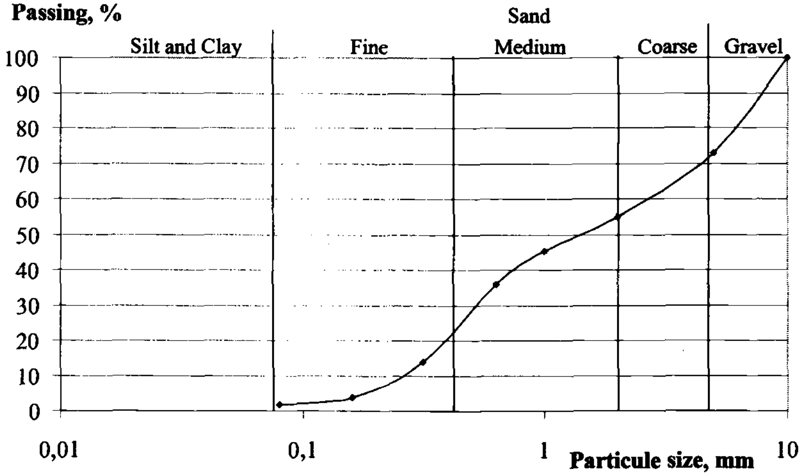

Figure 1 – *Soil particle size distribution and the ASTM texture scale.*

Table 1 – *Soil physico-chemical properties.*

pH	8.65
Carbonate content (%)	25
Organic matter (%)	2
CEC ($mol^{-1}.g$)	$2.75*10^{-5}$

Geotextiles – two geotextiles were tested. Both were nonwoven needlepunched geotextiles currently used for drainage and filtration. Before use, both geotextiles were washed with sulfochromic acid[4] to eliminate any chemicals entering the geotextiles during needlepunching. They were known to be made of different chemical derivatives

---

[4] Sulfochromic acid consists of 250 ml of concentrated sulfuric acid (H_2SO_4) added to 750ml of a 0.9 mol/l potassium dichromate ($K_2Cr_2O_7$) solution.

and therefore display different resistance to water penetration. Their properties are listed in Table 2.

Table 2 – *Properties of the geotextiles.*

	Geotextile G1	Geotextile G2
Thickness, cm	0.6	0.5
Weight, g/cm^2	800	630
Porosity, %	92	93
Permittivity, (s^{-1})	0.5	0.6

Experimental Setup and Transport Models

Characterization of heavy metals transfer and flow in the soil and soil-geotextile system was monitored through leaching column experiments. The same experimental setup was used to inject heavy metals and a tracer to determine the flow. Transfer models were used to characterize the transfer of the tracer more accurately and to assist in its interpretation.

Experimental Setup – The leaching columns were made of transparent PVC, 30 cm long and 10 cm in diameter. Both ends were closed with perforated caps. Glass marbles (5-mm diameter) were placed between the cap and the soil to ensure uniform solute distribution in the soil, allowing a real length of 28.5 cm for the soil and soil-geotextile systems. Before filling, the soil water content was adjusted to 8% with a 0.01 mol/l sodium nitrate ($NaNO_3$) solution (So). The columns were then filled with approximately 4.1 kg of soil for a final bulk density around 1.82 g/cm^3. The geotextiles, dry or wet, were always placed in the middle of the columns. The columns were then saturated upward using a Mariotte bottle for 48 hours with solution So. This natural saturation led to a pore water volume (Vo) around 510 cm^3.

After saturation, the percolation of the tracer and heavy metals was monitored with the experimental setup shown in Figure 2. The columns were connected to a peristaltic pump that could deliver two different solutions successively, i.e., solution So and the percolation solution (tracer or heavy metals) at a constant flowrate. The solutions percolated upward in the columns to expel the air from the columns.

The columns were first subjected to the injection of tracer solution in pulse mode. Bromide (Br^-) was used for its low reactivity, so that the tracer solution (S_T) consisted of a 0.01 mol/l potassium bromide (KBr) solution. The pulse consisted of successive injections of, at first, 1 Vo of solution So to establish steady state flow conditions, followed by 0.67 Vo of tracer solution (S_T), and finally 6.3 Vo of solution So. Eluate samples were collected at the upper cap and their bromide concentrations ($[Br^-]$) determined by ionic chromatography. Bromide elution was characterized by the breakthrough curves (BTC) that plotted the ratio $[Br^-]/[Br^-]_o$ against the ratio V/Vo, where $[Br^-]_o$, V and Vo are the bromide concentration of the percolation solution, the volume percolated and Vo the pore water volume respectively.

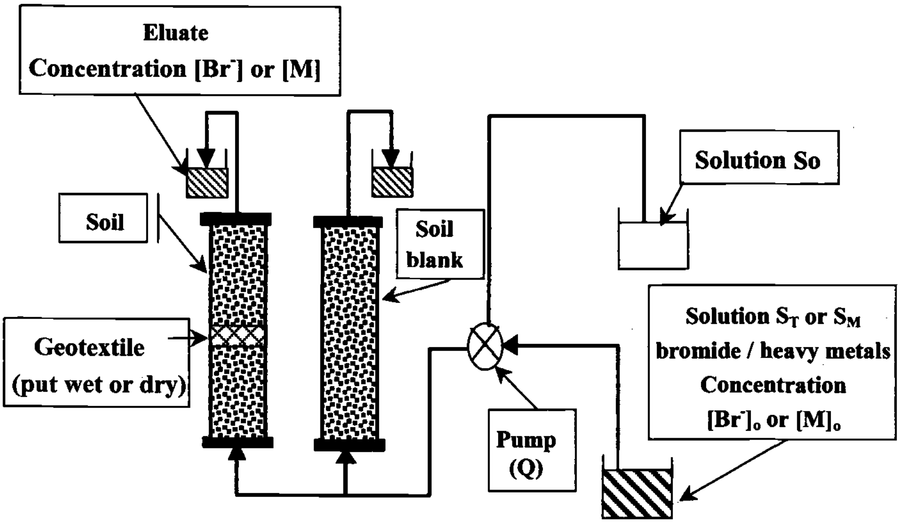

Figure 2 - *Experimental setup.*

The columns were then subjected to the injection of a solution contaminated with heavy metals (Zn, Pb and Cd) in step mode. This solution (S_M) was prepared by dissolving 10^{-3} mol/l of zinc, lead and cadmium nitrate ($Zn(NO_3)_2$, $Pb(NO_3)_2$, $Cd(NO_3)_2$). The ionic strength I of the solution S_M was kept constant and equal to that of the other solutions by adding sodium nitrate ($NaNO_3$). The step consisted of successive injections of 1 Vo of solution So to ensure steady state flow conditions and 7.5 Vo of solution S_M. The eluate concentrations of zinc, cadmium and lead were determined by flame atomic adsorption spectrometry. Heavy metals elution was then characterized by their BTCs ($[M]/[M]_o$ against V/Vo, where [ ] = total dissolved concentration and where M = Zn, Cd or Pb).

BTC Analysis and Transport Models – The flow was more accurately characterized by calculating parameters from the bromide BTCs and modeling the BTCs. At first, the mass balance was determined for each column by the zero order moment of the BTCs. The mean travel time and retardation factor (R) were determined by the first order moment of the BTCs. The retardation factor served to determine the real water volume "used" by the bromide. It estimated the ratio V_{Br}/Vo, where V_{Br} was the real water volume used by the bromide. This volume was smaller than the pore water volume due to anionic exclusion and to isolated water. Thus, a new water content $\theta_{Br}=R\theta$ was considered for BTC modeling.

The transport model used was a two region (mobile-immobile water) MIM transport model with a first-order exchange of solute. Previous studies have shown that this model was accurate for characterizing bromide transfer in our soil (Fevrier et al. 2000). The water is assumed to be divided into two fractions: a mobile fraction active in mass transport and a stagnant immobile fraction, and that solutes can only reach by diffusion from the mobile fraction. This diffusion is assumed to be governed by a first order law.

The MIM transfer model can be synthesized by the following equations (Van Genuchten and Wierenga 1976) :

$$\begin{cases} \theta_m \dfrac{\partial C_m}{\partial t} + \theta_{im} \dfrac{\partial C_{im}}{\partial t} = \theta_m D_m \dfrac{\partial^2 C_m}{\partial z^2} - q \dfrac{\partial C_m}{\partial z} \\ \theta_{im} \dfrac{\partial C_{im}}{\partial t} = \alpha (C_m - C_{im}) \end{cases} \qquad (1)$$

where
θ_m = volumetric water content of the mobile fraction (cm^3/cm3),
θ_{im} = volumetric water content of the immobile fraction (cm^3/cm3),
C_m = solute concentration in the mobile fraction (mol/L),
C_{im} = solute concentration in the immobile fraction (mol/,L)
q = Darcy water velocity in the mobile fraction (cm/min),
D_m = dispersion coefficient (cm^2/min) in the mobile fraction, and
α = solute exchange rate (min^{-1}) between the mobile and the immobile fractions.

The analytical solution Cm(x,t) of this model corresponds to the analytical solution of equations (1) for the following initial and boundary conditions :

$$\begin{cases} C_{im}(z,0) = C_m(z,0) = 0 \\ C_{im}(+\infty,t) = C_m(+\infty,t) = 0 \\ qC_m(0^+,t) - \theta_m D_m \cdot \dfrac{\partial C_m}{\partial z}(0^+,t) = qCo \quad when \quad t \le \delta t \\ qC_m(0^+,t) - \theta_m D_m \cdot \dfrac{\partial C_m}{\partial z}(0^+,t) = 0 \quad when \quad t \ge \delta t \end{cases} \qquad (2)$$

where
δt = time of injection of tracer solution S_T.

Some parameters (θ_{Br}, x = l = length of the column) and others including Dm, α and θ_m were then estimated to optimize the fitting of experimental BTC by the transfer model analytical solution Cm. These parameters can help determine flow homogeneity. For instance, the higher the mobile water content ratio ($f=\theta_m/(\theta_m+\theta_{im})$), the smaller the immobile fraction and the more homogeneous the flow. This means that, for quite similar values for Dm and α, the value of the water content ratio f can be considered as a good indicator of flow homogeneity.

Experimental Schedule

The experimental setup accounted for several experimental parameters such as injection rate Q, initial geotextile water content, when put into the columns, and type of geotextile (G1 or G2). The influence of the geotextiles on flow and heavy metals transfer was tested for the following experimental conditions :

- ✓ **Injection flowrate:** all the experiments were performed at a high injection flowrate Q = 14.02 cm^3/min, which corresponded to a pore water velocity equal to 0.80 cm/min, and at low injection flowrate q = 5.59 cm^3/min, that corresponded to a pore water velocity equal to 0.32 cm/min.
- ✓ **Initial geotextile water content:** for all injection rates, geotextile G1 was placed dry or wet. Geotextile G2 was always placed dry.
- ✓ **Type of geotextile:** both geotextiles were tested for all the injection rates.

All the experiments performed for this study are presented in Table 3. Three tests were performed for each type of column. The different columns were graded using the following code: the first letter for injection rate (q and Q respectively for the low and high rates), the second and the third for the system (S for soil, G1 for soil-geotextile G1 and G2 for soil-geotextile G2) and the last for the geotextile installation condition (d and w respectively for dry and wet).

Table 3 - *Experimental schedule.*

	Soil	Soil-geotextile G1	Soil-geotextile G2
q	qS	qG1d: geo G1 dry qG1w: geo G1 wet	qG2d: geo G2 dry
Q	QS	QG1d: geo G1 dry QG1w: geo G1 wet	QG2d: geo G2 dry

Results and Discussion

Influence of Geotextiles on Flow

At LowFlowrate – Figure 3 and Figure 4 show the mean BTCs plotting the averaged ratio $[Br-]/[Br-]_0$ against the averaged ratio V/Vo at the low flowrate.

Analysis of the BTCs reveals little difference between qS and qG2d. The BTCs qS, qG1w and qG1d were more different. qG1w and qG1d were characterized by a more symmetrical shape with a later breakthrough and a smaller tailing.

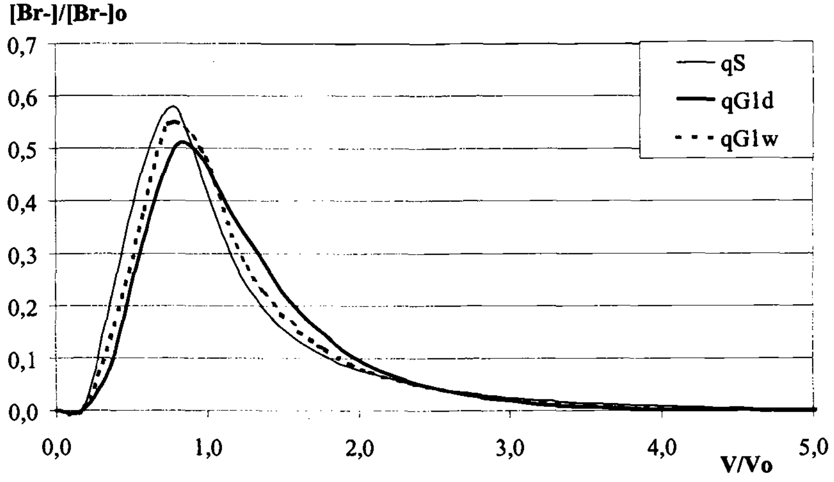

Figure 3 - *Mean BTCs of soil and soil-geotextile G1 columns at low flowrate.*

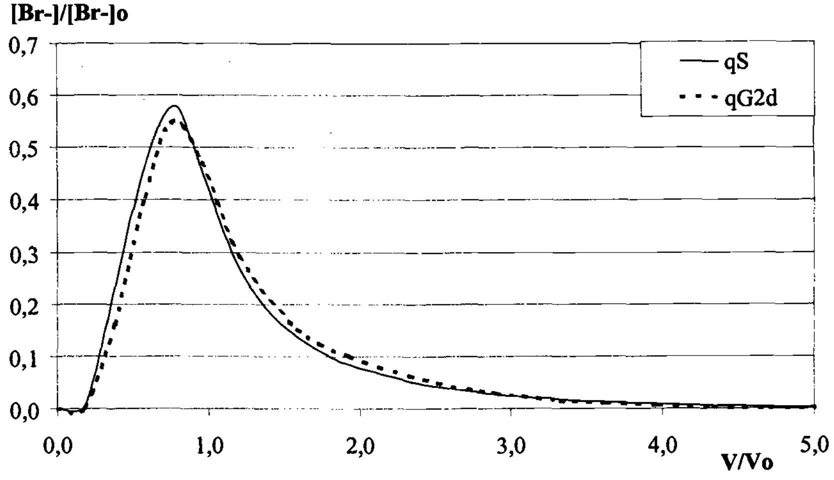

Figure 4 - *Mean BTCs of soil and soil-geotextile G2 columns at low flowrate.*

It can be proposed that the curve shape is an indicator of the homogeneity of the flow in the column. The earlier the breakthrough, the larger the tailing, and hence the more asymmetrical the BTC, the more heterogeneous the flow. This assumption is illustrated thanks to two particular columns of the qS and qG1d types, which are well representative of the mean BTCs. Figure 5 shows the experimental BTC curves (points) and model curves (continuous lines). The mass balance, retardation factors and all the parameters of the model curves are presented in Table 4. The shape of the BTC qS appeared more asymmetrical, with an earlier breakthrough and a larger tailing. As the solute exchange rate α and the dispersivities were close, the differences of shape resulted in a change in the mobile fraction ratio f. The ratio f was smaller for the column qS (52.2%) than for the column qG1d (76.2%). Thus the higher f for column qG1d was indicative of more homogeneous flow.

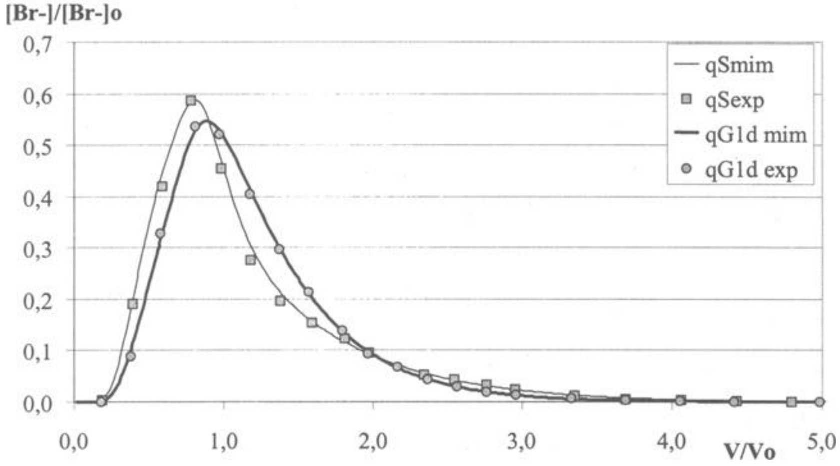

Figure 5 - *BTCs fitted with the MIM model for one of the columns qS, qG1d.*

Table 4 - Modeling parameters for one column qS and one column qG1d.

	qS	qG1d
Mass balance (MB)	0 926	0 918
Retardation factor (R)	0 816	0 935
Mobile fraction ratio (f) (%)	54.2	76.2
Solute exchange rate (α) (mn^{-1})	0 0017	0 002
Dispersivity (λ) (cm)	2.08	2.68

Thanks to the analysis of BTCs and of the modeling parameters, it seems accurate to conclude that geotextile G2 or geotextile G1 placed wet slightly homogenizes the flow, and that geotextile G1 placed dry homogenizes the flow significantly.

At High Flowrate – Figures 6 and 7 show the mean BTCs obtained at high flowrate. The standard deviations are not shown to keep the figures legible.

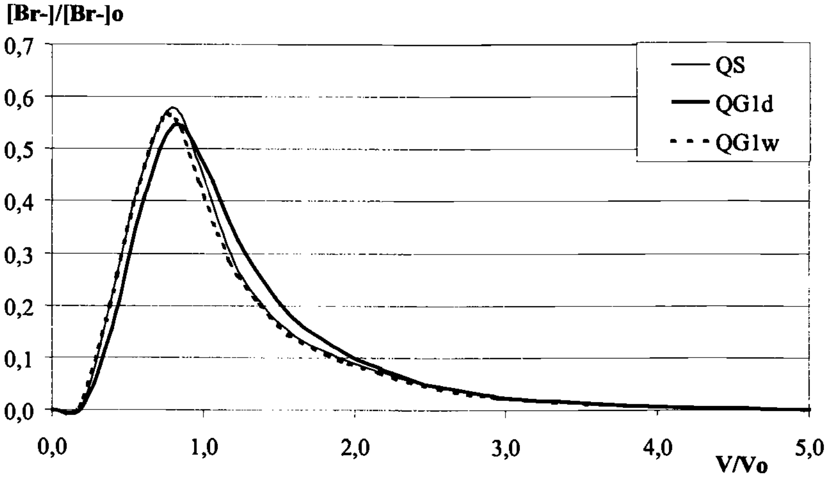

Figure 6 - *BTCs of soil and soil-geotextile G1 columns at high flowrate.*

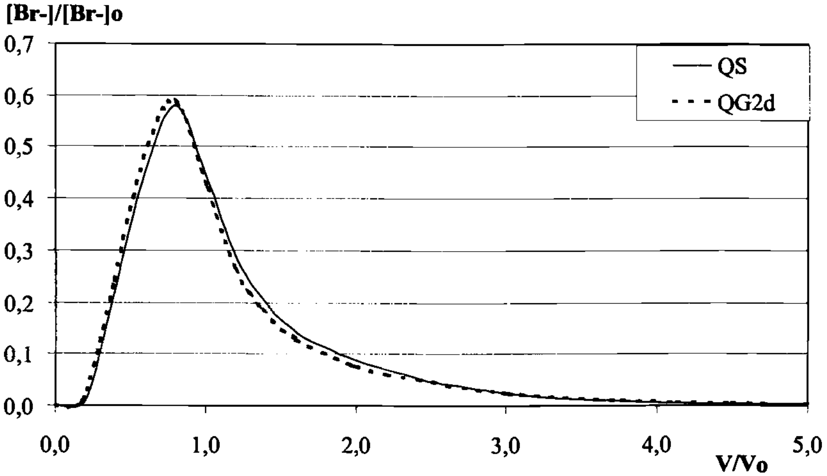

Figure 7 - *BTCs of soil and soil-geotextile G2 columns at high flowrate.*

There was no significant difference between QS and QG1w. QG2d appeared similar to QS except shifted slightly to the left, thus revealing an earlier breakthrough of bromide. QG1d seemed quite different from the other BTCs. The breakthrough was later, the tailing reduced, and the curve was more symmetrical. Geotextile G1 had little influence on the flow when introduced wet (QG1w), but homogenized the flow when introduced dry (QG1d). Geotextile G2 introduced dry caused some heterogenization of the flow. At high flowrate, the results have to be regarded cautiously: slight differences between the mean BTCs compared to the variability of triplicates. On the contrary, the reproducibility of triplicates was good at low flowrate.

Influence of Geotextile on Heavy Metals Transfer

Lead was not eluted at all in any of the experiments. This may have been due to lead carbonate and hydroxide precipitation (Plassard 1998). Thus the influence of the geotextiles on the heavy metals transfer could only be analyzed by their influence on the transfer of zinc and cadmium. These metals had similar elutions for all the experiments. The results shown deal only with the elution of cadmium. The same results and conclusions can be drawn for the elution of zinc.

Figure 8 and Figure 9 show the mean BTC obtained at high and low flowrates, respectively. All the BTCs had a linear shape and a late breakthrough. Retention mechanisms prevented heavy metals from eluting completely and rapidly.

At low injection rate (Figure 8), the standard deviation was quite small except for columns qG1w, which revealed good reproducibility of the results. The BTCs of columns qS, qG1w and qG2d were similar. In fact, cadmium elution seemed slightly less in columns qG1w and QG2d, although this difference was not really significant. The BTC qG1d was far lower than the other BTCs. Geotextile G1 placed wet and geotextile G2 did not significantly influence cadmium elution, while geotextile G1 put dry significantly reduced cadmium elution.

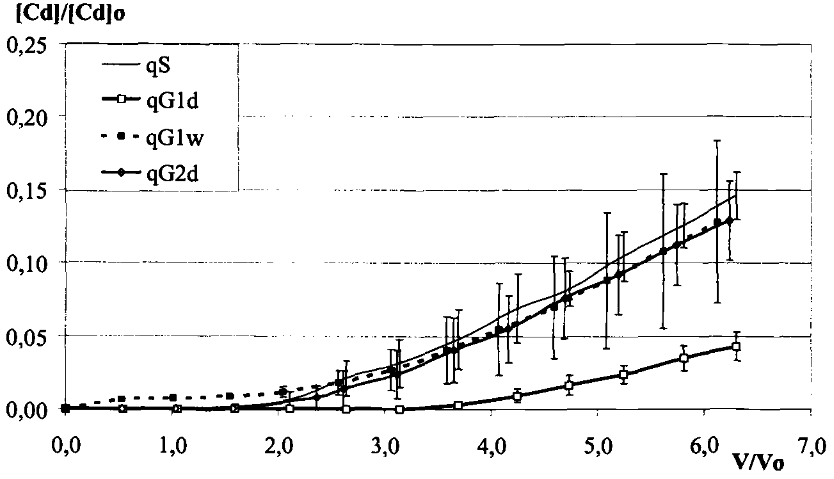

Figure 8 - *Cadmium BTCs at low injection rate.*

At high flowrate (Figure 9), standard deviations were quite high indicating a variability of the results, although some trends persisted. All the BTCs, except QG2d and QG1w, seemed different from each other. The BTCs QG2d and QG1w were above BTC QS, whereas BTC QG1d was lower than the others. When compared with columns QS, cadmium elution was higher in columns QG1w and QG2d and smaller in columns QG1d.

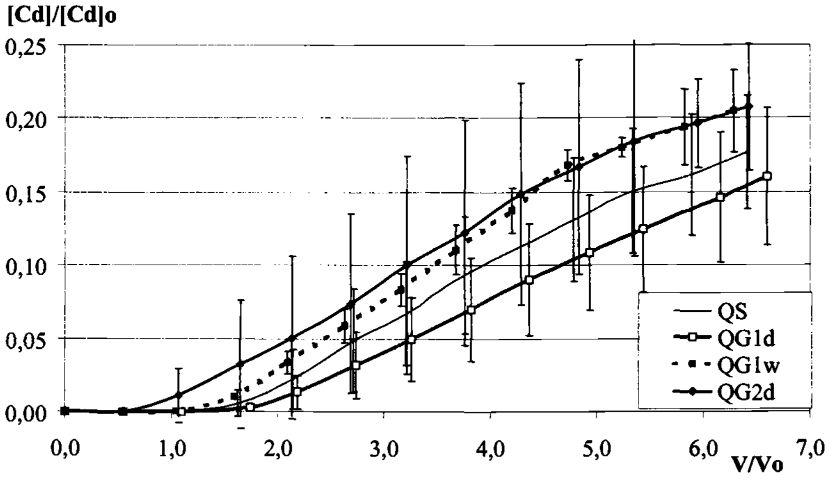

Figure 9 - *Cadmium BTCs at high injection rate.*

In short, at both flowrates, geotextile G1 placed dry reduced heavy metals transfer. Geotextile G1 placed wet and geotextile G2 had no influence on heavy metals elution at low injection rate and increased their elution at high flowrate.

Discussion

Flow modification and the elution of heavy metals appear to be related. When the geotextile led to homogenization of the flow (qG1d and QG1d), heavy metals were less eluted. When the geotextile led to a heterogenization (QG2d and QG1w) of the flow, heavy metals elution was increased. This is all the more accurate as each column is concerned. For instance, for the two specific columns presented above, the flow was much more heterogeneous in column qS than in column qG1d, while heavy metals elution was much higher in column qS than in column qG1d. At the end of percolation, the ratio $[Cd]/[Cd]_0$ scored 0.16 for qS and 0.03 for qG1d. These results were general and could be applied to most of the columns. The result indicated a strong correlation between flow homogeneity and heavy metals elution.

This correlation between flow and heavy metals transfer can be explained by considering the following assumptions. Flow heterogeneity can affect the transport process and retention mechanisms by reducing the contact between the soil and the contaminants (Birkholzer and Tsang 1997), the local increase in velocity causing a decrease in retention by kinetic mechanisms (Fryar and Schwartz 1998). Previous studies have shown that the retention mechanisms in the soil studied can be affected by the homogeneity of the flow and the quality of the contact between the soil and the heavy metals concerned (Zn, Cd and Pb) (Plassard 1998). The main retention mechanisms are in fact the precipitation of carbonates and hydroxide metals and the combination with carbonates (Plassard et al. 2000). These mechanisms need carbonate ions (CO_3^{2-}) and OH^-. These anions are provided by the dissolution of the soil carbonates, which increases with improved contact between carbonates and pore water. Carbonate dissolution may be favored by homogenizing the flow, thereby improving the quality of the contact between soil carbonates and pore water.

All these assumptions led to the conclusion that the geotextiles did not react directly with the heavy metals but influenced their transfer and retention by influencing the flow and mainly its homogeneity. Determining their influence on the heavy metals transfer is thus equivalent to determining their influence on flow.

Their influence on the flow can be characterized if we consider the water content of the geotextile as one of the main factors. For low water content, geotextiles, like most permeable materials, are characterized by very low permeability. They could form a lower permeability layer in the soil, reducing the flow in the macropores and thus homogenizing the flow. Moreover, a high water content in the geotextile must result in high hydraulic conductivity. The geotextile may form a layer interconnecting the macropores and high hydraulic conductivity zones, resulting in a heterogenization of the flow (Birkholzer et Tsang 1997).

Other parameters, such as injection flowrate, resistance to water penetration and initial water content, influenced the geotextile water content during the percolation of bromide and heavy metals and hence its influence on the flow. For instance, a high injection rate associated with high water head on the geotextile and a low resistance to water penetration (geotextile G2) ensured a high water content at both injection flowrates. This could explain the heterogenization of the flow by geotextile G2 for all cases. For geotextile G1, the injection flowrates did not seem high enough to ensure by themselves a high water content in all cases. Thus the water content must have been high only when geotextile G1 was placed wet. Thus geotextile G1 placed dry maintained a low water content at both flowrates, resulting in good homogenization of the flow.

Conclusions

This study demonstrated that the installation of geotextiles in a calcareous soil can change the flow and hence the transfer of some heavy metals (Zn, Cd). The influence of geotextiles on heavy metals appears to depend only upon their influence on the flow. The results suggested a correlation between their influence on flow homogeneity and their influence on heavy metals transfer. When the geotextiles homogenized the flow, they triggered an increase in heavy metals retention and thus decreased their elution. By contrast, when geotextiles triggered a flow heterogenization, heavy metals elution was increased and hence their soil retention was reduced. Thus determining their influence on heavy metals transfer is equivalent to determining their influence on flow. We assumed that one of the main factors was their water content, which appeared to condition their hydraulic conductivity and hence their influence on flow. Thus all parameters (injection rate, initial water content, resistance to water penetration of the geotextiles) that modified their water content could also modify their influence on the flow and on heavy metals transfer.

These assumptions lead to the conclusion that further studies are needed to clarify the processes explaining their influence on flow, and at least the way that flow modification can modify heavy metals transfer. A better understanding of these processes could help in monitoring the use of geotextiles in geoenvironmental works, as in infiltration basins.

Acknowledgments

We thank all the organizations that sponsored this study and primarily the Région Rhône Alpes, "Les Entretiens Jacques Cartier," the French Ministry of National Education and Research, and the French Ministry of Foreign Affairs.

References

Artières, O., Delmas, P., and Soyez, B., 1993, "Les Structures d'Etanchéité Combinées (Matériaux Naturels / Géosynthétiques) dans le Confinement des Sites de Stockage de Déchets Solides", *Geoconfine 93*, Arnould, Barrès & Côme (ed.), Rotterdam, pp. 291-296.

Bidim Geosynthetics, 1996, *Le Guide des Géosynthétiques*, Bidim Geosynthetics S.A. (ed.), Bezons, France.

Birkholzer, J., and Tsang, C. F., 1997, "Solute Channeling in Unsaturated Heterogeneous Porous Media," *Water Resources Research*, Vol. 33, No. 10, pp 2221-2238.

Farkouh, B., 1994, *Le Filtre Géosynthétique dans les Ouvrages de Drainage : Essais de Laboratoire et Observations in Situ*, PhD Thesis Joseph Fournier-Grenoble I, France.

Fevrier, L., Winiarski, T., Delolme, C. and Gaudet, J.-P., 2000, "Effect of Flow Rate on the Retention of Zinc, Cadmium and Lead in a Fluvio-Glacial Deposit Column," *International Conference on Heavy Metals in the Environement* (CD-ROM), J. Nriagu, Editor, University of Michigan An Arbor, Michigan, USA, 6-10 August 2000.

Fryar, E. A., and Schwartz, F. W., 1998, "Hydraulic-Conductivity Reduction, Reaction Front Propagation, and Preferential Flow within a Model Reactive Barrier," *Journal of Contaminant Hydrology*, Vol. 32, No. 3-4, pp. 333-351.

Koerner, G. R., and Koerner, R. M., 1990, "Biological Activity and Potential Remediation Involving Geotextile Landfill Leachate Filters", *Geosynthetic Testing for Waste Containment Applications,* ASTM STP 1081, Jan 23 1990, Las Vegas, pp. 313-321.

Mikkelsen, P.S., Weyer, G.,Berry, C., Walden, Y., Colandini, V., Poulsen, S., Grotehusman, D., and Rohlfing, R., 1994, "Pollution From Urban Stormwater Infiltration," *Water Sciences Technology*, Vol. 29, No. 1-2, pp.293-302.

Plassard F., 1998, *Influence de la Complexation de Trois Cations Métalliques sur leur Rétention par un Sol Alcalin. Application à un Bassin d'Infiltration d'Eaux Pluviales*, PhD Thesis Claude Bernard-Lyon 1, France.

Plassard, F., Winiarski, T., and Petit-Ramel, M., 2000, "Retention and Distribution of three heavy metals in a carbonated soil : comparison between batch and unsaturated column studies", *Journal of Contaminant Hydrology*, Vol. 42, pp. 99-111.

Van Genuchten, M.Th., and Wierenga, J.P., 1976, "Mass Transfer Studies in Sorbing Porous Media. I. Analytical solutions", *Soil Sciences Society American Journal*, Vol. 40, No. 4, pp. 473-480.

Narbutovskih, S.M.,[1] McDonald, J.P.,[1] Schalla, R.,[1] and Sweeney, M.D.[1]

Application of the Colloidal Borescope to Determine a Complex Groundwater Flow Pattern

Reference: Narbutovskih, S.M., McDonald, J.P., Schalla, R., and Sweeney, M.D., "**Application of the Colloidal Borescope to Determine A Complex Groundwater Flow Pattern,**" *Evaluation and Remediation of Low Permeability and Dual Porosity Environments, ASTM STP 1415*, M. N. Sara and L. G. Everett, Eds. ASTM International, West Conshohocken, PA, 2002.

Abstract: Pacific Northwest National Laboratory staff made in situ flow measurements in groundwater monitoring wells at the U.S. Department of Energy (DOE) Hanford Site to determine the flow direction in an aquifer with a flat water table. Given the total errors in water level elevations and a gradient of a few centimeters over 500 meters, flow directions based on the potentiometric surface are ambiguous across the 200 East Area at the Hanford Site. The colloidal borescope was used because it allows direct, real time observation of mobile colloidal particles in the open interval of a water well and, thus, avoids the use of water level data. The results characterize a complex groundwater flow pattern under several buried waste storage tank farms. The aquifer, artificially high due to the large volume of liquid discharges to the soil column from Hanford's nuclear production era, is currently receding to original conditions. The aquifer lies in unconsolidated gravel beds overlying an impermeable basalt surface that has a plucked, flood-scoured, scabland structure. The current aquifer thickness is similar to the relief on the basalt surface. Thus, the groundwater must flow around the impermeable basalt structures producing a complicated flow pattern under the waste storage unit. The original monitoring network was designed for northwest flow when the water table was held artificially high. Proper locations for new wells are dependent on our knowledge of the flow direction. The results of the colloidal borescope investigation agree with the southerly direction indicated from hydrographs, contaminant trends, other direct flow data and the general concept of a receding aquifer draining off the southern limb of a basalt anticline. Flow in the aquifer is diverted by irregular local structural highs of very low permeability basalt.

Keywords: Hydrology, flow direction, colloidal borescope, flat water table, in situ flow measurement, DOE Hanford Site, groundwater monitoring

---

[1] Senior Research Scientist, Senior Research Scientist, Senior Research Scientist, and Senior Research Engineer, respectively, Environmental Technology Division, Pacific Northwest National Laboratory, Richland, WA 99352

Introduction

In the 200 East Area on the U.S. DOE Hanford Site in eastern Washington, the hydraulic gradient is nearly flat making it difficult to determine upgradient versus down gradient groundwater monitoring wells from water level measurements. This paper describes the use of a unique in-well flowmeter, the colloidal borescope, to determine the direction and rate of groundwater flow under three single shell tank farms without the use of water level measurements. These farms comprise the RCRA Waste Manage Area (WMA) B-BX-BY (Figure 1).

In 1996, the waste management area was placed in a groundwater quality assessment program as required based on specific conductance values that were elevated above the critical mean in a downgradient well (Caggiano 1996, Narbutovskih 2000). The resulting assessment report documents evidence that waste from the area has, most likely, affected groundwater quality (Narbutovskih 1998). Because WMA B-BX-BY is regulated under RCRA interim status regulation (40 CFR 265.93 (d) paragraph [7]), DOE must determine the rate and extent of contaminant migration in groundwater associated with waste that has leaked from the WMA. The tanks at these farms contain a mixture of hazardous and radioactive waste left from processing to separate weapons-grade plutonium from reacted nuclear fuel rods. Consequently, monitoring is required to assess the impact of these storage facilities on the groundwater.

The discussion in this paper focuses on the description, use, and field application of the colloidal borescope during an evaluation to determine applicability of the method to measure flow directions in the 200 East Area. After a brief description of aquifer conditions at WMA B-BX-BY, the tool and ancillary equipment are described along with the approach used to guide the field application. Representative records of the field data are presented with an evaluation of the applicability of the method for further flow determination at the Hanford Site.

Background

The WMA B-BX-BY single-shell tank farms are nearly surrounded with effluent discharge facilities where large amounts of radioactive processing waste were discharged to the soil column (Figure 2). The chemistry of this waste was similar to the mixtures that were stored in the tanks. Consequently, it is difficult to differentiate groundwater contamination associated with these past-practice liquid discharge facilities from waste that has leaked from the tank farms, especially with the uncertainty associated with the direction of groundwater flow. The complexity of the groundwater contamination and the multiple release dates also negate the usefulness of plumes to clearly determine the flow direction.

Below WMA B-BX-BY are a series of unconsolidated Pleistocene sediments deposited during the Missoula Floods. These sediments consist of an upper unit of interbedded gravel and sand facies that are underlain by well-stratified, coarse to fine-grained sand that contains laterally discontinuous layers of silt (Figure 2). The

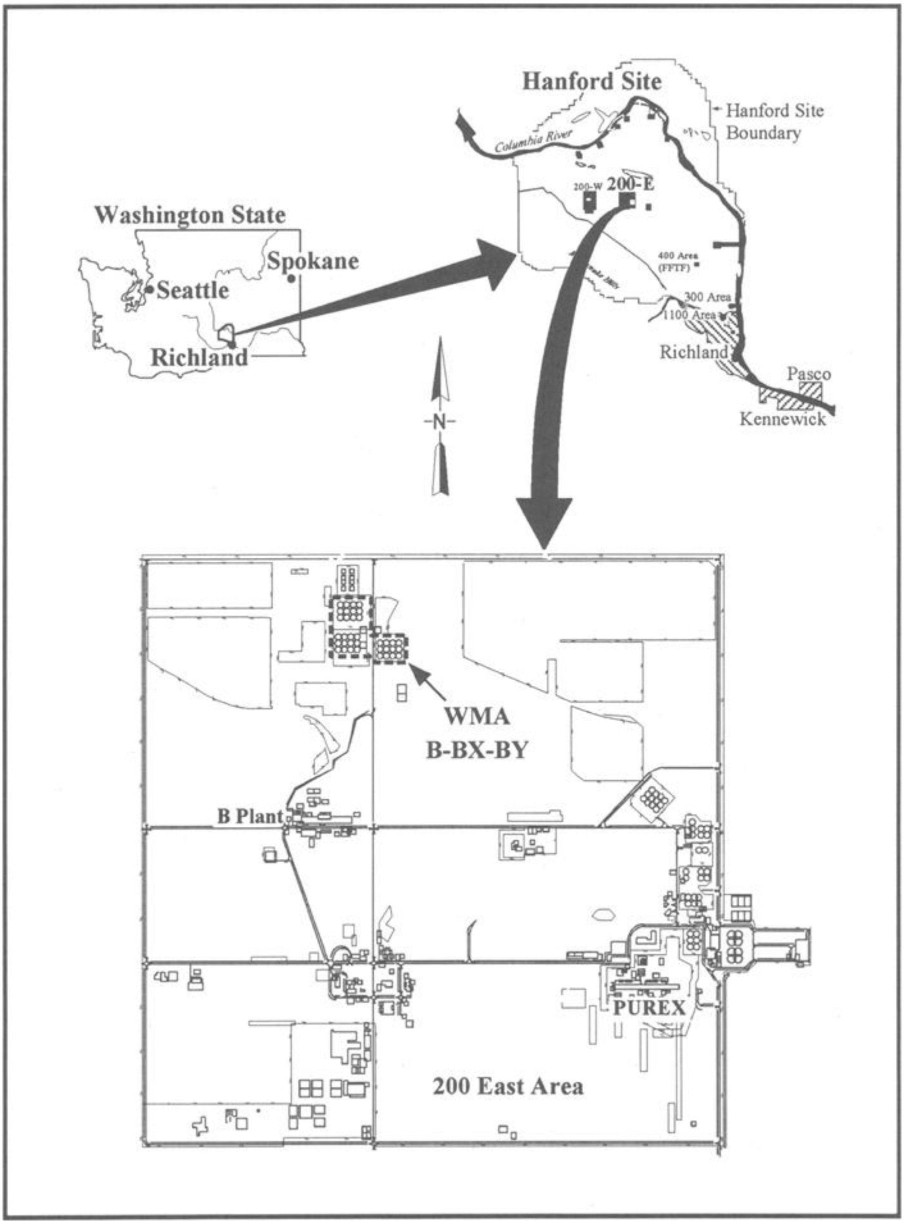

Figure 1- *Location map for waste management area B-BX-BY, located north of Richland, Washington.*

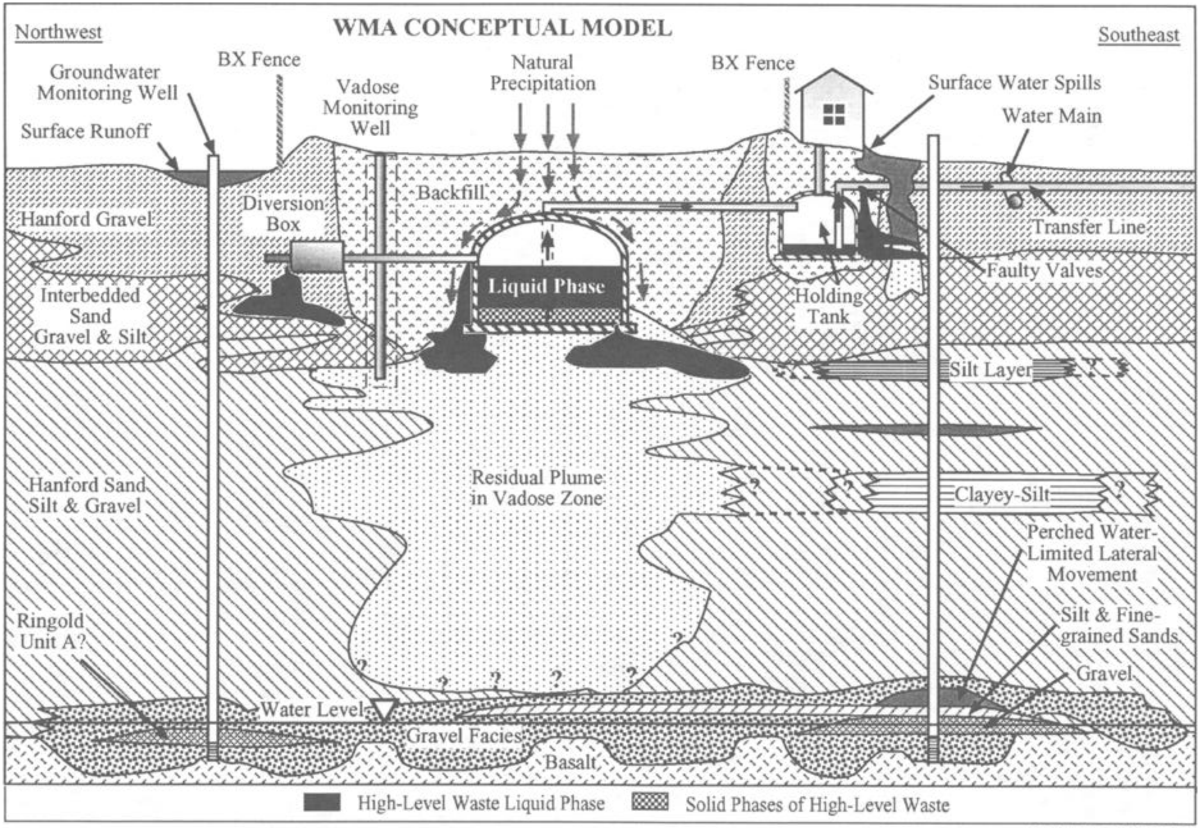

2001/DCL/B-BX-BY/004

Figure 2- *A conceptual model for WMA B-BX-BY. This area has a complicated history of nuclear waste discharged to the soil column, intentionally and accidentally that resulted in an intricate pattern of contaminant plumes in the groundwater.*

aquifer lies primarily in a basal, unconsolidated cobble to boulder gravel bed. This sediment package lies on an irregular, flood-scoured basalt surface. Based on results from pump tests, the hydraulic conductivity in this area is about 1615 meters per day. The estimated Darcy flow rate is calculated at 0.9 meters per day based on 30% porosity and a very small gradient of 0.000165 (Hartman et al. 2000).

The highly permeable sediments are the primary cause of the small gradient on the water table. The extremely small differences in water levels between wells make it difficult to determine flow direction from water-level measurements at this site. There are various sources of error in estimating water level elevations that compound this problem (Schalla et al. 1992). These sources are related to measurement errors, small errors in well elevation survey data, pressure effects associated with changing weather conditions, and small deviations from vertical of the borehole. Each of these sources can influence the relative position of a well's water elevation with respect to nearby wells (Hartman et al. 2000, Narbutovskih 2000, Narbutovskih and Horton 2001). The result may be a misinterpretation when multiple hydrographs are plotted together. Unless these errors are sufficiently minimized and corrected, or the error is identified and the well eliminated from the analysis at the 200 East Area of the Hanford Site, flow directions estimated from water elevations alone are uncertain when applied to a region as small as WMA B-BX-BY (Narbutovskih 2000).

Another issue that may cause misconception of the groundwater flow is the decreasing water-level elevations. Most of the region immediately underlying WMA B-BX-BY and the BY Cribs had little or no aquifer prior to Hanford operations in the mid-1940s. Groundwater in the area of the BY Cribs was artificially emplaced by releases of liquid wastes to the disposal facilities. Based on historic water-level data, the water table can be expected to drop at least 2.5 meters if conditions return to pre-Hanford conditions. The aquifer in the northern part of the site is only 1.2 meters thick in some areas. This thin aquifer is located on an uneven basalt surface with structural relief that varies from 1.5 to 3.4 meters. Consequently, local flow paths in this area may meander around these basalt features as the water level recedes.

Theoretically, given the conditions of a low hydraulic gradient and sharply contrasting hydraulic properties (e.g. impermeable basalt versus highly permeable gravel beds), complex flow patterns can be created (Cushman 1990). Such conditions appear to exist in the study area. Some water may even be ponded in local basalt surface depressions resulting in partially stagnant, no-flow conditions in the lower portion of the aquifer.

Approach

Colloidal borescope investigations were conducted in 15 wells by the tool vendor, AquaVision, Inc. (Narbutovskih 2000). This tool is an in situ borehole measurement device that detects the speed and direction of particulate matter in groundwater moving through the well bore. These data were planned to provide a measurement of the groundwater flow direction independent of water level elevations. In addition, the borescope data provided estimates on the relative rate or magnitude of groundwater flow in preferential flow zones.

Methods that rely on the borehole flow velocity to determine linear flow velocity in the aquifer have been questioned because the flow rate through the borehole may not be representative of the flow rate in the porous medium. However, it has been shown, both theoretically and experimentally in simulated aquifers, that the flow rate measured in the borehole can be related quantitatively to the flow velocity within the surrounding aquifer (Carslaw and Jaeger 1959, Wheatcraft and Winterberg 1985, Drost et al. 1968). An additional criticism is that there may also be some degree of distortion of the flow direction within the borehole. Numerous field experiments have also demonstrated the practicality of in situ borehole flow measurements (Kearl et al. 1992, Kearl et al. 1994, Kearl 1997, Kearl and Roemer 1998, Molz et al. 1994). The in-well flow meter was especially useful at WMA B-BX-BY because the uncertainty in the flow direction was as much as 180° in the present-day flow, varying from northerly to southerly. Thus, even an error of 35° in flow direction may be tolerated to significantly improve upon results of previous techniques.

There are several reasons why the colloidal borescope is especially useful at the DOE Hanford Site. First, the method has been verified in extensive laboratory testing and has a history of numerous successful field tests. Second, the method does not use water level data and therefore, avoids the many sources of error and ambiguity as discussed above. Third, the method is simple in concept and deployment, economic to operate and gives timely results with no lengthy data collection or processing. Finally, because no water is removed from the well, there are no liquid waste issues to hinder field operations.

Instrument Description and Operation

The colloidal borescope consists of a CCD (charge-coupled device) camera, a flux-gate compass, an optical magnification lens, an illumination source, and stainless steel housing. The device is approximately 89 cm long and has a diameter of 4.4 cm. This small size allows the use of the tool in small diameter monitoring wells. The tool is connected via electrical cables to a power source, a small video monitor, and laptop computer located at the surface.

The tool is lowered into the well over a pulley by hand. After the tool is placed at the desired depth in the well (discussed later), an electronic image magnified 140 times is transmitted to the camera and detector at the surface. This enlarged image allows the colloidal particles (typically 0.1 to 10 μm) to be viewed and the particle motion analyzed. The orientation of the tool in the borehole is found with the flux-gate compass.

As particles in the groundwater move past the camera lens, they are illuminated from behind with a cold lighting source similar to a conventional microscope with a lighted stage. At periodic intervals, a view is captured and digitized with a video frame grabber and stored in a computer. A comparison is made between two consecutive, digitized video frames with proprietary software developed by Oak Ridge National Laboratory (Kearl 1997). The particles from the two images are matched, and pixel addresses are assigned to the particles. These addresses are used to compute and record the average particle size, number of particles, speed, and direction.

Particle motion for a few to dozens of particles is analyzed every four seconds resulting in a large database after only a few minutes of observations. Kearl (1997) discusses the accuracy of the method stating that by collecting 30 frames per second, a particle moving 1 mm across the field of view is captured in subsequent frames 1/30 of a second apart. Thus, the upper range on velocity measurements is three cm/s. To operate in areas with very low flow rates, the delay between frames was set for a larger time interval. This allows the tool to collect data in near stagnant flow conditions.

Verification of the method was demonstrated at the Desert Research Institute in Boulder City, Nevada (Kearl 1997). Velocities determined with the colloidal borescope were verified using a laminar flow chamber. A flow rate of 0.11 cm/s was found with the colloidal borescope when the flow chamber was operated at 0.20 cm/s. This rate was verified by a tracer test. The borescope identified flow at ½ of the actual flow; this is not unusual even under field conditions. Estimating that the velocity in the well bore as half or less can provide a fairly good estimate of average linear flow velocity in the aquifer near the well.

Data Acquisition

The following general approach was used to interrogate each well with the borescope to determine flow direction and velocity. The tool was initially lowered to the middle of the aquifer (i.e., approximately the middle of the saturated interval of the well screen), where it was left for approximately 20 to 30 minutes to let the inertial disturbance caused by insertion of the tool to dissipate. The vendor has found this time interval to be adequate for initial screening in most aquifers, and ours was similar. If a recognizable direction was not obtained in this time period or if the data degraded into an incoherent scatter, the tool was moved either up or down by several feet. If a tight, well defined pattern of swirls was located, the tool was moved up and then down from that depth and monitored at increasingly smaller intervals, and always allowing at least a half hour to let the aquifer return to ambient conditions. Once a zone was found where the pattern defined a linear, consistent trend, indicative of an open flow zone, data was collected for at least 2 hours to assure that the observed flow direction was consistent over time and did not degrade into a random flow pattern.

Finding the preferential flow zone(s) within a well screen is necessary to allow successful use of this technology at the Hanford Site. As directed by the vendor, only flow directions that displayed relatively consistent flow over a substantial time, usually close to two hours, were deemed reliable directions. The locations of swirling flow zones usually are related to lower permeability zones adjacent to the more permeable laminar flow zone. Although these zones were recorded for usually less than an hour during the search for more permeable flow zones, they are not useful in determining steady flow directions.

Several factors such as aquifer heterogeneity, design of well screen and filter packs, effectiveness of well development and negative skin effects can influence both flow direction and rate through the open interval (Earlougher 1977, Gibs et al. 1993, Kearl 1997, Kerfoot and Massard 1985, Kerfoot 1988, Molz et al. 1994, Moss 1990, Nielsen 1991, Schalla and Walters 1990). Therefore, well construction and local stratigraphy were considered in evaluating the flow directions and rates estimated from the colloidal borescope measurements. Because only one aquifer was screened in each well and the saturated thickness was typically a few meters or less, significant differences in hydraulic head that might result in vertical flow were not expected or observed (Church and Granato 1996, Reilly et al. 1989).

The primary goal of the borescope investigation was to obtain an estimate of the general flow direction. Consequently, measurements were made in numerous wells. By making measurements in many wells, compensation can be made for local spatial variations in flow direction and for perturbations in flow direction due to borehole effects.

Results and Conclusions

Several general conclusions can be made about the aquifer based on the results of this study. The groundwater flow rate is considerably greater in the southern part of the WMA B-BX-BY with respect to the BY Crib area and the northeast corner of WMA Low Level Burial Grounds (LLBG) 1. The very low flow rate in the north appears to be related to slow drainage of the aquifer along the basalt surface. Second, the flow direction in the south of WMA B-BX-BY appears to be more consistent with time than in the north where the direction appears to vary slightly with time.

Plots of the data for two representative records are shown in Figures 3 and 4 for two different depths in the same well, 299-E33-334. Data collected at a depth of 82.9 meters, forms a well-defined linear pattern (Figure 3). The initial turbulent flow caused by insertion of the tool through the water in the well can be observed in the first 25 minutes of the record. Because the borescope tool imparts a momentum during insertion to the fluid in the well, the particles initially swirl. In addition, large particles are dislodged from the well that would not normally be carried by the flow. In this preferential flow zone, the ambient flow gradually dominated, and a steady flow of smaller particles (primarily 0.1 to 10 µm) were observed flowing in real-time through the well. Data were collected continuously for about two hours displaying an azimuth of about 125 ° for the flow direction. A record of similar quality was collected in a well nearby also displaying a well-defined southerly flow direction.

The data shown in Figure 4, however, display some variability in the flow direction in well 299-E33-334 at a depth of 82.3 meters. Although a southerly direction was defined in the first 10 minutes of data collection, the record decayed to display swirling flow swinging around through north after 11 minutes. Finally, the data decay to a scattered pattern indicating that this was not a preferential flow zone. No direction could be determined from these data. This record is included for comparison with a record for which a direction could be determined because it emphasizes one of the primary advantages of the colloidal borescope over other in situ devices, that is, the real-time determination of the validity of the measurement taken.

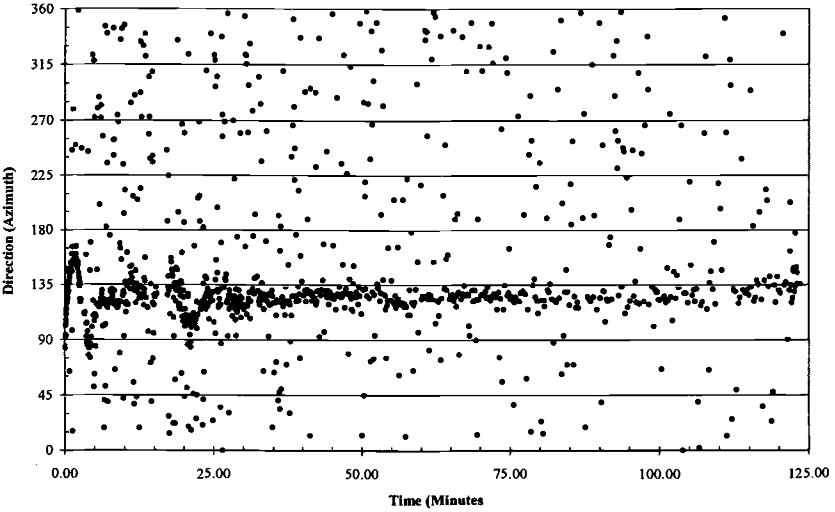

Figure 3. *Flow direction data collected in Well 299-E33-334 at a depth of 82.9 meters. Although there is some scatter in the data at this depth, the dominant flow direction is clearly to the south at about 125° azimuth. This direction held steady for two hours.*

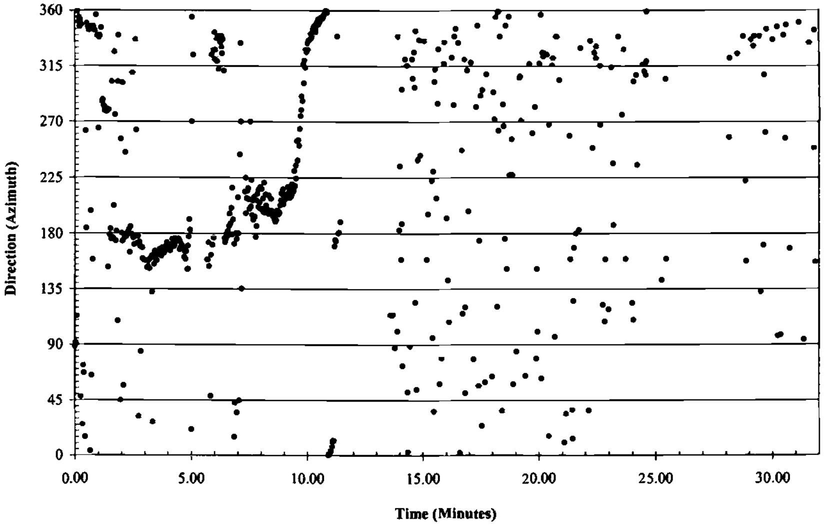

Figure 4. *Flow direction data collected in Well 299-E33-334 at a depth of 82.3 meters. Although a southerly direction was defined in the first 10 minutes of data acquisition, the record decayed from 180° direction swinging around to north after 11 minutes, and finally decaying to a scattered pattern without a defined direction at 14 minutes.*

Although the relationship of the borehole flow velocity to the flow velocity outside the well is not easily calculated with great precision, useful information was obtained on relative flow rates in preferential flow zones in each well screen and between such zones in other wells. The flow rate observed in wells from the northern part of the site was noticeably slower with respect to the wells in the southern half of WMA B-BX-BY. However, even in the northern part of the site, steady horizontal movement was observed as a particle was tracked across the viewing area. The difference in flow rates is probably associated with draining the artificially elevated portion of the aquifer in the north versus the deeper, natural aquifer in the south where the natural driving forces are still controlling aquifer movement.

Flow directions resulting from this study are shown in Figure 5. This figure also shows the local relief on the basalt surface and the approximate regional extent of the aquifer in pre-Hanford times when the alluvium in the northern portion of WMA B-BX-BY was dry. The estimated pre-Hanford groundwater table is shown in Figure 5. Only zones within the groundwater that displayed consistent horizontal laminar flow in a steady direction for about two hours are considered reliable flow zones. Data sets in which flow zones displayed a consistent flow direction for less than two hours are considered only qualitative indications of flow directions. Only the directions from reliable flow zones are shown at the associated well locations. Also provided are the results from the KV flowmeter study conducted in 1994 when the water table was about 0.6 meters higher than it is presently (Kasza 1995). The KV flowmeter discerns temperature variations across a flow zone delineating advective flow (Kerfoot, 1988). Although it may be expected that better-defined flow zones existed in the past when the aquifer was thicker, results between the two studies closely agree in most cases. Both methods indicate that the flow direction is primarily to the south, which is to be expected as the artificial groundwater mound that was centered at a location to the east-southeast dissipates. Local deviations from this general southerly flow are probably caused by structural highs in the basalt surface creating contorted flow paths.

There are limitations and advantages using the colloidal borescope to determine flow direction. The most significant limitation of the colloidal borescope technology the authors have found to date, relates primarily to the conditions within the borehole. Success in using the tool for a given well requires the well be properly screened and constructed to minimize disturbance of the ambient flow regime. For example, a well that is double screened, double sand packed, and incompletely developed is likely to have flow directions different, perhaps significantly, than the ambient flow direction in the adjacent aquifer sediments. Also, the well must be properly maintained including cleaning and, if necessary, redevelopment before using the borescope. Of course, the borescope is not used for at least 24 hours after redevelopment of the well to allow ambient flow patterns to return, and any pressure waves created by the development to diminish to negligible levels. If either of these requirements to assure open flow through the borehole cannot be met, there will be limited success in using the borescope to estimate flow direction or rate. The other dominant limitation to conducting a borescope investigation is the natural heterogeneity and anisotropy in the aquifer. Measurements with the borescope represent a relatively small area within the well screen interval. Consequently, data from numerous wells must be collected to recognize the effective flow direction from the local flow direction discerned in one well.

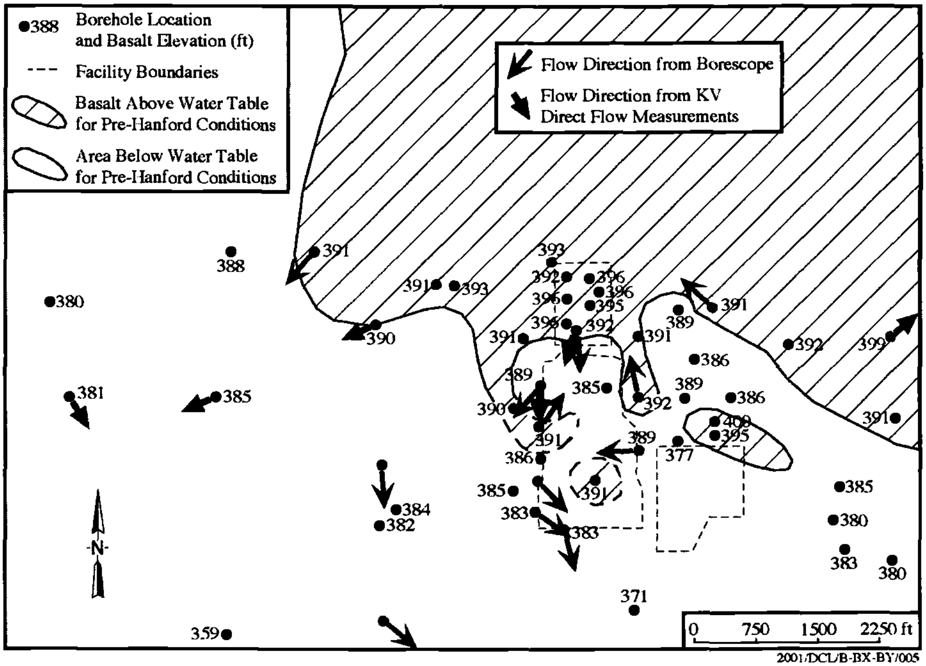

Figure 5- *Results of several in situ flow meter studies are shown for the area around WMA B-BX-BY. Dovetailed arrows depict the flow direction determined in a well using the colloidal borescope data. Shorter blocked arrows indicate the flow direction in 1994 using the KV flowmeter when the water table was about a meter higher. Note the correlation between results from the KV flowmeter and the colloidal borescope in the northern part of the study area. Contorted flow paths around structural basalt highs may cause local deviations from this general southern flow.*

One of the most important advantages of this technology over other in situ technologies even though the same fundamental physics apply, is that, it is possible to determine the reliability of the measurements by monitoring real-time changes in a continuous stream of particles flowing through the well. Because stagnant zones are easily identified by inconsistent flow direction, there is also a cost savings by reducing additional time that would be wasted collecting data from stagnant zones where ambient particles continue to swirl randomly. Finally, based on our experience, the colloidal borescope adds a useful technique to a toolbox of data collection methods. When combined with existing chemistry and potentiometric data, these point measurements will enable us to have a more comprehensive and accurate understanding of the groundwater flow system in areas subject to accuracy limitations of more conventional methods where extremely small gradients and complex flow patterns exist.

Acknowledgements

The authors wish to thank Peter Kearl and Kirk Roemer at AquaVision, Inc. for their assistance and mentoring during the course of the field project. We would also like to extend our appreciation to Dorothy "Dot" Stewart and Stuart Luttrell of the Pacific Northwest National Laboratory for their help and support in our efforts to field the colloidal borescope. David Lanigan created computer graphics and figures.

References

40 CFR 265, Code of Federal Regulations, Title 40, Part 265. *Interim Status Standards for Owners and Operators of Hazardous Waste Treatment Storage and Disposal Facilities.*

Caggiano, J. A., 1996, *Assessment Groundwater Monitoring Plan for Single-Shell tank Waste Management Area B-BX-BY.* WHC-SD-EN-AP-002, Westinghouse Hanford Company, Richland, Washington.

Carslaw, H. S. and Jaeger, K. C., 1959, *Conduction of Heat in Solids.* Oxford University Press, New York, 510 pp.

Church, P. E. and Granato, G. E., 1996, "Bias in Ground-Water Data Caused by Well-Bore Flow in Long-Screen Wells," *Groundwater* 134(2):262-273.

Cushman, J. H. (Ed.), 1990, *Dynamics of Fluids in Hierarchical Porous Media.* Cole, C. R. and Foote, H. P., Chapter 10, "Multigrid Methods for Solving Multiscale Transport Problems," Academic Press Inc., San Diego, California.

Drost, W., Klotz, D., Koch, A., Moser, H., Neumaier, F., and Rauert, V., 1968, "Point Dilution Methods of Investigating Ground Water Flow by Means of Radioisotopes," *Water Resources Research* 4(1), pp. 125-146.

Earlougher, R. C., 1977, "Advances in Well Test Analysis," *Society of Petroleum Engineers of AIME*, Dallas, Texas.

Gibs, J., Brown, G. A., Turner, K. S., MacLeod, C. L., Jelinski, J. C., and Koehnlein, S. A., 1993, "Effects of Small-Scale Vertical Variations in Well-Screen Inflow Rates and Concentrations of Organic Compounds on the Collection of Representative Ground-Water-Quality Samples," *Groundwater* 31(2): 201-208.

Hartman, M. J., Morasch, L. F., and Webber, W. D. (eds.), 2000, *Hanford Site Groundwater Monitoring for Fiscal Year 1999.* PNNL-13116, Pacific Northwest National Laboratory, Richland, Washington.

Kasza, G. L., 1995, *In Situ Flowmeter Results and Analysis for the 216-BY Cribs Vicinity.* BHI-00442, Bechtel Hanford, Inc., Richland, Washington.

Kearl, P. M., Korte, N. E., and Cronk, T. A., 1992, "Suggested Modifications to Groundwater Sampling Procedures Based on Observations from the Colloidal Borescope" *Groundwater Monitoring Review* 12(2), pp. 155-160. Dublin, Ohio.

Kearl, P. M., Korte, N. E., Stites, M., and Baker, J., 1994, "Field Comparison of Micropurging vs. Traditional Ground Water Sampling," *Groundwater Monitoring Review* 14(4), pp. 183-190. Dublin, Ohio.

Kearl, P. M., 1997, "Observations of Particle Movement in a Monitoring Well Using the Colloidal Borescope," *Journal of Hydrology*, pp. 323-344. New York, NY.

Kearl, P. M. and K. Roemer., 1998, "Evaluation of Groundwater Flow Directions in a Heterogeneous Aquifer Using the Colloidal Borescope," *Advances in Environmental Research* 2(1), pp. 12-23. Berkeley, CA.

Kerfoot, W. B., 1988, "Monitoring Well construction and Recommended Procedures for Direct Ground-Water Flow Measurements using a Heat-pulsing Flowmeter," In *Ground-Water Contamination – Field Methods, ASTM STP 963*, eds. A. G. Collins and A. I. Johnson, pp. 146-161, American Society for Testing Materials, West Conshohocken, Pennsylvania.

Kerfoot, W. B. and Massard, V. A., 1985, "Monitoring Well Screen Influences on Direct Flowmeter Measurements," *Groundwater Monitoring Review* 5(4), pp. 74-77. Dublin, Ohio.

Molz, F. J., Boman, G. K., Young, S. C., and Waldrop, W. R., 1994, "Borehole Flowmeters: Field Application and Data Analysis," *Journal of Hydrology* 163, pp. 347-371. New York, NY.

Moss, R. Jr. (ed.), 1990, *Handbook of Groundwater Development*. The Roscoe Moss Company, John Wiley & Sons Publishers, New York, New York, 493 pp.

Narbutovskih, S. M., 1998, *Results of Phase I Groundwater Quality Assessment for Single Shell Tank Waste Management Areas B-BX-BY at the Hanford Site*, PNNL-11826, Pacific Northwest National Laboratory, Richland, Washington.

Narbutovskih, S. M., 2000, *Groundwater Quality Assessment Plan for Single Shell Tank Waste Management Area B-BX-BY at the Hanford Site*, PNNL-13022, Pacific Northwest National Laboratory, Richland, Washington.

Narbutovskih, S. M. and Horton, D. G., 2001, *RCRA Groundwater Monitoring Plan for Single-Shell Tank Waste Management Areas A-AX at the Hanford Site*. PNNL-13023, Pacific Northwest National Laboratory, Richland, Washington

Nielsen, D. M. (ed.), 1991, *A Practical Handbook of Groundwater Monitoring*. Schalla R., Chapter 7, Design and Installation of Groundwater Monitoring Wells, Lewis Publishers, Chelsea, Michigan.

Reilly, T. E., Franke, O. L., and Bennett, G. D., 1989, "Bias in Groundwater Samples Caused by Wellbore Flow," *Journal of Hydraulic Engineering* 115(2): 270-276.

Schalla, R., Lewis, A. K., and Bates, D. J., 1992, "Accuracy and Precision of Well Casing Surveys and Water Level Measurements and Their Impact on Water-Level Contour Maps." *Mapping and Geographic Information Systems, ASTM Special Technical Publication 1126*, (Eds.), Johnson, I. A., Pettersson, C. B., and Fulton, J., Philadelphia, Pennsylvania. pp. 295-309.

Schalla, R. and Walters, W. H., 1990, "Rationale for the Design of Monitoring Well Screens and Filter Packs," *Standards Development for Groundwater and Vadose Zone Monitoring Investigations, ASTM STP 1053*, ed. D. M. Nielsen, pp. 64-75, American Society for Testing Materials, Philadelphia, Pennsylvania.

Wheatcraft, S. W. and Winterberg, F., 1985, "Steady State Flow Passing through a Cylinder of Permeability Different from the Surrounding Medium," *Water Resources Research* 21(12), pp. 1923-1929.